Isocitrate Dehydrogenase mutations in diffuse glioma

Unraveling metabolic rewiring in search of novel therapies

Krissie Lenting

Isocitrate Dehydrogenase mutations in diffuse glioma

Unraveling metabolic rewiring in search of novel therapies

Krissie Lenting

***Isocitrate Dehydrogenase* mutations in glioma – unraveling metabolic rewiring in search of novel therapies**

The research presented in this thesis was performed at the Department of Pathology, Radboud University Medical and the Department of Biochemistry, Radboud Institute of Molecular Life Sciences, Nijmegen, The Netherlands

Cover Design/Lay-out: Marco Prins Illustrations | www.marcoprins.nl
Print: Ridderprint | www.ridderprint.nl

Isocitrate Dehydrogenase mutations in diffuse glioma

Unraveling metabolic rewiring in search of novel therapies

Proefschrift ter verkrijging van de graad van doctor
aan de Radboud Universiteit Nijmegen
op gezag van de rector magnificus prof. dr. J.H.J.M. van Krieken,
volgens besluit van het college voor promoties
in het openbaar te verdedigen op

woensdag 18 januari 2023
om 16.30 uur precies

door

Krissie Lenting
geboren op 11 juni 1987
te Helmond

Promotoren:
Prof. dr. P. Wesseling (Vrije Universiteit Amsterdam)
Prof. dr. R.E. Brock

Copromotor:
Dr. W.P.J. Leenders

Manuscriptcommissie:
Prof. dr. J. Bussink (voorzitter)
Prof. dr. A.J. van Gool
Dr. E. Hulleman (Princes Máxima Centrum voor Kinderoncologie)

Isocitrate Dehydrogenase mutations in diffuse glioma

Unraveling metabolic rewiring in search of novel therapies

Dissertation to obtain the degree of
doctor from Radboud University Nijmegen
on the authority of the Rector Magnificus prof. dr. J.H.J.M. van Krieken,
according to the decision of the Doctorate Board
to be defended in public on

Wednesday, January 18, 2023
at 4.30 pm

by

Krissie Lenting
born on June 11, 1987
in Helmond (the Netherlands)

Supervisors:
Prof. dr. P. Wesseling (Vrije Universiteit Amsterdam)
Prof. dr. R.E. Brock

Co-supervisor:
Dr. W.P.J. Leenders

Manuscript Committee:
Prof. dr. J. Bussink (chair)
Prof. dr. A.J. van Gool
Dr. E. Hulleman (Princess Máxima Center for Pediatric Oncology)

Table of contents

LIST OF ABBREVIATIONS

6PGL	6-Phosphogluconolactonase
ABAT	γ-Aminobutyrate aminotransferase
Ac-CoA	Acetyl-CoA
ACLY	ATP citrate lyase
ACO	Aconitase
a-KG	Alpha ketoglutarate
ALDH5A1	Succinate semialdehyde dehydrogenase
ALKBH	AlkB homolog
AML	Acute myeloid leukemia
AR	Androgen receptor
ASCT2	Anti-neutral amino acid transporter 2
BBB	Blood brain barrier
BCAT	Branched chain amino acid transaminase
CAXII	Carbonic anhydrase 12
CNS	Central nervous system
CS	Citrate synthase
CT	Citrate
D-2-HG	D-2-Hydroxyglutarate
D_2O	Deuterated water
DNA-DSB	DNA double-strand break
EAAT	Glutamate transporters excitatory amino acid transporters
EGCG	Epigallocatechin-3-gallate
EGF	Epidermal growth factor
EGFR	Epidermal growth factor receptor
EGLN	Egg Laying Defective Nine
EMT	Epithelial-to-mesenchymal transition

F6P	Fructose-6-phosphate
FC	Fold change
FDG-PET	Fluorodeoxyglucose- positron emitter tomography
FDR	False discovery rate
FH	Fumarate Hydratase
FPKM	Fragments Per Kilobase per Million
FPM	Fragments Per Million
G6P	Glucose-6-phosphate
GAD1	Glutamate Decarboxylase 1
G-CIMP	Glioma CpG Island Methylator Phenotype
Glc	Glucose
Gln	Glutamine
GLS	Glutaminase
Glu	Glutamate
GLUD	Glutamate dehydrogenase
GLUT	Glucose transporter
GOT	Glutamic acid oxaloaminotransferases
GS	Glutamine synthase
GSH	reduced glutathione
GSLC	Glioma stem-like cell
H2AX	H2A histone family member X
HIF1α	Hypoxia Inducible Factor 1α
HK2	Hexokinase 2
ICT	Isocitrate
IDH	Isocitrate dehydrogenase
IHC	Immunohistochemistry

IR	ionizing radiation
JHDM	Jumonji-C-domain containing histone demethylase
LC-MS	Liquid chromatography mass spectroscopy
LDH	Lactate dehydrogenase
MCT	Monocarboyxlate transporter proteins
MDH1	Malate Dehydrogenase 1
MGMT	O(6)-Methylguanine-DNA methyltransferase
MRSI	Magnetic Resonance Spectroscopic Imaging
MS	Mass spectrometry
NGS	Next generation sequencing
NMR	Nuclear magnetic resonance
OAA	Oxaloacetate
OE	Overexpression
OGDH	α-ketoglutarate dehydrogenase
OXPHOS	Oxidative phosphorylation
PARP	Poly-ADP ribose polymerase
PC	Pyruvate carboxylase
PCV	Procarbazine, CCNU/lomustine, and vincristine
PDGFRα	Platelet derived growth factor receptor alpha
PDH	Pyruvate dehydrogenase
PDK1	Pyruvate Dehydrogenase Kinase 1
PEP	Phosphoenolpyruvate
PKM	Pyruvate Kinase M
PMS	Phenazine Methosulphate
PPP	Pentose phospate pathway
PSMA	Prostate specific membrane antigen

ROS	Reactive oxygen species
RSP	Ribose-5-phospate
RTK	Receptor tyrosine kinase
SDH	Succinate Dehydrogenase
smMIP	Single molecule Molecular Inversion Probe
SSA	Succinic semialdehyde
SSADH	Succinic semialdehydedehydrogenase
Suc	Succinate
t/RNA-NGS	Targeted RNA-next generation sequencing profiling assay
TCA	Tricarboxylic acid cycle
TCGA	The Cancer Genome Atlas
TET	Ten Eleven Translocation
TMZ	Temozolomide
VEGF	Vascular endothelial growth factor
w/RNA-NGS	Whole RNA next-generation sequencing
WHO	World Health Organization
γH2AX	Phosphorylated H2AX

CHAPTER 1

General introduction and outline of this thesis

According to the World Health Organization (WHO), cancer is a leading cause of death worldwide with an incidence of ~18 million and of 9.5 million people dying from cancer in 2018 [1]. With increased aging of the population the incidence and mortality rates of cancer are still increasing, despite the efforts of both (bio)medical researchers and the pharmaceutical industry to develop (therapeutic) strategies to fight and cure cancer.

Cancer is a group of diseases that involve abnormal cell growth in tissue. Most cancer-related deaths are associated with the capacity of many cancers to metastasize, a process involving a series of steps that include invasion of extracellular matrix at the primary site, detachment of (groups of) cancer cells from the primary tumour, intravasation into the lymphatic and/or circulatory system, and extravasation from distant capillaries, in order to eventually invade and proliferate in distant organs [2]. Initiation of metastasis is enabled by epithelial-to-mesenchymal transition (EMT) [3, 4], a dynamic and reversible process that involves a complex transcriptional program that leads to the loss of cell-to-cell interactions and cell polarity, facilitating migration and invasion [5].

Malignant neoplasms acquire various biological capabilities during their development, which are called 'the hallmarks of cancer', that include genome instability and mutations, sustained proliferative signalling, evasion of growth suppression, resistance to cell death, replicative immortality, induction of angiogenesis, and activation of invasion and metastasis (with metastasis being very rare in diffuse glioma), evasion immune destruction, and reprogramming of energy metabolism (Figure 1) [3, 4].

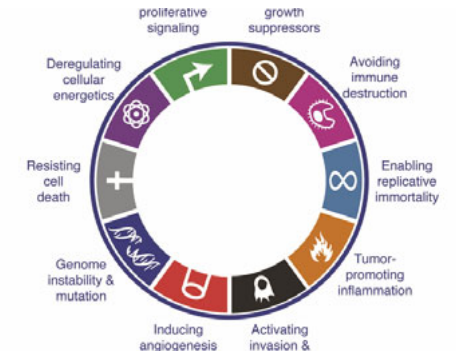

Figure 1: Hallmarks of cancer. *This illustration depicts the 10 hallmarks of cancer which are capabilities that each cancer cell acquires during malignant transformation. Figure adapted from Hanahan & Weinberg, Cell, 2011 [3].*

Especially the latter has been a major topic of interest in the past decade. Although the first observations of metabolic alterations were made nearly a century ago [6], the emergence of (new) biochemical and molecular tools, such as DNA and RNA sequencing, mass spectrometry (MS) techniques such as Liquid chromatography (LC-)MS, and metabolic flux tracing or stable

isotope tracing (^{13}C) has expanded our knowledge of tumour-associated metabolic alterations in tumorigenesis.

(Tumour)Metabolism

A classic example of reprogrammed metabolism in cancer is aerobic glycolysis, also known as the 'Warburg effect' [7]. In 1920, Otto Warburg observed that tumour cells preferentially metabolize glucose to pyruvate and then lactate rather than shuttling pyruvate via acetyl-CoA into the tricarboxylic acid (TCA) cycle, even under oxygen-rich conditions [6, 8].

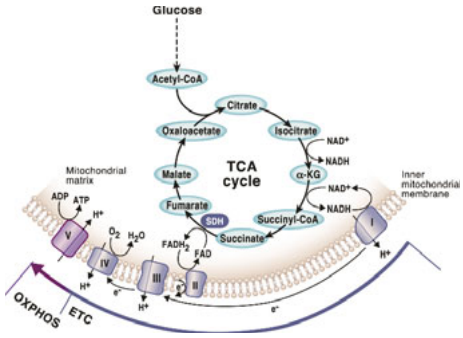

***Figure 2: The TCA cycle and OXPHOS**. The TCA Cycle generates reducing molecules such as NADH and $FADH_2$, which are required for electron transfer in the ETC. In a functional ETC, electrons move through the five (I-V) main protein complexes in the inner mitochondrial membrane, generating a mitochondrial membrane potential that is used to produce ATP. Oxygen is required for this process known as OXPHOS. Complex I and II in the ETC replenish NAD+ and FAD^+, necessary for the TCA cycle to function. SDH is the only enzyme that participates in both TCA cycle and ETC.*
ADP adenosine diphosphate, ATP adenosine triphosphate, ETC Electron transport chain, NAD nicotinamide-adenine-dinucleotide, NADH nicotine-adenine-dinucleotide hydride, FAD flavin adenine dinucleotide, FADH2 oxidized FAD, OXPHOS oxidative phosphorylation, TCA cycle tricarboxylic acid cycle [9].

In healthy cells and under normoxic conditions, the glycolytic pathway converts glucose to pyruvate through a series of enzymatic reactions. In the presence of oxygen, pyruvate formed in this multistep reaction can be further processed in the TCA cycle and oxidative phosphorylation (OXPHOS), ultimately providing the cell with the high energy ATP (Figure 2)[9]. Under conditions in which oxygen supply cannot fulfil energy demand (e.g. muscle hyperactivity and hypoxia occurring as a result of pathology), pyruvate derived from glucose is converted to lactate rather than shuttled into the TCA cycle [10]. The main source of lactate in the healthy body is from metabolically hyperactive cells and erythrocytes [11]). Lactate cannot be processed in the TCA cycle and can either be transported from peripheral tissues to the liver, where it is reconverted to pyruvate and glucose by a series of enzymes, starting with lactate dehydrogenase (the Cori cycle) [12, 13], or can be shuttled to nearby cells that use lactate as fuel for their metabolic processes. The latter process is also known as the lactate-shuttle and occurs in various tissues such as heart, skeletal muscle and brain [14, 15]. In heart and muscle, lactate that is produced by physical exercise, is transported out of the muscle cells

through monocarboxylate transporter proteins (MCTs), in order to be further processed in the Cori cycle. In the brain, both neurons and astrocytes express MCT, suggesting that the lactate shuttle may be involved in brain metabolism in which astrocytes produce and release lactate into the brain parenchyma, which is then taken up by adjacent neurons as fuel for their metabolic processes [15-17]. Lactate uptake is regulated via different MCTs that act as lactate importers.

Although much less efficient in terms of ATP production compared to OXPHOS, glucose to lactate conversion retains carbon from glucose that otherwise is exhaled in the form of CO_2, and which supports the biosynthetic requirements needed for proliferation, such as lipid components for cell membranes (via fatty acid metabolism), nucleic acid (through the pentose phosphate pathway; PPP), nitrogen (via glutaminolysis) and amino acid precursors [18-20]. One proposition for the 'Warburg effect' therefore is that cancer cells need to activate aerobic glycolysis, despite the presence of oxygen, for these proliferative purposes [21]. Excessive glucose uptake to compensate for reduced ATP production that is associated with glucose to lactate conversion, has emerged as a hallmark of cancer, and can be used clinically for tumour recognition and monitoring through positron-emission-tomography-based imaging of ^{18}F-fluorodeoxyglucose uptake (FDG–PET) [22].

The need for macromolecules is different in proliferating cells than in non-proliferating cells [23]. In the latter, the traditional view of the mitochondrial TCA cycle is to produce ATP from oxidizable substrates, needed as an energy source for cell homeostasis and survival. In proliferating cells however, many of the metabolites that are produced in the TCA cycle are exported from the mitochondria to the cytosol to be used in cytosolic pathways that consume rather than produce ATP (cataplerosis). This efflux (e.g. export of citrate for lipid synthesis) is needed to provide the necessary elements for cell division [24, 25]. To compensate for this loss of mitochondrial TCA cycle intermediates, the TCA cycle must be fuelled with other metabolites to keep it going, a process known as anaplerosis (the opposite to cataplerosis) [26]. In addition to glycolysis, glutaminolysis is an important pathway for anaplerosis of the TCA cycle [27].

Anaplerotic pathways

In the glutaminolysis pathway, glutamine not only contributes carbon, but also nitrogen for *de novo* biosynthesis of a number of nitrogen-containing molecules such as purines and pyrimidines [28]. Glutamine is converted in a two-step reaction to α-ketoglutarate (α-KG): 1) glutaminase (GLS) converts glutamine to glutamate, and 2) glutamate dehydrogenase (GLUD) converts glutamate to α-KG, a central metabolite in the TCA cycle [27]. α-KG can subsequently be converted to a.o. succinyl-CoA, succinate, fumarate, malate, and oxaloacetate (Figure 2) to support mitochondrial respiration and ATP production [29, 30].

With both glycolysis and glutaminolysis pathways often upregulated in cancer cells, inhibition of key enzymes involved in these pathways has provided an emerging therapeutic strategy in

cancer research, proven to be effective in slowing cancer cell proliferation and inducing cancer cell death in a preclinical setting [31, 32]. Efforts to block metabolic pathways involving glucose and glutamine have been initiated decades ago, but due to the lack of specificity of metabolic inhibitors, toxicity in patients has been a major issue, causing the abandonment of clinical trials [33-36]. Recent efforts to more specifically inhibit enzymes that are active in cancer cells have led to new clinical trials, with multiple inhibitors that are currently being tested in various cancer types, such as glioma [37], acute myeloid leukaemia (AML; ClinicalTrials.gov Identifier: NCT03245424), and solid malignancies (ClinicalTrials.gov identifier NCT02044861) [38].

Brain and neurotransmitters

The brain is composed of various types of cells including neurons, glial cells, neural stem cells and structures such as blood vessels. Neurons process and transmit information through electrical and chemical signals, while glial cells provide structural and metabolic support to the neurons, as well as isolate them from each other and protect them from pathogens [39]. Several types of glial cells can be distinguished: astrocytes, oligodendrocytes, and ependymal cells, of which astrocytes and oligodendrocytes are the most abundant. Oligodendrocytes form the myelin sheath that surround neuronal axons, thereby providing electrical insulation, as well as metabolic support [40]. Astrocytes are responsible for many functions, including supporting the endothelial cells that form the blood-brain barrier (BBB), metabolic support, and uptake of neurotransmitters released by neurons in the synaptic cleft [41].

Neurons communicate with other cells by releasing neurotransmitters that bind to chemical receptors of its target cell. The transmitter-molecules are released by the terminal axon of a presynaptic neuron, in the synaptic cleft that separates neurons from one another. The released neurotransmitters then bind to and react with the receptors on the postsynaptic neuron, which in turn reacts in an excitatory or inhibitory way, and can trigger short term changes such as changes in membrane potential, or long-term changes such as the initiation of signalling cascades [42, 43]. Many different types of neurotransmitters have been described [44], such as glycine, norepinephrine, serotonin, acetylcholine, dopamine, gamma-aminobutyric acid (GABA) [45], and glutamate [46]. In this thesis we will mainly focus on the neurotransmitter glutamate, which is the most prevalent neurotransmitter responsible for excitatory effects in 90% of synapses in the brain [47]. It plays a central role in both neurotransmission, and various pathways involved in cancer metabolism. Of note, GABA is the major inhibitory neurotransmitter in the brain [45].

Efficient glutamate-dependent neurotransmission in the brain relies on two requirements: Firstly, the level of glutamate in the synaptic cleft should be kept low in order to maximize the signal-to-noise ratio of newly released glutamate binding to (metabotropic and/or ionotropic) glutamate receptors on the post-synaptic cleft, and to prevent excessive excitations that can injure and even kill neurons (excitotoxicity) [48, 49]. Secondly, pools of glutamate should be available at all times to allow excitatory neurotransmission [50]. This can either be

accomplished by reuptake of the transmitter from the synaptic cleft, or resynthesis of the transmitter.

Both post- and presynaptic neurons have been shown to take up glutamate from the synaptic cleft, although inefficient [51]. One of the critical functions of astrocytes in the central nervous system (CNS) is regulation of neurotransmitter homeostasis, and a major role for astrocytes is therefore to take up excess glutamate [52]. In addition to uptake of neurotransmitters, astrocytes metabolize and release neurotransmitter-precursors back to the neurons [53], by participating in the so-called glutamate-glutamine cycle. In this cycle, astrocytes surrounding the synaptic cleft take up glutamate through the glutamate transporters excitatory amino acid transporters (EAAT) [52], and metabolize glutamate back into glutamine through the enzyme glutamine synthase (GS). Glutamine is then shuttled back to the neuron, to be converted to glutamate via GLS after which glutamate can again be used as a neurotransmitter, thus completing the cycle (Figure 3).

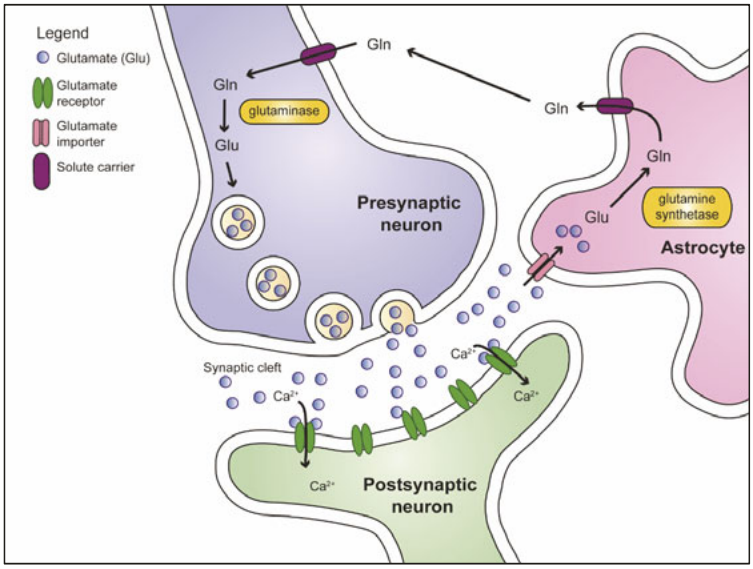

Figure 3: Schematic representation of the glutamine-glutamate cycle in the brain*. In the brain, glutamate (Glu) is released by presynaptic neurons to the synaptic cleft. Glutamate activates glutaminergic receptors that undergo a conformational change to allow influx of extracellular calcium. This triggers membrane depolarization in the postsynaptic neuron and induces signal transduction. The excess of glutamate in the synaptic cleft must be removed to prevent excitotoxicity. Astrocytes take up surplus glutamate through various glutamate importers and convert it to glutamine (Gln) through glutamine synthetase. Glutamine is exported to the capillaries (not shown) or is transferred back to the neurons. Subsequently, neurons can then convert back the glutamine to glutamate, closing the glutamine-glutamate cycle.*
Figure adapted from Lenting, K et al. Acta Neuropathologica, 2017 [54]

Glioma

Malignant transformation of (precursors of) glial cells may result in diffuse glioma (hereafter called glioma), a rare cancer of the CNS [55]. Gliomas are the most prevalent primary tumours of the brain and spinal cord [56, 57].

Glioma classification

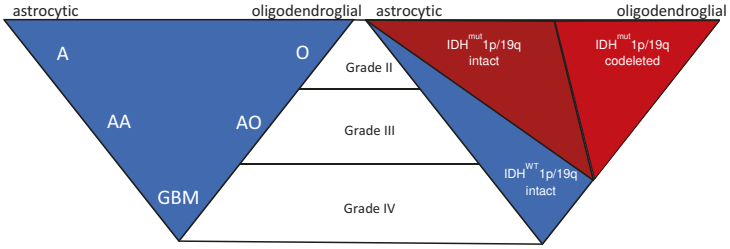

Figure 4: 2016 CNS WHO Grading and classification of glioma. *A: astrocytoma, AA: anaplastic astrocytoma, O: oligodendroglioma, AO: anaplastic oligodendroglioma, GBM: glioblastoma, IDH^{mut}: mutated isocitrate dehydrogenase, IDH^{wt}: wild-type isocitrate dehydrogenase.*
Figure adapted from Wesseling et al, Acta Neuropathologica, 2015 [58]

Gliomas share characteristics of non-neoplastic glial cells, and historically, have been diagnosed and classified based on histological characteristics [59]. According to the cell of origin gliomas are diagnosed as oligodendroglioma (derived from oligodendrocytes) or astrocytoma (derived from astrocytes) [60] and further assigned to either lower-grade (grade II-III) or high-grade grade (grade IV or glioblastoma). In 2016, the WHO revised the CNS tumour classification to include genotypic features in addition to the classical phenotypic features. Classification is now based on the extent of mitotic activity, necrosis and microvascular proliferation, and genetic properties such as *Isocitrate dehydrogenase (IDH)* mutational status (see below) and the combined loss of the short arm of chromosome 1 and the long arm of chromosome 19 (1p/19q codeletion) (Figure 4) [58-60].

Current treatment for glioma

Currently, treatment of grade II and III glioma consists of several options including 1) 'watchful waiting' until clinical progression of the patient (due to often slow development and growth of low-grade tumours) [61, 62], 2) resection of the tumour to the extent that is safe [63], 3) radio-chemotherapy with PCV (procarbazine, CCNU and vincristine)[60, 64].

The progress of treatment possibilities for glioma sharply contrasts that of other cancers, and only limited novel treatment protocols have been implemented in the last decades. In glioblastoma the concomitant addition of the DNA-alkylating agent temozolomide (TMZ) to radiotherapy increased median survival for only 3 months (from 12 to 15 months from diagnosis) [65, 66]. Implementation of optimized imaging [67, 68] and surgical techniques,

such as fluorescence-guided surgery using 5-aminolevulinic acid (5-ALA), resulted in the largest gain in patient survival due to better surgical resection of the tumour [69-71]. After resection to the extent that is safe, glioma cells that have invaded into the surrounding brain parenchyma, ultimately give rise to recurrence of the tumour within months.

Understanding the molecular events underlying gliomagenesis has been a major research effort in the last years, shedding light on a number of pathways that are frequently affected in glioma [72, 73]. Activating mutations or amplification of receptor tyrosine kinases (RTKs) such as epidermal growth factor receptor (EGFR), are often found in gliomas (as in other cancer types), and have therefore been investigated in various clinical trials over the years, trying to improve overall survival and patient outcomes. All of these trials have failed, including treatment with the VEGF-inhibitor bevacizumab [74], various EGFR-inhibitors, a.o. erlotinib and gefitinib [75-79], and c-MET inhibitors [80, 81].

Isocitrate Dehydrogenase (IDH) 1/2 mutations

A major breakthrough in understanding gliomagenesis was the identification of heterozygous hotspot mutations in the genes encoding the metabolic enzyme isocitrate dehydrogenase (IDH), that is found in 70-80% of grade II and III diffuse gliomas, and secondary glioblastomas that originate from IDH-mutated grade II and III gliomas [82, 83].

The dimeric IDH1 enzyme is responsible for the conversion of isocitrate to α-ketoglutarate (α-KG) in the cytosol. During this reaction, NADP+ is reduced to NADPH, which is necessary for multiple systems involved in fatty acid synthesis, cellular detoxification [84, 85], such as production of reduced glutathione (GSH) [86], thioredoxins [87], catalases [88] and activity of cytochrome P450 [89]. In the human brain, IDH1 is responsible for the generation of ~65% of the cytosolic NADPH [90, 91].

In addition to IDH1, there are two mitochondrial IDH isoforms: IDH2 and IDH3. IDH3 is dependent on NAD+ rather than NADP+. For IDH3, no tumour-associated mutations are reported [92], while IDH1 and IDH2 mutations are widely reported in cancers such as glioma, AML, chondrosarcoma and intrahepatic cholangiocarcinoma [93].

Mutations in *IDH* are one of the key events in low-grade gliomagenesis [94] and mainly involve a specific arginine residue on position 132 of IDH1 or residues R172 or R140 in IDH2 [83], present in the catalytic site of the enzyme. The R132H mutation induces a gain of function of the enzyme, resulting in rapid conversion of α-KG to D-2-hydroxyglutarate (*D*-2-HG) by the mutant subunit, while concomitantly oxidizing NADPH to $NADP^+$ [95] (Figure 5). *D*-2-HG is proposed to function as an 'oncometabolite', responsible for driving tumorigenesis. It is structurally similar to α-KG, and is thought to act as an competitive inhibitor of α-KG-dependent dioxygenases, such as histone demethylases and the TET family of hydroxylases which perform a rate limiting step in DNA-demethylation [96], and Jumonji-C-domain containing histone demethylases (JHDMs) [97]. This results in an overall increase of cellular DNA hypermethylation and alterations of epigenetics, ultimately leading to the glioma

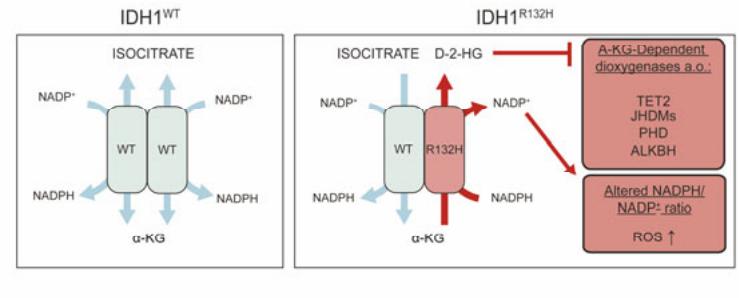

Figure 5: Biochemical and cellular effects of an IDH1 mutation. In homodimeric IDH1^{wt}, isocitrate is catalysed to α-ketoglutarate (α-KG), while also producing NADPH, important in scavenging of ROS (left panel). IDH1^{R132H} mutated enzymes are heterodimeric enzymes with one wild-type subunit (blue) and mutated subunit (red). The wild-type subunit produces α-KG from isocitrate. α-KG is then rapidly converted to D-2-HG by the mutant subunit. D-2-HG has inhibitory effects on α-KG-dependent dioxygenases, such as Tet methylcytosine dioxygenase 2 (TET2), Jumonji-C-domain containing histone demethylases (JHDMs), prolyl hydroxylases (PHD), and the DNA-repair protein ALKBH. In addition, the mutant subunit consumes NAPDH, altering the NADPH/NAPD$^+$ ratio, which ultimately leads to an increase in reactive oxygen species (ROS) in the cell.

CpG-island methylator phenotype (G-CIMP) [98, 99]. This is proposed to a.o. inhibit expression of DNA repair proteins, such as ALKBH, thereby increasing susceptibility to DNA-alkylating agents [100]. In addition metabolic enzymes such as Branched chain amino acid transaminase 1 (BCAT1) [101] and Lactate dehydrogenase A (LDH-A) [102] are silenced due to G-CIMP. Furthermore, D-2-HG serves as a cofactor for Egg Laying Defective Nine (EGLN), which hydroxylates specific proline residues in Hypoxia Inducible Factor 1α (HIF1α), after which the protein is ubiquinated and degraded [103]. HIF1α is a transcription factor that regulates expression of a number of hypoxia-related genes such as glucose transporter 1 (GLUT-1) and vascular endothelial growth factor A (VEGF-A), the central modulator of angiogenesis and vascular hyperpermeability [104]. Increased HIF1α degradation by *D*-2-HG fits with the notion that IDH-mutations are frequent in grade II/III glioma that lack signs of hypoxia and angiogenesis [105].

In addition to the role of *D*-2-HG in gliomagenesis through epigenetic alterations, the *IDH*-mutation also directly affects cellular metabolism. Due to the decrease in affinity for isocitrate, IDH-mutated enzymes are predicted to 1) produce *D*-2-HG, 2) deplete α-KG, and 3) decrease NADPH production and increase NADPH consumption. Since IDH1 activity is responsible for the production of the majority of cytosolic NADPH in glioma cells, IDH-mutations decrease the total NADPH production capacity [84, 85], thereby lowering the reductive potential of tumour cells [106] and probably interfering with fatty acid and membrane synthesis. This in turn might lead to a decreased ability of cellular proliferation and ROS detoxification, supporting the finding that patients with *IDH*-mutated glioma have a better prognosis and respond better to chemo- and/or radiotherapy [107].

Excessive consumption of α-KG and NADPH by IDH-mutant cancer cells is an important factor, impairing cell proliferation. Besides converting ICT to α-KG, IDH1 can also catalyse the reverse reaction forming ICT (reductive carboxylation), which can in turn be metabolized to citrate which is used for fatty acid synthesis [108, 109]. $IDH1^{R132H}$ lacks the capability of reductive carboxylation, and cancer cells carrying this mutation may therefore depend on metabolite anaplerosis via alternative metabolic pathways, such as mitochondrial IDH2, for citrate and α-KG production.

The high prevalence of *IDH*-mutations in low-grade and secondary high-grade glioma, strongly suggests that these *IDH*-mutations are an initiating event in gliomagenesis [94, 110]. Interestingly, the survival of patient with an *IDH*-mutant glioma is markedly better than for IDH wild type (IDH^{wt}) (31 vs 15 months for glioblastoma and 65 vs. 20 months for grade III astrocytoma [82, 83]).

The vast majority of IDH^{mut} in glioma concerns *IDH1* and of these, 90% are IDH1-R132H, while R132C, R132G, R132L, and R132S occur at lower frequencies. Equivalent mutations affect the catalytic site of IDH2 at position R172, but these have been found in <3% of glial tumours [83, 111]. Interestingly, *IDH2* mutations are much more prevalent in for instance AML [112, 113], for which no explanation has been suggested to date.

Outline of the thesis

Expression of $IDH1^{R132H}$ is expected to result in diminished levels of α-KG and NADPH in the cytosol. Depletion of α-KG results in cellular metabolic stress, for which cells must compensate. Previous work in our lab revealed that the murine xenograft model E478, which carries an endogenous $IDH1^{R132H}$ mutation, shows a 2-fold increase in mitochondrial density compared to the IDH^{wt} xenograft models E434 (derived from a tumour that was originally called an anaplastic oligodendroglioma, but is IDH^{wt}), and E98 (glioblastoma-derived) [114]. We therefore postulated that *IDH1*-mutated glioma cells might compensate for IDH1-functional loss by increasing mitochondrial IDH2 activity by induction of mitochondrial biosynthesis. This switch to increased mitochondrial activity might lead to impaired proliferation and thus relatively good prognosis of *IDH1*-mutated gliomas. An alternative manner in which to deal with decreased cytosolic α-KG, apart from increasing IDH2 activity, may be increased import of glutamine or glutamate from the microenvironment through importers such as SLC1A5 [115, 116]. Replenishment of α-KG can then be accomplished through the enzymes glutaminase (GLS; glutamine to glutamate) and glutamate dehydrogenase (GLUD; glutamate to a-KG) [117]. Therefore, it could be argued that with upregulation of glutamine import and GLS activity, inhibition of this pathway should be a promising target for metabolic targeting. The effect of GLS inhibition on proliferation has been only modest, however [118]. This together with the notion that low-grade glioma cells express the glutamate importer EAAT2 [119], led to the hypothesis that import and direct usage of glutamate, rather than glutamine, is an efficient anaplerotic pathway for the production of α-KG [120, 121].

The aim of this thesis is to identify altered metabolic pathways in clinical *IDH*^{mut} gliomas that may explain why *IDH*-mutations in glioma result in better prognosis and survival, by using a novel targeted RNA-next generation sequencing profiling assay (t/RNA-NGS), *in vitro* and *in vivo* experiments and exploring therapeutic options that target metabolic vulnerabilities in *IDH*^{mut} glioma.

Furthermore, we evaluate the diagnostic and prognostic value of t/RNA-NGS in human glioma tissues and aim to identify cancer-associated biomarkers (often found in other cancer types) in human glioma samples that may be used for personalized therapeutic strategies using existing drugs.

Most models of *IDH*-mutant glioma make use of overexpression of the IDH1^{R132H} enzyme in an otherwise *IDH*^{wt} background. Due to the vastly different metabolic activity and epigenetic status of *IDH*^{mut} glioma cells, results obtained from these models should be interpreted with care. In **chapter 2** we review available models of glioma in the context of molecular aberrations and tumour heterogeneity, and their application for the best interpretation of results in glioma research.

In **chapter 3,** we introduce t/RNA-NGS and show that this assay can generate tumour profiles that can stratify on *IDH*-mutational status, and prognosis. This test can aid in diagnosing gliomas and can be used to identify novel biomarkers which might be actionable targets, using a carefully selected panel of oncology related genes.

A different possibility for α-KG anaplerosis is through glutamine metabolism [122]. Upregulation of glutamine uptake combined with increased GLS activity results in increased glutamate levels which in turn can then be converted to α-KG by GLUD. *IDH*^{mut} cancer cells are more sensitive to inhibition of GLS than *IDH*^{wt} cells, but the effect on proliferative capacity is limited [122]. The question is why cancer cells might choose this pathway, when glutamate is readily available in the brain as a neurotransmitter [123]. Direct uptake of glutamate is facilitated by the glutamate importer EAAT2 [124]. This transporter is normally expressed by astrocytes to remove the excess of glutamate from the interstitium of synaptic clefts of neurons, in order to prevent excitotoxicity and to facilitate the glutamate-glutamine cycle [125, 126].

To investigate the hypothesis of a-KG anaplerosis through glutamate metabolism rather than glutamine metabolism in *IDH1*^{mut} gliomas, we previously analysed gene expression levels of metabolic pathways *in silico* [127]. We found clues that *IDH1*^{mut} gliomas primarily rely on glutamate and lactate for anaplerosis of α-KG, while *IDH*^{wt} gliomas mainly rely on glycolysis and acetate anaplerosis. This is in line with an earlier proposed hypothesis in which it was suggested that *IDH*^{mut} gliomas rely on glutamate for a-KG anaplerosis, a.o based on the notion that *IDH1*^{mut} gliomas cells express the glutamate transporter EAAT2 [124, 128, 129]. In **chapter 4,** we provide clinical, *in vivo* and *in vitro* data that strongly suggests that glutamate metabolism is the preferential pathway of α-KG anaplerosis in human glioma samples

harbouring an *IDH*-mutation. *In situ* enzymatic mapping reveals that GLUD activity is significantly higher in IDH^{mut} glioma, compared to GLS activity. t/RNA-NGS profiles are suggestive of glycolysis and lactate export in IDH^{wt} glioma compared to glutamatolysis and lactate metabolism as anaplerotic pathways in IDH^{mut} glioma. This dependency on glutamate and lactate opens the way for novel approaches of glioma treatment by inhibiting these pathways.

In **chapter 5**, we explore the possibilities of targeting glutamatolysis with the green tea polyphenol epigallocatechin-3-gallate (EGCG). EGCG is an inhibitor of $NADP^+$-dependent enzymes, among which GLUD and IDH1. We show that EGCG indeed inhibits these enzymes, and preferentially inhibits proliferation of HCT116 cells that carry an allelic knock-in of $IDH1^{R132H}$. Using ^{13}C-isotope tracing experiments we show that D-2-HG is mainly glutamate derived, further strengthening our hypothesis that IDH^{mut} gliomas preferentially rely on glutamate for α-KG anaplerosis. Furthermore, we provide evidence that IDH^{mut} cells are more sensitive to radiotherapy and that this sensitivity can be further increased by inhibition of glutamatolysis by EGCG. Treatment with the $IDH1^{mut}$ specific inhibitor AGI-5198 counteracts this sensitization and thus should not be given to patients when they receive radiotherapy.

Finally, chapter **6** provides a summary of the work presented in this thesis, as well as a discussion on the evidence that various models of IDH^{mut} *in vitro* and in *in vivo* are not representative of clinical gliomas that have an endogenous $IDH1^{R132H}$ mutation. Scientific results obtained using these models should be interpreted with caution and models used should be carefully selected based upon the research question at hand.

CHAPTER 2

Glioma: experimental models and reality

Krissie Lenting, Roel Verhaak, Mark ter Laan,
Pieter Wesseling, William Leenders

Acta Neuropathologica. 2017 Feb;133(2):263-282.

Abstract

In theory, *in vitro* and *in vivo* models for human gliomas have great potential to not only enhance our understanding of glioma biology, but also to facilitate the development of novel treatment strategies for these tumours. For reliable prediction and validation of the effects of different therapeutic modalities, however, glioma models need to comply with specific and more strict demands than other models of cancer, and these demands are directly related to the combination of genetic aberrations and the specific brain micro-environment gliomas grow in. This review starts with a brief introduction on the pathological and molecular characteristics of gliomas, followed by an overview of the models that have been used in the last decades in glioma research. Next, we will discuss how these models may play a role in better understanding glioma development and especially in how they can aid in the design and optimization of novel therapies. The strengths and weaknesses of the different models will be discussed in light of genotypic, phenotypic and metabolic characteristics of human gliomas. The last part of this review provides some examples of how therapy experiments using glioma models can lead to deceptive results when such characteristics are not properly taken into account.

1. Introduction

1.1 Clinicopathology of gliomas

Glioma is a rare cancer (6 diagnoses per 100,000 people annually) of the central nervous system (CNS) originating from (precursors of) glial cells [55]. The vast majority is characterized by diffuse infiltrative growth into the surrounding CNS parenchyma [130]. Based on the astrocytic, respectively oligodendroglial phenotype of the cancer cells these diffuse gliomas are traditionally histopathologically typed as diffuse astrocytomas, oligodendrogliomas, or as mixed gliomas/oligoastrocytomas. However, the latter diagnosis is disappearing because nowadays molecular testing generally provides an unambiguous diagnosis of either astrocytic or oligodendroglial tumour (see paragraph 1.2 and [60]). Furthermore, based on the presence/absence of marked mitotic activity, necrosis and florid microvascular proliferation (MVP) a malignancy grade is assigned to diffuse gliomas (World Health Organization (WHO) grade II - IV) [58, 131].

A shared characteristic of all grades of diffuse glioma is their extensive infiltration in the CNS parenchyma along white matter tracts and pre-existing blood vessels [130]. Surgical cure for diffuse gliomas is not available because complete resection cannot be achieved. Without treatment, survival of patients with glioblastoma (not only the most malignant, but also by far the most frequent glioma) is approximately 6 to 9 months after diagnosis, and even with current standard treatment using a combination of surgery irradiation and the DNA-alkylating agent temozolomide, survival rates remain dramatically poor [66, 132]. The limited progress in implementing novel, more effective treatment protocols for diffuse glioma sharply contrasts the situation of many other cancer types.

The most frequent examples of gliomas with a circumscribed rather than diffuse infiltrative growth pattern are pilocytic astrocytoma (relatively common in children and generally benign/WHO grade I) and different variants of ependymoma (occurring in both children and adults and with variable aggressiveness corresponding to WHO grade I–III) [133-135].

1.2 Molecular pathology of gliomas

Especially during the last decade, multiple studies have shed light on the molecular events underlying gliomagenesis and on their clinical relevance as diagnostic, prognostic and/or predictive markers. Some of these markers are now incorporated in the definitions of particular glioma entities in the recently published, revised WHO classification [60, 136]. Heterozygous mutations in the gene encoding the metabolic enzyme *isocitrate dehydrogenase (IDH)* are seen in 70-80% of grade II and III diffuse gliomas and in 12% of glioblastomas [82, 83]. These mutations (mostly involving cytosolic *IDH1*, lesser so mitochondrial *IDH2*) have important consequences for the epigenome and cause extensive DNA methylation in IDH-mutant diffuse gliomas ('glioma-CpG island methylator phenotype'/G-CIMP) [98, 99]. In ‘canonical’ oligodendrogliomas, according to the recently published WHO classification of CNS tumours, an *IDH1* or *IDH2* mutation co-occurs with

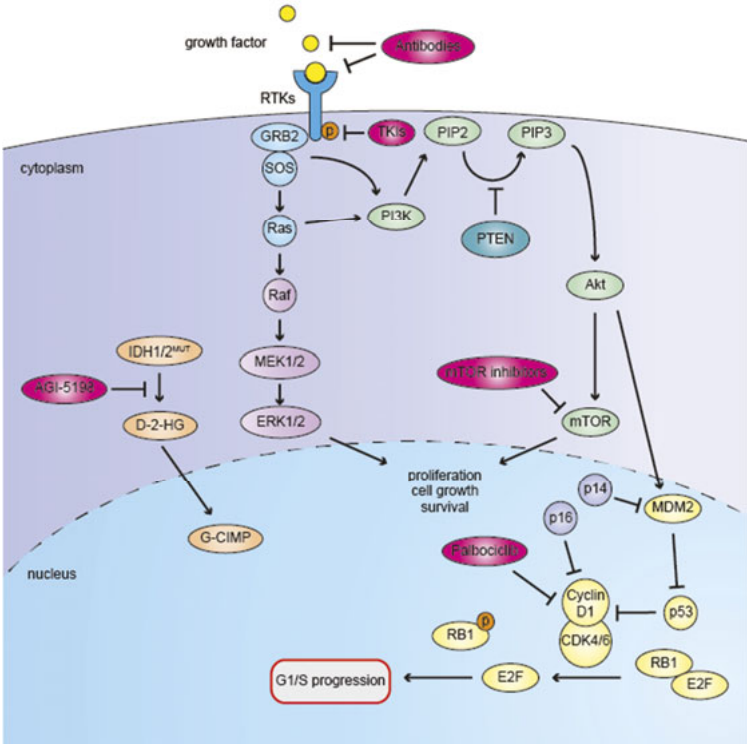

Figure 1: Overview of oncogenic pathways in glioma and possibilities for pharmacological interventions, relevant for the models described in this article. *Growth factors bind to RTKs resulting in phosphorylation and Ras/Raf and PI3K signalling to Akt and mTOR, thus driving cell growth and survival. In a substantial percentage of glioblastomas this process is amplified by loss of the counteracting phosphatase PTEN. Akt also can phosphorylate MDM2 thereby stabilizing the protein. This stabilization causes ubiquitinylation and degradation of the tumour suppressor P53, unleashing cyclin D1 complex activity and leading to uncontrolled G1-S progression. Loss of control over the cell cycle is also induced by CDKN2A mutations as CDKN2A products, $p14^{ARF}$ an $p16^{INK4A}$ are important G1-S checkpoint proteins.*

The PI3K pathway (activated by phosphorylated growth factor receptor tyrosine kinases [RTKs] such as EGFR, MET or PDGR) may be inhibited by small molecule RTK inhibitors or antibodies directed against ligand binding domains of RTKs or the ligands themselves, thus prevent ligand-receptor interaction. The cyclin D1 pathway (resulting in cell cycle progression from G1 to S phase) may be inhibited by the CDK4/6 inhibitor palbociclib. Finally, mutations in IDH1 or IDH2 result in mutant proteins that catalyse the conversion of α-KG to D-2-HG, causing the G-CIMP phenotype and a transcriptional profile leading to gliomagenesis. AGI-5198 specifically inhibits $IDH1^{R132H}$ activity by binding to the catalytic site of the protein.

complete and combined deletion of chromosome arms 1p and 19q [72, 137-140]. This complete 1p/19q codeletion not only constitutes the genetic hallmark of oligodendrogliomas, but also an important favourable prognostic and predictive marker. Diffuse astrocytic tumours

can be IDH mutant or wild-type. While most IDH mutant astrocytic tumours are at clinical presentation WHO grade II or III, they often progress to a grade IV lesion ('secondary glioblastoma'). It was recently shown that IDH1-mutated glioblastomas may experience loss of heterozygosity, resulting in absence of wild-type IDH1 expression [141]. It is not known yet whether and how heterozygosity or homozygosity for *IDH* mutations influences biological behaviour. The vast majority of diffuse gliomas presenting as glioblastoma at first diagnosis are IDH wild-type ('primary glioblastomas') [60, 136, 139, 142].

A number of dysregulated pathways are frequently operational in diffuse gliomas that may be amenable for pharmacologic intervention (see Figure 1).

Besides frequent mutations in the promoter of *TERT* (telomerase reverse transcriptase, involved in maintaining telomere length) [137], like in other cancer types three main pathways are frequently (alone or in combination) affected in diffuse gliomas/glioblastomas [73]: I) the *phosphoinositide 3-kinase (PI3K)/ AKT pathway* is often hyperactive as a result of activating mutations in or amplifications of genes encoding the upstream receptor tyrosine kinases (RTKs) and/or loss of PTEN, a negative regulator of the AKT pathway; II) *cell cycle control pathways*, e.g. caused by inactivating mutations in *CDKN2A*, the gene encoding the MDM2 inhibitor $p14^{ARF}$ and the cyclin D1-inhibitor $p16^{INK4A}$, or activating mutations in cyclin-dependent kinase (*CDK4*) resulting in uncontrolled progression from the G1 to the S-phase of the cell cycle [72, 143]; III) *inactivating mutations in TP53*, prohibiting apoptosis of cells with damaged DNA, and resulting in uncontrolled progression of the cell cycle, contributing to the gradual accumulation of mutations and increased intratumoral heterogeneity [144].

Of the most frequent non-diffuse gliomas, pilocytic astrocytomas are almost always affected by single abnormalities of the mitogen-activating protein kinase (MAPK) pathway (most frequently by KIAA1549-BRAF fusion, in other cases by a BRAF V600E or other mutation affecting this pathway), indicating that this neoplasm may be a ‘one pathway’ disease [133]. Ependymal tumours form a very heterogeneous group with regard to not only location, histology and clinical behaviour, but also molecular characteristics. Based on detailed molecular analyses combined with clinicopathological information, nine larger subgroups of ependymoma have been identified, some of these carrying a more grim prognosis while others behaving relatively indolent [145, 146].

1.3 Intratumoral heterogeneity

Intratumoral heterogeneity was firmly established by genetic analysis of multiple biopsies of the same tumour, and even on the level of single cells by single-cell RNA-seq analysis [147-150]. Gliomas may contain subpopulations of cells carrying mutually exclusive amplifications of oncogenes *EGFR* and *PDGFRα* [151]. In line with these observations, recurrent gliomas may be genetically markedly distinct from the tumours from which they originate [152].

A number of the frequently encountered molecular aberrations in diffuse gliomas are targetable with available drugs, examples being inhibitors of RTKs (antibodies and small

molecules against among others EGFR, MET, PDGFR [153]), inhibitors of CDK4/6 activity (palbociclib [154]) and inhibitors of mutant IDH enzymes [155] (see Figure 1). Despite the wealth of information on actionable molecular aberrations and the availability of corresponding targeted drugs, apart from bevacizumab (see paragraph 3.2) there has not been any change in approved drug-based treatment strategy for these cancers since the introduction of temozolomide. An important reason for this frustrating notion is the high diversity in genetic aberrations in glioma, combined with substantial intratumoral heterogeneity and the relatively low incidence of diffuse glioma, precluding testing of novel targeted therapies in groups of patients of sufficient size. Furthermore, validated predictive biomarkers for novel targeted drugs are often lacking. It is thus of great importance to have available appropriate preclinical glioma models.

2 Preclinical glioma models

Ideally, a preclinical glioma model meets the following requirements; I) Genetic background resembles that of (a subset of) human gliomas; II) Genetic, epigenetic and phenotypic intratumoral heterogeneity is similar to human glioma; III) Model involves an adequate microenvironment with regard to immunocompetence, presence of blood-brain barrier (BBB) and cell-cell interactions (both between tumour cells and with non-neoplastic cells) [156]; IV) Model is reproducible and stable over time.

In the following paragraphs we discuss currently employed preclinical glioma models, including their relevance with respect to molecular make-up, intratumoral heterogeneity, tumour microenvironment, stability and their usefulness for testing of novel therapies. Models that will be discussed can be categorized as carcinogen-induced gliomas in animals, *in vitro* glioma cell cultures derived from human or animal gliomas, glioma xenograft models (subcutaneous, orthotopic), and transgenic mouse models (Figure 2). Furthermore, some more 'exotic' glioma models (e.g. in zebrafish or fruit flies) will be briefly discussed.

2.1 Murine models of glioma

2.1.1 Ethyl-nitrosourea (ENU)-induced gliomas

A widely used model of diffuse glioma that was introduced in the 1970s is based on carcinogen-induced gliomagenesis (Figure 2a). In this model, pregnant animals (mostly rat) are injected intravenously with a single dose of N-ethyl-nitrosourea (ENU) [157]. The *in utero* exposure of embryos to this DNA-damaging compound induces predominantly brain tumours, possibly because DNA-repair mechanisms are less active in the brain than in other tissues, resulting in higher rates of stable mutations in neural cells. Interestingly, injection of ENU in adult animals does not result in brain tumours [158], suggesting that neural precursor cells in the developing brain pass through ENU-induced mutations to their progeny, that will cause problems in the event they affect oncogenes or tumour suppressor genes.

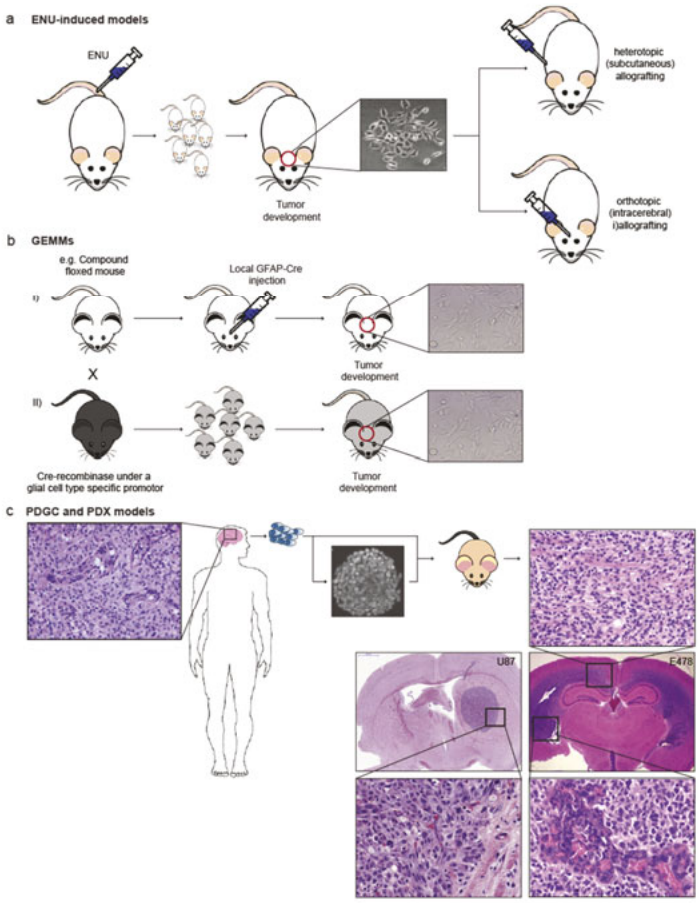

Figure 2: Schematic overview of in vitro and in vivo glioma models. *a) Intravenous injection of ENU into pregnant rat leads to offspring with a high chance of spontaneous glioma development. Resulting gliomas often carry mutations in oncogenes or tumour suppressor genes that are frequently encountered in human gliomas. ENU-induced gliomas have been processed to murine glioma cell lines that can be implanted as allografts in syngeneic animals. b) GEMMs. Shown are examples of compound flox-ed mouse, in which the floxed modifications can be activated by local transduction of cells with lentiviruses encoding Cre recombinase under control of ubiquitous or cell-type specific promoters, or by crossing with transgenic mice expressing Cre under control of neural- or glial-cell type-specific promoters (e.g. nestin or GFAP promoter). In these cases, modifications occur early during embryonal development, unless promoter activity is made inducible. These glioma models are molecularly highly defined and can be processed to novel murine cell lines that are amenable for allografting. c) PDGCs or PDX can be generated by preparing cell cultures of surgically obtained glioma material (nowadays mostly spheroid cultures) that can be implanted heterotopically (generally subcutaneously in the flank) or orthotopically (in the brain) of immunocompromised animals; alternatively, surgically obtained human glioma tissue can be directly implanted; ideally, an orthotopic xenograft of a diffuse high grade glioma/glioblastoma in the murine brain recapitulates not only the genotype, but also the phenotype of this tumour with e.g. florid microvascular proliferation (lower right image) and diffuse infiltrative growth in the white matter (upper right image). Of note, as illustrated by a xenograft derived from U87 cells, not all orthotopic glioma models show diffuse infiltration in brain parenchyma, and such models are less relevant for the study of glioma in the context of tumour-brain microenvironment interactions.*

This model thus may well represent gliomagenesis in humans and allows for the identification of key driver mutations and their roles in glioma development in a spatial and temporal fashion, especially since the tumours in this model have a relatively long latency time (i.e. they become symptomatic only months after birth) [159]. Like in a subset of human gliomas, *TP53* mutations have been identified as key cancer drivers in ENU-induced gliomas, resulting in genetic instability and accumulation of other mutations in oncogenes or tumour suppressor genes [160]. Additionally, other mutations that are frequently encountered in human gliomas, such as amplification of platelet derived growth factor receptor alpha (*PDGFRα*), deletion of the cell cycle regulator gene *CDKN2A,* and amplification of the EGFR gene can be present in these animal tumours [161], the combination of *TP53* and *PDGFRα* mutations being relatively frequent in paediatric high grade glioma [162-164]. A recent study demonstrated that a Braf codon 545 mutation (V545E, corresponding to the human BRAF V600E mutation) is a frequent early event in the development of ENU-induced rat gliomas [165]. This mutation can occur in human diffuse gliomas but is more frequently seen in 'non-diffuse' gliomas.

The ENU-induced model of gliomagenesis gives rise to genetically heterogeneous tumours and also involves a proper brain microenvironment, including an intact immune system and a blood brain barrier (BBB) [166], making it to a relevant model. One of the downsides of the model is the poorly reproducible character of glioma formation. Consequently, experiments with this model require costly and time-consuming studies with high numbers of animals. Yet, whereas in the early days' *in vivo* visualization of ENU-induced gliomas was impossible, current imaging techniques allow for therapy studies during which animals are longitudinally monitored. Obviously, testing of targeted drugs in this model requires that these are equipotent against the human and murine targets.

2.1.2 Transgenic mouse models

The knowledge of the driver mutations that are involved in gliomagenesis has resulted in innovative genetically engineered mouse models (GEMMs) of glioma (for systematic review of GEMMs, see [167]). An elegant approach made use of transgenic animals with GFAP-promoter-driven expression of tv-a, resulting in astrocyte specific expression of this retrovirus receptor. This makes these cells susceptible to infection with avian leukosis virus-derived RCAS vectors that carry expression cassettes for e.g. auto-active EGFR variants [168]. Infection with such viruses will result in astrocytic EGFR hyperactivity. To allow for astrocytic infection, RCAS-vector producing chicken fibroblasts need to be intracerebrally injected, resulting in infection of cells neighbouring the needle track.

Another example in this category is the model created by transcranially injecting lentiviruses expressing Cre-recombinase under control of the glial cell-specific GFAP promoter or the ubiquitously active CMV promoter, in LoxP-transgenic mice, conditionally lacking *p53* or *pten*, and $p16^{INK4a}$, and overexpressing the constitutively active $KRAS^{V12}$ mutant (Figure 2b). In this model high-grade gliomas develop within weeks after Cre-administration that resemble human glioma with respect to phenotype and BBB [169]. In a recent publication Bardella *et al.*

described a transgenic conditional mouse model in which mice carrying a floxed *Idh1* minigene, followed by an *Idh1*^{R132H} allele were crossed with mice carrying a tamoxifen-inducible P^{nestin}-Cre transgene [170]. Upon administering tamoxifen to the offspring mice, Cre is selectively expressed in nestin-positive neural progenitor cells in the subventricular zone (see also paragraph 2.2.2), resulting in deletion of the minigene and activation of the *Idh1*^{R132H} allele in this alleged stem cell population. The resulting cells were more proliferative and displayed invasive behaviour, suggestive of an early gliomagenesis phenotype. Such models may well be further developed into lower grade diffuse glioma models.

GEMMs are very suitable to investigate behaviour of genetically defined gliomas in an immune competent setting and allow for studies on drug distribution to glioma cells in the brain, taking potential BBB restrictions into consideration [171, 172]. These models however lack the intratumor heterogeneity that is observed in human gliomas. Furthermore, in these models targeted drugs that are tested ideally must have similar activity against human and murine targets in order to predict therapeutic outcome in patients.

2.1.3 Murine glioma cell lines and allograft models

The unpredictable character of glioma formation in ENU-induced models has stimulated researchers to create stable *in vitro* cell line cultures from ENU-induced rat gliomas, among which C6, 9L, T9, RG2, F98 and BT4C and RT-2 (molecular characteristics reviewed in detail in [173]), but also from transgenic mice [174]. The GL261 mouse cell line was generated by intracranial injection of the alkylating agent 3-methylcholantrene into C57BL/6 mice [175, 176]. These murine glioma cell lines have the advantage that they can be implanted orthotopically in syngeneic, immunocompetent animals [173] allowing for the study of tumour immunological aspects. An exception is the C6 glioma model that was generated from an ENU-induced glioma in an outbred strain of Wistar rats. As a consequence, inoculation of C6 cells in common Wistar rat strains results in an allogenic immune response and lack of tumour growth [177]. However, the cell lines that do grow in their syngenic hosts after intracerebral transplantation, develop to invasive cancers that have been used to investigate effects of targeted therapy and radiotherapy [178].

Novel immunotherapy concepts have been introduced in cancer treatment, such as dendritic cell vaccination and immune checkpoint inhibition (reviewed in [179]). Gliomas are considered by some to be good candidates for dendritic cell (DC) vaccination [180], but the efficacy of this and of other immunotherapeutic approaches is currently hampered by the immune suppressive milieu in (patients with) glioma [181, 182]. Glioma allografts in immunocompetent animals are highly valuable models to optimize immune-modulatory therapies and improve immunotherapeutic protocols [183]. Yet, as indicated above, one has to bear in mind that the intratumoral heterogeneity of human gliomas is probably not fully recapitulated in animal models. Another drawback of these murine glioma models in the context of immunotherapy is that humanized antibodies for clinical use are immunogenic in such models, precluding repeated administration. This problem can partly be circumvented

by using immune deficient animals (rats or mice), obviously not an adequate solution for studies in the field of immune therapy. Alternatively, immune-humanized mice may be used in which the mouse Ig-locus is exchanged for the human Ig-locus [184-186]. Clearly, in such models the targeting antibody should be reactive against the glioma target of interest. Genetic engineering of rat glioma cell lines aiming for expression of the human antigen of interest may be helpful in this respect. An example of this latter approach is the evaluation of therapeutic efficacy of anti-EGFRvIII antibodies using allografts of F98 rat glioma cells overexpressing human EGFRvIII [187]. So far, spontaneous *IDH1* mutations have not been reported in murine glioma cell lines, making these models less relevant for the study of IDH mutant human gliomas. Attempts to generate stable cell cultures from transgenic mice, expressing $IDH1^{R132H}$ in nestin-positive neural progenitor cells have so far also failed [170].

2.2. Models of human glioma

2.2.1 Human glioma cell lines: conventional cell cultures

In an attempt to work with glioma models that resemble as closely as possible the genetic make-up of their human counterparts, many research groups exploit patient-derived glioma cell lines. The two most widely studied cell lines, U87 and U251, were generated in the sixties of the last century from patients with a glioblastoma [188, 189]. In the past 4 decades experiments with these lines have been reported in over 2000 and 1000 publications, respectively. The U87 genome has recently been fully sequenced [190], and this effort revealed an enormous number of indels, copy number variations and translocations, most of which were probably acquired during decades of cell culture. Indeed, only recently the consequences of cell culture with fetal bovine serum for genetic instability have been recognized [191-194]. Still, genetic aberrations from the original tumours that are retained in these cell lines allow for the detailed study of their contribution to oncogenic cell signalling pathways in a controlled and reproducible fashion. Furthermore, such cell lines also allow for rapid and reproducible testing of targeted drugs *in vitro*, as a prescreen for further testing in appropriate preclinical *in vivo* models.

Of note, U87 cells have found their way to many labs in the world, and it may be expected that, due to genetic drift under serum culture conditions, there is a large number of subclones of U87 available that may affect experimental reproducibility. The need for regular cell line authentication is now widely recognized and cell line authentication is already required by a number of scientific journals [195].

2.2.2 Human glioma cell lines: neurosphere cultures

The genetic drift that is caused by culturing cells under serum conditions has resulted in a search for alternatives. In 1992, Weis and Reynolds reported that neural stem cells (NSC) can be stably maintained and propagated as neurospheres when cultured in growth-factor defined media in the absence of serum [196]. A subset of surgically obtained gliomas can be processed to genetically stable cell lines by growing tumour spheroids in a similar specialized

medium containing basic fibroblast growth factor (bFGF), epidermal growth factor (EGF) and neuronal viability supplement B27 [197-199]. Success rates of generating neurosphere cultures from gliomas is however largely dependent on tumour grade and *IDH* status. Especially generation of cell cultures from *IDH*-mutated lower grade (WHO grade II and III) gliomas is difficult, with only few examples reported in the literature [155, 200, 201]. Furthermore, considering the heterogeneous composition of human gliomas, it is quite likely that each patient-derived glioma spheroid line represents only a subset of the most aggressive cells from the original tumour.

This directly leads to the questions how the initiating glioma cells diverge into the heterogeneous population of progeny cells and what exactly are the initiating cells. This issue is still not resolved. Current ideas are that many gliomas originate from neural progenitor cells in e.g. the subventricular zone that during normal development differentiate into neuronal and glial cells. Based on the concepts of stem cells in healthy tissues, these glioma stem-like cells (GSLCs), also called glioma-initiating cells (GICs), are believed to divide asymmetrically, yielding a novel stem-like cell that is resistant to chemotherapy and radiotherapy and is responsible for tumour progression, and a non-stem-like daughter cell [202]. This hypothesis would qualify GSLCs as the cells that are most essential, but also most difficult to eradicate in glioma therapies.

Interestingly, glioma spheroid cultures contain characteristics of GSLCs, and may express stem cell markers such as CD133, Nestin, Sox2 and SSEA-1 [203]. However, expression of these markers varies widely, making it difficult to unequivocally define the initiating cells in gliomas. Furthermore, lack of expression of GSLC markers does not necessarily imply lack of the ability to generate tumours [204]. Even though *in vitro* and *in vivo* glioma models are promising tools for further elucidation of the molecular and functional characteristics of GSLCs/GICs (including identification of the best markers for recognizing these cells) [205], so far this has not led to broad consensus on what exactly GSLCs/GICs are and what their impact is in the pathobiology of gliomas.

When bFGF and EGF in the cell culture medium are replaced with serum, cells rapidly lose intercellular connections within the neurospheres and undergo marked phenotypical changes: cells start to adhere to plastic, flatten, acquire a more fibroblast appearance, and loose GSLC markers [206, 207]. When testing the effects of different culture conditions using the E98-model (derived from a human glioblastoma [208]) in our lab, upon intracerebral implantation only E98 cells cultured as neurospheres retained the capacity to diffusely infiltrate into the brain parenchyma, whereas E98 cells grown under serum conditions had lost this capacity (Figure 3). Similar observations were made by others [207]. The exact mechanism underlying this phenomenon is unclear, but may have to do with a GSLC population with invasive potential that is enriched in tumour spheroids [209, 210].

Nowadays, glioma cultures can be relatively easily modified with CRISPR/Cas9 technology, allowing for the elucidation of the role of individual oncogenes and tumour suppressor genes.

Furthermore, it is now common practice to generate luciferase-expressing glioma cells, enabling longitudinal non-invasive follow up of tumour development in the mouse brain [211, 212].

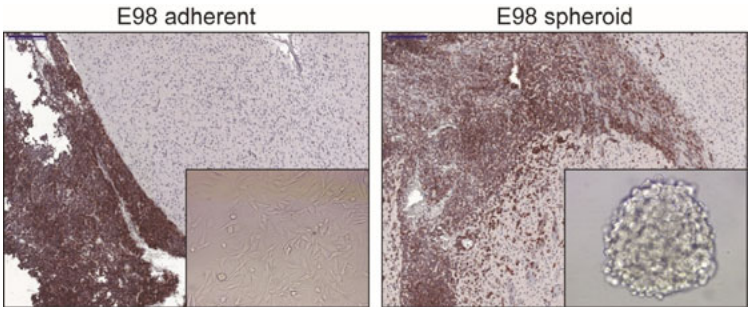

Figure 3: Cell culture conditions impact the phenotype of orthotopic E98 glioma xenografts. *E98 glioma cells grown as adherent cells in serum-supplemented culture medium lose the capacity to grow diffusely in the brain (left panel). Glioma cells are visualized via immunohistochemical staining for c-MET. Note the sharp demarcation between tumour (growing in the leptomeninges here) and brain parenchyma in the left panel, whereas E98 tumour cells diffusely infiltrate in the brain parenchyma after passaging as neurospheres (right panel). Of note, photographs are representative examples from experiments in which E98 cells, grown as adherent cultures or spheroid cultures, were injected in groups of 5 mice using exactly the same injection procedure. Bars indicate 200 µm.*

2.2.3 Heterotopic versus orthotopic grafts of glioma cell lines

Subcutaneous xenografting of human glioma cells in immunocompromised mice is a frequently used approach to obtain preclinical proof of concept for the efficacy of targeted drugs [213]. Glioma xenografts grown in the subcutaneous space have the advantage that tumour development can be followed visually and quantified in terms of tumour dimensions, allowing rapid testing of treatment efficacy. Such experiments may yield valuable results, especially if the drugs directly act on tumour cells (e.g. inhibitors of hyperactive oncogenes). Caution is however in place when drug activity is based on disturbing the interaction with the tumour microenvironment, such as in case of anti-angiogenic drugs or particular metabolic inhibitors. Subcutaneous glioma models lack the appropriate CNS microenvironment that has an essential role in glioma biology. Studies with such subcutaneous models may result in overinterpretation of effects of angiogenesis inhibitors [214] (see paragraph 3.2).

2.2.4 Orthotopic patient-derived xenografts

The desire to circumvent culture-related problems as described above combined with the increased understanding that glioma biology and therapy are heavily influenced by interactions between cancer cells and their microenvironment have increased the interest in the use of orthotopic glioma xenografts. Freshly obtained surgical human glioma samples can be directly injected into the brains of immune-deficient mice using stereotactic devices or by a freehand procedure and maintained by serial transplantation [200, 201, 208]. Using such an

approach we have created the *IDH1*^{R132H}-E478 xenograft model that is genetically highly similar to the anaplastic oligodendroglioma from which it was derived [215]. RNAseq analyses of such models allows the discrimination of human and mouse transcripts, preventing contaminating contributions of host non-neoplastic cell transcripts (which is an unavoidable flaw of studies on clinical cancer specimens).

A drawback of such glioma models is that xenografting is performed in immune-deficient animals and there will be a selection for the fastest growing cell clones resulting in reduced intratumor heterogeneity. Furthermore, orthotopic implantation of cell lines is not a guarantee for a clinically relevant phenotype: whereas orthotopic U251 xenografts have a striking phenotypic resemblance to human GBM [216], including diffuse infiltration in the brain parenchyma and palisading necrosis, U87 cells generally develop to bulky, sharply demarcated lesions that lack such infiltrative growth [130, 217] (see also Figure 2).

In light of the highly promising results that are obtained with immune checkpoint inhibitors for other cancer types, reconstituting a human immune system in xenografted mice will be of high importance to test these therapies for glioma in a preclinical setting [184, 186]. Whether patient-derived xenograft (PDX) models can be optimized by using humanized mice to allow for testing of clinically available immune checkpoint inhibitors, remains to be seen.

2.3 Other glioma models

The vast majority of glioma models reported in the literature concerns models for diffuse gliomas, but preclinical models for non-diffuse gliomas such as pilocytic astrocytomas and ependymomas have been reported as well (*in vitro*, heterotopic or orthotopic murine models, GEMMs) [218-221]. Obviously, like for diffuse gliomas, in an ideal situation the preclinical models for such gliomas are reproducible and closely resemble their human counterparts with regard to genetic background, intratumoral heterogeneity and tumour microenvironment.

As generation of mouse and rat models of glioma can be a slow process, *in vivo* detection of orthotopic gliomas requires sophisticated equipment, and drug screenings in these models are time-consuming and costly endeavours, some more 'exotic' glioma models have been developed. A potentially interesting example is the zebrafish (*Danio rerio*) model for the study of gliomas [222, 223]. Zebrafish embryos are increasingly used for cancer studies since the discovery that pathways of tumorigenesis are similar in humans and zebrafish [224]. In a typical experiment hundreds of day 3 post-fertilization zebrafish embryos are injected with tumour cells, stained with a fluorescent membrane dye. Using the pigmentation-mutated casper strain of zebrafish that remain transparent during life, cancer cells can be readily visualized using UV microscopy. Intracerebral implantation of human glioma cells in zebrafish was shown to result in xenografts with phenotypes that were similar to xenografts in mouse, grown from the same cells [225]. The zebrafish system allows semi-high-throughput drug screening, e.g. by adding compounds in the water [222]. A potentially serious drawback of the zebrafish system is that glioma cells need to adapt to function at 32^{o}C, with possible

consequences for metabolism and activity of oncogenic pathways. Furthermore, one needs to take into account that in zebrafish the BBB starts to develop from day 3 post fertilization and is fully developed only at day 15 post fertilization, and that the immune system has not matured in the early stages of development as well [226, 227]. Furthermore, it is not yet clear whether the zebrafish accommodates growth of all sorts of glioma cells, including the difficult-to-grow *IDH* mutant gliomas.

Another model of interest is the fruit fly (*Drosophila melanogaster*), a highly versatile genetic model system in which specific gene functions can be manipulated in a single-cell fashion in an *in vivo* setting [228]. This provides the opportunity to investigate the effect of genetic aberrations in an intact nervous system. Many molecular pathways, such as the RTK signalling pathways, are highly conserved between invertebrates and humans [229]. It has been reported that these models may recapitulate key characteristics of glioblastoma with regard to increased proliferation and migration [230].

The downsides of available experimental animal models of glioma has raised interest in using dogs with naturally occurring gliomas for testing of novel drugs and optimizing novel treatment concepts [231]. Although canine gliomas probably represent a good intermediate between murine models and humans, being more relevant in terms of intratumoral heterogeneity and immune system, low incidence and lack of canine-specific molecular testing facilities, hamper larger studies.

A recent development has been that human fibroblasts after p53 knock down are converted to inducible pluripotent stem cells (iPSCs) that can subsequently be differentiated to neural progenitor cells to yield TP53-mutated NPCs. These cells can be transformed to glioma initiating cells by lentiviral transduction of oncogenes [232].

Table I summarizes available models and indicates their strengths and weaknesses.

3 Glioma models and predictive medicine; a reality check

The exact glioma model used is an important determinant for the outcome of preclinical therapeutic studies. After briefly underscoring the importance of the molecular underpinnings and of the microenvironment of the model, anti-angiogenic therapy and tumour-cell metabolism will be discussed in more detail as examples where exploitation of inappropriate models may easily lead to deceptive information.

Table 1: Summary of available models of glioma

Model type	(Epi)genetic make up	Heterogeneity	Immunecompetent	Brain micro-environment	Blood brain barrier	Stable/ Reproducible
ENU-induced murine tumours	Partly relevant (among others p53, braf, pdgfrα). No IDH mutations identified	Genetically heterogeneous, different neural cells may be initiator cells	Yes	Relevant	Yes	No
GEMMs (conditional expression of oncogenes/loss of tumour suppressor genes)	Partly relevant, only few known driver mutations used (among others loss of p53/pten,CDKN2A, $kras^{V12}$) [38] Existing models expressing IDH1-R132H in neural stem cells have epigenetic alterations but are not tumour models [7]	Genetically homogeneous , initiator cell type dependent on promoter driving Cre expression (CMV/nestin/GFAP)	Yes	Relevant when cre expression is induced in the CNS (intracerebral injection of cre-lentivirus, crossing mice with developmental CNS-expression of Cre	Yes	Yes
PDX – subcutaneous	Partly relevant	Genetically homogeneous, but intratumoral heterogeneity due to lack of pre-existent vasculature, development of hypoxia and angiogenesis dependence	No	Non-relevant	No	Yes
PDX- orthotopic	Relevant	Partly, it is not known to which extent PDX models represent most aggressive parts of the originating tumour	No	Partly, only relevant in case PDXs have retained capacity to grow via diffuse infiltration	Yes	Yes
Cell lines – adherent	Less relevant	No	No	Non-relevant	No	Yes
Cell lines – spheroids	Possibly relevant	No	No	Non-relevant	No	Yes

Zebrafish	Non-relevant	No	No	Probably non-relevant	No	Yes
Canine	Possibly Relevant	Yes	Yes	Relevant	Yes	No
Fruit fly	Not relevant	No	No	Relevant	No	No

3.1 The importance of molecular underpinnings and microenvironment

Lots of (combinations of) mutations that are common in human glioma, are retained in human glioma cell lines. *In vitro* studies using appropriate cell lines are therefore well suited to investigate interactions between aberrant pathways and establish optimal concentrations of inhibitors, e.g. to achieve potential synthetic lethality [233]. A large proportion of gliomas have a dysfunctional *CDKN2A*, the gene encoding the cyclin D1 inhibitor $p16^{INK4A}$. These cells have a defective G1-S checkpoint that can however be corrected pharmacologically by palbociclib. This CDK4/6 inhibitor has recently been approved by the FDA and the European Medicine Agency (EMA) for treatment of women with advanced breast cancer [234]. Treatment of patient-derived $p16^{INK4a-/-}$glioma cell lines, grown as adherent cells or as spheroids, with palbociclib results in an effective block of cell cycle progression already at µmolar concentrations as shown by incorporation of nucleotide analogues bromo-deoxyuridine (BrdU) and 5-ethynyl-2'-deoxyuridine (EdU) (figure 4, unpublished work). These results confirm literature data that a large percentage of patient-derived glioma explants respond to palbociclib [235]. However, its clinical usability is strongly restricted because palbociclib is a substrate for P-glycoprotein (a family of ATP-dependent transporter proteins in the BBB that pump out the recognized substrate), reducing drug distribution behind the BBB [236]. Once the BBB limitations are overcome (see below) palbociclib may indeed be used to improve prognosis for a large proportion of glioma patients.

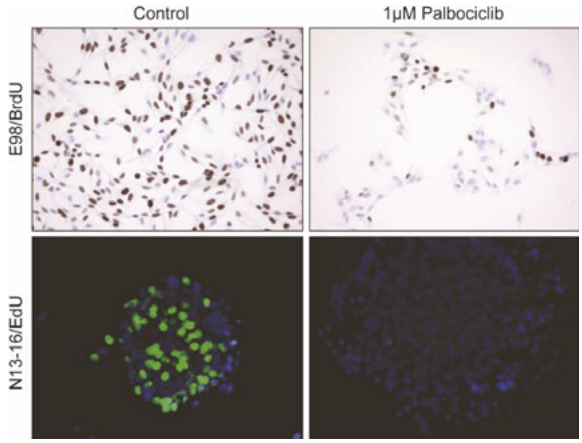

Figure 4: Example of promising in vitro effect of CDKN2A-mutation targeting that is difficult to translate into clinical efficacy. *Two different patient derived glioblastoma models (E98 adherent cells, N13-16 spheroid cultures, both characterized by dysfunctional CDKN2A), were incubated with placebo (left panels) or with the CDK4/6 inhibitor palbociclib (right panels). Visualization of DNA synthesis (S-phase of the cell cycle) with BrdU or EdU (as indicated) shows that palbociclib effectively prevents entry into the S-phase. Although such in vitro results are very promising, also because 80% of human glioblastomas have dysfunctional CDKN2A leading to a defective G1-arrest, in vivo diffuse gliomas may well be protected from palbociclib because this drug is substrate for p-glycoproteins of the BBB [236].*

Hyperactivity of the phosphoinositol-3-phosphate (PI3K) pathway in glioblastoma is common, due to (a combination of) amplified or otherwise mutationally activated oncogenic RTKs, and/or loss of the phosphatase *PTEN* [237, 238]. Aberrant expression of epidermal growth factor receptor (EGFR) and/or the ligand-independent EGFR mutant EGFRvIII (a product of a genetic deletion resulting in loss of exons 2-7 in the mRNA) is a frequent phenomenon in glioblastoma [239, 240], driving growth and migration of tumour cells [241].

Alterations in other RTKs that are frequently encountered in glioblastoma are mutations in *PDGFRα* and *MET* [242]. Also these mutations are retained in cell lines. We previously showed that targeted inhibition of MET by cabozantinib is highly effective in E98 cells *in vitro*, blocking MET phosphorylation and cell proliferation with IC_{50} in the nmolar range.

Testing the same drugs in orthotopic xenografts generated from the same cell line resulted in increased survival of mice, yet did not prevent development of treatment resistant cancers [243]. Such differences in effects of the same drug on the same cell line *in vitro* and *in vivo* illustrates the important role of the tumor microenvironment.

The BBB is designed to protect neural tissue from toxic substances in the blood. In large areas of diffuse infiltrative glioma this barrier also shields cancer cells from drugs. The BBB is composed of a relatively impermeable layer of endothelial cells that communicate with astrocytes via contacts with astrocytic end feet [244, 245]. Except for creating a physical barrier, endothelial cells of the BBB express a large diversity of P-glycoprotein family members, making the BBB impermeable to the vast majority of drugs [172, 246-249]. Therefore it is of high importance that drugs that have been positively tested on cell lines are subsequently tested in appropriate preclinical models that have retained diffuse growth, and in which cancer cells may 'hide' behind the BBB. For drugs that cannot pass the BBB, there is the need to find solutions for local and controlled BBB disruption, or to discover novel targeted drugs that are not substrate for the P-glycoprotein family of drug transporters [172, 248, 249]. Numerous research efforts to get drugs over the BBB are ongoing, including active transport of peptide- or antibody-coated nanoparticles [250-252]. Mechanical temporary and spatially restricted disruption of the BBB with high intensity focused ultrasound (HIFU) [253-255] or via stereotactic radiotherapy [256] is an alternative approach that may carry promise for the future but needs more preclinical validation.

One of the recent breakthroughs in oncology has been the implementation of immune checkpoint inhibitors, comprising antibodies against programmed death-1 (PD-1, nivolumab) or cytotoxic T-lymphocyte antigen-4 (CTLA-4, ipilimumab) on cytotoxic T-lymphocytes. These antibodies prevent the immune-suppressive interactions between cancer cells and cytotoxic T-cells, boosting anti-tumor immunity [152] and have now been FDA- and EMA-approved or are in clinical trial for a large number of tumor types. With currently available glioma models, preclinical testing of such highly promising approaches is an enormous challenge. PDXs are unfit for this purpose, given the immunocompromised status of the recipient mice, and humanized mice are probably required for preclinical testing of these concepts. Syngeneic

models would require that murine antibodies against the murine equivalents of PD-1 and CTLA-4 are generated, assuming that these immune checkpoint systems work alike in humans and rats or mice. Possibly, ENU-induced gliomas would recapitulate human gliomas best with respect to genetic heterogeneity and immunocompetence, but as discussed above this model lacks reproducibility.

3.2 Angiogenesis inhibition in preclinical glioma models

Whereas most targeted therapies in oncology focus on aberrations in tumour cells, anti-angiogenic treatment using bevacizumab, one of the very few FDA-approved new therapies for glioblastoma in the USA, is targeting the interactions between tumour cells and the tumour microenvironment. Based on the VEGF-induced florid MVP that is characteristic for glioblastoma, this cancer type has historically been looked at as angiogenesis-dependent, hence amenable for targeting with VEGF-pathway inhibitors. Obviously, *in vitro* glioma cell cultures are not suitable to investigate this concept. Lots of studies have concentrated on patient-derived glioma cell lines that were grown as subcutaneous xenografts in immune-deficient mice [257, 258]. These studies generally yielded highly promising results, with tumour stabilization or even regression, whether with anti-VEGF antibodies or with small compound VEGF RTK inhibitors. Combined data from such studies and radiological responses in phase II clinical studies for recurrent glioblastoma resulted in accelerated FDA-approval for bevacizumab as first line treatment for recurrent glioblastoma in 2009 [259]. Unfortunately, large phase III trials testing bevacizumab for newly diagnosed glioblastoma showed no positive effect on overall survival, often despite an initial radiological response [260, 261].

It is now broadly accepted that the FDA approval of anti-VEGF-A treatment for recurrent glioblastoma in 2009 was at least partly based on cases showing a radiological pseudoresponse (resulting from 'normalization' of activated tumour blood vessels) rather than from a tumoricidal response [262-265]. Of note, this phenomenon was demonstrated before in different animal models. For example, VEGF-expressing melanoma metastases in the murine brain that were readily visible in contrast-enhanced MRI became invisible upon treatment with the VEGFR2 inhibitor vandetanib, even while they progressed by growing in the space of Virchow-Robin via vessel co-option [266]. Similarly, several studies using orthotopic models of diffuse glioma had shown that these tumours can grow in CNS tissue independent of angiogenesis, especially cells that overexpress EGFR or MET [241, 242]. Accordingly, anti-angiogenic treatment does not prevent growth of these cancers [267] but it can increase hypoxia and glycolysis in angiogenic parts of glioma [268]. In this situation treatment with angiogenesis inhibitors diminishes contrast-enhancement in MRI scans without preventing diffuse infiltration in the brain parenchyma [243, 267], copying the phenomena seen in the clinic. Meanwhile, reduction of hyperpermeability of brain tumour microvessels by anti-VEGF-A treatment may have a rapid positive effect on edematous brain swelling, thereby temporarily improving the quality of life [264, 269].

It is important to consider the cellular principles underlying the different responses of subcutaneous and intracerebral tumours to anti-angiogenic treatment. Tumour growth in the originally avascular, subcutaneous space requires that tumour cells can initiate transcriptional programs that rescue them from starvation [270]. Normally this rescue is accomplished by switching on hypoxia-induced transcriptional programs in cells that are located beyond ~100-200 µm from the most nearby blood vessel (the maximum range of oxygen diffusion), including expression of the chemotactic factor VEGF-A, leading to blood vessel growth towards the tumour [271]. The situation in brain, one of the most vascularized organs in the body, is entirely different. Here, diffuse infiltrative glioma cells can incorporate the abundantly present, pre-existent brain microvessels (among others via vessel co-option) [272, 273] (Figure 5). Of note, orthotopic implantation of glioma cells may not necessarily lead to an adequate phenotype for diffuse glioma. For instance, orthotopic implantation of U87 cells generally results in bulky, well-demarcated tumours with a disrupted BBB, lacking diffuse infiltrative growth along white matter tracts [274]. Anti-angiogenic studies using subcutaneous or 'bulky' orthotopic glioma models thus carry the risk of overinterpretation of the therapeutic results, even more so if these studies use drugs that do not pass the BBB.

3.3 Metabolic considerations

Another important reason to study glioma in the orthotopic setting relates to tumour cell metabolism [8]. In the brain, ubiquitous amounts of glutamine and the neurotransmitter glutamate are present as part of the glutamine-glutamate cycle (Figure 6). Together with glucose, glutamine and/or glutamate may be important carbon and nitrogen donors for glioma cells

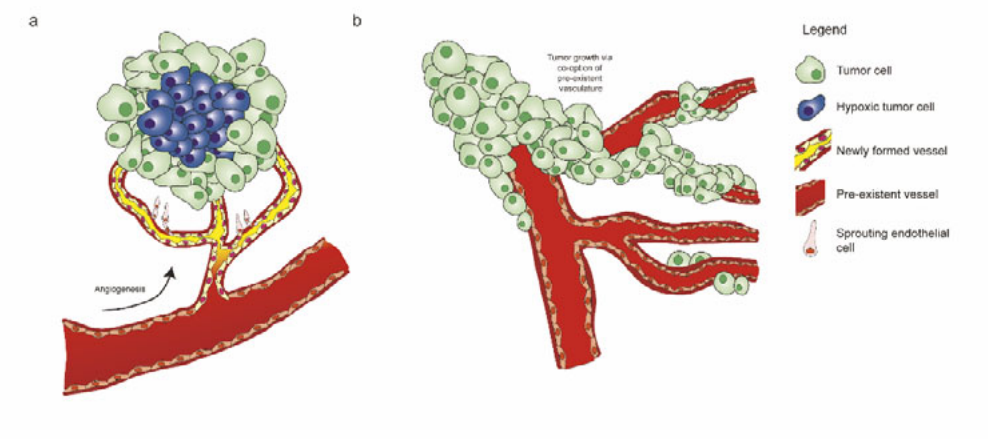

Figure 5: ***Schematic overview of tumour growth via angiogenesis versus vessel co-option.*** *a) Schematic representation of the dogma of angiogenesis-dependent growth of a tumour. When a tumour outgrows the capacity of the vasculature, hypoxic stress (indicated by blue cells) initiates sprouting angiogenesis as a rescue pathway (here presented as yellow vessels. b) Especially in tissue with rich pre-existent vasculature (such as brain tissue), tumours may grow through vessel co-option in an angiogenesis-independent fashion.*

[275], especially those with *IDH* mutations. The biology of *IDH* mutations has been extensively studied and is covered in excellent reviews e.g. [276, 277]. Whereas wild-type IDHs produce α-KG and NADPH from isocitrate and $NADP^+$, IDH mutants (mostly hotspot mutations $IDH1^{R132X}$ or $IDH2^{R140X}$/$IDH2^{R172X}$) consume α-KG and NADPH while producing the oncometabolite 2-hydroxyglutarate (D-2-HG) [83]. This has two important implications. Firstly, since α-KG and NADPH take important roles in fundamental processes such as fatty acid synthesis and maintenance of redox potential, expression of mutated IDH results in metabolic stress [128, 129]. Secondly, D-2-HG is an inhibitor of a large group of α-KG-dependent enzymes that are involved in epigenetic regulation and induces G-CIMP (see also paragraph 1.2) [278].

We previously suggested that one of the reasons for the unique phenotype of diffuse growth of *IDH*-mutated gliomas relates to the metabolic stress, translating into addiction to glutamate as an alternative carbon source, making this neurotransmitter to a potential chemotactic factor [129] (Figure 6). Because not all culture media routinely contain this non-essential amino acid, glutamate dependence would be incompatible with standard *in vitro* growth conditions and could partly explain the difficulty with producing stable glioma cell cultures carrying endogenous IDH mutations [279]. Only in the last years a number of IDH-mutated glioma models have become available, mostly as patient derived orthoptic xenografts [155, 200, 201, 215].

The high incidence of *IDH*-driver mutations in gliomas, combined with the lack of appropriate *in vitro* cell cultures has resulted in numerous studies in which effects of IDH-mutants are tested in cell models utilizing overexpression of mutated IDH. Whereas such models have proven valuable to investigate epigenetic phenomena and metabolic fluxes, they may also result in misinterpretation, depending on the specific cell system and desired read-out. For example, IDH^{wt} glioma cells routinely express the enzyme branched-chain amino acid transferase-1 (BCAT1) that converts α-KG to glutamate [280]. Together with the antiporter System Xc-, BCAT1 is responsible for maintaining redox potential. Glutamate is secreted from the cell via this transporter in exchange for cystine that entails reductive power [125]. In gliomas carrying the endogenous IDH mutation, *BCAT1* is silenced via promoter hypermethylation [101, 280]. Consequently, glutaminolysis in these cancers is a one-way reaction from glutamine/ glutamate to α-KG. Introduction of a mutated IDH gene in a cell with wild-type IDH background will thus result in a competition between BCAT-1 and mutated IDH1 for α-KG, a situation that does not reflect the endogenous situation. Whether full penetrance of D-2-HG-induced epigenetic effects in engineered cell lines can be achieved to the extent that the metabolic phenotype of clinical *IDH*-mutated glioma is fully mimicked, is an open question. Experience so far is that IDH^{mut} introduction in cells results in a gradual loss of the mutated protein, suggestive of a selection against mutant-expression, resulting in selective overgrowth of cells with no or low expression levels of the mutated protein [197, 279]. Introduction of mutant IDH disrupts metabolic balances that may result in model-specific artefacts.

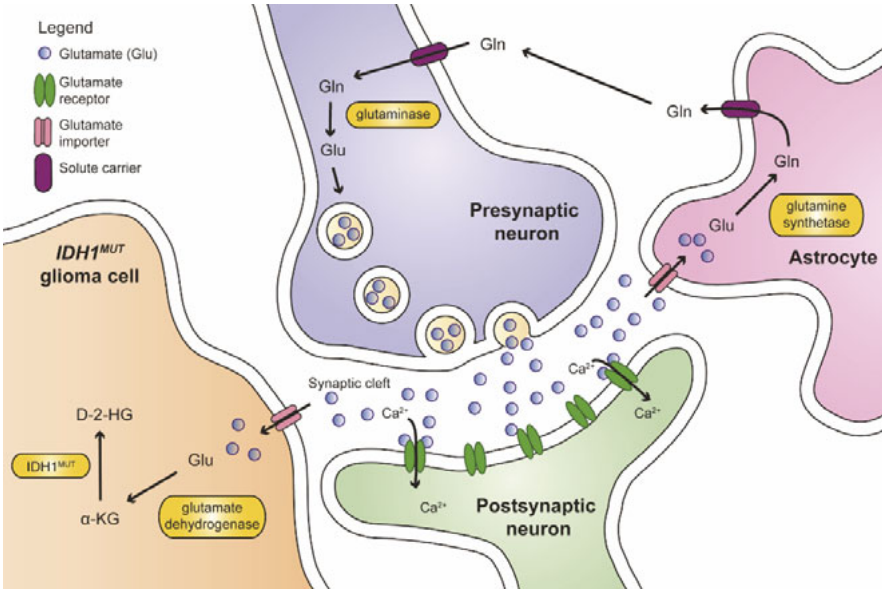

Figure 6: ***Schematic representation of the glutamine-glutamate cycle in the brain.*** *In the brain, glutamate (Glu) is released by presynaptic neurons to the synaptic cleft. Glutamate activates glutaminergic receptors that undergo a conformational change to allow influx of extracellular calcium. This triggers membrane depolarization in the postsynaptic neuron and induces signal transduction. The excess of glutamate in the synaptic cleft has to be removed to prevent excitotoxicity. Astrocytes take up surplus glutamate through various glutamate importers and convert it to glutamine (Gln) through glutamine synthetase. Glutamine is exported to the capillaries (not shown) or is transferred back to the neurons. Subsequently, neurons can then convert back the glutamine to glutamate, closing the glutamine-glutamate cycle. Glutamate can be imported by IDH^{mut} glioma cells in order to supply cells with αKG as a rescue pathway.*

4. Summarizing remarks

Glioma models that have been developed so far have greatly enhanced our understanding of glioma formation and metabolism and have contributed to the development and implementation of novel treatment strategies. As a recent example, partly based on in vitro studies and in vivo observations in mice and rabbits, in 2015 the FDA approved Tumour Treating Fields (TTF) as a therapeutic modality for patients with newly-diagnosed glioblastoma (http://www.fda.gov/NewsEvents/Newsroom/PressAnnouncements/ ucm465744.htm) [281].

Optimal exploitation of glioma models remains challenging though. Clearly, diffuse glioma remains a difficult tumour to treat, not in the least because of its diffuse infiltrative growth and the substantial inter- and intratumoral heterogeneity [282]. Up until now, creating adequate models for IDH mutant gliomas proves to be very difficult. Also, intratumoral heterogeneity of diffuse gliomas cannot be recapitulated to the fullest in *in vitro* or *in vivo*

models. For several therapies the BBB (which is relatively intact in large parts of diffuse glioma) is a true barrier, and modelling this barrier is a difficult task in itself. Yet another challenge lies in the development of appropriate models that can be used to test immunotherapy; *in vitro* studies using cell lines and xenograft models in immunodeficient animals are inherently unfit for this purpose. So far, a preclinical model that perfectly recapitulates (one or another subtype of) human glioma does not exist. Still, the models that are available may be very useful, but it is of paramount importance to carefully select the most appropriate glioma model for a particular research question, meanwhile realizing not only the strengths but also the weaknesses of the model used.

Financial support

KL is funded by KWF grant UvA2014-6839. This work was in part supported by a grant from Stichting StopHersentumoren and by Radboudumc. RGWV is supported by grants from the National Brain Tumour Society and NIH/NCI R01 CA190121.

CHAPTER 3

Mapping actionable pathways and mutations in brain tumours using targeted RNA next-generation sequencing

Krissie Lenting*, Corina N.A.M. van den Heuvel*, Anne van Ewijk, Elizabeth Tindall, Ge Wei, Benno Kusters, Maarten te Dorsthorst, Mark ter Laan, Martijn A. Huynen, William P. Leenders

* Authors contributed equally

Acta Neuropathologica Communications 2019 Nov 20;7(1):185.

Abstract

Many biology-based precision drugs are available that neutralize aberrant molecular pathways in cancer. Molecular heterogeneity and the lack of reliable companion diagnostic biomarkers for many drugs makes targeted treatment of cancer inaccurate for many individuals. Identifying actionable hyperactive biological pathways in individual cancers may improve this situation.

To achieve this, we applied a novel targeted RNA next-generation sequencing (t/RNA-NGS) technique to surgically obtained glioma tissues. The test combines mutation detection with analysis of biological pathway activities that are involved in tumour behaviour in many cancer types (e.g. tyrosine kinase signalling, angiogenesis signalling, immune response, metabolism), via quantitative measurement of transcript levels and splice variants of hundreds of genes. We here present proof of concept that the technique, which uses molecular inversion probes, generates a histology-independent molecular diagnosis and identifies classifiers that are strongly associated with conventional histopathology diagnoses and even with patient prognosis. The test not only confirmed known glioma-associated molecular aberrations but also identified aberrant expression levels of actionable genes and mutations that have so far been considered not to be associated with glioma, opening up the possibility of drug repurposing for individual patients. Its cost-effectiveness makes t/RNA-NGS to an attractive instrument to aid oncologists in therapy decision making.

Introduction

Many different cancer types share similar driver mutations. Examples are loss of function mutations in tumour suppressor genes (e.g. *p53* and *CDKN2A)* and DNA repair proteins, leading to genetic instability and loss of cell cycle control) [283-285], and activating mutations, amplifications or fusion events in proto-oncogenes [286, 287]. Other shared features are related to micro-environmental effectors, such as altered metabolism as a result of hypoxia [288, 289], induction of angiogenesis [290] and immune suppression [291].

Additionally, aberrations exist that are tumour-type specific. Examples are expression of hormone receptors in cancers of prostate, ovary and breast [292, 293]; mutations affecting metabolism (isocitrate dehydrogenase mutations [p.IDH1-R132H] in glioma and acute myeloid leukaemia [54]); and mutations affecting the PI3K and MAPK pathway (PIK3CA, p.KRAS-G12/G13 mutations in adenocarcinomas [294], p.BRAF-V600E in melanoma [295]). Such specificity is however never absolute. As an example, *IDH* and *BRAF* mutations are sporadically found in other cancers too [296-298]. Detection of such relatively rare, and therefore *a priori* unexpected mutations in individual patients could lead to repurposing of precision medicines in basket trials, in which precision drugs are administered to patients based on DNA profiling [299-302].

A number of actionable biological pathways in cancer involve the products of genes that are not mutated, but epigenetically regulated, for example by altered transcription factor availability, repressor activity or gene methylation, [303, 304]. Activity of such pathways cannot be directly inferred from DNA analyses. Whole genome methylation analysis has robust diagnostic power [305] but does not allow analysis of activity of biological pathways, involved in cancer development and progression. An example is angiogenesis, initiated by hypoxia-inducible factor (HIF-1α)- induced expression of an abundance of growth factors and followed by extensive crosstalk between tumour cells, tip- and stalk endothelial cells and pericytes [306, 307]. DNA analysis also does not provide information on post-transcriptional events. For example, expression of alternative splice variants of vascular endothelial growth factor (VEGFA) has implications for the regulation of angiogenesis [308] and splice variants of receptor tyrosine kinases can lead to auto-active and oncogenic PI3K signalling (e.g. EGFRvIII and $MET^{\Delta 7\text{-}8}$ in glioma and $MET^{\Delta 14}$ in lung cancer [242, 309-311]).

A comprehensive overview of gene expression levels and alternative splice variants can be obtained with whole RNA next-generation sequencing (w/RNA-NGS), provided sufficient coverage to detect alternative exon-exon boundaries. w/RNA-NGS is increasingly performed in a research setting but is cost-wise still not suitable for implementation in routine patient care. There is therefore a huge need for novel and cost-effective methods to obtain clinically actionable and reliable information for individual patients, to be able to implement personalized treatment approaches.

Due to its low incidence (6 per 100,000) and high molecular heterogeneity [147], glioma is a difficult tumour type to organize clinical trials with, although the molecular underpinnings of gliomagenesis and glioma progression are relatively well established [54]. In the absence of alternatives, treatment of its most malignant form, glioblastoma, is still confined to palliative surgery, followed by chemotherapy with temozolomide (TMZ) and radiotherapy [66] which extents median life expectancy with only few months. Surgical cure for this tumour type is not possible due to its diffuse infiltrative nature [130]. Glioma is therefore one of the most challenging tumours for which new treatment strategies are urgently needed.
We here analysed test and validation cohorts of in total 103 surgically derived brain tumours with quantitative targeted RNA next-generation sequencing (t/RNA-NGS) [312-315]. The technique uses single molecule molecular inversion probes (smMIPs) and sensitively and quantitatively measures expression levels of and mutations in actionable genes. We show that t/RNA-NGS provides a histology-independent molecular diagnosis and identifies classifier transcripts that are closely associated with histopathological diagnosis and prognosis. By measuring hyperactivity of cancer-related pathways the test may also stratify individual patients for treatment with appropriate medicine.

Materials and Methods

Patients
The study described here was performed with brain tumour tissue from newly diagnosed patients who were operated for a glioma between 2013 and 2018 (N=103). The cohort was separated in an experimental cohort (N=75, tumours that were operated between 2013 and 2017) and an independent validation set of 28 tumours (operated in 2017 and 2018). Researchers were blinded to histopathology and clinical outcome. The study protocol was approved by the Ethical Committee for Human Experimentation of the Radboudumc. All patients signed informed consent. Directly after surgery, tissue samples were snap frozen in liquid nitrogen and stored at -80^{o}C until further processing. In retrospect, patient characteristics were extracted from Radboudumc electronic patient files (EPIC) and documented in the electronic data capture system CASTOR. Histopathology and molecular diagnoses were extracted from the Dutch Pathology archive PALGA and summarized in Table 1.

RNA preparation and cDNA synthesis
Cryosections of 10 µm were cut for RNA isolation using TRIzol (ThermoFisher Scientific, Waltham, MA). For every sample a 4 µm serial section was stained with H&E to estimate percentage tumour area by an experienced neuropathologist (BK). RNA was reverse transcribed into cDNA using random hexamer primers and Superscript II (Invitrogen, CA) according to standard protocols. In parallel, tissue was processed to formalin-fixed paraffin-embedded (FFPE) tissue blocks for routine diagnosis. Samples from 2014 onwards were also subjected to genetic analysis using targeted DNA next-generation sequencing [300].

t/RNA-NGS with smMIPs

All enzymes were from NEB (Ipswich, MA) unless stated otherwise. The procedure of smMIP-based targeted RNA next-generation sequencing (t/RNA-NGS) to detect expression of metabolic genes has been described before [312, 314-316]. SmMIPs were designed by an adjusted version of the MIPgen algorithm [317] and were ordered from Integrated DNA Technologies (Leuven, Belgium). The set of smMIP probes used in [312] was expanded with probes for detection of regions of interest (ROI) in novel transcripts of interest that play a role in a wide variety of cancer types. Furthermore, smMIP probes were included for specific detection of splice variants by placing extension and ligation probes on neighbouring exons, e.g. probes on exons 1/8 of Epidermal Growth Factor Receptor (*EGFR*) for detection of *EGFR*vIII [314]. Probes for detection of Vascular Endothelial Growth Factor (*VEGF*) isoforms 121, 165 and 189 were designed with extension and ligation probes in exons 5/8, 5/7 and 5/6, respectively. Additional smMIPs were included that were directed against shared exons of transcript variants. For transcripts in which relevant mutations can be expected, smMIPs were selected with extension and ligation probes flanking the respective ROI. At least 5 smMIPs were used for each transcript of interest, evenly distributed along the transcript. cDNA was subjected to smMIP capture as described in [312, 313]. In short, a mixture of 936 phosphorylated smMIPs was hybridized to 15-50 ng of cDNA. After overnight hybridization and enzymatic gap-filling (KlenTaq polymerase, Epicentre, Madison, WI) and ligation (Ampligase, Epicentre) circular smMIPs are formed, the number of which is linearly related to the number of RNA molecules present in the original sample. After treatment with exonuclease to remove cDNA and linear smMIPs, the libraries of circular smMIPs were subjected to PCR with a unique barcoded primer set per sample. The PCR products of the expected length of 266 bp were purified with Ampure beads (Beckmann Coulter Genomics, High Wycombe, UK) and quantified on a TapeStation 2200 (Agilent Technologies, Santa Clara, CA). PCR libraries were sequenced on the Illumina Nextseq platform (Illumina, San Diego, CA) at the Radboudumc sequencing facility (output 2x151 bases). The barcode in the PCR primers allows for pooling of multiple samples into one sequencing library, followed by demultiplexing of reads, generating for all individual samples a FASTQ file.

Data processing

For each patient sample, all reads in the FASTQ file were mapped against reference transcripts (UCSC human genome assembly hg19) using the SeqNext module of JSI SequencePilot version 4.2.2 build 502 (JSI Medical Systems, Ettenheim, Germany). In all smMIP molecules a unique random 8N sequence is included (unique molecular identifier or UMI), allowing to assign all identical sequencing reads to one originating circularized (unique) smMIP. This excludes PCR amplification bias and makes the assay quantitative. Number of unique reads for each individual smMIP in a sample were normalized to the total of unique reads in that sample and expressed as fragment per million (FPM). Mean FPM values from all smMIPs covering different ROIs in the same transcript were considered to represent gene expression levels in the tumour

sample. Using the base calling algorithm of SeqNext a list of single nucleotide variations and insertions and deletions was generated for each sample. An in–house developed Python script (version 3.7) allowed direct coupling of gene expression values and mutation status of individual cancer samples.

Data analysis and statistics

Unsupervised hierarchical cluster analysis with the gene expression data was performed using R programming (version 3.4.3). Mean FPM values were log-transformed (after addition of 0.01 to prevent log0 transformation). Manhattan distance between gene expression profiles were calculated using the group average method for agglomerative clustering (Unweighted Pair Group Method with Arithmetic Mean) [318]. Other packages were heatmap.Plus (http://www.sciviews.org/SciViews-R.) and plyr (http://www.jstatsoft.org/v40/i01/). The Wilcoxon Mann-Whitney U test was used to find differentially expressed genes between clusters. Associations of mutations with clusters were calculated using Fisher's exact test. Multiple testing corrections were done using Benjamini Hochberg (FDR<0.05). Kaplan-Meier survival curves of 75 brain cancer patients in the test cohort were generated using Graphpad Prism, version 5.03. Patients who were still alive at the date of analysis or were lost to follow-up, were censored in the survival data. P-values were calculated using the Log-Rank test. All p-values are indicated as *($p<0.05$), ** ($p<0.01$), *** ($p<0.001$), **** ($p<0.0001$), unless specified otherwise. Survival analysis of the 28 patients in the validation cohort could not be performed due to short follow-up time.

Immunohistochemistry

Immunohistochemistry (IHC) was performed on 4 µm sections of FFPE tissue or on frozen sections, adjacent to those used for t/RNA-NGS. Frozen sections were air dried and fixed with 4% paraformaldehyde (PFA) solution for 20 min at room temperature before staining. After appropriate epitope retrieval (for FFPE sections), antibodies rabbit-anti-Prostate-Specific Membrane Antigen (PSMA; Abcam; ab133579), rabbit-anti-Carbonic Anhydrase 12 (CAXII; Sigma Life Sciences; HPA008773), mouse-anti-androgen receptor (AR; Santa Cruz; sc-7305), rabbit-anti-MET (Cell Signaling Technologies; #8198), and rabbit-anti-EGFR (Cell Signaling Technologies; #4267) were used. Sections were incubated with primary antibody in normal antibody diluent (Immunologic, Duiven, The Netherlands) overnight at 4^{o}C. Primary antibody detection was done using BrightVision polyHRP-anti-rabbit IgG (Immunologic, Duiven, The Netherlands), or BrightVision polyHRP-anti-mouse/rabbit/rat IgG (Immunologic) for AR staining. Sections were counterstained with haematoxylin and mounted with Quick-D mounting medium (Klinipath, Duiven, The Netherlands). As control staining, secondary antibody-only stainings were performed.

Whole transcriptome RNA-NGS (w/RNA-NGS)

Total RNA was isolated using the Qiagen AllPrep DNA/RNA Mini Kit following the manufacturer's protocol for animal tissues (Qiagen, Hilden, Germany). RNA sequencing

libraries were prepared from 16 gliomas using the KAPA RNA HyperPrep Kit with RiboErase (HMR; KAPA Biosystems, Wilmington, MA) following the manufacturer's protocol. Briefly, 100ng of total RNA was used to generate libraries, which were fragmented for 8 minutes at 94°C. Adapter stock concentration used was 750 nM and libraries were amplified for 11 cycles. Duplex "Y" adapter sequences with molecular barcodes were generated by IDT (Integrated DNA Technologies, Skokie, Illinois). Final libraries were quantified on a High Sensitivity Bioanalyzer chip (Agilent, Santa Clara, CA) and sequenced at 1.4pM with 10% PhiX on the Illumina NextSeq 550 Sequencer (Illumina, San Diego, CA). Raw FASTQ files were mapped to the human genome (hg19) with STAR (v2.5.3) aligner [319]. Mapped reads were filtered and deduplicated using sambamba v0.6.6 and feature quantification was performed using featureCounts v1.5.0-p1 against the RefSeq database (downloaded from the UCSC genome browser on 01/05/2017). Gene and exon-level fragments per kilobase per million mapped reads (FPKMs) were calculated using a custom python script.

Table 1. Summary of characteristics of human glioma samples. Histological type, WHO grade, and percentage tumour cells were confirmed by a trained neuropathologist (B.K.). IDH-mutational status was derived from the t/RNA-NGS data. All IDH1^{R132H}/IDH2 mutations were validated by routine diagnostic genetic analysis with the 'Radboud Cancer Hotspot Gene panel'.

Experimental Cohort						
Sample	**Sex**	**Age (at surgery)**	**Histological type**	**Grade**	**Mutation status**	**% tumour cells**
13-01	F	28	Ependymoma	2	IDH-WT	*
13-02	M	40	Astrocytoma	3	IDH1-R132H	70
13-03	M	58	Oligodendroglioma	3	IDH1-R132H	70
13-04	V	62	Glioblastoma	4	IDH-WT	60
13-05	M	56	Metastasis	**	IDH-WT	*
13-06	M	53	Oligodendroglioma	3	IDH2-R172K	60
13-07	F	20	Variant glioma	2	IDH-WT	*
13-08	M	67	Glioblastoma	4	IDH-WT	70
13-09	V	58	Glioblastoma	4	IDH-WT	70
13-10	M	45	Oligodendroglioma	3	IDH1-R132H	65
13-11	V	67	Glioblastoma	4	IDH-WT	70
13-13	M	52	Glioblastoma	4	IDH1-V178I	70
13-14	F	64	Glioblastoma	4	IDH-WT	70
13-15	V	44	Oligodendroglioma	3	IDH1-R132H	50
13-16	M	60	Glioblastoma	4	IDH-WT	70
13-17	M	45	Oligodendroglioma	2	IDH1-R132H	50
13-18	V	49	Oligodendroglioma	3	IDH1-R132H	50
14-01	V	52	Glioblastoma	4	IDH-WT	80
14-02	M	43	Oligodendroglioma	2	IDH1-R132H	50
14-03	V	62	Glioblastoma	4	IDH-WT	70
14-04	M	72	Glioblastoma	4	IDH-WT	60
14-05	M	21	Astrocytoma	2	IDH1-R132H	70

14-06	M	43	Oligodendroglioma	3	IDH1-R132H	50
14-07	M	65	Oligodendroglioma	3	IDH1-R132H	50
14-08	M	50	Astrocytoma	3	IDH1-R132H	50
14-09	V	43	Astrocytoma	3	IDH1-R132H	60
14-10	V	45	Glioblastoma	4	IDH1-R132H	50
14-11	M	50	Glioblastoma	4	IDH-WT	60
14-12	M	59	Oligodendroglioma	3	IDH1-R132H	50
14-13	M	39	Pleomorphous xanthoastrocytoma	3	IDH-WT, BRAF-V600E	70
15-01	M	66	Glioblastoma	4	IDH-WT	50
15-02	V	61	Glioblastoma	4	IDH-WT	70
15-03	V	76	Glioblastoma	4	IDH-WT	40
15-04	V	59	Glioblastoma	4	IDH-WT	40
15-05	M	31	Astrocytoma	3	IDH1-R132H	70
15-06	V	49	Astrocytoma	3	IDH1-R132H/V178I	70
15-07	M	63	Glioblastoma	4	IDH1-V178I	65
15-08	M	55	Astrocytoma	2	IDH1-R132H	60
15-09	M	70	Glioblastoma	4	IDH-WT	70
15-10	V	68	Oligodendroglioma	3	IDH1-R132H	70
15-11	M	33	LPD	**	IDH-WT	*
15-12	M	46	Glioblastoma	4	IDH-WT	70
15-13	V	78	Glioblastoma	4	IDH-WT	80
15-14	M	79	Glioblastoma	4	IDH-WT	70
15-15	V	58	Glioblastoma	4	IDH-WT	70
15-16	M	25	Astrocytoma	2	IDH1-R132H/V178I	50
15-17	M	68	Glioblastoma	4	IDH-WT	60
15-18	V	64	Glioblastoma	4	IDH-WT	70
16-01	M	61	Glioblastoma	4	IDH-WT	70
16-02	M	47	Glioblastoma	4	IDH-WT	70
16-03	V	46	Astrocytoma	3	IDH1-R132H	25
16-04	M	59	Oligodendroglioma	3	IDH1-R132H	60
16-05	M	51	Glioblastoma	4	IDH-WT	50
16-06	V	*	Astrocytoma	*	IDH1-R132H	50
16-07	M	74	Glioblastoma	4	IDH1-Y183C	60
16-08	F	68	Glioblastoma	4	IDH-WT	50
16-09	V	49	Glioblastoma	4	IDH-WT	70
16-10	M	*	Astrocytoma	*	IDH1-R132H	60
16-11	M	67	Glioblastoma	4	IDH-WT	50
16-12	M	23	Astrocytoma	3	IDH1-R132H	60
16-13	M	60	Glioblastoma	4	IDH-WT	70
16-14	V	60	Oligodendroglioma	3	IDH2-R172M	70
16-15	V	61	Oligodendroglioma	3	IDH1-R132H	70
16-16	M	58	Glioblastoma	4	IDH1-V178I	40
16-17	V	18	Oligodendroglioma	2	IDH2-R172K	40
16-18	*	30	Oligodendroglioma	3	IDH2-R172W	70
16-19	M	48	Glioblastoma	4	IDH-WT	70

17-01	M	58	Oligodendroglioma	2	IDH1-R132H	50
17-02	M	40	Astrocytoma	3	IDH1-R132H/V178I	70
17-03	V	76	Glioblastoma	4	IDH-WT	65
17-04	M	42	Oligodendroglioma	3	IDH1-R132H	70
17-05	M	59	Glioblastoma	4	IDH-WT	70
17-06	M	65	Glioblastoma	4	IDH-WT	70
17-07	M	63	Glioblastoma	4	IDH-WT	70
17-08	F	26	DNET	1	IDH-WT	*
Validation Cohort						
17-09	F	67	Glioblastoma	4	IDH-WT	*
17-10	F	67	Astrocytoma	2	IDH1-R132H	*
17-11	M	67	*	4	IDH-WT	*
17-12	*	*	*	*	IDH1-V178I	*
17-13	F	59	Glioblastoma	4	IDH-WT	75
17-14	M	46	Oligodendroglioma	2	IDH1-R132H	*
17-16	M	56	Astrocytoma	3	IDH1-R132H	*
18-01	F	48	oligodendroglioma	2	IDH1-R132H	60
18-02A	F	39	Astrocytoma	2	IDH-WT	*
18-02B	F	44	Astrocytoma	2	IDH-WT	*
18-04	M	65	Glioblastoma	4	IDH-WT	65
18-05	M	19	Astrocytoma	3	IDH-WT	45
18-06	M	48	Glioblastoma	4	IDH-WT	70
18-07	M	76	Glioblastoma	4	IDH-WT	*
18-08	M	69	*	*	IDH-WT	45
18-09	M	39	Astrocytoma	3	IDH1-R132H	80
18-10	M	53	Glioblastoma	4	IDH-WT	80
18-12	M	51	oligodendroglioma	2	IDH1-R132H	few
18-13	M	42	Pleomorphous xanthoastrocyoma	3	BRAF-V600E	*
18-14	M	53	Other		IDH-WT	40
18-15	M	67	Glioblastoma	4	IDH-WT	65
18-16	M	76	Glioblastoma	4	n.d.	70
18-17	F	45	Oligodendroglioma	2	IDH1-R132H	70
18-18	F	72	Glioblastoma	4	n.d.	75
18-19	M	55	Glioblastoma	4	n.d.	80
18-20	F	54	Glioblastoma	4	IDH1-V178I	80
18-21	M	53	Other	4	IDH-WT	75
18-23	*	*	*	*	*	80

Abbreviations. DNET, Dysembryoplastic neuroepithelial tumour; F, Female; IDH, Isocitrate Dehydrogenase; LPD, Lymphoproliferative disorder; M, male; IDH-WT, IDH wild-type; WHO, World Health Organization. * Data not available; ** Non-glioma, no WHO-grade

Results

t/RNA-NGS profiles have prognostic value

To investigate the prognostic value of t/RNA-NGS, we profiled an experimental cohort of 75 brain tumours, including 69 grade II-IV diffuse gliomas and 6 brain lesions that upon routine histopathology were diagnosed as an ependymoma (N=1), one dysembryoplastic neuroepithelial tumour (DNET), one pleomorphic xanthoastrocytoma, a variant glioma, a brain metastasis of lung adenocarcinoma and a lymphoproliferative disorder (LPD; Table 1). Annotated unique smMIP counts for each tumour sample ranged from 275,000 to 1,111,000 (not shown). Hierarchical unsupervised agglomerative clustering of the gene expression data of the grade II-IV gliomas (excluding the 6 rare cancers) resulted in 3 main clusters A, B and C, comprising of 26, 38 and 5 tumours, respectively (Figure 1).

In a next step we performed a Wilcoxon Mann-Whitney U test to find genes that were differentially expressed between clusters A and B; A and C; and B and C. A total of 83 genes were differentially expressed between clusters A and B with $p<0.05$ and False Discovery Rate (FDR) <0.05 (Table S2A). Among these were transcripts encoding transporters and enzymes involved in metabolism, as described before [316]. Membrane receptor tyrosine kinases (RTKs) *NTRK2*, *ERBB3*, *ERBB4* were higher expressed in cluster B with average fold changes (FC) of 3.5, 4.8 and 5.2 respectively, while cluster A was characterized by significantly higher expression levels of *EGFR*vIII (FC=250) and *VEGFA* isoforms *VEGFA-121*, *VEGFA-165* and *VEGFA-189* (all with FC>11, Table S1A). Between cluster B and C 69 genes were differentially expressed (Table S1B). Cluster A and C significantly differed with respect to expression levels of 9 genes (Table S1C). The functional significance of these differences was not subject of further investigation in this study.

We then coupled the profiles to survival data. As shown in Figure 2A, cluster B gene expression profiles of gliomas were associated with good prognosis (median survival, defined as time between surgery and death, >6 years; exact value could not be calculated for available follow-up time) whereas gene expression profiles in cluster A and C were associated with median survival of 467 and 135 days, respectively. Results were highly significant between clusters A and B ($p<0.0001$), A and C ($p=0.0078$), and C and B ($p<0.0001$). A Kaplan-Meier curve with survival data including also the non-glioma patients is presented in Supplementary Figure S1.

Mutation analysis

We next investigated whether we could identify nucleotide variations that significantly associate with the subgroups. To this end we included all identified sequence variants of potential clinical significance with a coverage of >10% of the unique reads. This analysis revealed that the well-known hotspot mutation in the metabolic enzyme isocitrate dehydrogenase 1 (p.IDH1-R132H) [54] was significantly associated with cluster B ($p<3x10^{-5}$ when compared to cluster A, see Supplementary Table S2).

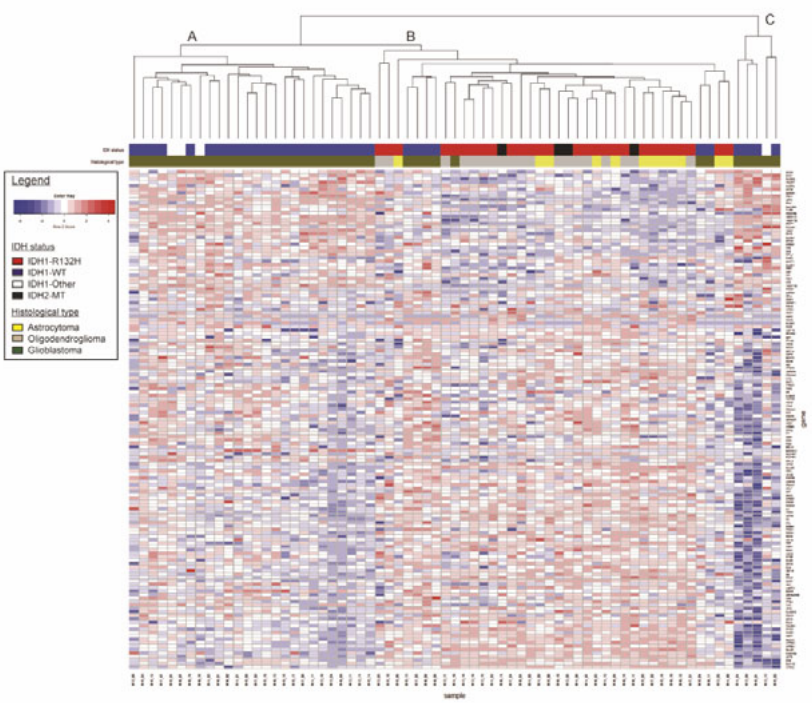

Figure 1. Agglomerative clustering of t/RNA-NGS profiles of 69 grade II-IV gliomas. *Clustering was based on expression levels of 145 genes of interest. Gene expression levels (in FPM) were transformed to a z-score for each individual transcript. After generating the dendrogram and heatmap using the average clustering method in R, histopathology results and mutation status were added in retrospect (legend and upper annotation bars). Cluster A and C strongly correlate with a wild-type IDH status, while cluster B is strongly associated with the IDH1^{R132H} mutation (see also Supplementary Table S3). IDH2 mutations (R172K, R172M, and R172W) are annotated as IDH2-MT (black in the annotation bar) and all co-clustered with the IDH1^{R132H} mutation. IDH1-other refers to variants other than the IDH1^{R132H} (see Table 1).*

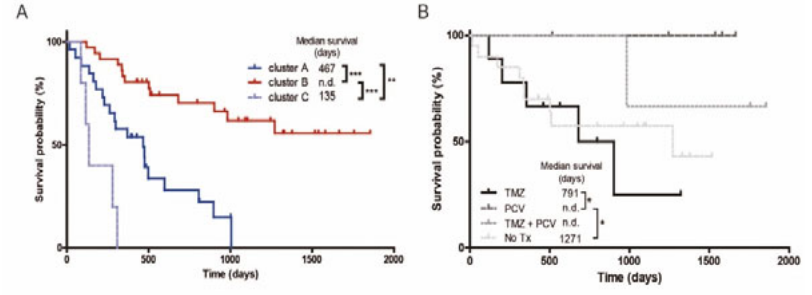

Figure 2. Kaplan-Meier analyses of unsupervised clusters. A) *For patients in clusters A (N=26) and C (N=5) median survival was 467 days and 135 days, respectively. For cluster B (N=38) the follow-up period was too short to determine median survival. Survival of patients in cluster B was significantly better than of clusters A and C (both p<0.0001). Survival in cluster A was significantly better than C (P=0.008).* ***B)*** *Oligodendroglioma patients in cluster B (diagnosed according to WHO 2016 classification, and treated with PCV) performed better than astrocytoma patients in this cluster (all treated with TMZ) (p=0.04). Two patients (N16-06 and N16-10) were excluded from analysis because no survival data was present.*

Additionally, a duplication in succinate dehydrogenase A (*SDHA*) of unknown significance was strongly associated with group B ($p=3x10^{-5}$). The test also identified known oncogenic mutations in mitochondrial *IDH2* in four patients (two p.R172K, one p.R172C and one p.R172M mutation, Table 1). Gene expression profiles from these gliomas co-clustered with those of the p.IDH1-R132H gliomas in cluster B (Figure 1, black in IDH-status annotation bar). All $IDH1^{R132}$ and $IDH2^{R172}$ mutations were in retrospect confirmed by routine genetic analyses (not shown). As described before, also other variants of *IDH1* (p.V178I, p.Y183C) were identified by the assay [316] (Table 1).

We then analysed the profiles in relation to survival with treatment and histopathology as additional parameters. Retrospective analysis of histopathology and clinical follow-up data revealed that all patients in clusters A and C received temozolomide (TMZ) and/or radiotherapy upon signs of tumour progression after surgery, suggesting that the differences in survival were not related to treatment. We therefore concentrated on patients in cluster B who were treated with TMZ (N=9, astrocytomas), procarbazine/lomustine/vincristine (PCV) chemotherapy (N=6, all 1p/19q co-deleted oligodendrogliomas), both adjuvant therapies (N=3), or did not receive additional treatment (N=19). Of 2 patients adjuvant therapy status was unknown (N=2). As shown in Figure 2B, outcome for oligodendroglioma patients treated with PCV was better than for astrocytoma patients treated with TMZ (p=0.04).

Whereas group B was dominated by IDH-mutated gliomas, this group also contained 6 IDH wild-type glioblastomas. Comparison of gene expression profiles of these gliomas with those of cluster A revealed that expression levels of all VEGF isoforms were significantly lower in the group B IDH^{wt} gliomas (Supplementary Table S3). This suggests that these 6 tumours grouped with the IDH^{mut} gliomas based on the lack of an angiogenic response.

t/RNA-NGS based molecular diagnosis

To investigate whether t/RNA-NGS profiles are associated with histopathology diagnoses, we performed a group-based analysis according to the WHO 2016 grading system [60] and compared grade II/III astrocytomas (N=12), grade II/III oligodendrogliomas (N=19) and glioblastomas (N=38). Wilcoxon Mann-Whitney U tests identified 79 genes that were differentially expressed between diffuse grade II/III oligodendrogliomas and glioblastomas (Table S4A). In the top 5 of differentially expressed genes were *LDHA* and *BCAT1*, genes that are known to be hypermethylated in low grade, IDH^{mut} gliomas [313, 320]. Expression levels of 50 genes were significantly different between grade II/III astrocytomas and glioblastomas (Table S4B), whereas expression levels of only 1 gene (*ALK*) differed significantly between astrocytomas and oligodendrogliomas (Table S4C). As expected, both oligodendrogliomas and astrocytomas were distinguished from glioblastomas by the p.IDH1-R132H mutation. *EGFR*vIII was expressed in 30% of glioblastomas (N=13; mean FPM=550, range 6-1450; Figure 3A) and never in grade II/III gliomas, in good agreement with literature [321]. Expression of wild-type *EGFR* was found among all gliomas, but was more prominent in glioblastomas than in grade II/III gliomas (mean FPM=612 vs. 126; p=0.0061). Levels of *EGFR* and *MET* expression in

glioblastomas were inversely correlated (Spearman R=-0.59, p<0.0001; Figure 3B). Not surprising given the strong association of IDH1 mutations and grade II/III gliomas with cluster B of Figure 1, the supervised histopathology-based analysis again identified ERBB3, ERBB4 and TRKB (the product of *NTRK2*) as potentially targetable proteins in grade II/III gliomas (Figure 3C).

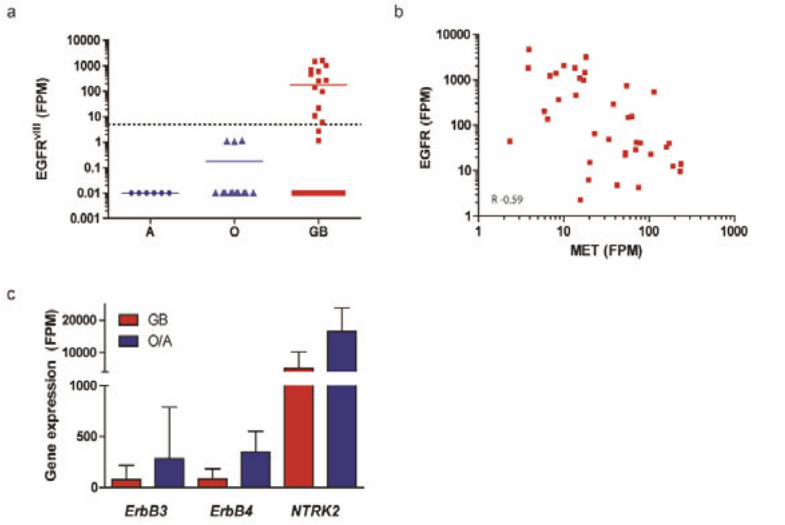

Figure 3. Actionable gene expression in grade II/III astrocytomas, oligodendrogliomas and glioblastoma. A) *$EGFR^{vIII}$ was detected at significant levels in 30% of glioblastomas (GB, red) but not in grade II/III astrocytomas (A) and oligodendrogliomas (O) (note the log scale of the Y-axis, expression <5 FPM was considered $EGFR^{vIII}$-negative).* ***B)*** *Wild-type EGFR expression is inversely correlated with expression of MET in glioblastoma (Spearman R=-0.59; p<0.0001).* ***C)*** *Mean expression of ErbB3, ErbB4, and NTRK2 in GB (red) and grade II/III O/A (blue). Error bars represent the standard deviation.*

Carbonic anhydrase 12 is a poor prognostic factor

To investigate whether prognostic factors other than *IDH1* mutations can be identified by t/RNA-NGS, we performed subgroup analysis on tumour profiles from IDH^{wt} patients with survival <14 months and >14 months (the median overall survival time of this group of patients). A Fisher's exact test on the sequence variations in these groups identified two different splice isoforms of *CAXII*: a full-length variant 1 (CAXIIv1), and a variant 2 (CAXIIv2) that lacks exon 9. Expression levels of *CAXII*v1 were associated with poor survival (Figure 4A). Detection of this variant was based on one smMIP with both exon 8-9 and exon 8-10 boundaries in its ROI. This smMIP can detect both isoforms due to the small size of exon 9 of 33 nucleotides. Interestingly, CAXIIv1 was never detected in IDH^{mut} gliomas. CAXIIv1 expression values higher than 50 FPM translated in poor prognosis as shown by Kaplan-Meier analysis (272 vs.1002 days from surgery to death, p=0.0137; Figure 4B).

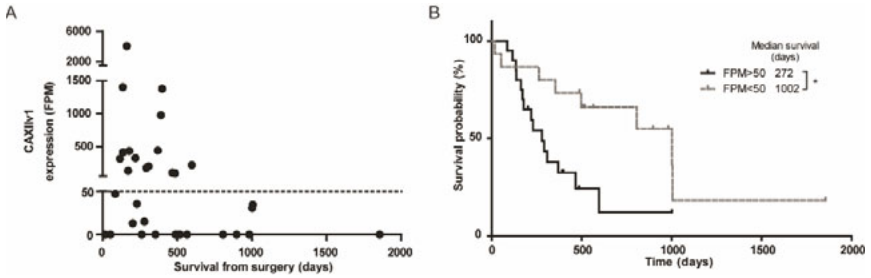

***Figure 4. Expression of CAXII is a poor prognostic factor**. **A)** CAXIIv1 expression levels in the positive patient samples included in panel A. Expression >50 FPM is a poor prognostic survival marker. **B)** Kaplan-Meier curve of IDH^{wt} gliomas, grouped based on CAXIIv1 expression.*

Validation of t/RNA-NGS data

We have previously shown that the quality of t/RNA-NGS data correlates well with w/RNA-NGS [312]. All IDH1 and IDH2 mutations that were found with regular molecular screening, were verified by t/RNA-NGS [313]. Interestingly, the broad set-up of our t/RNA-NGS assay allowed the frequent detection of androgen receptor (AR) in gliomas at relatively high levels. To confirm and validate these and other findings on the proteome level we performed immunohistochemical analyses for EGFR, MET, CAXII and AR on a number of

tumours with low or high FPM values for the corresponding genes. Transcript levels for *EGFR*, *MET*, *CAXII*, and *AR* correlated with protein levels (Figure 5). In one case we found that *EGFR*-transcript levels from frozen tumour tissue did not match with protein levels in FFPE blocks. This discrepancy could be attributed to tumour heterogeneity since the FFPE block contained both EGFR-positive and negative areas (Figure 5A).

We also detected prominent expression of *FOLH1*, the gene encoding prostate specific membrane antigen (PSMA), in approximately 70% of the gliomas. To validate this finding, we performed IHC analysis for PSMA on a number of tumours with either low or high *FOLH1* FPM values. IHC revealed expression of PSMA on the blood vessels of tumours with high *FOLH1* FPM values (Figure 5F).

Actionable markers in individual brain cancers

We then investigated whether t/RNA-NGS can stratify patient tumours based on relatively high expression of actionable targets (arbitrarily defined as >2-fold expression compared to the mean of all gliomas). Results of a selection of tyrosine kinases (*EGFR*, *MET*, *ALK*, *AXL*, *KIT*, *RET*, *ROS1*) for 12 gliomas are presented in Figure 6A. In only one tumour high expression levels of *CD2*, *CD3*, *CD4*, *CD8*, *CTLA4* and *PD-1* were found, suggesting an inflammatory phenotype (not shown). Many mutations were detected in the assay that are described as somatic mutations in the Cosmic database [322]. Potentially interesting mutations that we found (based on FATHMM score) included p.RET-S1002R, p.EGFR-G719D, p.EGFR-A289D, PTEN mutations ad TP53 mutations (not shown).

In the pleomorphic xanthoastrocyoma (PXA) in our test cohort a *BRAF*^{V600E} mutation was found which was confirmed via genetic testing (Table 1). This mutation has been described before in PXA [323]. These are mostly slow growing, low-grade gliomas but some patients will undergo malignant progression. Mutations in *BRAF* have been identified as poor prognostic factors for this tumour type [324, 325]. Interestingly, patient 14-03 was operated for a recurrent tumour 4 years later (sample 18-13 in the validation cohort).

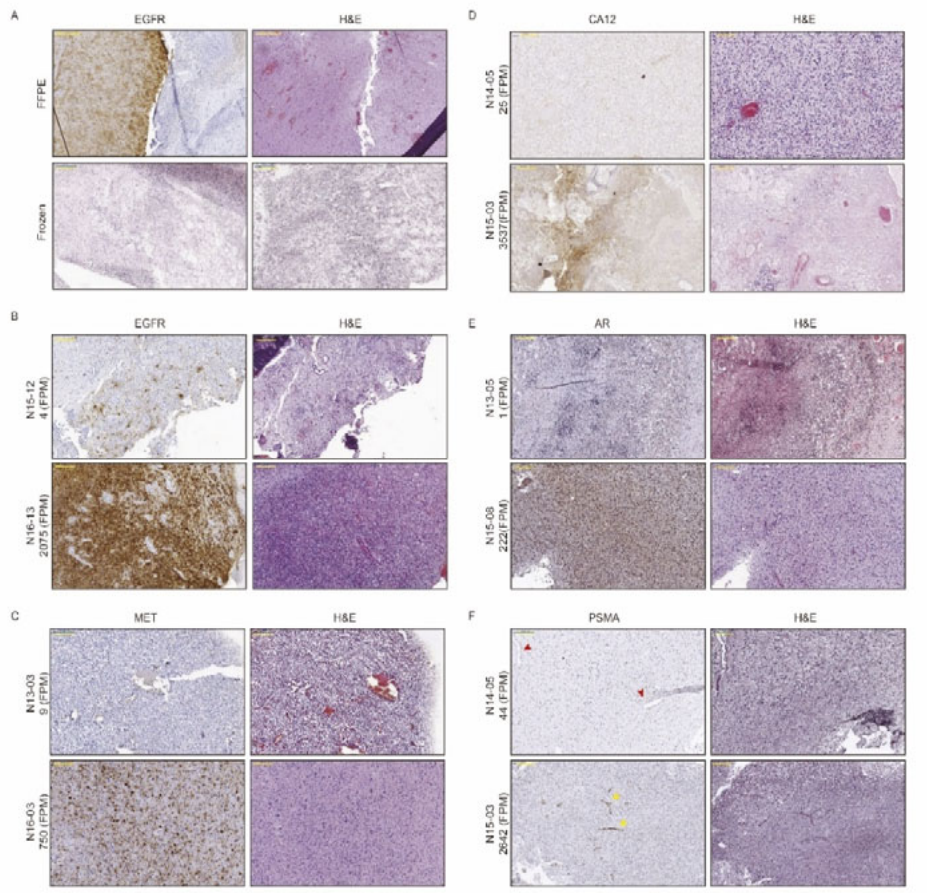

Figure 5. Immunohistochemical staining of EGFR, MET, CA12, AR, and PSMA. A, B) *EGFR staining of tumour N15-12 (negative in the smMIP assay) was negative in the frozen section, but partly positive in the FFPE section, indicating intratumoral heterogeneity of EGFR expression. High EGFR gene expression in tumour N16-13 was consistent with protein expression. IHC staining for MET* ***(C)****, CA12* ***(D)****, and AR* ***(E)*** *of tumour samples with low (upper panels) and high (lower panels) expression levels of MET, CA12 and AR respectively in the t/RNA-NGS assay. Expression levels in FPM are stated with the sample name.* ***F)*** *Staining for PSMA showed endothelial staining in gliomas with high PSMA (FOLH1) FPM values, as indicated with the yellow arrowheads in the lower panel. In gliomas with low expression (N14-05), no staining was observed (red arrowheads in upper panel point at blood vessels). Original magnification for upper panel in A, 5x. For lower panel of A and other panels, magnification is 10x. Yellow annotated bar for 5x 500µm, for 10x 200µm.*

Samples 14-03 and 18-13 were therefore re-analysed with t/RNA-NGS in the same sequencing run. The recurrent tumour showed a 70-80-fold increase of expression of transcription factors *ASCL1* and *HOXA1* and tyrosine kinases *FGFR3*, *HER3*, *HER4* and *MET* (Figure 6B). Another interesting finding was high expression of oestrogen receptor 2 (*ESR2*) in the recurrent, but not the primary tumour. Whereas the p.BRAF-V600E mutation was retained, the recurrent tumour showed an additional p.NF1-E1571* nonsense mutation (not shown). This mutation has been described as pathogenic in the Cosmic database [322] (FATHMM score=0.99).
Other observations that were of potential clinical relevance were that the brain metastasis of lung carcinoma expressed relatively high levels of *MET*, *RON* and *CTLA4* (Figure 6C). This may suggest sensitivity to the MET/RON inhibitor BMS777607/ASLAN002, combined with immune checkpoint inhibition [326]. The ependymoma showed high levels of *EGFR*vIII (not shown). One glioblastoma expressed the $MET^{\Delta 7\text{-}8}$ variant that we described previously [242]. In the DNET, considered as a benign grade I tumour, we found high expression levels of *ERBB3*, *FGFR2*, *FOLH1* and *AXL*.

Validation cohort
To validate these results, we next performed t/RNA-NGS on an independent validation cohort of 28 analysable human glioma samples. p.IDH1-R132H mutations were found in 7 samples, all diagnosed as grade II/III astrocytomas and oligodendrogliomas (Table 1). Differentially expressed genes between IDH^{mut} and IDH^{wt} gliomas in the experimental cohort were confirmed in the validation cohort (Supplementary Table S5). *EGFR*vIII expression was found in 4 of 19 (21%) of IDH^{wt} glioblastomas and not in p.IDH1-R132H cancers, confirming results in the test cohort. Thus, the test is robust and yields batch-independent clinically relevant information. Survival data in the validation set could not be interpreted due to short time of follow-up.

Discussion
We here describe the clinical application of a relatively novel and cost-effective multiplex next generation RNA sequencing assay for cancer pathway profiling. The assay generates expression profiles and sequence information of genes that have been identified by literature surveys as potentially important for diagnosis, prognosis and response to precision medicines in a variety of cancer types. We previously demonstrated that the test allows analysis of metabolism by measuring relative expression levels of metabolic enzymes [313, 315]. To analyse clinically actionable pathways, we expanded the assay with smMIPs to quantify expression levels of and detect mutations in the involved genes. Analysis of the cohort of 103 brain cancers, of which 97 well characterized gliomas, allowed robust group-based analysis, and confirmed high inter tumour molecular heterogeneity with respect to tyrosine kinase expression. Indeed, the biology in individual gliomas that drives progression is mostly a black box. Therefore, in the routine clinical setting molecular genetics is increasingly implemented as add-on to histopathology to aid the diagnostic process, but influence on therapeutic decision making is limited. Biomarkers that influence clinical management include *IDH*

mutations, combined with loss of chromosome arms 1p and 19q, leading to a diagnosis of oligodendroglioma that responds well to PCV, whereas methylation of the *MGMT* promoter in glioblastoma predicts a better response to TMZ [327-329]. *EGFR* status is also determined, amplification of which, in combination with the *EGFR* mutation, is associated with glioblastoma [330]. We here show that a single t/RNA-NGS test gives the same genetic information that can be derived from DNA analysis, but additionally provides information on gene activity from mutated but also non-mutated alleles. Thus, RNA-profiling is better suited than DNA-profiling to draw conclusions on activity of biological pathways, and thus may be more reliable as a guide to personalized treatment plans [331, 332]. It must be noted that for this study we isolated RNA from tumour tissue, snap-frozen directly after surgery. Although t/RNA-NGS can also be performed on RNA isolated from FFPE tissue, we found that whereas the quality of t/RNA-NGS data is good if tissue is formalin-fixed directly after surgery, it decreases in case of large time lags between surgery and formalin fixation (data not shown).

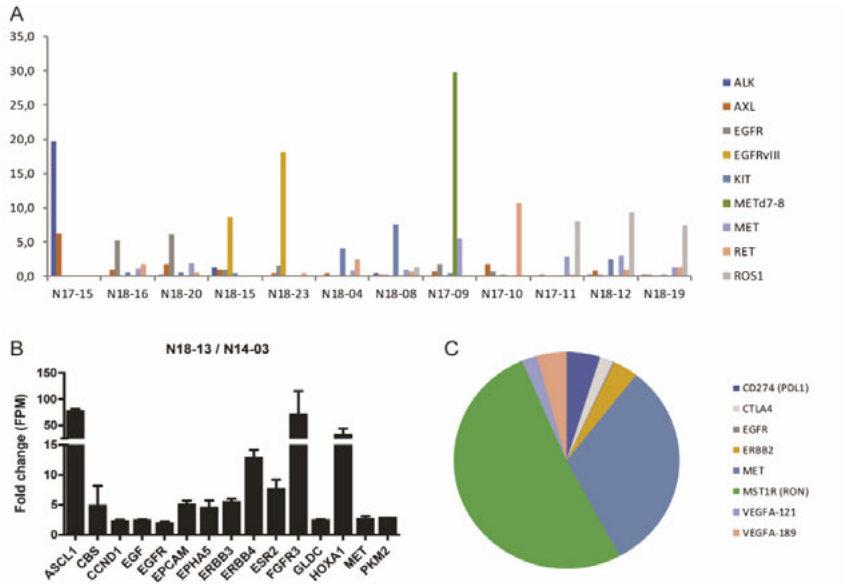

Figure 6. Actionable markers in brain tumours. A) *Overview of expression of potentially actionable targets in a subset of patients, expressed as fold change compared to the mean of the entire group. For clarity only tyrosine kinases are shown for a small selection of patients.* ***B)*** *Comparative analysis of a primary pleomorphous xantoastrocytoma and its recurrence 4 years later.* ***C) S****election of actionable targets in sample N13-05, a metastasis of a lung cancer. Note high expression levels of the macrophage receptor RON, MET and CTLA4. Also, VEGF isoforms 121 and 189 are detected.*

Tumours with overexpression of a targetable tyrosine kinase will be resistant to the corresponding inhibitor if other kinases are present that converge on the same signalling pathways [333]. Insight in the entire repertoire of expressed tyrosine kinases, downstream signalling intermediates and counteracting phosphatases may therefore predict intrinsic resistance or rapid development thereof [243, 334, 335]. t/RNA-NGS provides such insight for

individual glioma patients, and even can identify gene activities that have so far been associated with other cancer types, opening new avenues for targeted therapy. For example, expression of the prostate cancer marker PSMA on microvasculature of glioblastoma as we show here, may provide opportunities for tumour-vascular targeting [336-338]. Of interest, it was reported before that high expression levels of AR in glioblastoma translates into sensitivity to the AR antagonist enzalutamide [339]. Notably, our data also confirmed the identification of CAXIIv1 as a marker of poor prognosis in glioblastoma patients [340]. CAXII is a transmembrane enzyme that is involved in intracellular pH homeostasis and extracellular acidification, providing a biological explanation for the association with poor survival [341]. Overexpression of CAXIIv1, but not CAXIIv2, in cell models leads to acidification of the extracellular milieu, whereas overexpression of CAXIIv2 leads to increased oxygen consumption (manuscript in preparation). Because CAXII is expressed at low levels in normal brain, it is an interesting therapeutic target for the group of CAXII-positive glioblastomas [342].

In conclusion we here present a novel t/RNA-NGS 'one size fits all' assay that can provide a molecular diagnosis and prognosis for glioma and other cancers, as well as generate a list of (actionable) gene expression levels and mutations for individual cancers. The work described in this manuscript was performed with RNA, isolated from optimally biobanked tissue. The small size of the RNA regions of interest (150 bases) that is required for successful smMIP capture, however, also allows testing of RNA isolated from formalin fixed, paraffin embedded tissue blocks, provided that autolysis is prevented by proper and rapid processing. The low costs and high throughput capacity of the assay (up to 400 samples can be processed simultaneously due to barcoding) makes it highly interesting to further analyse biobanked tissues in future studies and identify classifier profiles that can predict prognosis and response to therapies. Thus, t/RNA-NGS may allow repurposing of drugs in an individualized manner.

Acknowledgements
We thank Carlijn van de Water and Tessa de Bitter (Radboudumc, Dept. of Pathology), for help with smMIP design. We thank Sanne van Lith (Radboudumc, Dept. of Radiology and nuclear medicine) and Kiek Verrijp (Radboudumc, Dept. of Pathology) for immunohistochemical stainings.

Supplementary material

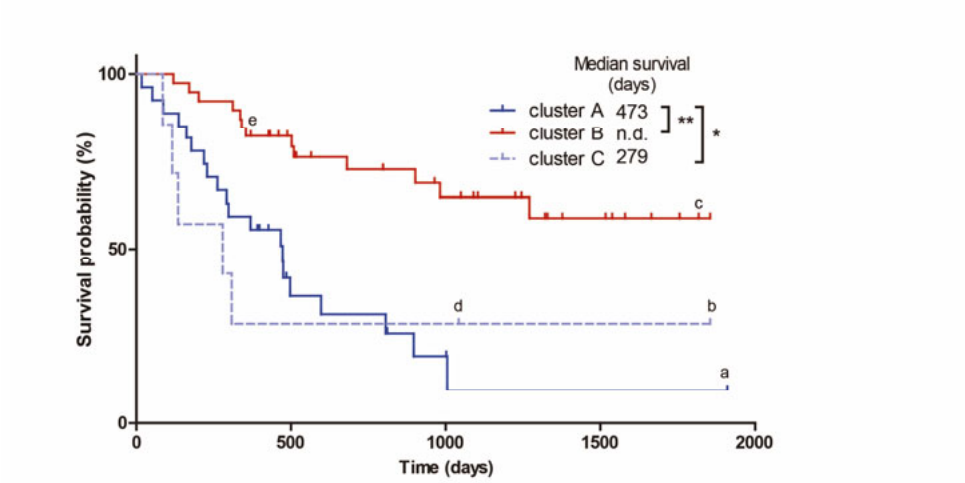

Figure S1. Kaplan-Meier analysis of unsupervised clusters of the entire cohort. *Indicated in the figure are (a) ependymoma, (b) lung metastasis, (c) DNET, (d) LPD, and (e) variant glioma.*

Table S1A: Differential gene expression in cluster A vs. B. A total of 83 genes were differentially expressed between the two clusters. Only genes that were significantly different are shown. Mean gene expression values (FPM) values for the clusters are given. For significance: A Wilcoxon-Mann-Whitney test with multiple testing correction was performed. Values are significant when the p-value is lower than the False Discovery Rate (FDR). The cut-off for the FDR was <0.05.

Gene	Mean FPM Cluster A	Mean FPM Cluster B	p-value	FDR
VEGF	315.843	18.989	0.000	0.000
VEGF165	1650.128	91.928	0.000	0.000
VEGF121	865.636	80.282	0.000	0.000
LDHA	4376.568	939.698	0.000	0.000
BCAT1	1605.473	244.772	0.000	0.000
PFKM	460.133	1206.420	0.000	0.000
ERBB4	62.190	326.643	0.000	0.000
ABAT	359.512	1282.089	0.000	0.001
GLUD1	839.99f3	4044.100	0.000	0.001
GLUD2	35.906	225.705	0.000	0.001
ATP5C1	1144.432	2469.982	0.000	0.001
VEGF189	997.068	40.234	0.000	0.001
LDHB	3783.220	7991.827	0.000	0.001
SLC16A3	454.556	131.831	0.000	0.001
MAPK8	117.256	295.313	0.000	0.001
NTRK2	4462.448	15774.166	0.000	0.001
GCLC	229.046	687.386	0.000	0.001
GAD1	94.355	557.142	0.000	0.001
CA12	1303.110	172.401	0.000	0.001
PGAM1	428.430	762.698	0.000	0.001
ACO2	202.578	380.995	0.000	0.001
ACACA	231.076	416.369	0.000	0.002
CBS	131.479	381.506	0.000	0.002
CA9	92.920	13.781	0.000	0.002
PC	135.112	336.137	0.000	0.002
IDH3G	330.658	556.237	0.000	0.002
SDHA	647.412	1055.310	0.000	0.002
CS	402.670	695.179	0.000	0.002
NAMPT	5014.847	883.489	0.000	0.002
PDK1	361.496	165.003	0.000	0.002
PGK1	3663.771	1848.398	0.000	0.002
GPI_1	749.152	444.488	0.000	0.002
IDH3A	145.390	249.574	0.000	0.002
GOT1	42.813	90.941	0.000	0.002
SOD1	410.087	758.264	0.000	0.002
HK2	65.428	18.863	0.000	0.002
ATP5A1	2196.228	3204.543	0.000	0.003
GAPDH	33982.269	24284.599	0.000	0.003
GLUL	1640.171	3617.271	0.000	0.003
SLC2A3	4293.117	1573.138	0.000	0.003

MDH1	349.529	572.232	0.000	0.003
L2HGDH	20.233	37.599	0.000	0.003
GPI_2	1076.352	644.286	0.000	0.003
CHKA	98.455	167.233	0.000	0.003
BRAF	244.947	377.284	0.000	0.003
D2HGDH	81.096	132.612	0.000	0.003
SOD2	20373.181	8933.506	0.000	0.003
IGF1R	459.821	566.188	0.000	0.003
MERTK	339.525	816.026	0.000	0.003
ERBB3	67.403	261.207	0.000	0.003
PDHA1	275.098	461.988	0.000	0.004
SLC7A1	983.578	1586.329	0.000	0.004
HK3	11.139	4.010	0.000	0.004
GPT	3.435	7.871	0.000	0.004
NOX4	103.698	62.475	0.000	0.004
ENO1	12011.763	8521.523	0.000	0.004
GCLM	159.109	99.892	0.000	0.004
PDGFRB	548.986	315.916	0.000	0.004
SDHC	899.070	1188.473	0.000	0.004
SLC9A1	336.077	215.883	0.000	0.004
TXN	2489.500	1721.999	0.000	0.004
ARHGAP26	715.163	1194.567	0.000	0.004
IDH2	504.126	827.137	0.000	0.004
SLC1A2	3676.856	9430.761	0.000	0.004
FASN	132.675	231.527	0.000	0.004
PDGFRA	5031.468	5126.429	0.000	0.005
PLXND1	275.485	191.349	0.000	0.005
PTEN	538.754	858.624	0.000	0.005
FBP1	47.942	28.475	0.000	0.005
CKB	3661.729	6620.678	0.000	0.005
EGFRvIII	253.316	1.001	0.001	0.005
MST1R	0.845	1.551	0.001	0.005
SDHD	625.821	818.604	0.001	0.005
CPT1A	256.524	358.950	0.001	0.005
MET	52.833	34.974	0.001	0.005
IDH1	1172.620	780.466	0.001	0.005
TALDO1	1145.332	1631.526	0.002	0.005
EGLN1	189.116	247.098	0.002	0.005
PRKAA2	32.568	48.941	0.002	0.005
PKM	4859.248	3775.165	0.003	0.006
NAPRT1	6.831	13.359	0.003	0.006
ACSS2	131.275	178.672	0.004	0.006
KIT	213.857	206.096	0.004	0.006

Table S1B: Differential gene expression in cluster B vs. C. A total of 69 genes were differentially expressed between the two clusters. Only genes that were significantly different are shown. Mean gene expression values (FPM) values for the clusters are given. For significance: A Wilcoxon-Mann-Whitney test with multiple testing correction was performed. Values are significant when the p-value is lower than the False Discovery Rate (FDR). The cut-off for the FDR was <0.05.

Gene	Mean FPM cluster B	Mean FPM cluster C	p-value	FDR
ABAT	1282.089	33.210	0.000	0.000
ALK	77.621	3.386	0.000	0.000
ATP5C1	2469.982	752.070	0.000	0.000
CBS	381.506	35.986	0.000	0.000
CHKA	167.233	45.718	0.000	0.000
ERBB3	261.207	3.718	0.000	0.000
ERBB4	326.643	2.236	0.000	0.000
GLUD1	4044.100	313.730	0.000	0.001
GLUD2	225.705	11.736	0.000	0.001
LDHB	7991.827	1867.272	0.000	0.001
NTRK2	15774.166	754.240	0.000	0.001
PC	336.137	45.400	0.000	0.001
SLC16A3	131.831	1405.726	0.000	0.001
GLDC	369.237	35.338	0.000	0.001
KIT	206.096	10.122	0.000	0.001
L2HGDH	37.599	7.534	0.000	0.001
VEGF121	80.282	1057.350	0.000	0.001
CKB	6620.678	486.208	0.000	0.001
GAD1	557.142	14.752	0.000	0.001
HK2	18.863	241.470	0.000	0.001
PFKM	1206.420	219.006	0.000	0.001
VEGF	18.989	513.152	0.000	0.002
ACO2	380.995	102.326	0.000	0.002
D2HGDH	132.612	40.816	0.000	0.002
ENO1	8521.523	19276.616	0.000	0.002
MAPK8	295.313	74.022	0.000	0.002
SDHC	1188.473	482.868	0.000	0.002
SLC2A3	1573.138	10808.804	0.000	0.002
CS	695.179	253.322	0.000	0.002
IDH2	827.137	221.878	0.000	0.002
LDHA	939.698	5143.006	0.000	0.002
SLC1A2	9430.761	369.618	0.000	0.002
SLC7A1	1586.329	409.818	0.000	0.002
PGK1	1848.398	5752.602	0.000	0.002
BCAT1	244.772	1294.698	0.000	0.002
NAMPT	883.489	10081.262	0.000	0.002
MDH1	572.232	230.760	0.000	0.003
RET	21.796	0.986	0.000	0.003
IDH3A	249.574	85.394	0.000	0.003

IDH3G	556.237	256.586	0.000	0.003
VEGF165	91.928	746.332	0.000	0.003
ACSS2	178.672	73.680	0.000	0.003
FGFR2	189.059	16.696	0.000	0.003
GCLC	687.386	150.580	0.000	0.003
PTEN	858.624	281.650	0.000	0.003
BRAF	377.284	148.594	0.000	0.003
PDHA1	461.988	163.292	0.000	0.003
SDHD	818.604	437.902	0.000	0.003
CAT	359.956	158.610	0.001	0.003
EGFR	233.221	18.110	0.001	0.003
PARP1	1327.669	543.882	0.001	0.004
PKM	3775.165	6456.298	0.001	0.004
VEGF189	40.234	934.224	0.001	0.004
ALDOA	9682.345	14013.498	0.001	0.004
ATP5A1	3204.543	1366.026	0.001	0.004
EGLN1	247.098	120.326	0.001	0.004
CA9	13.781	223.078	0.001	0.004
GOT1	90.941	36.028	0.001	0.004
SOD1	758.264	348.312	0.001	0.004
PRKAA2	48.941	16.718	0.001	0.004
VHL1	237.804	89.154	0.002	0.004
HK3	4.010	34.536	0.002	0.004
FH	209.338	101.728	0.002	0.004
ACACA	416.369	156.574	0.002	0.004
PFKFB1	2.239	0.544	0.004	0.004
AXL	374.522	134.300	0.004	0.005
MET	34.974	105.468	0.004	0.005
KDR	556.674	76.816	0.005	0.005
PDGFRA	5126.429	1009.234	0.005	0.005

Table S1C: Differential gene expression in cluster A vs. C. A total of 9 genes were differentially expressed between the two clusters. Only genes that were significantly different are shown. Mean gene expression values (FPM) values for the clusters are given. For significance: A Wilcoxon-Mann-Whitney test with multiple testing correction was performed. Values are significant when the p-value is lower than the False Discovery Rate (FDR). The cut-off for the FDR was <0.05.

Gene	Mean FMP cluster A	Mean FPM cluster C	p-value	FDR
ABAT	359.512	33.210	0.000	0.000
GLUD1	839.993	313.730	0.000	0.000
ERBB4	62.190	2.236	0.000	0.000
GLDC	276.017	35.338	0.000	0.000
KDR	388.283	76.816	0.000	0.000
FOLH1	473.184	30.216	0.000	0.000
FGFR2	129.527	16.696	0.000	0.000
GLUD2	35.906	11.736	0.000	0.000
NOX4	103.698	24.384	0.000	0.000

Table S2: Mutation detection in human glioma samples. A Fisher's exact test was performed to identify genetic mutations that distinguish the clusters A, B, and C as defined in Figure 1. Mutations that were present in at least 10 percent of the unique reads were tested for significance. There were no significant differences between cluster A vs. C. The cut-off for the FDR was set at 0.01. Genes shown here were significantly different between clusters.

Cluster A vs. B					
Gene mutation	**Gene mutation**	**Present in A**	**Present in B**	**p-value**	**FDR**
IDH1	p.Arg132His	0/26	28/38	4.44E-10	3.11E-05
Cluster B vs. C					
Gene mutation	**Gene mutation**	**Present in B**	**Present in C**	**p-value**	**FDR**
SDHA	p.Leu18_Ala19dup	37/38	0/5	6.23E-06	2.98E-05

Table S3: Differential gene expression in IDH^{wt} gliomas from cluster B vs cluster A. A total of 4 genes were differentially expressed between the cluster A and the IDH^{wt} gliomas that grouped in cluster B. Only genes that were significantly different are shown. Mean gene expression values (FPM) values for the clusters are given. For significance: A Wilcoxon-Mann-Whitney test with multiple testing correction was performed. Values are significant when the p-value is lower than the False Discovery Rate (FDR). The cut-off for the FDR was <0.05.

Gene	Mean FPM cluster A	mean FPM IDH^{wt} in cluster B	p-value	FDR
VEGF165	1666.451	58.500	0.000	0.000
VEGF189	977.172	41.042	0.000	0.000
VEGF	316.292	13.778	0.000	0.000
VEGF121	865.596	65.298	0.000	0.000

Table S4A: Differential gene expression in oligodendroglioma (O) vs. glioblastoma (G). A total of 79 genes were differentially expressed between the two histological types. Only genes that were significantly different are shown. Mean gene expression values (FPM) values for the histological type are given. For significance: A Wilcoxon-Mann-Whitney test with multiple testing correction was performed. Values are significant when the p-value is lower than the False Discovery Rate (FDR). The cut-off for the FDR was <0.05.

Gene	Mean FPM O	Mean FPM G	p-value	FDR
LDHA	463.02	4028.73	0.000	0.000
PFKM	1407.65	500.74	0.000	0.000
ABAT	1583.34	399.70	0.000	0.000
BCAT1	144.99	1381.35	0.000	0.000
LDHB	8884.68	4012.27	0.000	0.000
CBS	402.38	137.79	0.000	0.000
CS	736.33	404.79	0.000	0.000
SLC16A3	89.69	531.71	0.000	0.001
ACACA	472.83	242.18	0.000	0.001
GLUD1	4025.21	975.93	0.000	0.001
SOD2	5038.11	19897.21	0.000	0.001
GAD1	722.64	143.80	0.000	0.001
GPI_1	381.53	708.30	0.000	0.001
GLUD2	218.58	46.31	0.000	0.001
ERBB4	318.29	84.29	0.000	0.001
NAMPT	596.93	4997.24	0.000	0.001
PC	366.68	137.33	0.000	0.001
NTRK2	14968.00	5092.23	0.000	0.001
PGAM1	892.07	477.72	0.000	0.001
ATP5C1	2483.77	1222.98	0.000	0.001
SOD1	898.90	438.60	0.000	0.001
IDH3G	608.65	343.61	0.000	0.002
SDHA	1184.38	704.97	0.000	0.002
VEGF121	88.85	742.05	0.000	0.002
HK2	13.10	81.33	0.000	0.002
VEGF	23.96	285.94	0.000	0.002
GOT1	106.80	48.45	0.000	0.002
MAPK8	317.58	133.45	0.000	0.002
GPI_2	530.35	990.43	0.000	0.002
IGF1R	575.63	399.28	0.000	0.002
VEGF189	46.73	811.61	0.000	0.002
ACO2	409.97	210.37	0.000	0.002
GCLC	732.70	269.77	0.000	0.002
VEGF165	118.02	1236.81	0.000	0.002
IDH3A	277.82	154.24	0.000	0.002
D2HGDH	151.50	80.91	0.000	0.002
SLC7A1	1706.62	934.94	0.000	0.003
SLC2A3	1301.77	4686.36	0.000	0.003
SLC9A1	170.53	346.93	0.000	0.003
L2HGDH	40.92	20.11	0.000	0.003

ATP5A1	3468.10	2187.43	0.000	0.003
SDHC	1285.31	880.65	0.000	0.003
PDHA1	521.22	279.67	0.000	0.003
CA9	17.94	93.48	0.000	0.003
MDH1	603.55	369.90	0.000	0.003
MET	10.84	55.95	0.000	0.003
PGK1	1967.94	3595.70	0.000	0.003
FBP1	17.48	59.52	0.000	0.003
ALK	128.78	47.28	0.000	0.003
CHKA	177.20	106.08	0.000	0.003
CKB	7498.28	3500.81	0.000	0.004
BRAF	402.55	252.92	0.000	0.004
SLC16A7	176.87	136.02	0.000	0.004
SLC16A1	681.52	1137.67	0.000	0.004
CA12	227.88	1055.67	0.000	0.004
TALDO1	1782.59	1193.87	0.000	0.004
PDGFRA	5294.95	4427.43	0.000	0.004
ENO1	8027.94	12392.53	0.000	0.004
SDHD	868.54	628.45	0.000	0.004
ERBB3	349.27	78.66	0.000	0.004
EGLN1	274.98	185.77	0.000	0.004
FH	228.96	171.13	0.000	0.004
GAPDH	25070.21	32132.06	0.000	0.004
PDK1	179.88	312.18	0.000	0.004
FASN	242.72	158.25	0.001	0.004
HK3	4.04	12.87	0.001	0.005
CPT1A	410.11	276.92	0.001	0.005
GCLM	92.92	146.69	0.001	0.005
PFKFB1	2.55	1.51	0.001	0.005
GPT	8.25	3.66	0.001	0.005
G6PC	1.83	0.33	0.002	0.005
IDH2	854.75	520.60	0.002	0.005
GLUL	3973.52	1858.98	0.002	0.005
PLXND1	173.71	336.24	0.002	0.005
CD274	13.98	27.86	0.002	0.005
ADPGK	196.23	308.57	0.003	0.005
SLC1A2	9679.14	5159.91	0.003	0.005
PTEN	855.24	551.86	0.004	0.005
GLDC	409.85	247.87	0.005	0.005

Table S4B: Differential gene expression in Astrocytomas (A) vs. glioblastoma (G). A total of 50 genes were differentially expressed between the two histological types. Only genes that were significantly different are shown. Mean gene expression values (FPM) values for the histological type are given. For significance: A Wilcoxon-Mann-Whitney test with multiple testing correction was performed. Values are significant when the p-value is lower than the False Discovery Rate (FDR). The cut-off for the FDR was <0.05.

Gene	Mean FPM A	Mean FPM G	p-value	FDR
GLUD1	5293.31	975.93	0.000	0.000
GLUD2	304.69	46.31	0.000	0.000
BCAT1	189.25	1381.35	0.000	0.000
NTRK2	20109.69	5092.23	0.000	0.000
ATP5C1	2809.18	1222.98	0.000	0.000
CA12	82.87	1055.67	0.000	0.000
LDHA	1110.43	4028.73	0.000	0.000
PRKAA2	67.07	31.50	0.000	0.001
VEGF189	32.90	811.61	0.000	0.001
ERBB4	399.15	84.29	0.000	0.001
PFKM	1094.09	500.74	0.000	0.001
VEGF	14.87	285.94	0.000	0.001
MAPK8	294.62	133.45	0.000	0.001
GLUL	3749.54	1858.98	0.000	0.001
ABAT	1080.06	399.70	0.000	0.001
GCLC	721.35	269.77	0.000	0.001
PGK1	1686.07	3595.70	0.000	0.001
VEGF121	79.82	742.05	0.000	0.001
VEGF165	73.90	1236.81	0.000	0.001
PC	360.63	137.33	0.000	0.001
LDHB	7509.53	4012.27	0.000	0.001
ACO2	372.76	210.37	0.000	0.002
IDH3G	532.97	343.61	0.000	0.002
MYC	1673.47	638.66	0.000	0.002
ATP5A1	3057.38	2187.43	0.000	0.002
CBR1	77.69	236.58	0.000	0.002
MERTK	883.48	415.34	0.000	0.002
IGF1R	699.41	399.28	0.000	0.002
EPAS1	567.49	1146.52	0.000	0.002
CBS	434.54	137.79	0.000	0.002
SLC16A3	162.31	531.71	0.000	0.002
GAPDH	22245.75	32132.06	0.000	0.002
CS	731.72	404.79	0.000	0.002
PDK1	147.57	312.18	0.000	0.002
CA9	13.50	93.48	0.000	0.002
SLC7A1	1662.44	934.94	0.000	0.002
L2HGDH	37.57	20.11	0.000	0.003
GAD1	375.31	143.80	0.000	0.003
NAMPT	1094.00	4997.24	0.001	0.003
ACACA	368.84	242.18	0.001	0.003

GPI_1	462.18	708.30	0.001	0.003
PKM	3186.93	4822.66	0.001	0.003
ERBB3	172.65	78.66	0.001	0.003
D2HGDH	116.55	80.91	0.001	0.003
GPT	8.48	3.66	0.002	0.003
PTEN	901.95	551.86	0.002	0.003
SLC9A1	185.68	346.93	0.002	0.003
NQO1	69.02	171.00	0.002	0.003
SLC2A3	1885.76	4686.36	0.003	0.003
FASN	256.59	158.25	0.003	0.003

Table S4C: Differential gene expression in Astrocytomas (A) vs. oligodendroglioma (O). One gene was differentially expressed between the two histological types. Only genes that were significantly different are shown. Mean gene expression values (FPM) values for the histological type are given. For significance: A Wilcoxon-Mann-Whitney test with multiple testing correction was performed. Values are significant when the p-value is lower than the False Discovery Rate (FDR). The cut-off for the FDR was <0.05.

Gene	Mean FPM A	Mean FPM O	p-value	FDR
ALK	19.61	128.78	0.000	0.000

Table S5. Analysis of validation cohort. Shown are fold changes of gene expression values, calculated by dividing mean FPM values of each transcript in IDH^{wt} tumours by that in IDH mutant tumours, both in the experimental cohort and validation cohort. FC, fold change.

Transcript	Experimental cohort	Validation cohort
	FC IDH-WT/mutant	**FC IDH-WT/mutant**
ABAT	0.3	0.5
ACACA	0.6	0.5
ATP5C1	0.5	0.6
BCAT1	6.6	5.1
BRAF	0.6	0.7
CA12	7.6	5.1
CA9	6.7	24.1
EGFRvIII	253.1	200.0
EGLN1	0.8	1.0
ENO1	1.4	2.0
ERBB3	0.3	0.7
ERBB4	0.2	0.3
FASN	0.6	0.6
FBP1	1.7	1.4
GAD1	0.2	0.2
GAPDH	1.4	1.3
GCLC	0.3	0.7
GCLM	1.6	1.5
GLUD1	0.2	0.5
GLUD2	0.2	0.5

GLUL	0.5	0.8
GOT1	0.5	0.5
GPI (var3)	1.7	1.3
GPI (var4)	1.7	1.3
GPT	0.4	1.5
HK2	3.5	6.0
HK3	2.8	10.4
LDHA	4.7	3.5
LDHB	0.5	0.6
MAPK8	0.4	0.5
MET	1.5	1.8
MST1R	0.5	0.6
NAMPT	5.7	3.4
NAPRT1	0.5	2.4
NOX4	1.7	1.0
NTRK2	0.3	0.7
PC	0.4	0.9
PDGFRA	1.0	0.5
PDGFRB	1.7	1.8
PDK1	2.2	3.0
PFKM	0.4	0.7
SLC16A3	3.4	6.3
SLC1A2	0.4	0.4
SOD2	2.3	3.2
VEGFA	16.6	21.1
VEGFA-121	10.8	10.3
VEGFA-165	18.0	12.8
VEGFA-189	24.8	26.6

CHAPTER 4

Isocitrate dehydrogenase 1-mutated human gliomas depend on lactate and glutamate to alleviate metabolic stress

Krissie Lenting*, Mohammed Khurshed*, Tom H. Peeters*, Corina N.A.M. van den Heuvel, Sanne A.M. van Lith, Tessa de Bitter, Wiljan Hendriks, Paul N. Span, Remco J. Molenaar, Dennis Botman, Kiek Verrijp, Arend Heerschap, Mark ter Laan, Benno Kusters, Anne van Ewijk, Martijn A. Huynen, Cornelis J.F. van Noorden, William P.J. Leenders

*Authors contributed equally to this study

FASEB Journal 2019 Jan;33(1):557-571.

Abstract

Background: Diffuse gliomas often carry point mutations in isocitrate dehydrogenase (*IDH1*^{mut}), resulting in metabolic stress. Although *IDH*^{mut} gliomas are difficult to culture *in vitro*, they thrive in the brain via diffuse infiltration, suggesting brain-specific tumour-stroma interactions that can compensate for IDH1 deficits.

Methods: To elucidate the metabolic adjustments in clinical *IDH*^{mut} gliomas that contribute to their malignancy, we applied a recently developed method of targeted quantitative RNA next generation sequencing to 66 clinical gliomas and relevant orthotopic glioma xenografts, with and without the endogenous IDH1^{R132H} mutation. Datasets were analysed in R using Manhattan's to calculate distance between expression profiles, Ward's method to perform unsupervised agglomerative clustering and the Mann Whitney U test and Fisher's exact tests for supervised group analyses. Significance of transcriptome data was investigated by protein analysis, *in situ* enzymatic activity mapping, and *in vivo* magnetic resonance spectroscopy of orthotopic *IDH1*^{mut}- and *IDH*^{wt}-glioma xenografts.

Results: Gene set enrichment analyses of clinical *IDH1*^{mut} gliomas strongly suggest a role for catabolism of lactate and the neurotransmitter glutamate, whereas in *IDH*^{wt} gliomas processing of glucose and glutamine are the predominant metabolic pathways. Further evidence for the differential metabolic activity in these cancers comes from *in situ* enzymatic mapping studies and preclinical *in vivo* magnetic resonance spectroscopy imaging.

Conclusions: Our data support an evolutionary model in which *IDH*^{mut} glioma cells exist in symbiosis with supportive neuronal cells and astrocytes as suppliers of glutamate and lactate, possibly explaining the diffuse nature of these cancers. The dependency on glutamate and lactate opens the way for novel approaches in the treatment of *IDH*^{mut} gliomas.

Keywords: glioma; isocitrate dehydrogenase; IDH-mutations; metabolism; glutamate; lactate; anaplerosis; glycolysis

Background

Heterozygous hotspot mutations in cytosolic isocitrate dehydrogenase 1 (*IDH1^{mut}*) and, less frequently, mitochondrial *IDH2* occur in 80% of WHO grade II-III and secondary grade IV gliomas, and are considered to be driving events in the formation of these and other neoplasms [82, 343, 344]. IDH1 is a cytosolic $NADP^+$-dependent homodimeric enzyme that reversibly oxidizes isocitrate to alpha-ketoglutarate (α-KG) with concomitant NADPH production. This enzyme reaction is responsible for 65% of total NADPH production capacity in the cytoplasm of IDH wild-type (*IDH^{wt}*) glioblastoma cells [84].

IDH1 mutations mainly involve Arg^{132} in the isocitrate binding pocket and introduce a neomorphic activity of reducing α-KG to *D*-2-hydroxyglutarate (*D*-2-HG) and oxidizing NADPH to $NADP^+$. Because *D*-2-HG is metabolized slowly, it accumulates intracellularly to millimolar concentrations at which it competitively inhibits a range of α-KG-dependent enzymes, ultimately resulting in epigenetic alterations that are associated with malignant transformation [96, 129, 344-347].

Although these *IDH* mutations are oncogenic, patients with *IDH^{mut}* gliomas have a better prognosis than patients with *IDH^{wt}* gliomas [83, 84]. This may be related to metabolic and oxidative stress, resulting from excessive consumption of α-KG and oxidation of NADPH [348]. Diminished NADPH levels translate into decreased production of reduced glutathione, an important scavenger of reactive oxygen species (ROS) in oxidative stress conditions such as irradiation [349]. This provides an explanation for increased radiotherapy sensitivity of *IDH^{mut}* gliomas [84, 350-352].

Previous studies have shown that *IDH1^{mut}* cancers have significantly rewired their metabolism [353-355]. This rewiring likely relieves *IDH1^{mut}*-associated metabolic stress by upregulating compensatory metabolic pathways that supply cancer cells with sufficient amounts of NADPH and α-KG for anaplerosis and allowing tumour progression. In a previous study, we reported that cells of the patient-derived *IDH1^{mut}* oligodendroglioma xenograft model E478 contain an extremely high density of mitochondria, suggesting that *IDH1^{mut}* gliomas revert to mitochondrial metabolism as a rescue pathway [215]. Emerging evidence shows that the tricarboxylic acid (TCA) cycle in *IDH1^{mut}* cells is however not fed by glucose, and *in vitro* studies have suggested that *IDH1^{mut}* cells use glutamine as a source for TCA cycle anaplerosis [122, 356]. According to this concept, *IDH1^{mut}* cells preferentially convert glutamine to α-KG through the sequential activities of glutaminase (GLS) and glutamate dehydrogenases (GLUD1/2) or glutamic acid oxaloaminotransferases (GOT1/2), unlike *IDH1^{wt}* cells that besides glutamine use glucose as a predominant fuel (Figure 1, route B) [354]. In contrast to primary glioblastomas, grade II and III (mostly *IDH^{mut}*) gliomas express the glutamate importer EAAT2 (the product of *SLC1A2*) [124]. Based on this finding we previously postulated that *IDH1^{mut}* cells may also directly utilize glutamate, a ubiquitous neurotransmitter, as a source for α-KG and NADPH production [129].

Gliomas are subject to intratumoral evolution, resulting in genetically heterogeneous subclones in one tumour [147]. Generation of cell lines under *in vitro* culture conditions therefore has a risk of outgrowth of artificially selected subclones that have undergone epigenetic reprogramming due to IDH locus loss or amplification [357]. To bypass these events we here concentrated on metabolism in a cohort of surgically obtained glioma tissues, using metabolic gene expression levels as surrogate marker for metabolic pathways. To this end we applied a targeted RNA next generation sequencing technology to profile metabolic gene expression in a large cohort of surgically obtained glioma tissues [312], combined with *in situ* and *in vivo* functional studies.

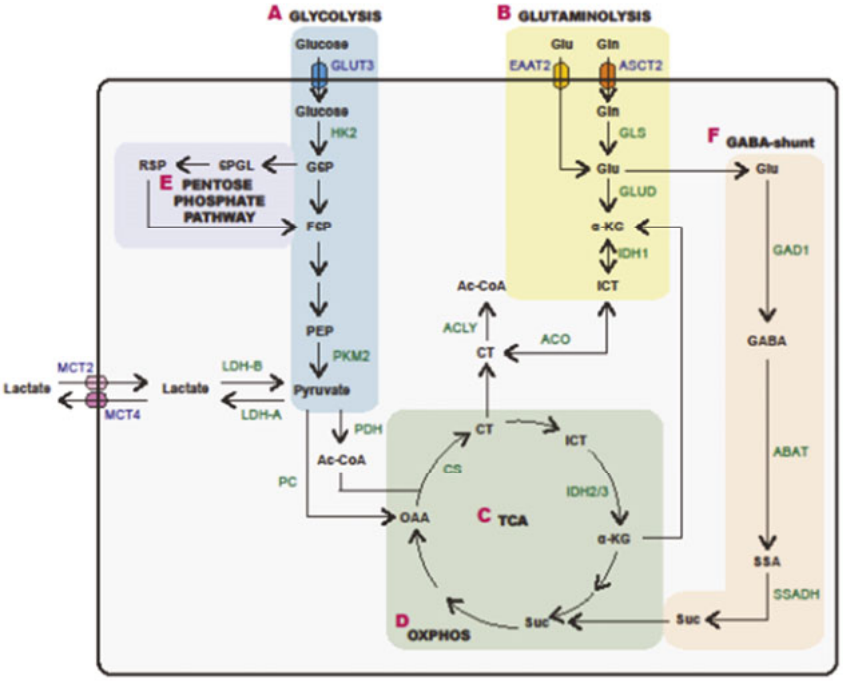

Figure 1: Overview of the metabolic pathways of investigation in this study. Indicated are the pathways of glycolysis (A), glutaminolysis (B), tricarboxylic acid (TCA) cycle (C), oxidative phosphorylation (D), pentose phosphate pathway that is responsible for nucleotide and NADPH synthesis (E) and the GABA-shunt (F). Enzymes and transporters in the different pathways are indicated in the figure.

6PGL 6-Phosphogluconolactonase; ABAT γ-Aminobutyrate aminotransferase; Ac-CoA Acetyl-CoA; αKG α-Ketoglutarate; ACLY ATP citrate lyase; ACO Aconitase; ASCT2 Anti-neutral amino acid transporter 2; CS Citrate synthase; CT Citrate; EAAT2 Excitatory amino acid transporter 2; F6P Fructose-6-phosphate; G6P Glucose-6-phosphate; GABA γ-Aminobutaric acid; GAD1 Glutamate decarboxylase 1; Gln Glutamine; Glu Glutamate; GLUD Glutamate dehydrogenase; GLS Glutaminase; GLUT3 Glucose transporter 3; HK2 Hexokinase 2; ICT Isocitrate; IDH Isocitrate dehydrogenase; LDH Lactate dehydrogenase; MCT Monocarboxylate transporter; OAA Oxaloacetate; OXPHOS Oxidative phosphorylation; PC Pyruvate carboxylase; PEP Phosphoenolpyruvate; PKM Pyruvate Kinase M; RSP Ribose-5-phospate; SSA Succinic semialdehyde; SSADH Succinic semialdehydedehydrogenase; Suc Succinate; TCA Tricarboxylic acid.

The combined data show that the TCA cycle in *IDH1*^{mut} gliomas is fuelled at multiple entry points by glutamate-derived α-KG and lactate-derived oxaloacetate, whereas *IDH*^{wt} gliomas are primarily dependent on glucose and glutamine. Furthermore, high expression of γ-aminobutyrate aminotransferase (ABAT) and succinic semialdehyde dehydrogenase (SSADH/ALDH5A1), together responsible for processing γ-aminobutyric acid (GABA) to succinate, suggest a role for the GABA-shunt in TCA anaplerosis in *IDH*^{mut} gliomas. These data put forward glutamate, lactate and possibly GABA as neuron- and astrocyte-derived chemotactic factors that fuel invasive progression of *IDH*^{mut} glioma.

Materials and Methods

The aim of this study was to map metabolic pathways *IDH*^{mut} gliomas that distinguish these tumours from *IDH*^{wt} gliomas. To avoid potential artefacts that may arise during *in vitro* culture of glioma cells carrying the endogenous mutation [357], we concentrated on analyses of surgically derived clinical glioma tissues and preclinical orthotopic models. Knowledge of these pathways may give insight in the biology of these highly diffuse infiltrating cancers, in conjunction with their micro-environment and may provide opportunities for metabolic targeting.

Patient tissues

All experiments involving human tissues were performed according to institutional guidelines of Radboudumc Nijmegen and Academic Medical Centre Amsterdam and involved informed consent. All research was performed on 'waste' material that was stored in a coded fashion. From Radboudumc, biobanked frozen human glioma samples (n=66), collected between 2013 and 2017, were used for targeted RNA sequencing (see below) and immunohistochemistry (IHC) analysis. Clinical and histopathological information was not available to the research team at the time of analysis, but was coupled to the datasets in retrospect. All tumour samples in this study contained 40-80% cancer cells, as was verified by an experienced neuropathologist (B.K.) using H&E-stained sections. Patient characteristics and WHO-2016-based histopathological diagnoses are listed in Table SI.

For enzymatic mapping experiments, human glioma samples (*IDH1*^{R132H}, n=7; *IDH*^{wt}, n=5, all astrocytomas) were obtained from the tumour archive maintained by the Departments of Neurosurgery and Neuropathology of the Academic Medical Centre (Amsterdam, The Netherlands). Written consent for tissue storage in the tumour bank for research purposes was obtained and documented in the patients' medical records and approved by the Medical Ethics Review Committee of the Academic Medical Centre at the University of Amsterdam (reference number W14_224 # 14.17.0286).

Targeted RNA next generation sequencing

Enzymes were from New England Biolabs (NEB; Ipswich, MA) unless indicated otherwise. Total RNA was isolated from glioma cryostat sections with documented percentages cancer cells

(see Table SI), using the standard TRIzol method. After treatment with DNase, 1 µg of RNA was reverse transcribed using Superscript II according to routine protocols in a volume of 20 µl. Fifty ng of cDNA was used for targeted next generation sequencing (NGS) according to a recently described method using single-molecule Molecular Inversion Probes (smMIPs) [312]. In short, smMIP-based NGS is based on the hybridization of an extension and ligation probe, joined by a backbone sequence, in an inverted manner to a cDNA of interest, followed by gap-filling/ligation and PCR. SmMIPs against the antisense strand of 104 predicted transcripts (UCSC human genome assembly hg19), encoding enzymes involved in lipid metabolism, glycolysis, oxidative phosphorylation (OXPHOS), TCA cycle, pentose phosphate pathway (PPP), glutaminolysis and control of reductive potential were designed on the basis of the MIPgen algorithm as described by Boyle *et al.* [358]. For each transcript, a minimum of 5 smMIPs targeting different regions were included in the panel to compensate for inter-smMIP variations in efficiency. In case mutations in a transcript were expected, extension and ligation probes in smMIPs were selected to flank the area with the potentially variant nucleotide. If possible, smMIPs were included with ligation and extension probes located on adjacent exons to ensure a reaction with matured mRNAs. The smMIP set also contained probes for detection of β-actin and β-tubulin as housekeeping gene transcripts.

Libraries were generated with a procedure adapted from O'Roak *et al.* [317]. In short, a total of 642 smMIPs (IDT, Leuven, Belgium) were pooled at 100 µM/smMIP. The smMIP pool was phosphorylated using T4 polynucleotide kinase in T4 DNA ligase buffer at 37°C for 45 min, followed by enzyme inactivation for 20 min at 65°C. The capture reaction was performed with 50 ng of cDNA and an estimated 8000-fold molar excess of the phosphorylated smMIP pool [300] in a 25 µL reaction mixture containing Ampligase buffer (Epicentre, Madison, WI), dNTPs, Hemo KlenTaq enzyme and thermostable DNA ligase (Epicentre). The capture mix was incubated for 10 min at 95°C (denaturation), followed by incubation for 18 h at 60°C, during which hybridization and concomitant primer extension and ligation occurred. Immediately after this step, non-circularized smMIPs, RNA and cDNA were removed by treatment with 10 U exonuclease I and 50 U of exonuclease III for 45 min at 37°C, followed by heat inactivation (95°C, 2 min). The circularized smMIP library was subjected to standard PCR with 2x iProof High-Fidelity DNA Polymerase master Mix (Bio-Rad, Hercules, CA) with a backbone-specific primer set containing a unique barcoded reverse primer for each sample. Generation of PCR products of the correct size (266 bp) was validated on agarose gel electrophoresis, and PCR libraries of different samples were pooled based on relative band intensity. The pool was then purified using AMPureXP beads (Beckman Coulter Genomics, High Wycombe, UK) according to manufacturers' instructions. The purified library was run on a TapeStation 2200 (Agilent Technologies, Santa Clara, CA) and quantified via Qubit (Life Technologies, ThermoFisher Scientific, Waltham, MA) to assess quality of the library.

Sequencing and annotation

Libraries were sequenced on the Illumina NextSeq platform (Illumina, San Diego, CA) at the Radboudumc sequencing facility to produce 2x 150 bp paired-end reads. Reads were

mapped to the reference transcriptome (hg19) using the SeqNext module of JSI SequencePilot version 4.2.2 build 502 (JSI Medical Systems, Ettenheim, Germany). The random 8 nt sequence flanking the ligation probe was used to reduce PCR amplicates to one original hybridized and circularized smMIP (unique reads), making the assay quantitative. Transcript levels were expressed as fragments per million (FPM), calculated by $\frac{mean\ \#\ unique\ smMIPs\ per\ transcript * 10E6}{total\ \#\ unique\ smMIPs\ in\ sample}$. Nucleotide calling was considered reliable when a coverage >10 was achieved.

The profiling test delivers for each sample a list of quantitative values for each detected gene transcript in mean fragments per million (mean FPM) and a list of base variations that are found after annotation of all reads.

Data processing

Unsupervised cluster analysis was performed with R, using log transformed gene expression values (mean FPM+0.01, to prevent taking the logarithm of 0), Manhattan distance to calculate the distance between gene expression profiles, and Ward's method for agglomerative clustering. Based on base calling using the SeqNext software package (with hg19 as reference human transcriptome) and histopathology diagnosis, we annotated each sample as *IDH*^{wt} or *IDH1*^{R132H} astrocytoma, oligodendroglioma or glioblastoma.

Whole transcriptome RNA next generation sequencing

Whole-transcriptome RNAseq of E478 xenografts (derived from oligodendroglioma; *IDH1*^{R132H}), E434 xenografts (derived from oligodendroglioma, *IDH1*^{wt}) and E98 xenografts (derived from astrocytoma) and E98^{FM} and E98$^{FM\text{-}IDH1\text{-}R132H}$ cell lines [208, 212] was performed at ServiceXS (Leiden, The Netherlands). Samples were prepared using the NEBNext Ultra Directional RNA Library Prep Kit for Illumina (NEB #7420S/L). Ribosomal RNA was removed using the NEBNext rRNA removal kit. After fragmentation of the rRNA-depleted RNA, cDNA synthesis was performed, after which sequencing adapters were ligated and PCR was performed. The quality and yield of the product was measured with a fragment analyzer. Size of the resulting products was consistent with the expected size distribution of 300-500 bp. Sequencing was performed on an Illumina NextSeq500 and yielded 40-60 million reads per sample (single-end sequencing protocol). The dataset was analysed using the 'Tuxedo' protocol [359]; reads were mapped against the RefSeq human genome (hg19) with TopHat and final transcript assembly was performed with the Cufflinks package [359]. For xenografts, mouse reads were filtered from the data sets using Xenome [360] prior to the 'Tuxedo' protocol. Transcript values were expressed as FPKM (fragment per kilobase per million human reads). Since all sequencing data were obtained during the same Illumina run, comparison of FPKM values between samples was allowed.

Gene Set Enrichment Analysis (GSEA) was run based on genes sorted on the ratio of their FPKMs between E478 and E434, using the Reactome pathways as gene set, an False Discovery

Rate (FDR) of 0.05, and run in the "classic" mode (http://software.broadinstitute.org/gsea/index.jsp) [361].

Metabolic mapping of GLUD and GLS activity and immunohistochemical GLUD and GLS stainings

All chemicals were from Sigma-Aldrich (St. Louis, MO), unless stated otherwise. Maximum production capacities of glutaminolysis enzymes were investigated by metabolic mapping of clinical glioma tissue and glioma xenografts [155, 362, 363]. For Glutamate Dehydrogenase (GLUD) activity measurements, 7 µm-thick cryostat sections were dried on microscope slides and incubated for 1 h at 37°C with different concentrations of glutamate (0-10 mM) in 100 mM phosphate buffer (pH 8.0) containing 18% polyvinyl alcohol (PVA), 3 mM NAD^+, 2 mM ADP, 5 mM nitroblue tetrazolium chloride (NBT) and 0.2 mM phenazine methosulphate (PMS). NADH production was measured indirectly via conversion of NBT to water-insoluble formazan. Reactions were stopped after 1 h by incubation of the sections in 100 mM phosphate buffer (pH 5.3) for >30 min at 60°C. After mounting the sections in glycerol/gelatin mounting solution, formazan production was quantified using image cytometry [364]. Images of tissue sections were captured using ImageJ (NIH, Bethesda, MD) on a Vanox-T microscope fitted with a x20 objective (Olympus, Tokyo, Japan) and a Scion cfw-1312 gray scale camera (Scion, Tucson, AZ). Images were recorded at a resolution of 1360x1024 pixels. White light was used for illumination and filtered by an infrared light blocking filter and a 585 nm monochromatic filter [364].

Glutaminase (GLS) activity in cryostat sections was measured indirectly as described before [363]. In short, sections were positioned on glass slides coated with a film containing >40 units bovine GLUD (Serva, Heidelberg, Germany) and incubated with medium containing 18% PVA, 37.5 mM glutamine, 5 mM NBT, 3 mM NAD^+, 2 mM ADP and 0.2 mM PMS. NADH production was quantified indirectly by measuring NBT-formazan production as described above. This method enables zero-order GLUD kinetics and therefore NADH and α-KG are generated stoichiometrically by GLS via GLUD activity. Negative control reactions were performed in the absence of substrate (glutamate and glutamine for GLUD and GLS activity, respectively).

IHC was performed on 4 µm-thick sections of formalin-fixed paraffin-embedded tissue. After epitope retrieval by boiling in Tris-EDTA buffer, pH 9.0 (Klinipath, Duiven, The Netherlands), sections were stained with rabbit-anti-GLUD1/2 (Cell Signaling Technologies, Danvers, MA #12793), rabbit anti-GLS (Abcam, Cambridge, UK, ab156876) or rabbit anti-human vimentin (Thermo Scientific, MA5-16409). Primary antibodies were detected using BrightVision polyHRP-anti-rabbit IgG (Immunologic, Duiven, The Netherlands). All IHC-stained sections were counterstained with haematoxylin and mounted in Quick-D mounting medium (Klinipath, Duiven, The Netherlands). For all tissue samples, control staining with secondary antibody-only was performed.

TCGA datamining

RNA expression data *of* IDH^{wt} (N=112) and $IDH1^{R132H}$ *(*N=399) was analysed as described previously [354].

Xenograft models

All animal experiments were approved by the local committee for animal welfare of the Radboud University. The patient-derived orthotopic $IDH1^{R132H}$- and IDH^{wt}-xenograft models E478 and E434 have been described before and were maintained by direct serial transplantation in BALB/c nude mice (Janvier Labs, Le Genest-Saint-Isle, France) [54, 208, 243]. Expression of $IDH1^{R132H}$ in the different models was validated by western blotting of cell extracts and by *D*-2-HG measurements via liquid chromatography mass spectroscopy (LC-MS, Quattro LC, Micromass, Waters, Milford, MA) [215]. Mice presenting with tumour-related symptoms were sacrificed and brains were harvested. After trimming of macroscopically unaffected brain, tumours were processed to cell suspensions (see below).

In vivo MRSI

Healthy mice (n = 3) and mice carrying E478 and E434 xenografts (n = 5 for each model) were subjected to *in vivo* magnetic resonance spectroscopic imaging (MRSI) [268]. Animals were anesthetized using an isoflurane/N_2O/O_2 mixture and investigated on a 7T MR system (ClinScan, Bruker, Ettlingen, Germany) with a dedicated mouse brain transmit-receive-coil. Breathing of the mice was monitored throughout the MR experiment, and body temperature was maintained at 37.5°C using a continuous flow of warm air (SA Instruments, Stony Brook, NY). The presence of tumour was verified in retrospect by comparing T2-weighted MR images to hematoxylin-eosin staining of corresponding brain sections. Guided by these MR images, voxels of interest (VOI) were selected for further analysis while preventing partial volume artifacts.

3D MRSI was performed with a semi-LASER short echo time (TE = 24 ms, n = 5) and a long echo time (TE = 144 ms, n = 3) sequence using a 12x12x16 elliptical weighted phase encoding scheme, interpolated to 16x16x16. The 11x11x16 mm FOV contained 0.85 mm^3 nominal voxels. For all measurements, the repetition time (TR) was set at 1500 ms. Water signal was suppressed using WET over a bandwidth of 120 Hz and residual signals from surrounding fat and bone tissue were suppressed with 1 mm thick saturation slabs. The RF saturation pulse was positioned at -3.40 ppm relative to the water resonance. Four averages were acquired; total acquisition time was 28 minutes. A non-water suppressed short TE dataset was acquired (1 average) for calibration of the metabolites to the water signal. For absolute quantification we used known T1 and T2 relaxation times available from literature [365-367]. Water content was assumed to be 79% [368]. As an anatomical reference, multi-slice T2-weighted images were made in 3 directions parallel to the MRSI grid.

Unfiltered spectra in the chemical shift range of 0.5 – 4.2 ppm were fitted with LCModel software [369] using simulated spectral basis sets of 23 metabolites for 7T with TE = 24 ms (for detection of glutamate and glutamine) or TE = 144 ms (for detection of lactate and N-acetylaspartate). Cramér Rao Lower Bound (CRLB) values were reported for all integrated peak values. In case peak intensities could not be assessed independently (metabolite correlation coefficient (MCC) << -0.3), values were excluded from analysis (http://s-provencher.com/pub/LCModel/manual/manual.pdf).

Statistical analysis

Statistically significant differences between gene expression levels in IDH^{wt} and $IDH1^{R132H}$ gliomas were identified using the Mann-Whitney U-test. Associations between mutations and clusters were calculated using Fisher's exact test. Multiple testing corrections were performed for the association of identified mutations with IDH^{wt} and $IDH1^{R132H}$ using Benjamini-Hochberg with an FDR of 0.01. Heatmaps of mean FPM values for each transcript were generated using heatmap.2 in R.
Statistical analyses for enzymatic mapping assays and proliferation rates were performed in Graphpad Prism v5.03 (GraphPad Software, LaJolla, CA). P-values are marked as follows: <0.05 (*); <0.01 (**); <0.001 (***), <0.0001 (****). For MRSI data analysis, a two-sided unpaired T-test was performed, assuming normal distribution.

Results

Metabolic gene expression profiles separate gliomas in two groups

To map metabolic pathways, we applied quantitative targeted RNA deep-sequencing of 104 metabolic gene transcripts [312] to 66 clinical gliomas. Unsupervised agglomerative clustering of the gene expression data separated the cohort into 2 main groups A and B (Figure 2a). Among mutations that discriminated these groups, $IDH1^{R132H}$ and a variety of SLC2A3 mutations stood out (Fishers' exact test, $p<10^{-11}$; Table SII). A representative example of a detected $c.IDH1^{G395A}$ mutation is shown in Figure 2b. IDH^{mut} astrocytomas and oligodendrogliomas clustered together showing that the major differences in metabolic gene expression profiles among the gliomas studied were not related to histopathological characteristics (see histological type annotation in Figure 2a). Of note, we also identified other amino acid alterations than R132H in IDH1 (1 case of heterozygous $IDH1^{Y183C}$ of unknown significance [370] and 6 cases of $IDH1^{V78I}$, a known polymorphism) [371]. These variants clustered with the group of IDH^{wt} tumours (annotated as IDH-other in Figure 2a). Four cases with IDH2 mutations ($IDH2^{R172K}$, $IDH2^{R172W}$, $IDH2^{R172M}$, all known to produce *D*-2-HG [372]) grouped with $IDH1^{R132H}$-mutated gliomas (annotated as IDH-other in group A). In all cases, the $IDH1^{R132H}$ and IDH2 mutations were in retrospect confirmed by standard genetic analysis (Table SI).

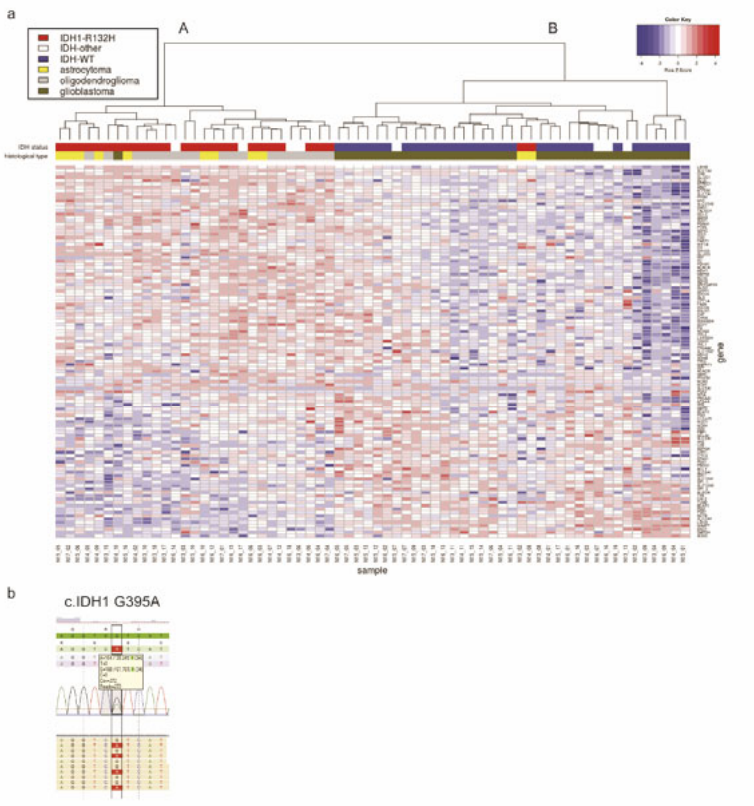

Figure 2: Targeted RNAseq of human glioma samples. *a) Heatmap and unsupervised hierarchical clustering of metabolic genes in 66 sequenced clinical gliomas. Gene expression levels (as fragment per million) were transformed to a Z-score for each gene transcript. The dendrogram at the top is based on gene expression and has been derived using Ward's method (see Materials and Methods). The IDH1^{R132H} mutation strongly correlates with gene expression cluster A. IDH mutations other than IDH1^{R132H} (annotated as IDH-other in the annotation bar) are shown in Table SI. b) SeqNext sequence analysis output showing the c.IDH1 G395A mutation, leading to IDH1R132H*

The metabolic transcriptome reveals high expression levels of glutamine/glutamate/GABA-processing enzymes in clinical IDH1^{R132H}-glioma

To investigate in more detail how the IDH1^{R132H} mutation affects metabolism, we performed a comparative analysis of the gene expression profiles of *IDH^{wt}* and *IDH1^{R132H}* gliomas (Table SIII). Because functional studies on IDH1^{Y183C} and IDH1^{V78I} are lacking, we did not include these tumours in these analyses. In the *IDH1^{R132H}* group, levels of transcripts encoding glucose-processing transporters or enzymes were strongly reduced in comparison to the *IDH^{wt}* group. Assuming a false discovery rate of 0.01, the genes being differentially lowly expressed in *IDH1^{R132H}*-gliomas included those encoding glucose transporter 3 (GLUT3/*SLC2A3;* fold change (FC) = -3.2; p<0.0001), hexokinase 2 (*HK2;* FC=-5.6; p<0.0001) and lactate dehydrogenase A

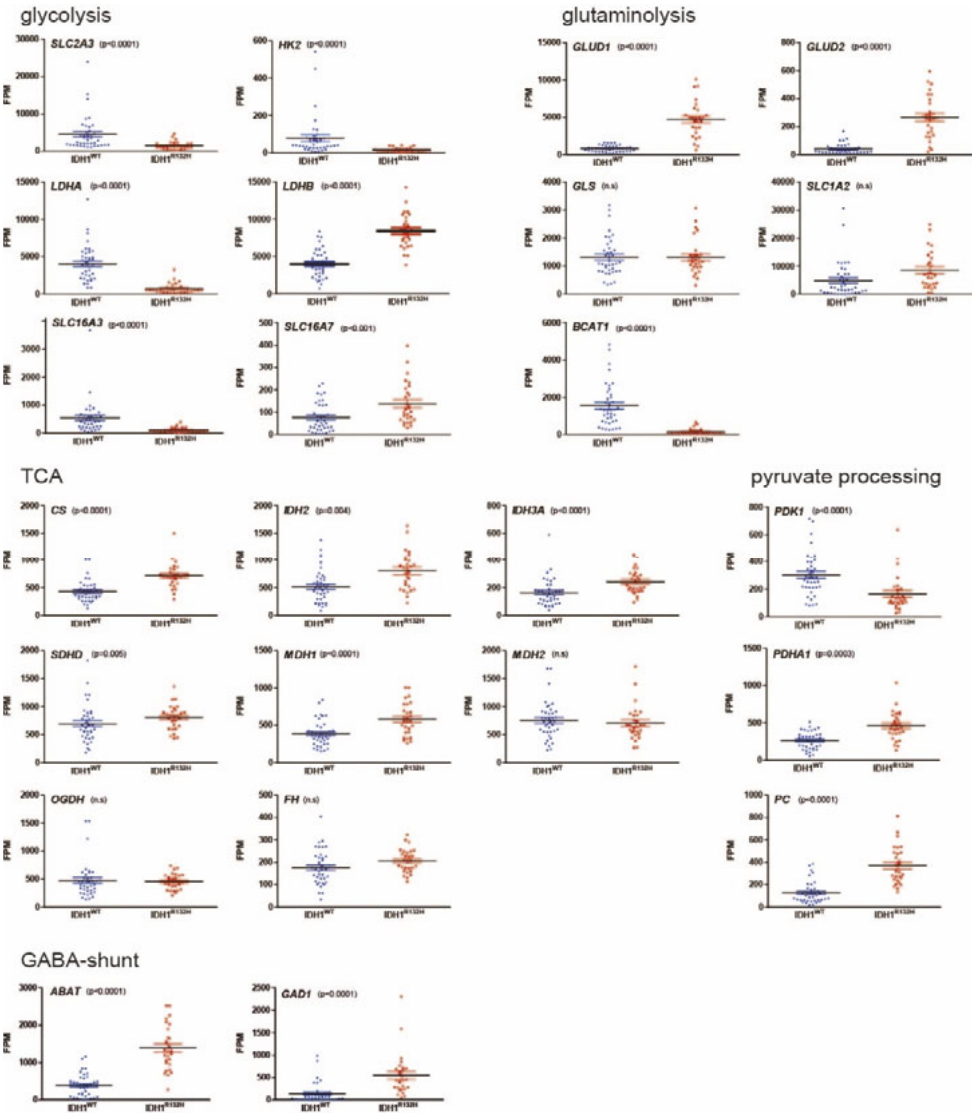

Figure 3: Overview of gene expression levels of enzymes in the metabolic pathways depending on IDH status. *Boxplots of expression of genes involved in glycolysis, glutaminolysis, TCA, pyruvate processing enzymes and GABA shunt, expressed as fragments per million (FPM). Note that IDH1^{R132H}-mutated gliomas express significantly higher levels of genes involved in glutaminolysis, whereas in IDH1^{wt} gliomas a glycolytic metabolotype is more prominent. IDH1^{wt} glioma cells display the typical Warburg effect by upregulating transporters and enzymes involved in glycolysis, such as GLUT3 and HK2, to ultimately generate pyruvate. Pyruvate can either be metabolized to lactate by LDH-A and exported out of the cell, or can feed into the TCA via Ac-CoA through the activity of pyruvate dehydrogenase (PDH). IDH1^{mut} cells express high levels of glutamate importer EAAT2 (SLC1A2) suggesting glutamate import and GLUD-dependent production of α-KG that may enter the TCA. Increased levels of the lactate importer MCT2, LDHB and PC suggest that alternatively, lactate from the tumour environment is used to produce pyruvate that is converted to oxaloacetate (OAA) by pyruvate carboxylase (PC) as a TCA shortcut. P-values were calculated with the Benjamini-Hochberg procedure.*

(*LDH-A;* FC= -5.7; p<0.0001) (Figure 3 and Table SIII, a negative FC represents lower and a positive FC higher expression in *IDH1*^{R132H}-gliomas). *SLC16A3*, the gene encoding monocarboxylate transporter 4 (MCT4), an exporter of lactate that is expressed on hypoxic/glycolytic cells [243], was also significantly lower in *IDH1*^{mut} glioma (FC= -4.4; p<0.0001), whereas *SLC16A7*, the gene encoding the lactate/pyruvate importer MCT2, was expressed at significantly higher levels in *IDH1*^{mut} gliomas (FC= 2.2; p<0.001). Expression of GLUD1 and GLUD2 was significantly elevated in *IDH1*^{mut} gliomas (FC= 5.4 and 7.1 respectively, both p<0.0001), whereas expression levels of GLS did not differ between groups (p=0.608; Figure 3). *SLC1A2*, the gene encoding glutamate importer EAAT2, was expressed at higher levels in *IDH1*^{mut} gliomas (FC= 1.7; p=0.008, FDR=0.006). Levels of transcripts encoding BCAT1, the enzyme catalysing the reversible conversion of α-KG to glutamate, were close to zero in *IDH*^{mut} gliomas in contrast to *IDH*^{wt} gliomas (FC= -8.3; Figure 3; p<0.0001). This corroborates reports that the BCAT1 promoter is inactivated by hypermethylation in *IDH1*^{mut} glioma [280, 354]. Expression levels of the majority of enzymes involved in the TCA cycle were significantly higher in *IDH*^{mut} gliomas [citrate synthase (CS), FC= 1.8; p<0.0001; IDH2, FC= 1.5; p=0.004; IDH3A, FC= 1.7 p<0.0001 and malate dehydrogenase 1 (MDH1), FC= 1.7; p<0.0001, Figure 3].

In our targeted RNA sequencing panel, we also assessed expression levels of genes encoding enzymes that are responsible for pyruvate metabolism in mitochondria. Whereas pyruvate dehydrogenase (*PDHA1)* expression was significantly higher (FC= 1.7, p=0.0003), expression of its inhibitor enzyme pyruvate dehydrogenase kinase (*PDK1*) was significantly lower in *IDH1*^{mut} compared to *IDH1*^{wt} (FC= -1.9, p<0.0001). Pyruvate carboxylase (*PC*), the enzyme responsible for production of oxaloacetate that has an anaplerotic role in the TCA cycle, was significantly higher in *IDH1*^{mut} gliomas (FC= 2.7, p<0.0001) (Figure 3).

Two other metabolic genes that are highly upregulated in *IDH1*^{mut} gliomas are the GABA shunt enzymes glutamate decarboxylase 1 (GAD1, FC 4.4, P<0.0001), and ABAT (FC = 3.9, p<0.001), the enzymes converting glutamate to GABA and GABA to succinic semialdehyde, respectively. To confirm these findings and to investigate expression levels of ALDH5A1, the enzyme converting succinic semialdehyde to succinate, the last step of the GABA shunt, Figure 1a, route F), we consulted the TCGA (The Cancer Genome Atlas) database. TCGA expression data confirmed higher expression of GAD1 and ABAT and additionally revealed higher expression of ALDH5A1 in *IDH1*^{mut} glioma, suggesting a higher capacity of *IDH1*^{mut} gliomas to use the GABA shunt for TCA cycle anaplerosis (Figure S1).

In situ metabolic activity mapping suggests glutamate catabolism in IDH1^{R132H} gliomas

To investigate the impact of the altered transcript levels at the functional level, we mapped *in situ* enzymatic activities of GLS1/2 and GLUD1/2 in glioblastoma with known IDH status (Figure 4). GLUD1/2 activity was significantly higher (P<0.01) in *IDH1*^{mut} gliomas as compared to *IDH*^{wt} counterparts whereas, conversely, GLS activity was significantly lower (p<0.05). The high expression levels of glutamate importers and GLUD1/2 and the high activity levels of these

enzymes, combined with lower levels of glutamine- and glucose-processing enzymes, suggest that *IDH1*^{mut} gliomas depend on glutamate, rather than glutamine and glucose, to fuel the TCA cycle. Direct *in situ* detection of ABAT and GAD1 activity via redox reactions was unfortunately not possible using the enzymatic mapping technique.

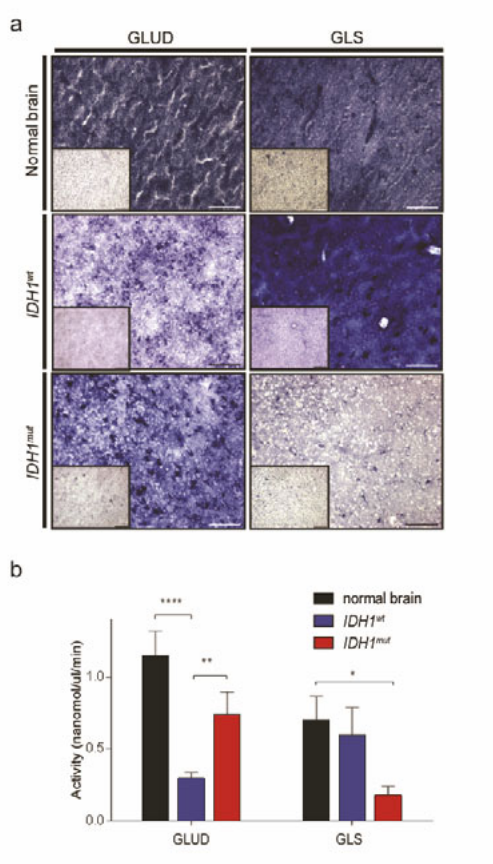

Figure 4: In situ metabolic mapping of GLUD and GLS activity in IDH^{wt} and IDH1^{mut} glioma. a) Representative examples of cryostat sections of normal brain, IDH1^{wt} or IDH1^{mut} gliomas after in situ metabolic mapping of activity of GLUD1/2 and GLS. Production of reduced insoluble formazan salt (blue dye) is used as readout to visualize NADH and NADPH production capacity. b) Quantification of GLUD and GLS activity levels derived from metabolic mapping in IDH1^{wt} (n=5) and IDH1^{mut} (n=7) gliomas. *: p<0.05; **: p<0.01; ***: p<0.0001

Glutamine-glutamate and glucose metabolism in orthotopic IDH1^{mut} glioma model E478 resemble that of clinical IDH1^{mut} gliomas

Glutamine- and glutamate-processing enzymes are part of the glutamine-glutamate cycle and are therefore highly expressed in normal brain astrocytes and neurons [373]. The same holds for the enzymes of the GABA shunt in the brain. To ascertain that the metabolic differences observed between *IDH*^{mut} and *IDH*^{wt} gliomas are attributable to cancer cells and not tumour stroma, we took advantage of the xenograft setting of our patient-derived glioma xenograft models. Whereas it is impossible to discriminate mouse and human enzymes by IHC or enzymatic activity mapping (due to the highly conserved structures of these fundamentally important enzymes), at the nucleotide level the inter-species sequence differences allow reliable distinctions between mouse and human-derived transcripts after processing of the

datasets by the Xenome routine [360]. Our E478 model is a stable, non-engineered xenograft model of *IDH1*^{R132H} glioma [208, 374] whereas E434 was used as a counterpart *IDH1*^{wt} model. Both models have codeletion of chromosome arms 1p and 19q [208], a characteristic of oligodendrogliomas [60]. RNAseq analysis of the human reads in E478 in the Integrative Genomics Viewer (IGV, version 2.3.72, www.broadinstitute.org/igv) identified the IDH1c.G395A mutation in 62% of the reads, in line with a prevalence of 55% of reads as identified in targeted RNAseq (data not shown). Xenome-based RNAseq analysis of the human transcripts in E478 and E434 xenografts confirmed the differences in expression profiles of metabolic genes that we found in our cohort of clinical gliomas, except for the GABA-shunt enzymes GAD1, which was expressed at 4-fold lower levels in E478 than in E434, and ABAT which was expressed at approximately similar levels in E434 and E478 (data not shown). GLUD1 expression was higher in E478 cancer cells than in E434 cells (Figure 5a), whereas BCAT1 expression levels were 28-fold lower. Consistent with the high density of mitochondria in E478 cancer cells [374] and the elevated levels of mitochondrial enzymes in clinical *IDH*^{mut} human glioma samples, TCA cycle enzymes CS, ketoglutarate dehydrogenase (OGDH), succinate dehydrogenases (SDHD), fumarate hydratase (FH), MDH2 and all subunits of the NAD^+-dependent IDH3 were expressed at higher levels in E478 than in E434 cells (Figure 5a). To obtain significant differential expression results at the level of complete pathways, we ran a Gene Set Enrichment Analysis [361] with genes sorted on the basis of the ratio of the gene expression values between E478 and E434 cells. The TCA cycle and oxidative phosphorylation pathways are among the 65 Reactome pathways significantly enriched in E478 xenografts (at an FDR of 0.05, Table SIVa). Glucose transport was among the pathways that were significantly lower in E478 relative to E434 (Table SIVb). Western blotting with a human-specific antibody against BCAT1 (Figure 5b) confirmed low gene expression levels of this enzyme in E478 xenografts compared to E434. Expression of the IDH1^{R132H} mutant protein was also confirmed on western blot (Figure 5b). Increased GLUD expression and activity in E478 cells were verified at the protein and enzyme activity level with the use of IHC and *in situ* metabolic mapping (Figure 5c).

To investigate the relative contributions of glucose and glutamate to the TCA cycle, we investigated gene expression levels of enzymes that determine the fate of glucose. In line with the clinical dataset, the rate-limiting glycolysis enzyme hexokinase 2 (HK2) was expressed 160-fold lower in E478 (*IDH*^{mut}) cells than in E434 (*IDH*^{wt}) cells (FPKM values of 2 and 327, respectively; Figure 5a). Also, with respect to lactate producing enzymes, E478 closely resembled clinical *IDH*^{mut} glioma. LDH-A levels were lower, whereas LDH-B expression levels were higher in E478 cells than in E434 cells. Expression of PC was 4-fold higher in *IDH*^{mut} E478 than in *IDH*^{wt} E434 cells (FPKM values of 436 vs. 114).

Differences in metabolic gene expression levels between E434 and E478 xenografts were largely confirmed using targeted RNAseq (Figure S2).

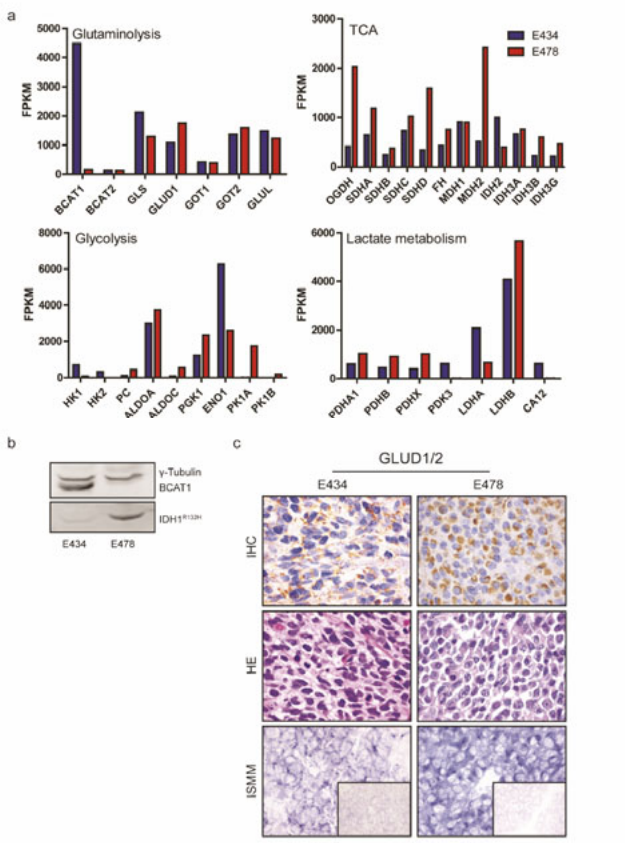

Figure 5: Transcript levels of genes of metabolic enzymes in E434 and E478 xenografts. *Human reads in whole transcriptome RNAseq were mined from the xenografts. For each transcript, levels are expressed as fragments per kilobase per million reads (FPKM). Genes are shown that are involved in glutaminolysis, TCA, glycolysis and pyruvate fate (lactate formation vs. TCA entry), respectively. b) Western blot of E434 and E478 protein extracts, stained with an antibody specific for human BCAT1 and IDH1^{R132H,} confirming low BCAT1 transcript levels in E478-IDH1^{R132H} xenografts at the protein level. γ-Tubulin served as a loading control. c) IHC analysis and in situ metabolic mapping (ISMM) of the glioma xenograft models E434 and E478 for GLUD1/2. Note that GLUD expression levels as determined with IHC (upper panels), and activity as determined with metabolic mapping (lower panels), are considerably higher in E478 as compared to GLS. Inserts represent control metabolic mapping staining patterns in the absence of substrate*

In vivo MRSI

Metabolic activity is a net result of a combination of factors, among which concentrations of substrate and product, availability of cofactors such as NAD(P)(H), and enzyme concentrations. Furthermore, enzyme activity is determined by enzyme stability at the protein level. Therefore, to test whether the highly significant differences in the metabolic transcriptome of *IDH^{mut}* and *IDH^{wt}* gliomas have bearing on metabolic pathways in cancer, we performed *in vivo* MRSI on mice carrying orthotopic E478 and E434 xenografts. The tumour

location in the brain of mice as observed on T2-weighted anatomical MR images matched with H&E-stained histopathological sections (Figure 6a). Analysis of spectra of selected voxels in the brain showed that the neuronal signals of N-acetylaspartate and N-acetylaspartate-glutamate, collectively termed tNAA, were almost absent in tumour tissue of both xenograft models, which is in agreement with recent *in situ* metabolome analyses [375]. The signal of lactate is inverted at TE = 144 ms and could be detected properly in all animals. We observed distinctly lower lactate concentrations in E478 than in E434 xenografts which is in line with the low LDH-A:LDH-B RNA ratios in *IDH*^{mut} E478 xenografts (Figs. 5a and 6a).

The levels of glutamine and glutamate were assessed from short echo time spectra (TE = 24 ms). Even though these resonances partially overlapped with other metabolites between 2.0 and 2.4 ppm, we successfully detected glutamine and glutamate in all selected E478 tumour voxels. Glutamine levels in E434 xenografts were substantially lower than in normal brain, suggesting glutamine usage in this model. In contrast, in *IDH*^{mut} E478 xenografts higher levels of glutamine were detected as compared to normal brain, whereas glutamate levels were significantly lower than in normal brain tissue, suggesting that in *IDH*^{mut} tumours glutamate is consumed, while glutamine is not processed and accumulates (Figure 6b).

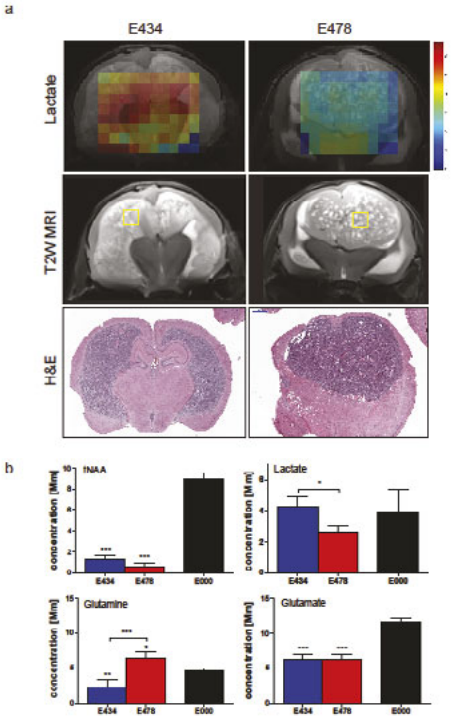

Figure 6: In vivo multivoxel magnetic resonance spectroscopic imaging (MRSI) of E434 and E478 xenografts. *a) Local concentrations of lactate, as determined with MRSI, mapped to corresponding T2-weighted MR images. Left column: E434 (IDH*^{wt}*), right column: E478 (IDH1*^{R132H}*). The middle panel shows an example of selected voxels for analysis of tumour tissue (yellow). The bottom panel shows corresponding H&E-stained sections. b) Quantification of tNAA, lactate, glutamine and glutamate levels in both xenografts and healthy mice, based on MRSI data. Values represent the mean concentrations (± standard error) of metabolites in tumour-related quantifiable voxels in 3 or 5 mice per model, and in 3 healthy animals. Asterisk (*) without a bar indicates significantly different levels of the metabolite relative to healthy brain (E000), whereas asterisks with a bar indicate significantly different metabolite levels of E434 relative to E478.*

Discussion

Since the discovery that *IDH1* mutations occur frequently in diffuse gliomas, research has focused on unravelling the effects of *D*-2-HG on epigenetics and metabolism [96, 122]. Recognizing the important role of this oncometabolite in glioma development [376] specific inhibitors of mutant IDH function have been developed [155]. These inhibitors prevent *D*-2-HG production and, supposedly, tumour initiation. In established tumours, these inhibitors prevent NADPH oxidation to $NADP^+$. NADPH oxidation is thought to increase tumour radiosensitivity and prolong patient survival [350]. Application of mutant IDH inhibitors may therefore counteract the prognostically-favourable characteristics of the IDH1 mutation by normalizing redox status and *reducing* metabolic stress [349]. From a therapeutic perspective, it should be advantageous to instead *increase* metabolic stress. This requires detailed knowledge of metabolic pathways in these tumours *in vivo*. Here, we present data that give important insight in the metabolic relationships between IDH^{mut} glioma cells and the brain microenvironment.

Using datasets from The Cancer Genome Atlas we previously showed that metabolic differences between IDH^{wt} and IDH^{mut} gliomas can be inferred from transcriptome analyses [354] which makes sense as the transcriptome is to a large extent correlated with the proteome [377]. Therefore we performed targeted next generation sequencing of transcripts of metabolic genes [312] and confirmed protein expression for a number of associated transcripts. Bioinformatic analysis of the resulting 66 tumour metabolic gene expression profiles readily separated the cohort in two groups. Further analyses revealed that this grouping was associated with the IDH mutation status with high significance.

Based on our data, we propose a metabolic model in which cells adapt to $IDH1^{R132H}$–induced metabolic stress by increasing mitochondrial metabolism and anaplerotic feeding of the TCA cycle at different entry points. Figure 7 depicts these proposed metabolic fluxes in a model of IDH^{wt} and IDH^{mut} glioma metabolism. First, increased expression of PC serves to shuttle as much pyruvate as possible into the TCA cycle via oxaloacetate, simultaneously preventing the energy-inefficient flux from pyruvate to lactate. Because IDH^{mut} -gliomas are inefficient in processing glucose (our data and (34)), the question is what fuels pyruvate production. The high expression levels of the lactate importer MCT2 and LDHB in IDH^{mut} gliomas suggest that these cancer cells import lactate from the tumour microenvironment to produce pyruvate. Use of lactate as a fuel by cancer cells is not unique; similar results were recently reported for non-small cell lung cancer [378]. Furthermore, in normal brain physiology lactate is continuously produced by astrocytes and oligodendrocytes to fuel neurons [379-381].

In addition to increased transporter and enzyme levels involved in lactate catabolism, we found that GLUD1 and GLUD2 were expressed at significantly higher levels in IDHmut gliomas in comparison to IDHwt glioma, endowing these with the capacity to directly convert glutamate to α-KG, producing ammonia as by-product (Figure 1 and 7). Interestingly, astrocytes release lactate in response to increased ammonium levels [382]. This combination

of metabolic adaptations thus creates a triple entry point for metabolites into the TCA cycle via lactate-pyruvate derived oxaloacetate and GLUD-derived α-KG. The high expression levels of GAD1, ABAT and SSADH in clinical IDHmut gliomas were not reproduced in the E478 model, making it difficult to assign a role for the GABA shunt as anaplerotic flux in direct relation to the IDH mutation.

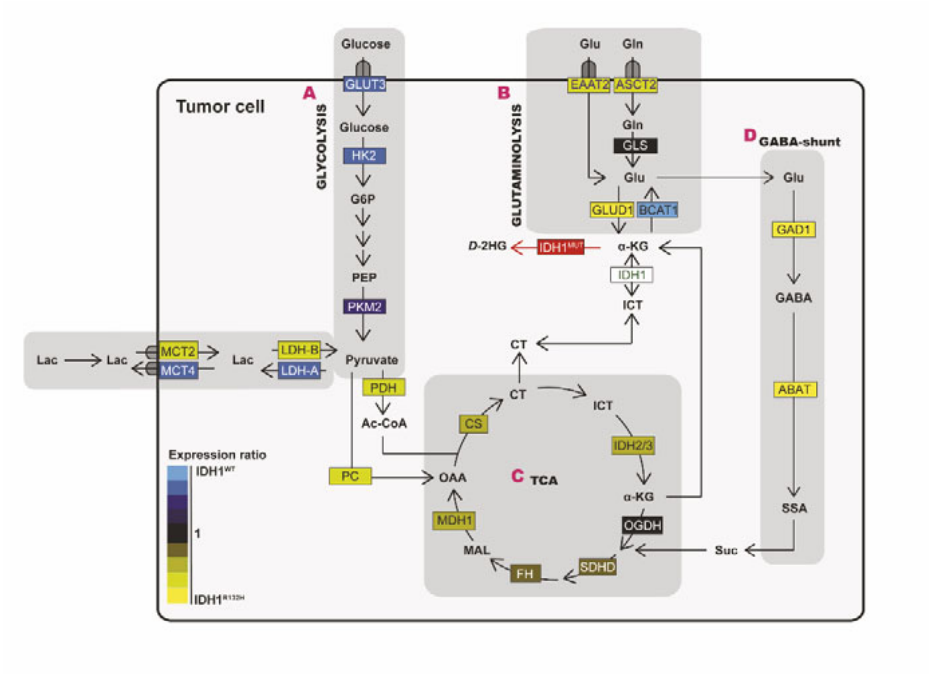

Figure 7: Cartoonized expression levels of genes involved in glycolysis (A), glutaminolysis (B), TCA cycle (C) and GABA-shunt (D). *$IDH1^{wt}$/$IDH1^{R132H}$ ratios were calculated on the basis of gene expression levels to indicate the relative contribution to a particular pathway. Genes in blue indicate higher gene expression in $IDH1^{wt}$ gliomas, whereas yellow indicates higher gene expression in $IDH1^{R132H}$-mutated gliomas. ABAT γ-Aminobutyrate aminotransferase; Ac-CoA Acetyl-CoA; aKG Alpha-ketoglutarate; ASCT2 Anti-neutral amino acid transporter 2; BCAT Branched-chain amino acid transaminase; CS Citrate synthase; CT Citrate; D-2HG D-2-hydroxyglutarate; EAAT2 Excitatory amino acid transporter 2; F6P Fructose-6-phosphate; FH Fumarate hydratase; G6P Glucose-6-phosphate; GABA γ-Aminobutyric acid; GAD1 Glutamate decarboxylase 1; Gln Glutamine; GLS Glutaminase; Glu Glutamate; GLUD Glutamate dehydrogenase; GLUT3 Glucose transporter 3; HK2 Hexokinase 2; ICT Isocitrate; IDH Isocitrate dehydrogenase; LDH Lactate dehydrogenase; MCT Monocarboxylate transporter; MDH1 Malate dehydrogenase1; OAA Oxaloacetate; OGDH α-Ketoglutarate dehydrogenase; OXPHOS Oxidative phosphorylation; PC Pyruvate carboxylase; PDH Pyruvate dehydrogenase; PEP Phosphoenolpyruvate; PKM Pyruvate kinase M; SDHD Succinate dehydrogenase D; SSA Succinic semialdehyde; Suc Succinate; TCA Tricarboxylic acid cycle.*

Our findings favour a model of an intimate relationship between *IDH^{mut}* cancer cells and stromal cells, in which cancer cells import neuron-derived glutamate (and possibly GABA) for conversion to α-KG (and possibly succinate) and produce ammonia during glutamate processing. Ammonia triggers lactate release by astrocytes in the tumour stroma, which is

then imported by the cancer cells, resulting in a glutamate-lactate shuttle (Figure 7). This model is supported by our *in vivo* MRSI data in Figure 6 revealing a) low levels of lactate in E478 xenografts in comparison with E434 xenografts and normal brain, in line with lactate consumption; b) high levels of glutamine in E478 xenografts in comparison to normal brain and E434 xenografts, in line with lack of glutamine consumption and c) low levels of glutamate in E478 as compared with normal brain, suggesting glutamate consumption [383]. Increased lactate and decreased glutamine and glutamate levels in E434 xenografts, combined with the gene set enrichment analyses and targeted RNAseq profiles suggest that these IDH^{wt} xenografts are dependent on glucose and glutamine for pyruvate and α-KG production.

Our findings assign a role to glutamate and lactate in the brain as chemotactic fuels for IDH^{mut} glioma cells. The search and use of these neuron- and astrocyte products by tumour cells may explain the diffuse invasive character of IDH^{mut}-gliomas [59, 384].

Conclusions

Results from a variety of independent technologies suggest that IDH^{mut} gliomas depend on lactate and the neurotransmitter glutamate as metabolic substrates to rescue cells from the metabolic stress that results from defective isocitrate processing. Whereas glutaminolysis has been suggested as a promising target in IDH^{mut} cancers [122], our data pinpoint glutamatolysis by GLUD as preferred therapeutic targets.

It is important to realize that the approach that we have used in this work is correlative in nature with conclusions being based on differential expression of metabolic genes between clinical IDH^{mut} and IDH^{wt} tumours. Because metabolic gene expression is not necessarily correlated with metabolic enzyme activity, it will be important to validate our conclusions by performing metabolic flux analysis in clinically relevant models of IDH^{mut} and IDH^{wt} glioma, or detecting the relevant metabolites *in vivo* in clinical gliomas using magnetic resonance spectroscopic imaging. If glutamate indeed is an essential carbon source for IDH^{mut} gliomas, pharmacological inhibition of glutamate processing in IDH^{mut}-cells is expected to prevent mitochondrial metabolism and to reduce levels of NADPH, inducing energy crisis and sensitizing cells to chemotherapy and radiation therapy. Experiments to test these concepts are currently ongoing in our lab. An intriguing question is to what extent these metabolic adaptations are specific for gliomas. It would be highly interesting to investigate metabolic adaptation in other IDH^{mut} tumour types that cannot rely on brain-specific metabolites such as neurotransmitters and lactate.

Declarations

Ethics approval

Studies on patient material were approved by the local Medical Ethics Review Committee of the Academic Medical Centre at the University of Amsterdam (reference number W14_224 # 14.17.0286) and Radboudumc (reference number NL nr 37097.091.11). Animal studies were

approved by the Animal Experiment Committee of Radboud University (reference number 2014-18).

Availability of data and materials:

The datasets generated and/or analysed during the current study are available from the corresponding author on reasonable request.

Competing interests: All authors have declared that no conflict of interest exists.

Funding: This work was supported by Dutch Cancer Society grant UvA 2014-6839 (KL, MK), by Stichting StopHersentumoren (CNAMvdH) and Eurostars (CNAMvdH, WL). RJM was supported by an AMC PhD scholarship. THP was supported by EFRO/GO project Ultrasense NMR.

Authors' contributions

MtL collected surgical material, BK assessed tumour sections and provided histological diagnoses. KV and SvL did IHC stainings. TP and KL performed and analysed in vivo MRSI studies. MK and DB performed and analysed ISMM experiments. CvdH, TdB were responsible for the smMIP assay. WL, RM, RH, PS, WJAJH and RvN designed and interpreted experiments. AvE wrote R-scripts used for smMIP analysis. WL, MH and KL were responsible for analysis. KL, WL wrote the manuscript. All authors read and approved the final manuscript.

Acknowledgements

We thank Dr Alex Hoischen for helpful discussions. Carlijn van de Water is acknowledged for the help with smMIP design.

Supplementary material

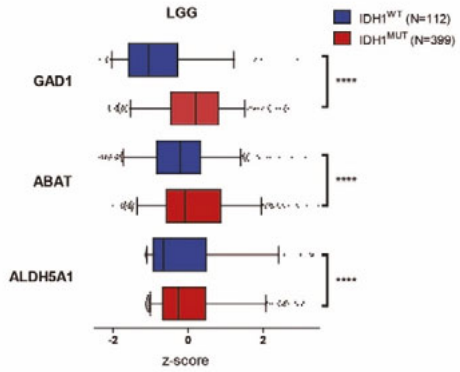

Supplementary Figure 1: TCGA datamining of the gene expression levels of GABA-shunt in low-grade glioma. a) Gene expression of genes involved in the GABA-shunt in low-grade glioma (LGG). GAD1, ABAT, and ALDH5A1 are significantly (P<0.0001) upregulated in IDH^{mut}-gliomas. ALDH5A1 Succinate semidaldehyde dehydrogenase; GAD1 Glutamate decarboxylase 1 SSA Succinate semialdehyde.

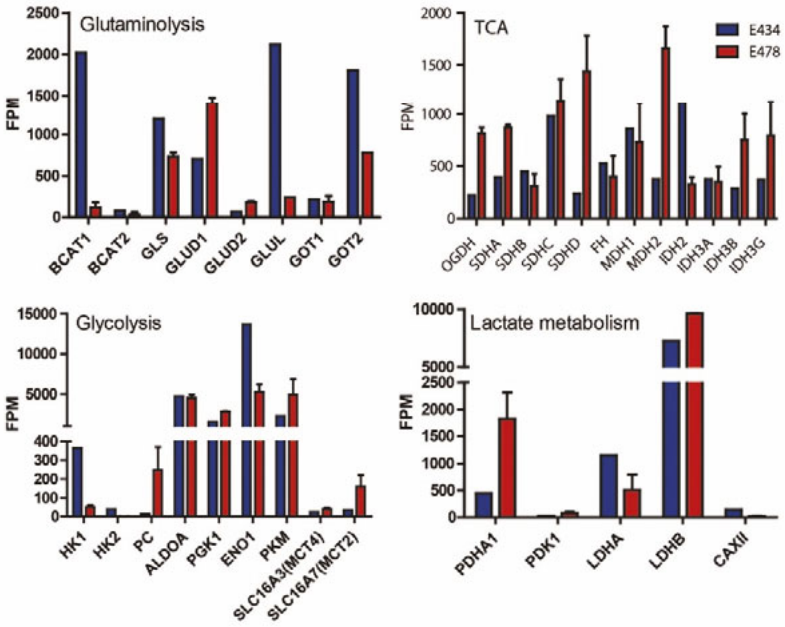

Supplementary Figure 2: Part of the metabolic transcriptome in xenografts E478 and E434 using targeted RNAseq. The same metabolic genes are presented in Figure 5, bt were obtained in different assays (whole transcriptome RNAseq vs. smMIP assay) Data from both assays show the same trends in gene expression.

Supplementary Table I: Clinical information of human glioma samples. Diagnosis, histological type, and percentage tumour cells were confirmed by a trained pathologist. Annotations as marked in this table are used in the heatmap. A students T-test was performed on the $IDH1^{wt}$ vs. IDH^{-R132H} to test differences in percentage tumour cells. There was no significant difference between groups. Abbreviations: M male; F female; WT wild-type; IDH isocitrate dehydrogenase, n/a Not available.

Sample name	Sex	Age (at time of surgery)	Histological type	IDH mutation	% tumour cells
13-02	M	40	Astrocytoma	IDH1-R132H	70
13-03	M	58	Oligodendroglioma	IDH1-R132H	70
13-04	F	62	Glioblastoma	WT	60
13-06	M	53	Oligodendroglioma	IDH2-R172K	60
13-08	M	67	Glioblastoma	WT	70
13-09	F	58	Glioblastoma	WT	70
13-10	M	45	Oligodendroglioma	IDH1-R132H	65
13-11	F	67	Glioblastoma	WT	70
13-13	M	52	Glioblastoma	IDH1-V178I	70
13-15	F	44	Oligodendroglioma	IDH1-R132H	50
13-16	M	60	Glioblastoma	WT	70
13-17	M	45	Oligodendroglioma	IDH1-R132H	50
13-18	F	49	Oligodendroglioma	IDH1-R132H	50
14-01	F	52	Glioblastoma	WT	80
14-02	M	43	Oligodendroglioma	IDH1-R132H	50
14-03	F	62	Glioblastoma	WT	70
14-04	M	72	Glioblastoma	WT	60
14-05	M	21	Oligodendroglioma	IDH1-R132H	70
14-06	M	43	Oligodendroglioma	IDH1-R132H	50
14-07	M	65	Oligodendroglioma	IDH1-R132H	50
14-08	M	50	Astrocytoma	IDH1-R132H	50
14-09	F	43	Astrocytoma	IDH1-R132H	60
14-10	F	45	Glioblastoma	IDH1-R132H	50
14-11	M	50	Glioblastoma	WT	60
14-12	M	59	Oligodendroglioma	IDH1-R132H	50
15-01	M	66	Glioblastoma	WT	50
15-02	F	61	Glioblastoma	WT	70
15-03	F	76	Glioblastoma	WT	40
15-04	F	59	Glioblastoma	WT	40
15-05	M	31	Astrocytoma	IDH1-R132H	70
15-06	F	49	Astrocytoma	IDH1-R132H/V178I	70
15-07	M	63	Glioblastoma	IDH1-V178I	65
15-09	M	70	Glioblastoma	WT	70
15-10	F	68	Oligodendroglioma	IDH1-R132H	70
15-12	M	46	Glioblastoma	WT	70

15-13	F	78	Glioblastoma	WT	80
15-14	M	79	Glioblastoma	WT	70
15-15	F	58	Glioblastoma	WT	70
15-16	M	25	Astrocytoma	IDH1-R132H/V178I	50
15-17	M	68	Glioblastoma	WT	60
15-18	F	64	Glioblastoma	WT	70
16-01	M	61	Glioblastoma	WT	70
16-02	M	47	Glioblastoma	WT	70
16-03	F	46	Astrocytoma	IDH1-R132H	25
16-04	M	59	Oligodendroglioma	IDH1-R132H	60
16-05	M	51	Glioblastoma	WT	50
16-06	F	n/a	Astrocytoma	IDH1-R132H	50
16-07	M	74	Glioblastoma	IDH1-Y183C	60
16-09	F	49	Glioblastoma	WT	70
16-10	M	n/a	Astrocytoma	IDH1-R132H	60
16-11	M	67	Glioblastoma	WT	50
16-12	M	23	Astrocytoma	IDH1-R132H	60
16-13	M	60	Glioblastoma	WT	70
16-14	F	60	Oligodendroglioma	IDH2-R172M	70
16-15	F	61	Oligodendroglioma	IDH1-R132H	70
16-16	M	58	Glioblastoma	IDH1-V178I	40
16-17	F	18	Oligodendroglioma	IDH2-R172K	40
16-18	n/a	30	Oligodendroglioma	IDH2-R172W	70
16-19	M	48	Glioblastoma	WT	70
17-01	M	58	Oligodendroglioma	IDH1-R132H	50
17-02	M	40	Astrocytoma	IDH1-R132H/V178I	70
17-03	F	76	Glioblastoma	WT	65
17-04	M	42	Oligodendroglioma	IDH1-R132H	70
17-05	M	59	Astrocytoma	WT	70
17-06	M	65	Glioblastoma	WT	70
17-07	M	63	Glioblastoma	WT	70

Supplementary table II: Mutation detection in clinical gliomas. A Fisher's exact test was performed to identify gene mutations that distinguished gliomas from cluster A (IDH^{mut}) from cluster B (IDH^{wt}). Mutations were present in at least 10 percent of the reads and were tested for significance with an FDR of 0.01. Cluster A consists of 29 gliomas in total, of which 25 have the $IDH1^{R132H}$ mutation, cluster B consists of 37 gliomas, of which 2 have the $IDH1^{R132H}$ mutation. Genes shown in here were significantly different between the clusters

Gene	Gene mutation	Present in cluster A	Present in cluster B	p-value	FDR
IDH1	p.Arg132His	25	2	6,51E-12	3,06E-05
SLC2A3	p.Glu459Lys	11	0	3,22E-05	6,12E-05

SLC2A3	p.Arg463Ter	11	0	3,22E-05	9,17E-05
SLC2A3	p.Gly471Asp	11	0	3,22E-05	1,22E-04
SLC2A3	p.Asp473Asn	11	0	3,22E-05	1,53E-04
SLC2A3	p.Lys477Argfs*7	11	0	3,22E-05	1,83E-04
SLC2A3	p.Gly479Cys	11	0	3,22E-05	2,14E-04
SLC2A3	p.Glu487Gln	11	0	3,22E-05	2,45E-04
SLC2A3	p.Thr453_Gly455delinsMetCysTyr	10	0	9,49E-05	2,75E-04

Table 2 Supplementary table III: Statistical analysis of differential gene expression of IDH^{R132H}-mutated versus IDH^{wt} glioma. Differential expression was calculated with a Benjamini-Hochberg procedure with a cut-off of 0.01. Analysis was done on predefined clusters based on IDH status, only patient samples with an $IDH1^{R132H}$ mutation validated by routine genetic analysis, and IDH^{wt} samples were included in the analysis. $IDH2^{mut}$, $IDH1^{Y183C}$ and $IDH1^{V178I}$ samples were excluded. P-values that are lower than the FDR-value are significantly different, values higher than the FDR are not significant. Fold change (FC) was calculated by dividing the mean of $IDH1^{R132H}$ by the mean IDH^{wt}. Genes with a value higher than 1 were upregulated in $IDH1^{R132H}$, whereas genes with a negative FC were upregulated in IDH^{wt}. For significance: Y yes; N no

Gene	Mean IDH^{WT}	Mean $IDH1^{R132H}$	p-value	FDR	FC	Significant?
LDHA	4087,22	720,88	1,28E-12	8,93E-05	-5,7	Y
BCAT1	1446,23	174,11	9,43E-12	1,79E-04	-8,3	Y
GLUD1	831,41	4524,64	3,51E-11	2,68E-04	5,4	Y
ABAT	361,07	1395,86	4,32E-11	3,57E-04	3,9	Y
PFKM	506,47	1291,98	6,49E-11	4,46E-04	2,6	Y
GLUD2	36,62	258,38	3,55E-10	0,001	7,1	Y
CS	400,70	734,82	4,25E-10	0,001	1,8	Y
LDHB	3866,22	8394,96	1,19E-09	0,001	2,2	Y
ACACA	225,64	452,38	2,66E-09	0,001	2,0	Y
SLC16A3	463,28	106,12	4,23E-09	0,001	-4,4	Y
PC	132,00	354,96	8,95E-09	0,001	2,7	Y
MAPK8	120,50	314,57	1,20E-08	0,001	2,6	Y
GPI_1	724,37	406,58	1,83E-08	0,001	-1,8	Y
GCLC	246,70	645,51	2,42E-08	0,001	2,6	Y
ATP5C1	1190,22	2570,76	3,17E-08	0,001	2,2	Y
SDHA	640,74	1093,88	3,63E-08	0,001	1,7	Y
CBS	129,40	388,01	4,74E-08	0,002	3,0	Y
ATP5A1	2194,97	3425,85	6,17E-08	0,002	1,6	Y
SOD1	421,18	845,49	7,02E-08	0,002	2,0	Y
ACO2	201,11	403,52	1,17E-07	0,002	2,0	Y
GAD1	135,29	591,27	1,17E-07	0,002	4,4	Y
NAMPT	5299,62	809,82	1,32E-07	0,002	-6,5	Y
PGAM1	457,50	822,34	1,69E-07	0,002	1,8	Y
HK2	84,11	15,01	3,11E-07	0,002	-5,6	Y
IDH3G	333,93	578,63	4,38E-07	0,002	1,7	Y

CA9	99,92	14,99	4,44E-07	0,002	-6,7	Y
GPI_2	1010,88	572,04	6,91E-07	0,002	-1,8	Y
CA12	1204,13	177,35	9,64E-07	0,003	-6,8	Y
PGK1	3665,82	1859,31	1,20E-06	0,003	-2,0	Y
SOD2	19592,75	7735,23	1,20E-06	0,003	-2,5	Y
GOT1	46,48	98,13	1,49E-06	0,003	2,1	Y
SLC2A3	4915,27	1519,43	4,19E-06	0,003	-3,2	Y
L2HGDH	18,77	38,34	4,79E-06	0,003	2,0	Y
PDK1	308,46	161,65	1,60E-05	0,003	-1,9	Y
GAPDH	33503,48	24450,72	1,92E-05	0,003	-1,4	Y
IDH3A	150,13	251,76	3,26E-05	0,003	1,7	Y
D2HGDH	78,12	127,50	3,56E-05	0,003	1,6	Y
PRKAA2	31,56	53,18	4,23E-05	0,003	1,7	Y
GLUL	1867,77	3909,82	4,60E-05	0,003	2,1	Y
SLC9A1	346,61	190,81	4,60E-05	0,004	-1,8	Y
MDH1	362,03	597,48	6,99E-05	0,004	1,7	Y
CHKA	102,00	165,15	8,24E-05	0,004	1,6	Y
SLC7A1	942,50	1538,78	8,24E-05	0,004	1,6	Y
FBP1	55,17	19,00	9,82E-05	0,004	-2,9	Y
SLC16A7	67,67	148,71	1,68E-04	0,004	2,2	Y
MYC	572,05	1109,76	2,45E-04	0,004	1,9	Y
HK3	12,46	3,92	2,46E-04	0,004	-3,2	Y
GCLM	151,80	93,46	3,06E-04	0,004	-1,6	Y
PDHA1	277,19	464,32	3,54E-04	0,004	1,7	Y
FASN	130,05	228,62	0,001	0,004	1,8	Y
GPT	3,55	7,81	0,001	0,005	2,2	Y
CBR1	222,41	118,85	0,001	0,005	-1,9	Y
EGLN1	182,36	255,42	0,001	0,005	1,4	Y
CKB	3483,82	6467,28	0,001	0,005	1,9	Y
NOX4	90,70	47,11	0,001	0,005	-1,9	Y
SDHC	880,22	1184,92	0,001	0,005	1,3	Y
TALDO1	1118,85	1511,38	0,002	0,005	1,4	Y
ENO1	12349,89	8997,88	0,003	0,005	-1,4	Y
TXN	2260,16	1690,50	0,003	0,005	-1,3	Y
NAPRT1	7,01	13,86	0,004	0,005	2,0	Y
GLDC	253,39	389,35	0,004	0,005	1,5	Y
IDH2	525,32	800,42	0,004	0,006	1,5	Y
SDHD	621,27	799,74	0,005	0,006	1,3	Y
FH	170,28	215,34	0,006	0,006	1,3	N
SLC16A1	1116,59	787,48	0,007	0,006	-1,4	N
IDH3B	382,86	502,88	0,008	0,006	1,3	N
PKM	5023,68	3856,18	0,008	0,006	-1,3	N
PTEN	548,24	821,28	0,008	0,006	1,5	N
SLC1A2	5397,16	9073,26	0,008	0,006	1,7	N

G6PC	0,33	1,50	0,009	0,006	4,5	N
CPT1A	255,25	348,45	0,009	0,006	1,4	N
PARP1	1035,53	1345,83	0,014	0,006	1,3	N
NOX1	0,13	0,48	0,016	0,007	3,6	N
ARHGAP 26	820,27	1078,44	0,018	0,007	1,3	N
ADPGK	301,13	209,59	0,028	0,007	-1,4	N
PFKFB1	1,51	2,20	0,029	0,007	1,5	N
GFPT1	699,68	865,61	0,031	0,007	1,2	N
SLC2A1	324,13	217,01	0,034	0,007	-1,5	N
ACSS2	133,11	162,03	0,042	0,007	1,2	N
NQO1	175,16	128,95	0,042	0,007	-1,4	N
SLC5A1	0,34	0,71	0,059	0,007	2,1	N
CAT	282,63	323,47	0,063	0,007	1,1	N
HK1	1372,67	1664,80	0,063	0,007	1,2	N
ACTB	12932,07	11289,82	0,065	0,008	-1,1	N
BCAT2	90,76	56,53	0,065	0,008	-1,6	N
IDH1	1046,01	755,35	0,073	0,008	-1,4	N
NOX3	0,23	0,91	0,077	0,008	4,0	N
SLC25A5	1355,40	1753,02	0,098	0,008	1,3	N
VHL2	102,05	126,23	0,098	0,008	1,2	N
TP53I3	87,55	71,43	0,114	0,008	-1,2	N
EPAS1	1187,43	978,91	0,173	0,008	-1,2	N
PRKAA1	167,06	180,06	0,190	0,008	1,1	N
ACLY	1166,47	991,07	0,202	0,008	-1,2	N
RPIA	88,78	94,80	0,247	0,008	1,1	N
OGDH	426,13	455,52	0,254	0,008	1,1	N
HIF1A	2649,63	3307,82	0,261	0,009	1,2	N
SDHB	226,49	251,27	0,332	0,009	1,1	N
TUBB	5108,25	4852,67	0,332	0,009	-1,1	N
PRDX1	841,22	692,32	0,423	0,009	-1,2	N
C12orf5	112,30	96,00	0,484	0,009	-1,2	N
CYCS	861,73	805,92	0,584	0,009	-1,1	N
GLS	1240,26	1346,17	0,608	0,009	1,1	N
ATG4A	58,34	56,83	0,655	0,009	1,0	N
MDH2	713,97	718,15	0,655	0,009	1,0	N
VHL1	212,04	217,46	0,680	0,009	1,0	N
PGK2	0,28	0,16	0,689	0,009	-1,7	N
TP53	81,40	80,29	0,705	0,010	1,0	N
ALDOA	10399,64	10008,24	0,743	0,010	1,0	N
PGD	787,72	745,31	0,781	0,010	-1,1	N
GSS	232,53	212,51	0,847	0,010	-1,1	N
ACACB	72,59	76,19	0,865	0,010	1,0	N
G6PD	273,50	285,54	0,913	0,010	1,0	N

Supplementary table IVa: Gene set enrichment analysis of pathways that are enriched in E478 ($IDH1^{R132H}$) compared to E434 (IDH^{wt}). GSEA was run on genes using Reactome pathways as a gene set. The enrichment score (ES), Normalized Enrichment Scores (NES), Nominal p-value (NOM p-val, and False Discovery Rate q-value (FDR q-val), using (http://software.broadinstitute.org/gsea/index.jsp).[361] An FDR value of 0.05 was chosen as a cut-off to identify significantly upregulated pathways in E478.

Name of pathway	# genes in pathway	ES	NES	NOM p-val	FDR q-val
TCA cycle and respiratory electron transport	106	0.2860566	3.4708712	0.0	0.0
Respiratory electron transport	61	0.33840853	3.139408	0.0	0.0
Respiratory electron transport ATP synthesis by chemiosmotic coupling and heat production by uncoupling proteins	74	0.29975075	3.008204	0.0	0.0
Translation	135	0.17705296	2.3625908	0.0	0.017995128
Regulation of apoptosis	52	0.26844937	2.339759	0.0019493178	0.01704688
Proteolytic cleavage of snare complex proteins	15	0.49458942	2.3231874	0.0	0.016149795
3 UTR mediated translational regulation	96	0.20032889	2.2914696	0.0	0.017132146
Activation of the mRNA upon binding of the cap binding complex and eIFs and subsequent binding to 43s	50	0.2636738	2.2291439	0.002008032	0.023830138
Vif mediated degradation of APOBEC3G	44	0.27730942	2.1544049	0.0061728396	0.03316279
Pyruvate metabolism and citric acid cycle	36	0.30188543	2.1516216	0.0018867925	0.030139262
Peptide chain elongation	77	0.20794405	2.145787	0.001980198	0.028752333
regulation of ornithine decarboxylase odc	45	0.27399728	2.1397586	0.0021321962	0.027723063
Nonsense mediated decay enhanced by the exon junction complex	97	0.19017804	2.138099	0.0038095238	0.026100954
Formation of the ternary complex and subsequently the 43s complex	43	0.27100584	2.1267729	0.002074689	0.025832746
Botulinum neurotoxicity	16	0.4362245	2.1214886	0.0	0.025214633
Autodegradation of the E3 ubiquitin ligase COP1	44	0.26891106	2.1047227	0.010570824	0.026282508
Influenza viral RNAtranscription and replication	93	0.17795895	2.0735006	0.0061099795	0.030472804
Metabolism of mRNA	192	0.12877095	2.0658453	0.0058365758	0.029876838
Metabolism of RNA	234	0.11570477	2.0512772	0.002074689	0.030260226
CDT1 association with the CDC6:ORC origin complex	51	0.24059549	2.0487657	0.0078125	0.029268626
Mitochondrial protein import	42	0.2637869	2.0268478	0.0040983604	0.03190501
activation of NF-kappaB in B cells	56	0.22840573	2.0268264	0.004048583	0.03045478
SRP-dependent cotranslational protein targeting to membrane	99	0.17048825	1.9895797	0.008032128	0.03674765

citric acid cycle (TCA cycle)	18	0.38493603	1.9760294	0.0019762847	0.03842362
p53 independent Ga/S DNA damage checkpoint	45	0.25170302	1.9483076	0.0038834952	0.04362312
Destabilization of mRNA by AUF1 hnRNP D0	47	0.24082775	1.9428527	0.00998004	0.04308282

Supplementary table IVb: Gene set enrichment analysis of pathways that are downregulated in E478 (IDH1^{R132H}) compared to E434 (IDH^{wt}). GSEA was run on genes using Reactome pathways as a gene set. The enrichment score (ES), Normalized Enrichment Scores (NES), Nominal p-value (NOM p-val, and False Discovery Rate q-value (FDR q-val) using (http://software.broadinstitute.org/gsea/index.jsp) [361]. An FDR value of 0.05 was chosen as a cut-off to identify significantly downregulated pathways in E478.

Pathway name	# genes in pathway	ES	NES	NOM p-val	FDR q-val
Generic transcription pathway	282	-0.17326634	-3.3634012	0.0	0.0
RNA Polymerase I promoter opening	39	-0.39645863	-3.001081	0.0	0.0012542009
Amyloids	45	-0.36197886	-2.864934	0.0	8,36E+03
Processing of capped intron containing pre-mRNA	123	-0.22066908	-2.8583617	0.0	9,48E+03
mRNA processing	140	-0.20656902	-2.8516946	0.0019880715	7,58E+02
Cell cycle	357	-0.13062505	-2.813871	0.0	0.0012619899
Factors involved in megakaryocyte development and platelet production	86	-0.26000288	-2.7841518	0.0	0.0012614732
Keratan sulfate (keratin metabolism)	24	-0.4664222	-2.7403607	0.0	0.0012588598
Deposition of new CENPA-containing nucleosomes at the centromere	48	-0.33210889	-2.7224896	0.0	0.0011189865
Meiotic recombination	59	-0.29424793	-2.697666	0.0	0.0012523746
Axon guidance	188	-0.1662002	-2.6620042	0.0	0.0015824524
Cell cycle mitotic	284	-0.13598752	-2.648057	0.001953125	0.0016726375
Glycosaminoglycan metabolism	78	-0.24130769	-2.56538	0.0	0.0025155917
GPCR downstream signalling	193	-0.15663365	-2.5188065	0.0	0.0027860478
Extracellular matrix organization	37	-0.34553936	-2.4875574	0.0	0.0031748777
Keratan sulfate biosynthesis	20	-0.46628812	-2.484481	0.001996008	0.0029764478
Developmental biology	287	-0.12537703	-2.4570723	0.0	0.0034004005
Hemostasis	287	-0.12645438	-2.4441097	0.0	0.0037002228
Mitotic prometaphase	76	-0.22820818	-2.365997	0.0	0.00672554
mRNA splicing	98	-0.2008037	-2.3581479	0.0	0.0068911235

SLC mediated transmembrane transport	144	-0.16467215	-2.3194113	0.0	0.00888539
Chromosome maintenance	98	-0.20112972	-2.3099377	0.0020242915	0.009002479
Transport of mature transcript to cytoplasm	46	-0.28674796	-2.3058965	0.0019762847	0.008717472
Meiosis	84	-0.20590903	-2.2684135	0.0	0.010626784
GPCR ligand binding	103	-0.18470399	-2.2578337	0.0	0.010858051
Transcription	169	-0.14618391	-2.229108	0.0	0.01312703
DNA replication	171	-0.1441985	-2.1687753	0.00407332	0.0190664
RNA polymerase I transcription	62	-0.22559482	-2.1366763	0.0	0.021573167
G alpha1213 signalling events	60	-0.23303051	-2.101063	0.002020202	0.026466828
Transport of inorganic cations anions and amino acids oligopeptides	56	-0.22956385	-2.0878057	0.002096436	0.027498193
Mitotic M-M/G1 phases	153	-0.14459343	-2.0658216	0.0020491802	0.030724218
Signaling by GPCR	255	-0.11302958	-2.056083	0.008	0.031611387
Signaling by FGFR1 mutants	20	-0.37648076	-2.045577	0.003929273	0.03317718
Signaling by RHO GTPpases	92	-0.17784616	-1.9841524	0.0060728746	0.04585799
Metabolism of carbohydrates	173	-0.12952195	-1.9828523	0.005905512	0.04476136
Potassium channels	51	-0.23473476	-1.9651031	0.007905139	0.04890171
Glucose transport	29	-0.3081424	-1.9643099	0.0019607844	0.047783744
G alpha (q) signalling events	77	-0.190544	-1.9608874	0.011904762	0.047358997
Activation of the pre replicative complex	29	-0.29903743	-1.9527317	0.005952381	0.048350856
NEP/NS2 interacts with the cellular export machinery	25	-0.31551597	-1.9463599	0.010080645	0.049005564

CHAPTER 5

Isocitrate dehydrogenase 1-mutated cancers are sensitive to the green tea polyphenol epigallocatechin-3-gallate

Tom H. Peeters*, Krissie Lenting*, Vincent Breukels, Sanne A.M. van Lith, Corina N.A.M. van den Heuvel, Arno van Rooij, Ron Wevers, Paul N. Span, Arend Heerschap, William P.J. Leenders

* authors contributed equally to this work

Cancer & Metabolism, 2019 May 20;7:4.

Abstract

Background: Mutations in isocitrate dehydrogenase 1 (*IDH1*) occur in various types of cancer and induce metabolic alterations resulting from the neomorphic activity that causes production of *D*-2-hydroxyglutarate (*D*-2-HG) at the expense of α-ketoglutarate (α-KG) and NADPH. To overcome metabolic stress induced by these alterations, *IDH*-mutated (IDH^{mut}) cancers utilize rescue mechanisms comprising pathways in which glutaminase and glutamate dehydrogenase (GLUD) are involved. We hypothesized that inhibition of glutamate processing with the pleiotropic GLUD-inhibitor epigallocatechin-3-gallate (EGCG) would not only hamper *D*-2-HG production, but also decrease NAD(P)H and α-KG synthesis in IDH^{mut} cancers, resulting in increased metabolic stress and increased sensitivity to radiotherapy.

Methods: We performed ^{13}C-tracing studies to show that HCT116 colorectal cancer cells with an $IDH1^{R132H}$ knock-in allele depend more on glutaminolysis than on glycolysis for replenishment of the depleted pools of α-KG and NADPH. We treated HCT116 cells, HCT116-$IDH1^{wt/R132H}$ cells and HT1080 cells (carrying an $IDH1^{R132C}$ mutation) with EGCG and evaluated *D*-2-HG production, cell proliferation rates and sensitivity to radiotherapy.

Results: Significant amounts of ^{13}C from glutamate accumulate in *D*-2-HG in HCT116-$IDH1^{wt/R132H}$ but not in HCT116. Preventing glutamate processing in HCT116-$IDH1^{wt/R132H}$ cells with EGCG resulted in reduction of *D*-2-HG production. In addition, EGCG treatment decreased proliferation rates of $IDH1^{mut}$ cells and sensitized cancer cells to ionizing radiation. Effects of EGCG in IDH-mutated cell lines were diminished by treatment with the $IDH1^{mut}$ inhibitor AGI-5198.

Conclusions: This work shows that glutamate can be directly processed into *D*-2-HG and that reduction of glutamatolysis by EGCG is an effective and promising new treatment option for IDH^{mut} cancers.

Key words: IDH mutations, metabolism, EGCG, radiotherapy, glutamate

Background

Acquisition of hotspot mutations in *IDH1* and *IDH2* are key events in the development of various types of cancer. The mutations are found in 80-90% of gliomas [82, 83, 385], in substantial percentages of acute myeloid leukaemia [386], chondrosarcoma [387], osteosarcoma [388] and intrahepatic cholangiocarcinoma [389] and are sporadically found in other cancer types [390, 391].

IDH1 and IDH2 are $NADP^+$-dependent homodimeric enzymes that oxidize isocitrate (ICT) to α-ketoglutarate (α-KG) in cytosol and mitochondria, respectively [392]. The NADPH produced by these reactions contributes to the reductive potential of the cell [84]. Cancer-related mutations in *IDH1* and *IDH2* are mostly heterozygous and are always hotspot mutations involving arginine residues R132 in IDH1 and R140 or R172 in IDH2. The mutated subunits have acquired a neomorphic activity of reducing α-KG to *D*-2-hydroxyglutarate (*D*-2-HG) while oxidizing NAPDH. Accumulation of *D*-2-HG competitively inhibits α-KG-dependent enzymes, including the Ten Eleven Translocation (TET) family of methylcytosine dioxygenases, resulting in a CpG island hypermethylator phenotype that is considered as a first step in malignant transformation [346, 347]. Whereas *IDH* mutations are involved in the initial steps of carcinogenesis, the metabolic and oxidative stress that comes with the mutation may eventually slow down tumour progression, explaining the better survival of patients carrying IDH^{mut} gliomas [129, 344]. *IDH* mutations are however not associated with prolonged survival in non-glioma cancer patients, indicating tissue-specific effects that are currently not understood [82, 83, 393].

Small molecule inhibitors of mutant IDH1 and IDH2 enzymes have been developed to prevent production of the alleged oncometabolite *D*-2-HG [155, 394]. However, blocking *D*-2-HG production also blocks NADPH oxidation and consequently decreases oxidative stress, desensitizing IDH^{mut} cells for radiotherapy, chemotherapy and inhibitors of poly-ADP ribose polymerase (PARP), an important enzyme involved in DNA double-strand break (DSB) repair [350, 395-397].

To improve the clinical outcomes of patients with IDH^{mut} cancers it is essential to increase, rather than decrease metabolic stress. We previously showed that clinical IDH^{mut} gliomas have dramatically altered expression profiles of genes involved in metabolism as compared to IDH^{wt} gliomas. Based on these data we proposed a model in which IDH^{mut} gliomas utilize the neurotransmitter glutamate and lactate as fuels [316], whereas IDH^{wt} gliomas predominantly use glucose [345]. According to that model the shortage of α-KG in IDH^{mut} gliomas is partially rescued by direct import of glutamate that is converted to α-KG by the NAD^+/$NADP^+$ dependent enzymes glutamate dehydrogenase 1/2 (GLUD1/2). Alpha-KG can then be shuttled into the TCA cycle or converted to *D*-2-HG. We therefore hypothesized that inhibition of glutamate processing would not only prevent *D*-2-HG production, but also NAD(P)H and α-KG synthesis, thus increasing metabolic stress and sensitizing IDH^{mut} gliomas to radiotherapy and chemotherapy [316, 354]. Non-glioma IDH^{mut} cancers however reside in environments with

lower glutamate concentrations than in the brain. To test how different nutrients contribute to *D*-2-HG production in non-glioma tumours, we here employed HCT116 and HCT116-*IDH1*$^{wt/R132H}$ knock-in colorectal cancer cells and HT1080 cells, a fibrosarcoma containing an endogenous IDH1^{R132C} mutation. We performed carbon tracing studies and investigated the effects of epigallocatechin-3-gallate (EGCG), an inhibitor of GLUD1/2 and of NADP-dependent enzymes, on *D*-2-HG synthesis and radiosensitivity of these cell lines.

Methods

Cell lines and compounds

HCT116 (parental) and HCT116-*IDH1*$^{wt/R132H}$ knock-in human colorectal cell lines were generated by AAV targeting technology GENESIS [398] and obtained from Horizon Discovery (Cambridge, UK). HT1080 fibrosarcoma cells (containing an endogenous *IDH1*$^{wt/R132C}$ mutation) were a kind gift of Dr. W. Hendriks (Dept. of Cell Biology, Radboudumc). Cell lines were cultured in DMEM (LONZA, Basel, Switzerland) supplemented with 10% FCS (Gibco, Waltham, MA) and 40µg/µl gentamycin (Centrafarm, Etten-Leur, the Netherlands). Cell lines were checked for IDH1^{R132H} expression by Western blotting of cytosolic protein extracts, using a mutation-specific antibody (Dianova, Hamburg, Germany; DIAH09). All experiments in this study were performed with cells below passage number 25 as IDH1^{R132H} expression levels gradually dropped at higher passage numbers (data not shown). All chemicals were obtained from Sigma Aldrich (St. Louis, MO) unless stated otherwise. EGCG (E4268) was stored in DMSO at a concentration of 25 mM under nitrogen gas and kept from light, or dissolved in distilled water directly before use. The IDH1^{mut} inhibitor AGI-5198 was from MedChemExpress (Monmouth Junction, NJ).

^{13}C-isotope tracing experiments

Nuclear magnetic resonance (NMR) spectroscopy and LC-MS experiments were performed to investigate the contribution of glutamine (Gln), glutamate (Glu) and glucose (Glc) as carbon donors for *D*-2-HG (see figure 1A). For NMR, HCT116-*IDH1*$^{wt/R132H}$ and HCT116 cells were grown to 50% confluency in T175 culture flasks (Greiner Bio-One, Kremsmünster, Austria) and incubated with glutamine-free DMEM (Gibco) supplemented with 10% FCS and 4 mM [1-^{13}C]-glutamine or 4 mM [1-^{13}C]-glutamate. EGCG (100 µM final concentration in distilled H_2O) or solvent control was administered 2 hours prior to the start of incubation. After 20 hours of incubation, cells were placed on ice, washed twice with ice-cold PBS and lysed in 2.5 ml methanol (MeOH) (-20°C) containing 280 mM formic acid as a ^{1}H and ^{13}C (naturally abundant) NMR reference compound. After 10 min, cell material was collected with a rubber policeman, thoroughly vortexed and centrifuged for 5 min at 1,200 x g to precipitate proteins. The protein content of the precipitated pellets was measured using a Pierce BCA protein assay kit (ThermoScientific, Rockford, IL) and used for data normalization. The metabolites in the supernatant were dried in a SpeedVac evaporator (Savant, Waltham, MA) and redissolved in 400 µl D_2O for NMR analysis (Avance III 500MHz, Bruker BioSpin, Rheinstetten, Germany).

NMR spectra were acquired with pulse-acquire experiments. For ^{1}H NMR the settings were: TR = 18s, 90° flip angle, NS = 16; and for ^{13}C: TR = 5.1s, 30° flip angle, NS = 7000 and proton-decoupling. The spectra were analysed with Bruker Topspin software. Integrated peak intensities of *D*-2-HG, Glu and Gln were corrected for T_1 saturation, number of contributing spins and cell number, and were referenced to formic acid to obtain concentrations.

Because total amounts of *D*-2-HG are difficult to obtain from ^{1}H spectra, due to overlapping resonances of *D*-2-HG and glutamate, total and ^{13}C-labeled *D*-2-HG pools were examined with LC-MS. To this end, HCT116 and HCT116-*IDH1*$^{wt/R132H}$ cells were grown to 50% confluency in 10 cm culture dishes (Greiner Bio-One) and incubated with Glc- and Gln-free DMEM with and without 10% FCS and different combinations of non-labelled and ^{13}C-labeled Glc, Gln or Glu. In all experiments the final total Glc concentration was 5.5 mM and Glu and/or Gln concentrations were 4 mM. LC-MS was performed as described before [215].

Proliferation assays

Cells were seeded in 96-well plates at 500 cells/well (HCT116 cell lines) or 1000 cells/well (HT1080) and left to adhere overnight. The following day varying concentrations of EGCG or vehicle were added. For AGI-5198 experiments, cells were cultured at least 3 days in the presence of 5 µM AGI-5198, and the compound was left on the cells during the entire experiment. At days 2, 4, and 6 after seeding, total cell protein content was measured using SRB assays, as described [399]. In short, cells were washed twice with PBS and fixated overnight at 4°C in 10% (w/v) trichloroacetic acid. After fixation, plates were washed four times with distilled H_2O and stored at -20°C until analysis. Plates were stained with 0.5% (w/v) SRB dissolved in 1% (v/v) acetic acid (Merck, Darmstadt, Germany) and incubated in the dark for 20 min. After washing four times with 1% acetic acid, plates were dried at 60°C. Protein-bound SRB was solubilized with 150 µl 10mM Tris-HCl, pH 10. Optical densities were measured at 560 nm on a microplate reader (Bio-rad, Hercules, CA). Proliferation is expressed as fold increase, normalized for the protein content of control cells one day after plating.

Alternatively, cell proliferation was measured using the xCELLigence Real-Time Cell Analyzer system (ACEA Biosciences, San Diego, CA). Cells were plated in duplicate at a density of 1,000 cells/well on ACEA E16 view plates. The next day EGCG or vehicle was added to the wells. Doubling times were calculated over 48 hours, using dedicated ACEA software.

GLUD1/2 and IDH enzymatic assays

IDH1 was expressed as glutathione S-tranferase (GST)-fusion protein in pDEST15 and purified on glutathione beads (GE Healthcare, Chicago, IL) as described [400]. Purified bovine GLUD1/2 was purchased from Serva (Heidelberg, Germany). Enzyme reactions were initiated by adding 4 µg IDH1 enzyme to a mixture of 100 µM NADP+, 2 mM $MgCl_2$, 0.5 mM isocitrate, 100 mM Tris-HCl (pH 7.4). GLUD1/2 activity was measured in reactions containing 0.1 U bovine GLUD1/2 enzyme, 500 µM NAD^+, 10 mM glutamate and 2 mM ADP in phosphate buffer (pH 8.0). Stoichiometric production of NADPH and NADH was measured by real-time monitoring

of NADPH or NADH absorbance at 340 nm with 20 sec intervals on an Omega Fluostar (BMG Labtech, Ortneberg, Germany).

Colony-forming assays after ionizing radiation (IR)

Cells, cultured with or without AGI-5198, were seeded in 6-well plates (30-5,000 cells/well) and left to adhere overnight. Cells were treated with 0, 20, 50 or 100 µM EGCG for 24 hours and irradiated with 0, 2 or 4 Gy (IR, 3.1 Gy/min; XRAD 320 ix; Precision XRT; N. Brandford, CT, USA). After 72 hours, medium was refreshed and cells were cultured for another 7 days (without EGCG) and fixated with 70% ethanol (10 min, 4 °C). After drying at 60°C, colonies were stained with 0.5% (w/v) crystal violet (Merck) in distilled water. Colonies consisting of 50 cells or more were considered to be derived from cells surviving radiotherapy and were manually counted. The effect of EGCG on radiotherapy-induced cell death was expressed as surviving fraction, normalized to plating efficiency.

DNA-double strand break (DSB) detection

Cells (cultured with or without AGI-5198) were plated at a density of 300,000 cells/well in 6-well plates and left to adhere overnight. After 24 h incubation with EGCG (0, 50 or 100 µM) cells were irradiated with 0, 2 or 4 Gy. After 30 min, cytosolic extracts were prepared in 1 x RIPA buffer (Cell Signaling Technologies) containing 1 mM phenylmethylsulfonyl fluoride (PMSF). Cell extracts were sonicated to release nuclear proteins. Protein samples (25 µg) were electrophoresed on 10% SDS-PAGE gels and electroblotted onto nitrocellulose (GE Healthcare). Blots were stained with anti-γH2AX antibody (Ser139; #2577; Cell Signaling Technologies) and anti-γ-tubulin (C20) (Santa Cruz Biotechnology, Dallas, TX, sc-7396), followed by appropriate secondary antibodies labelled with IRDye680 or IRDye800 (ThermoFisher). Signals were visualized and quantified using the Odyssey system (Li-COR, Lincoln, NE).

Statistical analysis

Statistical analyses were performed in Graphpad Prism v5.03 (GraphPad Software, LaJolla, CA). The difference in mean values between various groups was assessed using an unpaired Students' t-test, unless mentioned otherwise. P-values are marked as follows: <0.05 (*); <0.01 (**); <0.001 (***), <0.0001 (****). Differences were considered statistically significant when p-values were < 0.05.

Results

Glutamine and glutamate are carbon donors for *D*-2-HG production

To find support for the hypothesis that glutaminolysis and/or glutamatolysis is a rescue mechanism for IDH^{mut} cancers, we used the HCT116 cell line and its isogenic knock-in variant HCT116-$IDH1^{wt/R132H}$. The balanced expression of both alleles makes this variant more representative for clinical cancers than overexpression models [401]. We used [1-^{13}C]-labelled

glutamine (Gln*) and glutamate (Glu*) to trace the routing of carbons from Gln and Glu to *D*-2-HG. Labelled carbon from Glu or Gln that enters the TCA-cycle is lost as carbon dioxide by oxidative decarboxylation of α-KG (see Figure 1A).

^{13}C-NMR spectra of extracts of *IDH1^{mut}* cells, cultured for 20 hours in Gln*-containing DMEM, showed ^{13}C resonances for Glu and *D*-2-HG, demonstrating significant carbon fluxes from Gln to Glu and to *D*-2-HG (see blue graph in upper panel of Figure 1B for a representative NMR spectrum).

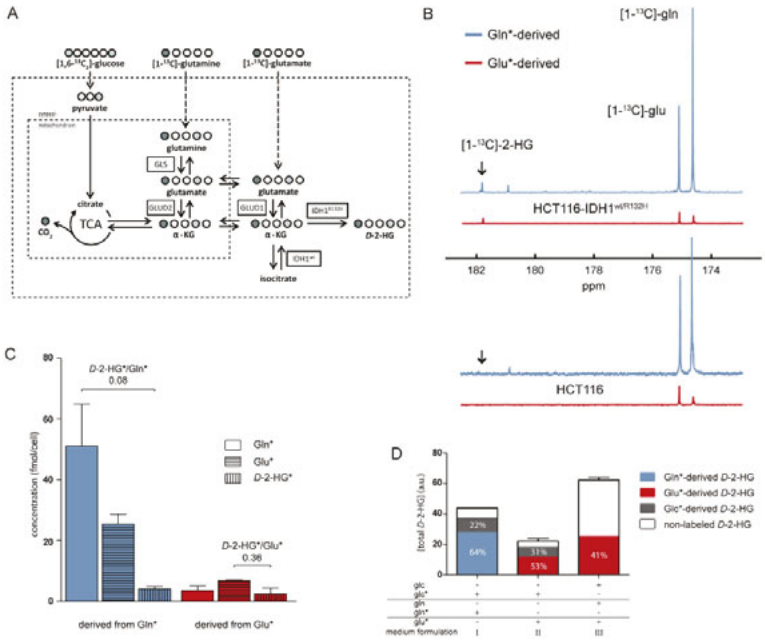

Figure 1 Carbon sources for D-2-HG production and ^{13}C tracing studies A) *Schematic model of metabolic pathways involved in production of D-2-HG from extracellular glucose, glutamine and glutamate; and the ^{13}C labelling patterns following incubation in culture medium containing ^{13}C-labeled glucose (light circles), and glutamine or glutamate (dark circles).* ***B)*** *Example of ^{13}C NMR spectra of extracts of HCT116-IDH1$^{wt/R132H}$ and HCT116 cells cultured in medium with [1-^{13}C]-glutamine (Gln*, blue) or [1-^{13}C]-glutamate (Glu*, red). [1-^{13}C]-D-2-HG (D-2-HG*) was detected at 181.8 ppm and could not be observed in parental HCT116 cells.* ***C)*** *Quantified NMR results showing levels of Glu*, Gln* and D-2-HG* in HCT116-IDH1$^{wt/R132H}$ cells, after incubation in medium with Gln* (blue) or Glu* (red).* ***D)*** *LC-MS analysis of D-2-HG pool fractional enrichments in HCT116-IDH1$^{wt/R132H}$ cells after incubation with ^{13}C-labeled substrates. Bar I displays the total amount of D-2-HG and the fractions that were derived from Gln* (blue) and Glc* (gray). Results were obtained from two separate measurements: in the first measurement cells were incubated in DMEM with Glc and Gln*; in the second measurement DMEM was supplemented with Glc* and Gln*. The difference in labelled fractions from these two measurements was assigned as the Glc* fraction. In a parallel experiment Gln and Gln* were substituted by Glu and Glu* respectively. Bar II shows the total amount of D-2-HG and the fractions that were derived from Glu* (red) and Glc* (gray). A third experiment was performed with DMEM containing Glu*, Gln and Glc. Bar III displays the total amount of D-2-HG and the fraction that was derived from Glu* (red). Provided that both Glu and Gln are available from the culture medium, production of Glu-derived D-2-HG (red) was substantial. Gln* and Glc* fractions were not measured in experiment III. Supplemented metabolite concentrations were always the same: 5.5 mM glucose and 4 mM glutamine and/or 4 mM glutamate.*

In similar experiments with Glu* instead of Gln* in the medium we observed ^{13}C resonances for Gln and *D*-2-HG, next to that for Glu, demonstrating carbon flux from Glu to Gln and to *D*-2-HG (see red spectrum in upper panel Figure 1B and Figure 1C). Whereas cells take up less Glu* than Gln*, the ratio *D*-2-HG*/Glu* (0.36, n=2) was higher than that of *D*-2-HG*/Gln* in the Gln* incubation experiments (0.08, n=6; see Figure 1C). Since *D*-2-HG was not detected in parental HCT116 cells (see lower panel of Figure 1B) these cells were not used for further ^{13}C experiments.

Relative contributions of Glu, Gln and Glc carbons to the total pool of *D*-2-HG were assessed with LC-MS of extracts of cells, cultured 20 hours in medium with Glu* or Gln*, together with Glc* ([1,6-$^{13}C_2$]-glucose). Experiments with Gln*+Glc* in the medium revealed that 64 ± 8.5% of *D*-2-HG was derived from Gln* whereas 22 ± 3.8% was derived from Glc* (n=5; see Figure 1D; medium formulation I). When cells were cultured in Glu*+Glc*-containing DMEM in the absence of Gln, the total amount of *D*-2-HG decreased, with 53 ± 3.1% of carbons originating from Glu* and 31 ± 1.8% from Glc* (n=3; Fig 1D, formulation II). Only small amounts of non-labelled *D*-2-HG were detected when cells were cultured in medium formulations I and II. When cultured in DMEM with Glu* and non-labelled Gln and Glc, the total amount of *D*-2-HG was highest (Figure 1D, formulation III). Of all intracellular *D*-2-HG, 41 ± 0.2% was derived from Glu* (n=3). The latter experiment showed that direct glutamate contribution is substantial even in the presence of glutamine, and that the availability of Gln is a prerequisite for increased *D*-2-HG production.

EGCG inhibits proliferation of *IDH*^{mut} cells more effectively than proliferation of *IDH*^{wt} cells

Our finding that the glutamine-glutamate pathway is an important carbon donor for *D*-2-HG via α-KG suggests that blocking this pathway not only decreases α-KG availability and *D*-2-HG production, but also increases oxidative stress [350]. In line with this hypothesis, inhibiting GLUD1/2 by EGCG dose-dependently reduced growth rates of HCT116-*IDH1*$^{wt/R132H}$ cells more than of parental HCT116 cells (Figure 2A). Because the IDH1^{mut} inhibitor AGI-5198 prevents *D*-2-HG production and NADPH oxidation, it is expected to annihilate the metabolic stress that is caused by the *IDH* mutation, thereby reducing the effects of EGCG. Indeed, AGI-5198 treatment antagonized the inhibitory effect of EGCG to the level that was observed for parental HCT116 cells (Fig 2B). This finding was supported in experiments with HT1080 cells, in which AGI-5198 treatment resulted in significantly increased proliferation rates, while decreasing sensitivity to EGCG (Figure 2C).

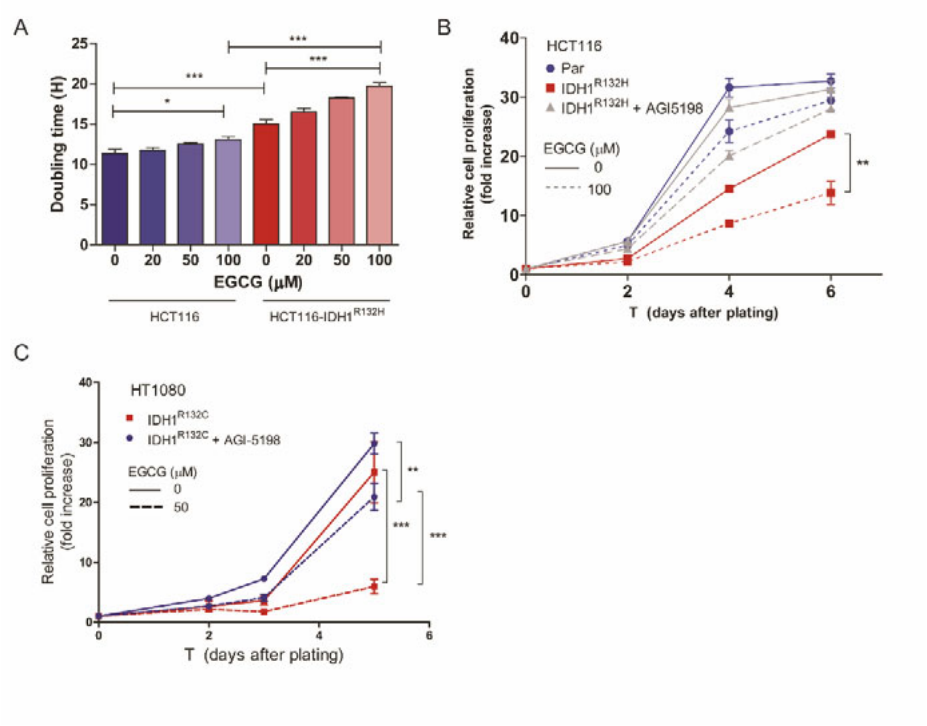

Figure 2: Proliferation assays of the isogenic cell line pair HCT116 and HCT116-IDH1$^{wt/R132H}$ with EGCG. A) *Doubling times of cells as measured on the xCELLigence. Doubling times for HCT116-IDH1$^{wt/R132H}$ (red bars) were significantly higher compared to its wild-type counterpart (blue bars). Supplementation of EGCG to the culture medium increased doubling times in both cell lines, but this effect was more significant in HCT116-IDH1$^{wt/R132H}$.* ***B)*** *SRB assay of HCT116 cells cultured with EGCG (dotted lines), or vehicle (solid lines). HCT116-IDH1$^{wt/R132H}$ (red lines) cells had slower proliferation rates as compared to HCT116 (blue lines). Addition of AGI-5198 (grey lines) rescued the proliferation rates of IDH1^{R132H} cells to HCT116 baseline levels. EGCG inhibited proliferation of HCT116-IDH1$^{wt/R132H}$ more than HCT116, and this inhibitory effect was abolished by AGI-5198. Similar results were obtained for HT10180 cells* ***(C)****.*

EGCG inhibits GLUD1/2 and IDH1 activity

EGCG is an inhibitor of GLUD but also of other NADP$^+$-dependent enzymes [402], which could contribute to the reduction in growth rates of HCT116 and HT1080 cells. We therefore tested the effects of EGCG on enzymatic activities of wild-type IDH1 and GLUD1/2 in biochemical assays, quantifying NAD(P)H production by 340 nm absorption. These experiments revealed dose-dependent inhibition of both GLUD1/2 and of IDH1 activity (Figure 3).

EGCG reduces *D*-2-HG production in HCT116-*IDH1$^{wt/R132H}$*

The effect of EGCG on IDH1 and GLUD1/2 activity predicts that EGCG inhibits the formation of α-KG and *D*-2-HG in *IDH1^{mut}* cells. To test this hypothesis we analysed the effects of EGCG on *D*-2-HG production in HCT116-*IDH1$^{wt/R132H}$* cells using LC-MS. Total amounts of *D*-2-HG were

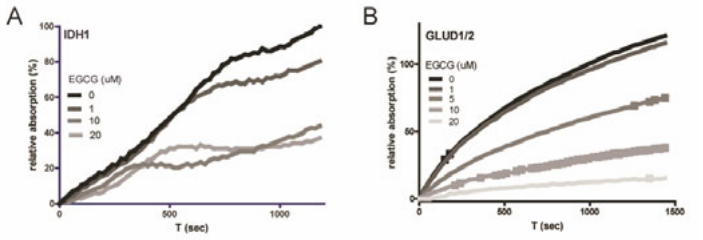

Figure 3: EGCG inhibits the activity of IDH1 and GLUD1/2. *IDH1* ***(A)*** *and GLUD1/2* ***(B)*** *activities were inhibited by EGCG, but this effect was much more pronounced in GLUD1/2. Activity was determined by measuring NADP(H)-generated absorption at 340nm. Activity was corrected for absorption measured with cofactors, without the addition of enzyme.*

decreased in cells treated with EGCG (Figure 4A). This alteration was most apparent in cells incubated in DMEM containing Glc, Glu and Gln. EGCG treatment decreased carbon flux from Glu* to *D*-2-HG, although this difference was not statistically significant (Figure 4B). Because EGCG binds to serum albumin [403], possibly diminishing cellular uptake, we repeated the LC-MS experiment, but now cultured cells in serum-free medium. Under these conditions EGCG treatment resulted in a significant reduction of ^{13}C- flux from *Glu to *D*-2-HG (Figure S1).

EGCG increases sensitivity of HCT116-*IDH1*$^{wt/R132H}$ cells to radiotherapy

Because EGCG inhibits GLUD1/2 and IDH1 activity and thus NADH and NADPH production, it is expected to increase oxidative stress and sensitize cells for ionizing radiation. Colony formation assays showed that EGCG increased the sensitivity to IR of both cell lines, although at low doses (20µM) EGCG appeared to protect cells against radiotherapy (Figure 5A, Table 1).At higher doses of EGCG, HCT116-*IDH1*$^{wt/R132H}$ cells were significantly more sensitive to IR than HCT116 cells. Inhibition of IDH1^{R132H} activity with AGI-5198 resulted in decreased radiosensitivity of EGCG-treated HCT116-*IDH1*$^{wt/R132H}$ cells (dotted grey lines).

EGCG increases DNA-DSB in IDH^{mut} cells

In addition to colony assays we also measured γH2AX to assess IR sensitivity. Phosphorylation of histone H2AX is a rapid response to DNA-DSBs [404]. To test the direct IR-induced DNA damage, we determined levels of γH2AX in HCT116, HCT116-*IDH*$^{wt/R132H}$ and HT1080 cells with and without AGI-5198, 30 min after irradiation with 0, 2 or 4 Gy. Endogenous levels of γH2AX were higher in HCT116-*IDH1*$^{wt/R132H}$ than in HCT116 cells (Figure 5B) as reported before [350]. Higher irradiation doses resulted in increased levels of γH2AX, and this effect was increased by EGCG in HCT116-*IDH*$^{wt/R132H}$. Similar effects were observed in HT1080 cells. Of note, treatment with AGI-5198 reduced the amount of γH2AX, suggesting a protective effect of this compound towards IR.

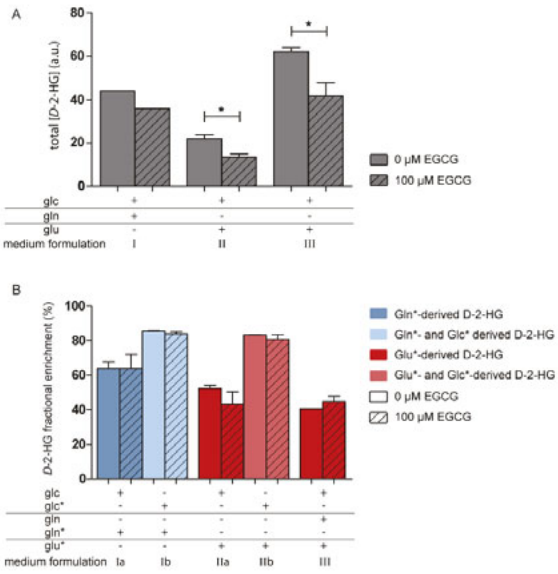

Figure 4 LC-MS analysis of D-2-HG pools after treatment with EGCG. *HCT116-IDH1$^{wt/R132H}$ cells were incubated in DMEM with 10% FCS, supplemented with glucose, glutamine and/or glutamate as indicated in the presence or absence of EGCG (shaded vs. non-shaded bars respectively).* ***A)*** *shows total pools of D-2-HG after incubation in medium containing Glc and Gln (I), Glc and Glu (II), or Glc, Gln and Glu (III). Total D-2-HG levels decreased when cultured with EGCG. Fractional enrichments (FE) of D-2-HG are displayed in* ***(B)****. Blue bars display the fractions of D-2-HG that were derived from Gln* (dark blue) and both Gln* and Glc* (light blue) after incubation in DMEM with Glc + Gln* (formulation Ia) and Glc* + Gln* (formulation Ib) respectively. Red bars display the fractions of D-2-HG that were derived from Glu* (dark red) and both Glu* and Glc* (light red) after incubation in DMEM with Glc + Glu* (formulation IIa) and Glc* + Glu* (formulation IIb) respectively, and the fraction of D-2-HG derived from Glu* (dark red) after incubation in DMEM with Glc, Gln and Glu* (formulation III).*

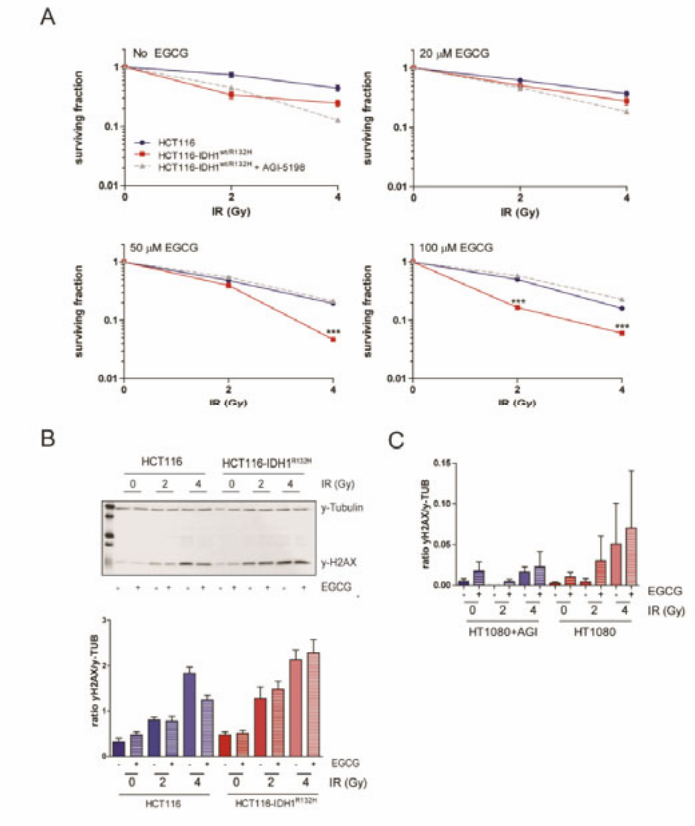

Figure 5: EGCG increases radiosensitivity in HCT116-IDH1$^{wt/R132H}$ cells. A) *Colony formation assay of HCT116-IDH1$^{wt/R132H}$ cells shows increased sensitivity to IR after treatment with EGCG compared to in HCT116. Surviving fractions were 5% (± 0.5%) vs. 16% (± 2%) for IDH1$^{wt/R132H}$ and IDH1^{wt} cells, respectively, when cultured with 100µM EGCG and irradiated with 4Gy.* ***B)*** *Western blot quantification of phosphorylated H2AX foci in HCT116-IDH1$^{wt/R132H}$ and HCT116 cells, cultured with or without 100µM EGCG and irradiated at 2 or 4 Gy. EndogeAnous H2AX-phosphorylation was higher in HCT116-IDH1$^{wt/R132H}$ cells than in HCT116 cells. 30 min After IR, γH2AX levels further increased to higher levels in HCT116-IDH1$^{wt/R132H}$ than in*

Table 1: Cell survival of irradiated cells. Surviving fractions are presented as percentage surviving colonies (± standard deviation), normalized to the non-irradiated control per EGCG treatment condition. Colonies >50 cells were considered to be derived from cells that survived radiotherapy. Surviving fractions were normalized to plating efficiency.
The surviving fractions are also visualized in Figure 5A.

HCT116				
	EGCG (μM)			
IR (Gy)	**0**	**20**	**50**	**100**
0	100 (± 0)	100 (± 0)	100 (± 0)	100 (± 0)
2	74 (±12)	62 (± 3)	48 (± 11)	50 (± 3)
4	44 (± 9)	37 (± 6)	19 (± 1)	16 (± 2)
HCT116-IDH1$^{wt/R132H}$				
	EGCG (μM)			
IR (Gy)	**0**	**20**	**50**	**100**
0	100 (± 0)	100 (± 0)	100 (± 0)	100 (± 0)
2	33 (± 8)	50 (± 3)	39 (± 6)	16 (± 0.5)
4	24 (± 5)	28 (± 7)	5 (± 0.5)	5 (± 0.5)
HCT116-IDH1$^{wt/R132H}$ + AGI-5198				
	EGCG (μM)			
IR (Gy)	**0**	**20**	**50**	**100**
0	100 (± 0)	100 (± 0)	100 (± 0)	100 (± 0)
2	44 (± 11)	46 (± 9)	55 (± 3)	57 (± 17)
4	13 (± 4)	18 (± 2)	21 (± 2)	22 (± 6)

Discussion

Since the discovery of the frequent occurrence of *IDH1* mutations in various types of cancer, research has mainly focused on the oncogenic effects of *D*-2-HG, the product of the mutant enzyme [405]. Recognizing the oncogenic role of *D*-2-HG, IDH1^{mut}- and IDH2^{mut}-specific drugs have been developed that inhibit the activity of the mutant enzymes [155]. We recently showed that these inhibitors not only inhibit production of *D*-2-HG, but also prevent NADPH oxidation [350]. This results in normalization of the redox status of the cell and thus decreased sensitivity to IR, which may imply that these inhibitors are contra-indicated for combination treatment with IR. In glioma, mutations in *IDH1* are considered ancestral, driving gliomagenesis but not necessarily glioma progression [344]. In the initial stages of neoplastic transformation, *D*-2-HG affects the epigenome through inhibition of α-KG-dependent DNA- and histone-demethylases [376]. However, to overcome metabolic stress induced by depletion of α-KG and NADPH production [349] during progression of the disease, *IDH^{mut}* cells need to adopt rescue mechanisms. Identification of such pathways potentially allows the rational selection of metabolic inhibitors for therapeutic applications.

Previous *in vitro* and *in vivo* studies reported that *IDH^{mut}* cells rely on glutaminolysis for anaplerosis of glutamate and production of reduced glutathione, an important scavenger of reactive oxygen species [345, 406-408]. We recently postulated that metabolic rescue

mechanisms involve direct import and anaplerotic consumption of glutamate and lactate in *IDH*^{mut}, but not *IDH*^{wt} gliomas based on transcriptome and MR spectroscopy experiments [129, 316, 354]. Glutamate import is regulated via excitatory amino acid transporters (EAAT) which are expressed at high levels in IDH^{mut}-glioma cells [316] but at low levels in HCT116 cells [409]. In the present work we provide direct evidence using ^{13}C-tracing that glutamine and glutamate are carbon sources for *D*-2-HG production.

As shown in Figure 1 the presence of glutamine in culture medium increased the intracellular pool of *D*-2-HG HCT116-*IDH1*$^{wt/R132H}$ cells. In medium with *Glu in the absence of Gln, less *D*-2-HG was produced but the contribution of *Glu-derived carbon in *D*-2-HG was relatively high. We postulate that the lower total *D*-2-HG pools are attributed to lower uptake of glutamate relative to glutamine by HCT116-*IDH1*$^{wt/R132H}$ cells.

Most research on *IDH*^{mut} cancers is currently performed on cell lines that overexpress IDH1^{mut} [122, 410]. Recent evidence suggests that the *IDH* mutation may be one of the initial mutations that occur in glioma [94, 110]. Establishing tumour models that carry the endogenous *IDH1*$^{wt/R132H}$ mutation is difficult [201, 279] and overexpression models are not necessarily representative for the heterozygous mutation that occurs in these cancers [411]. Therefore, we here used the heterozygous HCT116-*IDH1*$^{wt/R132H}$ knock-in cell line, one of the few *in vitro* models carrying a heterozygous *IDH1*$^{wt/R132H}$ mutation. The use of the isogenic cell line pair (HCT116-*IDH1*$^{wt/R132H}$ and HCT116) allowed us to link the *IDH1* mutation to sensitivity to GLUD inhibition. Our results may also have relevance to other *IDH1*^{mut} cancer types, as *IDH* mutations are also found in colorectal cancers, although at low frequency [344, 412]. Even though the importance of glutamate and glutamine as an anaplerotic fuel might differ between cancer types due to the nature of cells, inhibition of the processing pathway downstream of glutamine will hamper the cancer cells either way.

Previous studies have shown that the glutaminase (GLS) inhibitor BPTES inhibits proliferation of *IDH*^{mut} cells [122]. The potential of cells to bypass GLS activity by directly using glutamate instead of glutamine is a possible explanation for the relatively small inhibitory effect of BPTES in that study. Therefore, inhibiting glutamatolysis at the level of GLUD1/2 with compounds such as EGCG may be a more effective strategy. EGCG affects the production of *D*-2-HG, among others by diminishing the supply of α-KG by inhibition of GLUD1/2 but likely also by inhibition of the IDH1^{wt} subunit, and simultaneously deteriorates the redox status by inhibiting NAD(P)H production. In this way EGCG has clear benefits over inhibitors that only inhibit GLS or mutant IDH activity directly. Glu-derived *D*-2-HG production was inhibited more by EGCG than Gln-derived *D*-2-HG. We explain this by the fact that GLUD has both a mitochondrial and cytosolic isoform, while GLS is mitochondrial. As EGCG cannot enter the mitochondrial matrix [413] Gln may lead to the production of mitochondrial glutamate and α-KG that may be processed in the TCA cycle instead of being converted in the cytosol *D*-2-HG.

Cell growth was reduced by EGCG in both HCT116 and HCT116-*IDH1*$^{wt/R132H}$ cell lines. We attribute this to the fact that EGCG inhibits multiple NADP$^+$-dependent enzymes including

IDH1^{wt} [402]. We hypothesize that the significantly larger effect of EGCG on HCT116-*IDH1*$^{wt/R132H}$ cells is caused by a higher GLUD-dependency compared to HCT116 cells.

A direct relationship between EGCG and increased oxidative stress was established by its sensitizing effect on radiotherapy, which was significantly higher in HCT116-*IDH1*$^{wt/R132H}$ cells, as demonstrated by increased DNA-DSB after IR, and decreased survival in colony forming assays. Interestingly, a recent report described that *D*-2-HG in IDH1^{mut} cancers inhibits the activity of the α-KG-dependent DNA repair enzyme alkB homolog (ALKBH) [100]. This may provide an additional explanation for increased baseline sensitivity of *IDH1*^{mut} cancers to radiation therapy and alkylating chemotherapy. The decreased IR sensitivity of HCT116-*IDH1*$^{wt/R132H}$ treated with AGI-5198 is in agreement with this hypothesis.

EGCG has several other effects next to the inhibition of GLUD. It can inhibit histone- and DNA demethylases; reactivate tumour suppressor genes [414-416], and inhibit fatty acid synthase [417] and glucose-6-phosphate dehydrogenase, the rate-limiting enzyme in the pentose phosphate pathway and a provider of NADPH [418]. Furthermore, EGCG has been reported to inhibit epidermal growth factor (EGF)-induced activation of the EGF-receptor (EGFR) [419], a frequently encountered aberrant oncogenic pathway in glioblastoma and many other cancers. The combination of these effects provides a solid rationale to test EGCG as an adjuvant treatment to radiotherapy, and possibly chemotherapy, also in *IDH*^{wt} cancers. However, our data also show that the effects of EGCG may be dose dependent, having a radioprotective effect on HCT116-*IDH1*$^{wt/R132H}$ cells at low doses. This may be due to both is anti-oxidative and pro-oxidative effects [420] and warrants extra investigation.

One problem that requires attention is the bioavailability and stability of EGCG *in vivo* [413, 421, 422]. Anticancer effects of EGCG can be diminished due to oxidation of the compound [423], resulting in low circulating doses after oral administration [424]. Furthermore EGCG in the circulation is mostly albumin-associated, increasing stability but decreasing bioavailability [403]. Methods to increase bioavailability via nanomedicine and controlled delivery are currently being explored [425, 426].

Conclusions

HCT116-*IDH1*$^{wt/R132H}$ cells use glutamine and glutamate as direct sources for α-KG anaplerosis and *D*-2-HG production. EGCG, an inexpensive and safe derivative of green tea, inhibits glutamate processing at the level of GLUD1/2, reduces proliferation rates, decreases production of *D*-2-HG and increases sensitivity to radiotherapy in *IDH1*$^{wt/R132H}$ cells. Additional studies are required to test these concepts *in vivo* and to investigate effective ways of delivering EGCG to the brain.

Declarations

Acknowledgements
We thank Dr. S. Pusch from DKFZ Heidelberg, Germany for providing IDH1 GST-fusion proteins and prof. Dr. R. van Noorden and M. Khurshed (Amsterdam UMC) for helpful discussions.

Funding
This work was supported by Dutch Cancer Society grant UvA 2014-6839 (KL). TP was supported by EFRO/GO project Ultrasense NMR.

Availability of data and materials

Data is available from the corresponding author upon request.

Authors' contributions

KL, TP and CH were responsible for cell culture. TP and VB designed, performed and analysed all NMR experiments, supervised by AH. AR and SL performed LC-MS experiments, supervised by RW, analysed together with TP and VB. Cell proliferation and enzymatic assays were performed and analysed by KL. Colony-forming assays and DNA-DSB experiments were designed by, performed and analysed by KL, RM and PS. TP, KL, RM, WL, AH and VB interpreted experimental results. TP, KL, WL and AH wrote the manuscript. All authors read and approved the final manuscript.

Ethics approval and consent to participate

Not applicable.

Consent for publication

Not applicable.

Competing interests

The authors declare that they have no competing interests.

Supplementary material

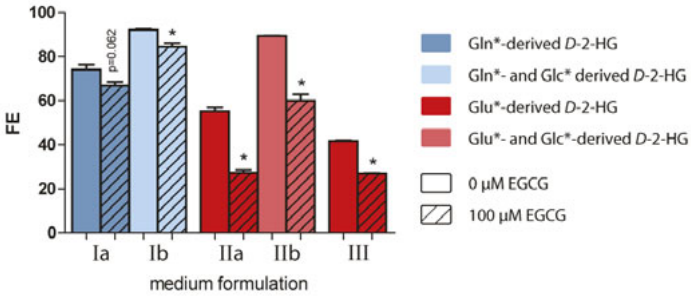

Figure S1 LC-MS analysis of D-2-HG pools in cells cultured in serum-free medium. *HCT116-IDH1$^{wt/R132H}$ cells were incubated in DMEM without FCS and with and without EGCG (shaded vs. non-shaded bars respectively). Blue bars display the fractions of D-2-HG that were derived from Gln* (dark blue) and both Gln* and Glc* (light blue) after incubation in DMEM supplemented with Glc + Gln* (formulation Ia) and Glc* + Gln* (formulation Ib) respectively. Red bars display the fractions of D-2-HG that were derived from Glu* (dark red) and both Glu* and Glc* (light red) after incubation in DMEM with Glc + Glu* (formulation IIa) and Glc* + Glu* (formulation IIb) respectively, and the fraction of D-2-HG that was derived from Glu* (dark red) after incubation in DMEM with Glc, Gln and Glu* (formulation III). Fractional enrichments of D-2-HG decreased significantly when incubated with EGCG. The glucose fraction can be obtained by calculating the difference Ib-Ia and IIb-IIa. Supplemented metabolite concentrations were always the same: 5.5 mM glucose and 4 mM glutamine and/or 4 mM glutamate.*

CHAPTER 6

General discussion and conclusion

Diffuse gliomas are malignant cancers of the central nervous system (CNS). Patients with glioblastomas suffer from very poor prognosis, with a median overall survival of little over a year [66]. In lower grade (grade II-III) tumours, survival is markedly better, but a cure remains unavailable for all these types of tumour. One hallmark of diffuse glioma is its capability of invasion of tumour cells into the brain parenchyma, which makes complete resection impossible. Current therapy options are limited to resection to the extent that is feasibly safe often followed by chemoradiation [132]. The development of novel treatment strategies has been relatively ineffective due to the complexity of the disease and the compartmentalized nature of the brain, which is protected from the blood circulation by the blood-brain barrier (BBB). This barrier is only highly selectively permeable for many drug compounds, and drugs need to be designed in a specific way that allows crossing of the BBB [427-429]. In addition, inter- and intratumoral heterogeneity is found in glioma, with sometimes multiple distinct molecular patterns found in one tumour [430-432]. Taken together, it makes it difficult to design effective therapeutic strategies due to resistance mechanisms, and clonal selection and expansion of the tumour, resulting in relapse after treatment [432].

In the last decades, significant progress has been made to improve the understanding of gliomagenesis, not in the least through technological advances that have made it possible to perform extensive genomic, transcriptomic, and metabolic profiling of human (glioma) tissues. The identification of the *IDH1*^{R132H} mutation in glioma has been a key finding in understanding gliomagenesis [82], and has led to an updated World Health Organization CNS tumour classification in 2016 [60]. Testing for the IDH1-mutation in glioma has become routine practice, and has led to a better diagnosis and assessment of prognosis for the patient, since treatment can be given on a more personalized basis (e.g. treatment with PCV instead of temozolomide for low-grade glioma) [64, 433]. Despite these efforts, there is still an urgent need for improving our understanding of glioma biology and to develop novel treatment strategies.

Glioma models and their limitations

Multiple studies have tried to improve understanding of how molecular aberrations are involved in gliomagenesis and cancer progression, with the aim to identify biomarkers that predict prognosis and give hints to personalized treatments. However, thus far we have not been able to fully take advantage of these understandings, partly due to the difficulties of generating *in vivo* and *in vitro* models that recapitulate the intricate metabolic equilibrium found in clinical glioma. Only a handful of *in vivo* models exist, among which our own E478 xenograft model, harbouring an endogenous *IDH1*^{R132H} mutation [434]. Many different types of preclinical models are used in glioma research, each of them with their own advantages and limitations as we discussed in **chapter 2**. Limitations of models used in a research setting are especially relevant for *IDH1*^{mut} models, since cells with an endogenous *IDH1*^{R132H}-mutation have been proven to be hard to culture *in vitro* [279]. For one, the brain tumour microenvironment plays a crucial role in the development and progression of the cancer [435,

436]. The proposed importance of the glutamine-glutamate cycle for survival and progression of *IDH*^{mut} glioma cells may explain this difficulty, as it is not easily mimicked under culture conditions. Very few models of endogenous *IDH1*^{R132H} have been established worldwide [155, 200, 201], and most research groups revert to models of IDH-mutations by overexpression (OE) of the mutant enzyme in a cell with an otherwise *IDH*^{wt} background (such as U87, U251 and E98 cell glioma cell lines) [406, 437, 438], or switch to heterozygous models other than glioma, such as the colorectal cancer cell line HCT116 [278], or the fibrosarcoma cell line HT1080 (harbouring an endogenous *IDH1*^{R132C} mutation) [439, 440]. Although these cell models produce the oncometabolite *D*-2-HG [441], they lack the metabolic rewiring that endogenous *IDH*^{mut} models of glioma undergo. Since the *IDH1*^{R132H} is considered an ancestral mutation [94, 110], tumour cells that arise have had ample time to adapt their metabolism to cope with the metabolic burden that is induced by the mutation. More evidence has been presented that OE models of IDH1^{R132H} do not recapitulate the metabolic rewiring and gene expression profiles of endogenous models [411].

Unpublished work from our own lab has shown that IDH1^{R132H} OE models are different from endogenous *IDH*^{mut} models. We generated an OE model by transducing IDH1^{R132H} in our E98^{FM} glioblastoma-derived cell model [434]. The model showed production of *D*-2-HG and decreased cell proliferation i*n vitro*, but complete IDH1^{R132H}-characteristic metabolic rewiring was not resembles in these celles, as evidenced by the lack of silencing of BCAT1 and LDH-A, two genes that are known to be silenced in clinical *IDH*^{mut} gliomas, as was also shown previously [127, 442]. BCAT1 catalyses the reversible transamination of α-KG to glutamate, and thus it can be hypothesized that co-expression of BCAT1, GLUD and IDH1^{R132H} in E98$^{FM\text{-}IDH1R132H}$ can lead to a situation in which BCAT1 converts α-KG back to glutamate, resulting in a futile glutamate-α-KG-glutamate cycle. It must however be noted that the *D*-2-HG-induced glioma CpG island methylator phenotype (G-CIMP) in endogenous *IDH*^{mut} glioma, takes many passages to fully develop [54]. The toxicity of *D*-2-HG production does not allow such long lasting *in vitro* experiments [443].

Alternative models of *IDH1*^{R132H}, such as HCT116 with a heterozygous knock in of the *IDH1*^{R132H} gene (HCT116-*IDH1*$^{wt/R132H}$) exist and are often used as a research model for *IDH1*^{mut} gliomas [395, 418, 444-447]. Although this cell model also produces the oncometabolite *D*-2-HG, it is of colorectal origin, and therefore is not fully representative for glioma, since these cells originate from different microenvironments. Indeed, comparison of RNA levels of the HCT116 and HCT116-*IDH1*$^{wt/R132H}$, revealed a complete lack of expression of BCAT1 in both IDH1^{R132H} as well as IDH1^{wt} cell lines, and the expression of LDH-A was higher HCT116-*IDH1*$^{wt/R132H}$ compared to HCT116, opposite to clinical gliomas (Figure 1, unpublished data) [127, 442]. Other differences we found between the two cell lines include increased expression of GLS, but not GLUD1/2, which may be indicative of increased glutaminolysis rather than glutamatolysis. When comparing the cell models to human glioma samples, more differences in metabolic fingerprints become apparent, such as expression of genes involved in shuttling pyruvate into the TCA cycle

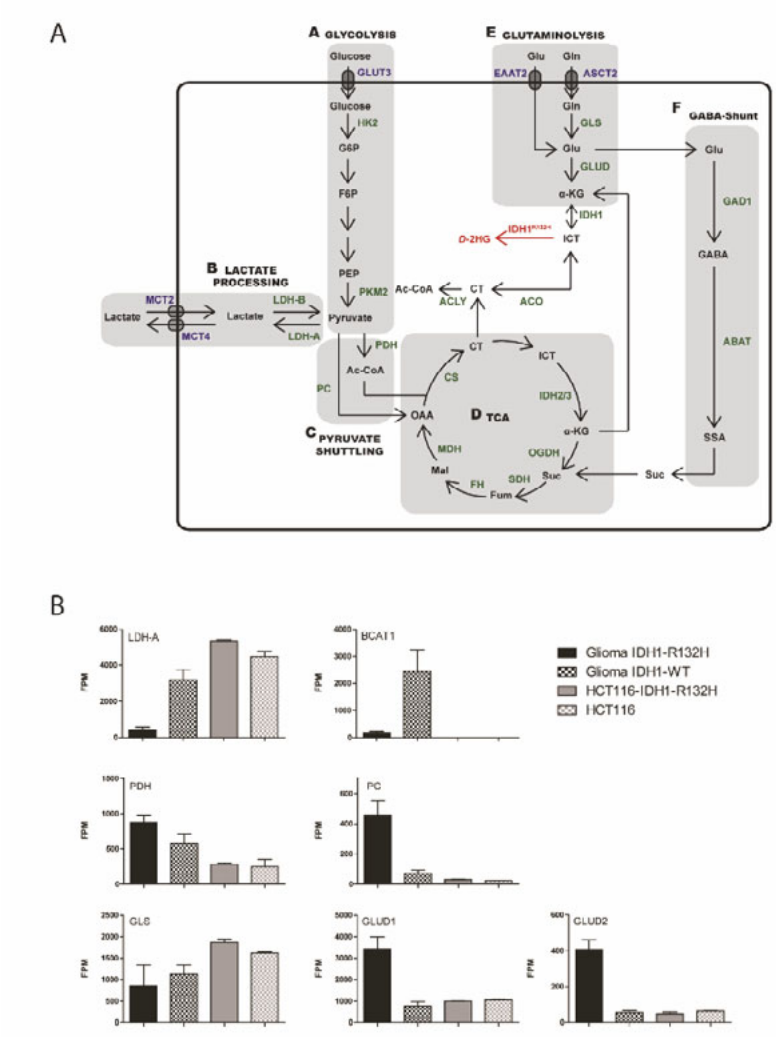

Figure 1: RNA expression of enzymes involved in glioma metabolism. *A) schematic overview of metabolic pathways involved in (IDHR^{r132H}-mutated) glioma. B) RNA expression of various enzymes in original human glioma samples and the HCT116 cell line which is often used in IDH-1 mutant glioma research. ABAT γ-Aminobutyrate aminotransferase; Ac-CoA Acetyl-CoA; aKG Alpha-ketoglutarate; ASCT2 Anti-neutral amino acid transporter 2; BCAT Branched-chain amino acid transaminase; CS Citrate synthase; CT Citrate; D-2HG D-2-hydroxyglutarate; EAAT2 Excitatory amino acid transporter 2; F6P Fructose-6-phosphate; FH Fumarate hydratase; G6P Glucose-6-phosphate; GABA γ-Aminobutyric acid; GAD1 Glutamate decarboxylase 1; Gln Glutamine; GLS Glutaminase; Glu Glutamate; GLUD Glutamate dehydrogenase; GLUT3 Glucose transporter 3; HK2 Hexokinase 2; ICT Isocitrate; IDH Isocitrate dehydrogenase; LDH Lactate dehydrogenase; MCT Monocarboxylate transporter; MDH1 Malate dehydrogenase1; OAA Oxaloacetate; OGDH α-Ketoglutarate dehydrogenase; OXPHOS Oxidative phosphorylation; PC Pyruvate carboxylase; PDH Pyruvate dehydrogenase; PEP Phosphoenolpyruvate; PKM Pyruvate kinase M; SDHD Succinate dehydrogenase D; SSA Succinic semialdehyde; Suc Succinate; TCA Tricarboxylic acid cycle.*

(such as pyruvate dehydrogenase (PDH) and pyruvate carboxylase (PC)), which were expressed at much lower levels than in human glioma samples (Figure 1B). This together with high expression of LDH-A in the cell lines, might indicate completely reversed lactate shuttling in the cell model as opposed to clinical glioma [127, 313].

The best option to study glioma biology and possible novel therapeutic interventions, of course is through human gliomas, but this is not always an option. Therefore, the second-best option might be through studying *in vivo* models in which cancer cells are directly xenografted in the brain after surgical resection [436]. Culturing freshly resected (cancer) cells under serum conditions *in vitro* before xenografting is known to change the metabolic, genetic and morphologic properties of many cells, including those of IDH^{mut} cells, as we have also seen in our own E98-xenograft model [54, 448-452]. This, in combination with the increased understanding of the interactions between glioma cells and their microenvironment, increases the interest in the use of orthotopic glioma models such as E478 that are generated by direct inoculation of surgically derived cancer cells without prior culturing. This model was generated in our laboratory and is one of the few $IDH1^{R132H}$ xenograft models in the world. This model is highly similar to the anaplastic oligodendroglioma from which it was originally derived [114]. The metabolic fingerprint of this model closely resembles that of IDH^{mut} gliomas, but because these models are grown in (immunodeficient) mice, they cannot fully recapitulate the microenvironment found in a human setting. In addition, research with these models is slow, because it takes 3-4 months to fully develop a glioma in these mice. Many attempts have been made of culturing these cells *in vitro*, under many different culture conditions, but thus far we have not been able to successfully propagate these cells for longer than 5 passages.

Although all these models have proven valuable for investigation of metabolic fluxes, epigenetic alterations and novel therapeutic strategies, they may also result in misinterpretation of the results and thus should be carefully selected and results should be interpreted with caution.

Cancer metabolism and metabolic profiling of IDH^{mut} glioma

Metabolism is a set of chemical reactions that occur in living organisms (and each individual cell) in order to maintain life. The main purposes of metabolism are the conversion of nutrients to energy to run cellular processes, conversion to building blocks for proteins, lipids, nucleic acids and carbohydrates, and the elimination of nitrogenous waste. It involves complex sequences of controlled biochemical reactions that occur in distinct metabolic pathways that convert one (bio)chemical into another (bio)chemical through a series of steps that are facilitated by specific enzymes. These processes allow organisms to grow and reproduce, maintain tissue (and cellular) structures, and respond to environmental changes.

Cellular metabolic reprogramming is an important mechanism by which cells alter their metabolism in order to support specific energetic demands, e.g. to promote proliferation and

cell growth and is mostly studied in light of cancer and tumorigenesis [453]. Cancer metabolism has been one of the earliest areas of research in understanding cancer biology, with the first observations made by Otto Warburg nearly a century ago [6, 454-456]. Reprogramming of pathways to meet the high bioenergetic need of fast proliferating malignant cells is both direct and indirect consequences of oncogenic mutations, and is required for oncogenesis and malignant progression, including invasion and metastasis. Reprogramming of metabolism is observed in general across many cancer types and therefore is considered a 'hallmark of cancer' [3]. Activation of key oncogenic signalling pathways (PI3K/Akt/mTORc, HIF1), or inactivation of tumour suppressor genes (e.g. p53, PTEN, CDKN2A) due to mutations can directly affect cancer cell metabolism by upregulation of nutrient transporters or enzymes in anabolic pathways including glycolysis and glutaminolysis [457]. In addition, metabolic enzymes can act as oncogenes or tumour suppressors directly. Mutations in TCA cycle-associated enzymes such as *SDH, FH*, and *IDH* have been found in multiple types of cancer. Inactivating mutations in both SDH and FH lead to accumulation of their respective substrates succinate and fumarate, and mutations in *IDH* lead to a depletion of α-KG, while simultaneously producing high amounts of the oncometabolite *D*-2-HG. These metabolic adaptations have been linked to epigenetic changes that result in epithelial-to-mesenchymal (EMT) transition and thus tumour progression, or inhibition of several α-KG-dependent dioxygenases [458-460] that affect multiple cellular processes.

Comprehensive metabolic profiling or 'metabolomics' is increasingly being applied to many pathologies, including cancer and cardiovascular disease [461, 462]. Metabolomics is the measurement of low-molecular-weight metabolites and their intermediates, that provides (semi-)quantitative information of steady-state abundance of intermediates from many different metabolic pathways [463, 464]. This method requires analytical techniques such as nuclear magnetic resonance spectroscopy (NMR), magnetic resonance spectroscopy (MRS), mass-spectrometry (MS), and liquid chromatography MS (LC-MS) [462]. Due to the complexity (and costs) of these methods, these are often restricted to a research setting [465].

In order to provide a more cost-effective, less time-consuming, and easier to analyse technique to map actionable metabolic pathways and identify new biomarkers in diffuse glioma, in **chapter 3**, we show that with a novel technique of targeted RNA next generation sequencing (t/RNA-NGS) [312], we can generate histology-independent molecular diagnoses, and identify classifiers that are strongly related to conventional diagnostic histopathologic diagnoses [466]. The gene panel used consists of genes involved in metabolism, tyrosine kinase signalling, angiogenesis signalling and immune response, which are known to be affected in glioma and many other different cancer types. One of the main advantages of this type of profiling, in addition to being cost-effective, is that it can also identify new actionable biomarkers, which are already often found in other types of cancer, such as lung cancer, renal cell carcinoma and head and neck cancers.

The assay has also been designed to give us clues about the specific metabolic rewiring in *IDH*^{mut} gliomas. Many studies have shown that the metabolism of *IDH*^{mut} glioma greatly differs from that of *IDH*^{wt}, which most likely relieves metabolic stress that is inflicted by the IDH1 mutation [127, 353, 355]. Compensatory pathways resupply the glioma with both NAPDH and α-KG, which allows for tumour progression. We previously showed using *in silico* analyses, that *IDH*^{mut} gliomas mainly express genes that are involved in glutamate and lactate anaplerosis, whereas *IDH*^{wt} gliomas mainly express enzymes that are involved in glycolysis and acetate anaplerosis [127]. This observation is in line with our hypothesis that indeed, *IDH*^{mut} gliomas rely on glutamate more than glutamine [120, 128, 465]. In **chapter 4** we provide evidence that *IDH*^{mut} gliomas might alleviate their metabolic stress by fuelling the TCA cycle via glutamate-derived α-KG- and lactate-derived oxaloacetate, through the combined methods of gene expression profiling, *in situ* and *in vivo* functional studies. *In vivo* MRSI data from our xenograft model E478 (*IDH1*^{R132H}) and E434 (*IDH1*^{wt}), showed that E478 had much lower glutamate levels compared to E434, accompanied by a decreased choline/NAA ratio, which has also been described by others [467]. These decreased levels of glutamate might indicate higher uptake and metabolism of glutamate. We also found increased levels of glutamine, which could be indicative of accumulating glutamine due to decreased glutaminase (GLS) activity, which has been supported by various studies [353, 467, 468]. The GLS inhibitor BPTES has been shown to be primarily effective in IDH1^{R132H} glioma cells, but effects were limited [122]. The lack of efficacy could be explained by our model that suggests that there is a preferential role for glutamate processing though GLUD1/2, as we show with ^{13}C-tracing studies in **chapter 5**. Inhibition of GLUD1/2 could therefore be a more appropriate targeting approach, also given te notion that GLUD1/2 is downstream of GLS, which we discuss further below.

In addition to lactate and glutamate, we also found clues for the possible role of the neurotransmitter GABA, through the GABA-shuttle, in *IDH*^{mut} glioma TCA anaplerosis (**Chapter 4,** figure 7). This finding suggests that neurotransmitters that are readily available in the brain can be used by glioma cells for resupplying metabolites that are diminished by the IDH1^{R132H} mutation. The alleviation of metabolic stress can allow tumour progression in these cancer cells and might also explain the diffuse infiltrating growth of glioma cells, and *IDH*^{mut} glioma cells in particular. [469, 470] As recently shown by Venkartaramani *et al.* [471] and Venkatesh *et al.* [472], there is a direct communication channel between presynaptic neurons an post-synaptic glioma cells via AMPA receptors (a glutamate receptor in the brain [116]), which might also hold true for *IDH*^{mut} glioma cells. They describe that glioma growth is promoted through microenvironmental interactions such as neuron-to-glioma synaptic transmission. This, together with the relatively high expression of EAAT2 (a glutamate importer) on *IDH*^{mut} glioma cells [124, 313], may further strengthen our hypothesis that these gliomas indeed utilize glutamate to their advantage in growth and survival. Very interesting new information was recently published on how glioblastomas interact with neurons [473], and a roadmap was presented on how to shape the emerging field of Cancer Neuroscience. [474]. These recent

understandings might pave the way to develop novel treatment strategies targeting neuron-glioma interactions.

Mapping of genes shared across many different cancer types possibly also makes our t/RNA-NGS assay applicable in a routine diagnostic setting [475-477]. In addition, identification of mutations and active metabolic pathways could allow for a personalized treatment approach. Protocols that allow for off-label use of anticancer drugs have already proven to be of significant value in patient care [478], and research regarding this is still ongoing (e.g. CPCT-02 (NCT01855477) and DRUP (NCT02925234)), and further exploitation of a tumour agnostic approach needs to be validated.

Personalized medicine in glioma

Targeted therapy is a type of treatment that specifically targets oncogenic pathways, such as signal transduction pathways and metabolic pathways, with relative sparing of healthy cells. An increasing understanding of molecular underpinnings of tumorigenesis has enabled the development drugs that specifically target the aberrant pathways in cancer. Most of these drugs are small molecule tyrosine-kinase inhibitors, monoclonal antibodies, or antibody-drug conjugates. High-throughput analysis of many glioma patient samples has shown that gliomas contain many types of mutations and aberrant oncogenic pathways, including mutations in *TP53,* amplification of *EGFR*, homozygous deletion of *CDKN2a*, mutations in *PTEN,* and *IDH* [73, 479, 480]. These molecular advances provide a rationale for precision medicine, in which cancer therapy is tailored specifically to a patient, based on genomic or epigenomic alterations in individual cancers [481, 482]. A few examples of targeted therapies are gefitinib or erlotinib in *EGFR*-mutated lung cancers [483, 484], vemurafenib in *BRAFV600E*-mutated melanomas [485, 486], and olaparib for *BRCA1/2* mutated ovarian, [487], breast [488] and prostate cancer [489]. Trials investigating targeted therapies in glioma, including the VEGF-inhibitor bevacizumab [74], various EGFR(vIII) inhibitors, a.o. erlotinib and gefitinib [75-79], and c-MET inhibitors [80, 81] have failed to improve patient outcomes thus far, partly due to resistance mechanisms such as the BBB, which limits drug entry into the brain parenchyma [490]. A high unmet need for novel therapeutic strategies for glioma still exists. However, due to the low incidence and high molecular heterogeneity of glioma, it is a difficult tumour type to organize clinical trials for, resulting in almost no significant advancement of patient outcomes in the last decades. As described in chapter 3, with t/RNA-NGS we can identify gene activities that have been associated with other cancer types, such as PSMA, AR, ErbB3/4, and NTRK2 expression. It can be hypothesized that the possibility to detect expression of these proteins on the transcript level will open up ways for novel therapies such as vascular targeting with ^{177}Lutetium-PSMA (currently under investigation in prostate cancer), targeting of AR with enzalutamide [339] or apalutamide [491], ErbB3/4 targeting with ibrutinib (ClinicalTrials.gov Identifier: NCT03535350), or targeting of NTRK2 expression with the novel tumour-agnostic NTRK-inhibitor larotrectinib [492] (if an *NRTK*-fusion gene is present, which are found in a small subset of gliomas [493-495]).

Metabolic targeting of *IDH*^{mut} glioma

Metabolic reprogramming by cancer cells introduces liabilities that can be exploited to treat cancer. For decades now, chemotherapy that targets metabolism has been effective in many different cancer types. In 1947, Sidney Farber, an American paediatric pathologist, discovered that folic acid plays a key role in the progression of acute lymphoblastic leukaemia in children, and that this could be exploited to combat the disease [496]. He used folic acid antagonists that inhibit one-carbon transfer reactions necessary for *de novo* nucleotide synthesis [497]. This discovery led to an entire class of antimetabolic drugs, that resemble nucleotide metabolites and inhibit the enzymes involved in nucleotide base synthesis [498-500]. The clinical success of antimetabolites can be attributed to the increased demand of cancer cells to produce nucleotides for DNA replication needed for cell division. Biosynthesis of nucleotides, however, is only one of the many different metabolic pathways that are altered in cancer cell proliferation that can be targeted [501, 502]. These pathways may be attractive therapeutic targets. However, non-neoplastic proliferating cells have similar metabolic requirements. Finding a therapeutic window for distinguishing between cancer cells and normal cells remains a major challenge in developing metabolically targeted cancer therapies [502]. Another major hurdle in metabolism-targeted therapy development, is identifying which patients will most likely respond to a given therapy. With targeted cancer therapy, patient selection is often predicted based on genomics and expression of oncogenes or increased activity of a downstream signalling pathway. Many emerging metabolic targets are widely expressed in many different cancers, but dependency on altered metabolism is not a universal cancer trait [32]. So why is targeting metabolism in cancer still a much sought-after area of research? One of the reasons is that metabolism is linked to cancer initiation and progression, for instance by activation of the PI3K signal transduction pathway via Insulin Growth Factor 1 (influencing metabolic pathways downstream), or mTOR activation (regulated by nutrient availability) [503, 504]. Another reason is that metabolic targeting may synergize with other therapies.

As we discuss in **chapter 4 and 5,** understanding the consequences of metabolic rewiring inflicted by oncogenic mutations is the first step in developing novel treatment approaches targeting tumour cell metabolism. We show in **chapter 5** that *IDH*^{mut} cancer cells can directly utilize glutamate for anaplerosis of the TCA cycle, and ultimately production of *D*-2-HG. IDH1 and IDH2 are both $NADP^+$-dependent homodimeric enzymes that oxidize isocitrate to α-KG. In the process of this reaction, NADPH is formed which contributes to the reductive potential of the cell [91, 392]. In cells harbouring a mutation in *IDH1*, α-KG is quickly converted to *D*-2-HG, which diminishes the levels of α-KG as well as NADPH. To alleviate metabolic stress inflicted by the mutation, the cells need to supply α-KG through alternative routes, one of which is through glutamate. We show that by directly targeting glutamate metabolism through the glutamate dehydrogenase (GLUD) inhibitor epigallocatechin-3-gallate (EGCG), we could inhibit *D*-2-HG production, as well as sensitize the tumour cells to radiotherapy.

EGCG has been studied over the last three decades for its beneficial effects in obesity, diabetes, inflammatory diseases and cancer [505]. Concentrations of EGCG in the circulation have been reported to be very low after oral ingestion [506, 507] and it is therefore uncertain which concentrations can be reached in the brain when the compound is taken orally. As we show in chapter 5, rather high concentrations of EGCG are needed for a sensitizing effect, with even radioprotective effects reported when concentrations of EGCG are low [508]. This is in line with the notion that EGCG can have oxidative as well as antioxidative properties [509]. This warrants further research into delivery strategies of EGCG to the brain, in order to achieve the high concentrations of EGCG needed for its radiosensitizing effects. Other compounds that inhibit GLUD1/2, such as chloroquine [510, 511] might also prove to be effective in targeting *IDH*^{mut} glioma, and is currently being tested in clinical trials (NCT02378532, and NCT00224978).

Additionally, we also show that inhibition of the mutation directly via the IDH1^{R132H} specific inhibitor AGI-5198 decreased sensitivity to radiotherapy. Direct targeting of the aberrant IDH enzyme through various small molecule inhibitors might at first seem like a promising strategy. However, it directly prevents the production of *D*-2-HG and decreases oxidative stress, thereby desensitizing cells to ionizing radiation and chemotherapy [350, 395]. Although direct inhibition of mutant IDH1 might be effective at first, ultimately resistance will develop through e.g. isoform switching or *trans* or *cis* dimer-interface mutations [394, 512, 513].

Understanding the full effects or metabolic rewiring might provide us with new clues to exploit compensatory metabolic pathways in addition to targeting mutated proteins directly. In this regard, targeting of enzymes involved in glycolysis such as hexokinase 2/3 or pyruvate kinase M2, or enzymes involved in acetate metabolism, such as MCT1/4 or acetyl-coA synthetase (ACSS1/2), might be viable treatment strategy in *IDH*^{wt} glioma, which mainly rely on glucose and acetate for TCA cycle anaplerosis [127].

Concluding remarks and future perspectives

With this thesis we contribute to a better understanding of the changes in metabolism inflicted by the *IDH1*^{R132H}-mutation in glioma. Via a novel targeted RNA-NGS assay, we identified possible novel therapeutic targets such as ErbB3, ErbB4, and NTRK2, and showed that *IDH*^{mut} gliomas have a different metabolic RNA expression signature than *IDH*^{wt} gliomas. We provide clues that the *IDH*-mutation causes rewiring of active metabolic pathways towards a dependency of glutaminolysis for replenishment of the TCA both in an *in vitro* and *in vivo* setting. Furthermore, we found clues that suggest that glutamate, rather than glutamine plays a central role in this metabolic rewiring, as this neurotransmitter is readily available in the brain. Relatively high expression levels of the glutamate transporter EAAT2 may indicate an important role of glutamate in these cells.

Although cancer metabolism is a widely studied field, we still do not have a solid understanding of the implications of rewiring of metabolism in cancer cells. Further

unravelling of the cancer specific metabolic fingerprints is necessary to develop novel strategies that will deprive cancer cells of metabolites needed for growth and progression. In addition, more research should focus on exploring the efficacy of combining treatments that inhibit metabolic rewiring with sensitizing tumour cells to e.g. DNA damaging agents such as chemotherapy or radiotherapy. In this work we showed that inhibition of glutamate processing through the GLUD1/2 inhibitor EGCG, affected *IDH1*^{mut} cells more than *IDH1*^{wt} cells, and that we could even sensitize *IDH*^{mut} cells to radiotherapy in *in vitro* studies. Before moving into the clinic, future efforts should concentrate on corroborating these findings in an *in vivo* setting. Novel delivery strategies should be exploited to be certain that the necessary concentrations of EGCG are delivered to the brain and that EGCG can have its oxidative and thus radiosensitizing effects.

To conclude, although recent efforts in metabolic characterization of glioma has provided us with better insights into gliomagenesis, metabolic rewiring in these cancers in still not fully understood. In the future we need to gain more knowledge of the drivers of this altered metabolism, and put more efforts into treatment strategies that either deprive tumour cells of the metabolites necessary for rewiring, or come up with therapeutic combination strategies that will allow us to use the altered metabolism to our advantage, such as sensitizing cancer cells to ionizing radiation.

SUMMARY

Cancer is one of the leading causes of death worldwide, and with an increasingly aging population, incidence and mortality rates of cancer are increasing, despite expanding understanding of cancer biology. This improved understanding has resulted in a multitude of novel treatments for various types of cancers. For diffuse gliomas, however, over the last decades only a limited number of novel treatment protocols have been implemented. A major hurdle in delivering systemic therapies in the brain is the presence of a blood-brain barrier (BBB), which is impermeable for many different molecules (of note, in high-grade glioma the BBB is partly leaky due to angiogenesis).

The largest gain in patient survival has been accomplished through novel imaging techniques that result in better surgical resection of the tumour. Due the infiltrative growth of glioma cells into the brain parenchyma, complete resection of diffuse gliomas however is not possible. Development of novel, more efficacious therapeutic options for the treatment of diffuse gliomas are therefore urgently needed.

The discovery of heterozygous mutations in the metabolic gene *isocitrate dehydrogenase (IDH)* in the majority of diffuse low-grade gliomas and in high-grade neoplasms derived from such lower grade gliomas, has been a major breakthrough in the understanding of gliomagenesis, and fits with the (re)gained interest in tumour metabolism, one of the 'hallmarks of cancer', in which aberrant metabolic pathways of tumour cells are used as a therapeutic strategy. IDH plays a central role in the TCA cycle, an important metabolic pathway. Mutations in IDH mostly involve Arg132 in IDH1 and Arg172 or Arg140 in IDH2, and results in a gain-of-function of the enzyme. Whereas normal IDH1 converts isocitrate to alpha-ketoglutarate (α-KG) with simultaneous reduction of $NAPD^+$ to NADPH, mutant IDH reduces α-KG to *D*-2-HG, while oxidizing NADPH. *D*-2-HG acts as an oncometabolite via competitive inhibition of α-KG-dependent enzymes that are involved in metabolism and epigenetic regulation. Of note, patients with *IDH*-mutant gliomas or GBMs have longer overall survival than patients with *IDH* wild-type gliomas.

The aim of this thesis therefore is to better understand 1) the metabolic pathways involved in gliomagenesis, 2) the rewiring that *IDH*-mutated gliomas have undergone in their malignant transformation, as well as 3) investigate how we can exploit these aberrant pathways for novel therapeutic approaches. In addition, we aim to identify cancer-associated biomarkers in human glioma samples that may be used for personalized therapies. In **chapter 1**, the context of the work described in this thesis is introduced.

Glioma research often makes use of glioma models that not necessarily reflect the complex metabolic and epigenetic status of human glioma samples with an *IDH*-mutation. In **chapter 2**, we discuss which research models, both *in vitro* and *in vivo,* are available and which advantages and limitations these models have. Although several different models have proven valuable for investigation of the effects of *IDH*-mutations on both metabolism and epigenetics, they may also result in misconceptions. Careful selection of the models used to answer research questions is therefore warranted.

In **chapter 3**, we introduce a novel targeted RNA-NGS assay that can generate a histology-independent molecular diagnosis for glioma, and that can identify actionable metabolic pathways as well as new markers for glioma, such as ErbB3, ErbB4, and NTRK2 (which are often found in other cancer types) that might be used as targeting strategies with already existing therapeutics.

In order to further unravel the rewired metabolism in *IDH*^{mut} gliomas, in **chapter 4** we focus on changes in metabolic pathways that are involved in fuelling these gliomas. Human glioma samples provided us clues on which metabolic pathways are preferentially used for anaplerosis of TCA cycle metabolites. We propose a model in which *IDH*-mutant gliomas are mainly dependent on glutamate and lactate anaplerosis, while for *IDH* wild-type gliomas, glucose and glutamine processing are more predominant. The data was supported by quantified metabolite levels in *in vivo* MRS in orthotopic *IDH*^{mut} and *IDH*^{wt} glioma xenografts, as well as *in situ* enzymatic activity mapping.

In **chapter 5** we further show that glutamate can be directly processed by cells harbouring mutated IDH1^{R132H}, via NMR and MS experiment using ^{13}C- glucose, -glutamine or -glutamate tracing experiments. Glutamate-dependency opens the way for novel treatment approaches that directly target the glutamate pathway. We provide clues that this pathway is indeed targetable, using the green tea extract EGCG, which inhibits cell proliferation in *IDH*^{mut} cells significantly more than *IDH*^{wt} cells. In addition, we show that inhibition of the glutamate processing pathways with EGCG sensitizes the *IDH*^{mut} cells for radiotherapy. This possibly opens up the way for combination treatment of glutamatolysis-inhibiting therapies with DNA-damaging therapies such as chemotherapy or radiotherapy.

Before starting clinical trials, further research in an *in vivo* setting is required to determine the efficacy of the proposed combination therapy.

Chapter 6 presents a genral discussion of the findings of our own work, and puts these findings in a broader context.

SAMENVATTING

Kanker is een van de belangrijkste doodsoorzaken wereldwijd. Ondanks dat we steeds meer van de ziekte begrijpen, nemen zowel de incidentie als het sterftecijfer van kanker toe door de toenemende vergrijzing van de bevolking. Het toegenomen begrip van kankerbiologie heeft geresulteerd in een veelvoud aan nieuwe behandelingen voor verschillende soorten kanker. Voor de behandeling van diffuse gliomen zijn de afgelopen decennia echter slechts een beperkt aantal nieuwe behandelprotocollen geïmplementeerd. Een belangrijke hindernis bij het toedienen van systemische therapieën bij de behandeling van diffuus glioma is de aanwezigheid van een bloed-hersenbarrière (BBB) die ondoordringbaar is voor veel verschillende moleculen (let wel: bij hooggradig glioom is de BBB gedeeltelijk lek als gevolg van angiogenese en is daarmee niet compleet ondoordringbaar). De grootste winst in overleving is bereikt door nieuwe beeldvormingstechnieken die benut kunnen worden voor een betere chirurgische resectie van de tumor. Door de infiltratieve groei van glioma cellen in het hersenparenchym is volledige resectie van de tumor echter niet mogelijk. De ontwikkeling van nieuwe therapeutische opties voor de behandeling van glioom is daarom dringend nodig.

De ontdekking van heterozygote mutaties in het metabole enzym isocitraat dehydrogenase (IDH) in de meeste diffuse laaggradige gliomen en in glioblastoma die uit zulke minder maligne gliomen ontstaan, is een belangrijke doorbraak in het begrip van gliomagenese geweest. Dit past bij de toegenomen (her)interesse in onderzoek naar tumormetabolisme. Bepaalde metabole veranderingen in tumorcellen vormen één van de 'kenmerken van kanker' (‘hallmarks of cancer’), en het onderzoek richt zich o.a. op het remmen van de metabole routes waarvan tumorcellen afhankelijk zijn. IDH speelt een centrale rol in de citroenzuurcyclus (TCA cyclus). Mutaties in *IDH* komen voornamelijk voor op positie Arg132 in IDH1 en Arg172 of Arg140 in IDH2. Deze mutaties resulteren in een nieuwe functie van het enzym (gain-of-function). Terwijl normaal IDH1 isocitraat omzet in alfa-ketoglutaraat (α-KG) met gelijktijdige reductie van NAPD+ naar NAPDH, reduceert mutant IDH α-KG tot D-2-HG, terwijl NAPDH wordt geoxideerd. D-2-HG zorgt voor competitieve remming van α-KG-afhankelijke enzymen die betrokken zijn bij het metabolisme en de epigenetische regulatie en wordt daarom een ‘oncometaboliet’ genoemd. Interessant is dat patiënten met *IDH*-mutante gliomen of GBM’s een langere overleving hebben dan patiënten IDH wild-type gliomen van histologisch dezelfde maligniteitsgraad.

Het doel van dit proefschrift is daarom ook om een beter begrip te krijgen van 1) de metabole routes die betrokken zijn bij gliomagenese, 2) hoe het metabolisme van *IDH*-mutante gliomen veranderd is door de mutatie in het enzym IDH, en 3) hoe we dit afwijkende metabolisme kunnen gebruiken voor nieuwe therapeutische benaderingen. Daarnaast willen we kanker gerelateerde biomarkers identificeren die kunnen worden gebruikt voor gepersonaliseerde therapieën. In **hoofdstuk 1** wordt de context van het werk beschreven in dit proefschrift geintroduceerd.

Bij glioma onderzoek wordt vaak gebruik gemaakt van glioma modellen die niet noodzakelijkerwijs de complexe metabole en epigenetische staat van de oorspronkelijke

gliomen met een *IDH*-mutatie weerspiegelen. In **hoofdstuk 2** bespreken we welke onderzoeksmodellen, zowel *in vitro* als *in vivo*, beschikbaar zijn en welke voordelen en beperkingen deze modellen hebben. Hoewel verschillende modellen waardevol zijn gebleken voor het onderzoeken van de effecten van *IDH*-mutaties op zowel het metabolisme als de epigenetica, kunnen ze ook resulteren in een verkeerde interpretatie van de resultaten omdat ze in veel opzichten geen accurate afspiegeling zijn van wat we in de humane situatie vinden. Een zorgvuldige selectie van de modellen die worden gebruikt om onderzoeksvragen te beantwoorden, is daarom cruciaal.

In **hoofdstuk 3** introduceren we een nieuwe gerichte RNA-NGS-test die precieze, moleculair-gebaseerde diagnose kan genereren zonder histologisch onderzoek. Deze test identificeert welke metabole routes 'aan' staan in de tumor, alsmede nieuwe predictieve biomarkers voor glioma, zoals ErbB3, ErbB4 en NTRK2 (die gevonden worden in andere kankertypes). Deze biomarkers kunnen wellicht ook worden gebruikt om nieuwe therapie opties te bieden voor patiënten met een glioom.

Om het veranderde metabolisme in *IDH* mutante-gliomen verder te ontrafelen, hebben we ons in **hoofdstuk 4** gericht op het in kaart brengen van veranderingen in metabole routes die betrokken zijn bij het onderhouden van deze gliomen. Weefselmonsters van gliomen geven aanwijzingen over welke metabole routes bij voorkeur worden gebruikt voor anaplerose (het weer aanvullen van metabolieten) van TCA cyclus. We stellen een model voor waarin *IDH*-mutante gliomen voornamelijk afhankelijk zijn van glutamaat en lactaat, terwijl voor *IDH* wild-type gliomen glucose en glutamine de voornaamste metabolieten zijn die gebruikt worden voor anaplerose van de TCA cyclus. Deze bevindingen worden ondersteund door gekwantificeerde niveaus van metabolieten gevonden in *in vivo* MRS proeven die zijn uitgevoerd in orthotope modellen voor *IDH*-mutante of *IDH*-wild-type gliomen. *In situ* enzymatische activiteitsproeven onderbouwen deze bevindingen verder.

In **hoofdstuk 5** laten we via Nuclear Magnetic Resonance spectroscopie en massa spectroscopie-experimenten zien dat zien dat cellen met de $IDH1^{R132H}$-mutatie direct glutamaat verwerken. Deze afhankelijkheid van glutamaat kan leiden tot nieuwe behandelmogelijkheden die direct gericht zijn op het remmen van de metabole routes die verantwoordelijk is voor glutamaat verwerking. Het remmen van deze route met het groene thee extract EGCG liet zien dat groei van *IDH*-mutante cellen sterker werd geremd dan de groei van wild-type *IDH*-cellen. Bovendien laten we zien dat het behandelen van *IDH*-mutante cellen met EGCG de cellen gevoeliger maakt voor radiotherapie. Dit opent mogelijkerwijs de weg naar behandeling van IDH-mutante gliomen met glutamatolyse-remmende middelen in combinatie met therapieën gericht op het veroorzaken van DNA-schade zoals chemo- of radiotherapie. Er zal verder onderzoek gedaan moeten worden naar de effectiviteit van deze combinatie in dierproeven, voordat het in klinische trials getest kan worden.

Hoofdstuk 6 beschrijft een algemene discussie van de bevingdingen van het werk beschreven in dit proefschrift en zet deze bevindingen in een bredere context.

REFERENCES

1. Bray, F., et al., *Global cancer statistics 2018: GLOBOCAN estimates of incidence and mortality worldwide for 36 cancers in 185 countries.* CA Cancer J Clin, 2018. **68**(6): p. 394-424.
2. Seyfried, T.N. and L.C. Huysentruyt, *On the origin of cancer metastasis.* Crit Rev Oncog, 2013. **18**(1-2): p. 43-73.
3. Hanahan, D. and R.A. Weinberg, *Hallmarks of cancer: the next generation.* Cell, 2011. **144**(5): p. 646-74.
4. Hanahan, D. and R.A. Weinberg, *The hallmarks of cancer.* Cell, 2000. **100**(1): p. 57-70.
5. da Silva-Diz, V., et al., *Cancer cell plasticity: Impact on tumor progression and therapy response.* Semin Cancer Biol, 2018. **53**: p. 48-58.
6. Warburg, O., F. Wind, and E. Negelein, *The Metabolism of Tumors in the Body.* J Gen Physiol, 1927. **8**(6): p. 519-30.
7. Pavlova, N.N. and C.B. Thompson, *The Emerging Hallmarks of Cancer Metabolism.* Cell Metab, 2016. **23**(1): p. 27-47.
8. DeBerardinis, R.J. and N.S. Chandel, *Fundamentals of cancer metabolism.* Sci Adv, 2016. **2**(5): p. e1600200.
9. Martinez-Reyes, I. and N.S. Chandel, *Mitochondrial TCA cycle metabolites control physiology and disease.* Nat Commun, 2020. **11**(1): p. 102.
10. Eales, K.L., K.E. Hollinshead, and D.A. Tennant, *Hypoxia and metabolic adaptation of cancer cells.* Oncogenesis, 2016. **5**: p. e190.
11. Feig, S.A., et al., *Energy metabolism in human erythrocytes. II. Effects of glucose depletion.* J Clin Invest, 1972. **51**(6): p. 1547-54.
12. Brooks, G.A., *Cell-cell and intracellular lactate shuttles.* J Physiol, 2009. **587**(Pt 23): p. 5591-600.
13. Adeva-Andany, M., et al., *Comprehensive review on lactate metabolism in human health.* Mitochondrion, 2014. **17**: p. 76-100.
14. Brooks, G.A., *Lactate shuttles in nature.* Biochem Soc Trans, 2002. **30**(2): p. 258-64.
15. Gladden, L.B., *Lactate metabolism: a new paradigm for the third millennium.* J Physiol, 2004. **558**(Pt 1): p. 5-30.
16. Bergersen, L.H., *Is lactate food for neurons? Comparison of monocarboxylate transporter subtypes in brain and muscle.* Neuroscience, 2007. **145**(1): p. 11-9.
17. Magistretti, P.J. and I. Allaman, *Lactate in the brain: from metabolic end-product to signalling molecule.* Nat Rev Neurosci, 2018. **19**(4): p. 235-249.
18. Boroughs, L.K. and R.J. DeBerardinis, *Metabolic pathways promoting cancer cell survival and growth.* Nat Cell Biol, 2015. **17**(4): p. 351-9.
19. Vander Heiden, M.G., L.C. Cantley, and C.B. Thompson, *Understanding the Warburg effect: the metabolic requirements of cell proliferation.* Science, 2009. **324**(5930): p. 1029-33.
20. Potter, V.R., *The biochemical approach to the cancer problem.* Fed Proc, 1958. **17**(2): p. 691-7.
21. Lopez-Lazaro, M., *The warburg effect: why and how do cancer cells activate glycolysis in the presence of oxygen?* Anticancer Agents Med Chem, 2008. **8**(3): p. 305-12.
22. Almuhaideb, A., N. Papathanasiou, and J. Bomanji, *18F-FDG PET/CT imaging in oncology.* Ann Saudi Med, 2011. **31**(1): p. 3-13.
23. Zhu, J. and C.B. Thompson, *Metabolic regulation of cell growth and proliferation.* Nat Rev Mol Cell Biol, 2019. **20**(7): p. 436-450.
24. Hatzivassiliou, G., et al., *ATP citrate lyase inhibition can suppress tumor cell growth.* Cancer Cell, 2005. **8**(4): p. 311-21.
25. DeBerardinis, R.J., et al., *The biology of cancer: metabolic reprogramming fuels cell growth and proliferation.* Cell Metab, 2008. **7**(1): p. 11-20.
26. Ahn, C.S. and C.M. Metallo, *Mitochondria as biosynthetic factories for cancer proliferation.* Cancer Metab, 2015. **3**(1): p. 1.

27. DeBerardinis, R.J., et al., *Beyond aerobic glycolysis: transformed cells can engage in glutamine metabolism that exceeds the requirement for protein and nucleotide synthesis.* Proc Natl Acad Sci U S A, 2007. **104**(49): p. 19345-50.
28. Yang, L., S. Venneti, and D. Nagrath, *Glutaminolysis: A Hallmark of Cancer Metabolism.* Annu Rev Biomed Eng, 2017. **19**: p. 163-194.
29. Tanaka, K., et al., *Compensatory glutamine metabolism promotes glioblastoma resistance to mTOR inhibitor treatment.* J Clin Invest, 2015. **125**(4): p. 1591-602.
30. Wise, D.R. and C.B. Thompson, *Glutamine addiction: a new therapeutic target in cancer.* Trends Biochem Sci, 2010. **35**(8): p. 427-33.
31. Akins, N.S., T.C. Nielson, and H.V. Le, *Inhibition of Glycolysis and Glutaminolysis: An Emerging Drug Discovery Approach to Combat Cancer.* Curr Top Med Chem, 2018. **18**(6): p. 494-504.
32. Luengo, A., D.Y. Gui, and M.G. Vander Heiden, *Targeting Metabolism for Cancer Therapy.* Cell Chem Biol, 2017. **24**(9): p. 1161-1180.
33. Livingston, R.B., et al., *Glutamine antagonists in chemotherapy.* Adv Pharmacol Chemother, 1970. **8**: p. 57-120.
34. O'Dwyer, P.J., M.T. Alonso, and B. Leyland-Jones, *Acivicin: a new glutamine antagonist in clinical trials.* J Clin Oncol, 1984. **2**(9): p. 1064-71.
35. Doherty, J.R. and J.L. Cleveland, *Targeting lactate metabolism for cancer therapeutics.* J Clin Invest, 2013. **123**(9): p. 3685-92.
36. Hay, N., *Reprogramming glucose metabolism in cancer: can it be exploited for cancer therapy?* Nat Rev Cancer, 2016. **16**(10): p. 635-49.
37. Natsume, A., et al., *Phase I study of a brain penetrant mutant IDH1 inhibitor DS-1001b in patients with recurrent or progressive IDH1 mutant gliomas.* Journal of Clinical Oncology, 2019. **37**(15).
38. Punekar, S. and D.C. Cho, *Novel Therapeutics Affecting Metabolic Pathways.* Am Soc Clin Oncol Educ Book, 2019. **39**: p. e79-e87.
39. Jessen, K.R. and R. Mirsky, *Glial cells in the enteric nervous system contain glial fibrillary acidic protein.* Nature, 1980. **286**(5774): p. 736-7.
40. Baumann, N. and D. Pham-Dinh, *Biology of oligodendrocyte and myelin in the mammalian central nervous system.* Physiol Rev, 2001. **81**(2): p. 871-927.
41. Siracusa, R., R. Fusco, and S. Cuzzocrea, *Astrocytes: Role and Functions in Brain Pathologies.* Front Pharmacol, 2019. **10**: p. 1114.
42. Nagatsu, T., *[Molecular mechanisms of neurotransmission].* Rinsho Shinkeigaku, 2000. **40**(12): p. 1185-8.
43. Andreae, L.C. and J. Burrone, *The role of spontaneous neurotransmission in synapse and circuit development.* J Neurosci Res, 2018. **96**(3): p. 354-359.
44. Snyder, S.H., *Neurotransmitters, Receptors, and Second Messengers Galore in 40 Years.* Journal of Neuroscience, 2009. **29**(41): p. 12717-12721.
45. Bowery, N.G. and T.G. Smart, *GABA and glycine as neurotransmitters: a brief history.* British Journal of Pharmacology, 2006. **147**: p. S109-S119.
46. Jiang, S.H., et al., *Neurotransmitters: emerging targets in cancer.* Oncogene, 2020. **39**(3): p. 503-515.
47. Meldrum, B.S., *Glutamate as a neurotransmitter in the brain: Review of physiology and pathology.* Journal of Nutrition, 2000. **130**(4): p. 1007s-1015s.
48. Daikhin, Y. and M. Yudkoff, *Compartmentation of brain glutamate metabolism in neurons and glia.* J Nutr, 2000. **130**(4S Suppl): p. 1026S-31S.
49. Debanne, D., et al., *Brain plasticity and ion channels.* Journal of Physiology-Paris, 2003. **97**(4-6): p. 403-414.
50. Marx, M.C., D. Billups, and B. Billups, *Maintaining the presynaptic glutamate supply for excitatory neurotransmission.* Journal of Neuroscience Research, 2015. **93**(7): p. 1031-1044.
51. Anderson, C.M. and R.A. Swanson, *Astrocyte glutamate transport: review of properties, regulation, and physiological functions.* Glia, 2000. **32**(1): p. 1-14.

52. Mahmoud, S., et al., *Astrocytes Maintain Glutamate Homeostasis in the CNS by Controlling the Balance between Glutamate Uptake and Release.* Cells, 2019. **8**(2).
53. Sofroniew, M.V. and H.V. Vinters, *Astrocytes: biology and pathology.* Acta Neuropathol, 2010. **119**(1): p. 7-35.
54. Lenting, K., et al., *Glioma: experimental models and reality.* Acta Neuropathol, 2017. **133**(2): p. 263-282.
55. DeAngelis, L.M., *Brain tumors.* N Engl J Med, 2001. **344**(2): p. 114-23.
56. Rasmussen, B.K., et al., *Epidemiology of glioma: clinical characteristics, symptoms, and predictors of glioma patients grade I-IV in the the Danish Neuro-Oncology Registry.* J Neurooncol, 2017. **135**(3): p. 571-579.
57. Ostrom, Q.T., et al., *Epidemiology of gliomas.* Cancer Treat Res, 2015. **163**: p. 1-14.
58. Wesseling, P., M. van den Bent, and A. Perry, *Oligodendroglioma: pathology, molecular mechanisms and markers.* Acta Neuropathol, 2015. **129**(6): p. 809-27.
59. Louis, D.N., et al., *The 2007 WHO classification of tumours of the central nervous system.* Acta Neuropathol, 2007. **114**(2): p. 97-109.
60. Louis, D.N., et al., *The 2016 World Health Organization Classification of Tumors of the Central Nervous System: a summary.* Acta Neuropathol, 2016. **131**(6): p. 803-20.
61. Mandonnet, E., et al., *Continuous growth of mean tumor diameter in a subset of grade II gliomas.* Ann Neurol, 2003. **53**(4): p. 524-8.
62. Pallud, J., et al., *Prognostic significance of imaging contrast enhancement for WHO grade II gliomas.* Neuro Oncol, 2009. **11**(2): p. 176-82.
63. Keles, G.E., K.R. Lamborn, and M.S. Berger, *Low-grade hemispheric gliomas in adults: a critical review of extent of resection as a factor influencing outcome.* J Neurosurg, 2001. **95**(5): p. 735-45.
64. Hafazalla, K., et al., *Procarbazine, CCNU and vincristine (PCV) versus temozolomide chemotherapy for patients with low-grade glioma: a systematic review.* Oncotarget, 2018. **9**(72): p. 33623-33633.
65. Gilbert, M.R., et al., *Dose-dense temozolomide for newly diagnosed glioblastoma: a randomized phase III clinical trial.* J Clin Oncol, 2013. **31**(32): p. 4085-91.
66. Stupp, R., et al., *Radiotherapy plus concomitant and adjuvant temozolomide for glioblastoma.* N Engl J Med, 2005. **352**(10): p. 987-96.
67. Coburger, J., et al., *Low-grade Glioma Surgery in Intraoperative Magnetic Resonance Imaging: Results of a Multicenter Retrospective Assessment of the German Study Group for Intraoperative Magnetic Resonance Imaging.* Neurosurgery, 2016. **78**(6): p. 775-86.
68. Senft, C., et al., *Intraoperative MRI guidance and extent of resection in glioma surgery: a randomised, controlled trial.* Lancet Oncol, 2011. **12**(11): p. 997-1003.
69. Stummer, W., et al., *Fluorescence-guided surgery with 5-aminolevulinic acid for resection of malignant glioma: a randomised controlled multicentre phase III trial.* Lancet Oncol, 2006. **7**(5): p. 392-401.
70. Thon, N., J.C. Tonn, and F.W. Kreth, *The surgical perspective in precision treatment of diffuse gliomas.* Onco Targets Ther, 2019. **12**: p. 1497-1508.
71. Stummer, W., et al., *Counterbalancing risks and gains from extended resections in malignant glioma surgery: a supplemental analysis from the randomized 5-aminolevulinic acid glioma resection study. Clinical article.* J Neurosurg, 2011. **114**(3): p. 613-23.
72. Cancer Genome Atlas Research, N., et al., *Comprehensive, Integrative Genomic Analysis of Diffuse Lower-Grade Gliomas.* N Engl J Med, 2015. **372**(26): p. 2481-98.
73. Cancer Genome Atlas Research, N., *Comprehensive genomic characterization defines human glioblastoma genes and core pathways.* Nature, 2008. **455**(7216): p. 1061-8.
74. Chinot, O.L., et al., *Bevacizumab plus radiotherapy-temozolomide for newly diagnosed glioblastoma.* N Engl J Med, 2014. **370**(8): p. 709-22.

75. Uhm, J.H., et al., *Phase II evaluation of gefitinib in patients with newly diagnosed Grade 4 astrocytoma: Mayo/North Central Cancer Treatment Group Study N0074.* Int J Radiat Oncol Biol Phys, 2011. **80**(2): p. 347-53.
76. Peereboom, D.M., et al., *Phase II trial of erlotinib with temozolomide and radiation in patients with newly diagnosed glioblastoma multiforme.* J Neurooncol, 2010. **98**(1): p. 93-9.
77. Wen, P.Y., et al., *Phase I/II study of erlotinib and temsirolimus for patients with recurrent malignant gliomas: North American Brain Tumor Consortium trial 04-02.* Neuro-Oncology, 2014. **16**(4): p. 567-578.
78. Raizer, J.J., et al., *A phase II study of bevacizumab and erlotinib after radiation and temozolomide in MGMT unmethylated GBM patients.* Journal of Neuro-Oncology, 2016. **126**(1): p. 185-192.
79. Reardon, D.A., et al., *Phase I/randomized phase II study of afatinib, an irreversible ErbB family blocker, with or without protracted temozolomide in adults with recurrent glioblastoma.* Neuro-Oncology, 2015. **17**(3): p. 430-439.
80. Wen, P.Y., et al., *Phase II study of cabozantinib in patients with progressive glioblastoma: subset analysis of patients naive to antiangiogenic therapy.* Neuro Oncol, 2018. **20**(2): p. 249-258.
81. Schiff, D., et al., *Phase 1 dose escalation trial of the safety and pharmacokinetics of cabozantinib concurrent with temozolomide and radiotherapy or temozolomide after radiotherapy in newly diagnosed patients with high-grade gliomas.* Cancer, 2016. **122**(4): p. 582-7.
82. Parsons, D.W., et al., *An integrated genomic analysis of human glioblastoma multiforme.* Science, 2008. **321**(5897): p. 1807-12.
83. Yan, H., et al., *IDH1 and IDH2 mutations in gliomas.* N Engl J Med, 2009. **360**(8): p. 765-73.
84. Bleeker, F.E., et al., *The prognostic IDH1(R132) mutation is associated with reduced NADP+-dependent IDH activity in glioblastoma.* Acta Neuropathol, 2010. **119**(4): p. 487-94.
85. Atai, N.A., et al., *Differential activity of NADPH-producing dehydrogenases renders rodents unsuitable models to study IDH1R132 mutation effects in human glioblastoma.* J Histochem Cytochem, 2011. **59**(5): p. 489-503.
86. Koehler, A. and C.J.F. Van Noorden, *Reduced nicotinamide adenine dinucleotide phosphate and the higher incidence of pollution-induced liver cancer in female flounder.* Environmental Toxicology and Chemistry, 2003. **22**(11): p. 2703-2710.
87. Holmgren, A. and J. Lu, *Thioredoxin and thioredoxin reductase: Current research with special reference to human disease.* Biochemical and Biophysical Research Communications, 2010. **396**(1): p. 120-124.
88. Salvemini, F., et al., *Enhanced glutathione levels and oxidoresistance mediated by increased glucose-6-phosphate dehydrogenase expression.* Journal of Biological Chemistry, 1999. **274**(5): p. 2750-2757.
89. Van Noorden, C.J. and R.G. Butcher, *A quantitative histochemical study of NADPH-ferrihemoprotein reductase activity.* Histochem J, 1986. **18**(7): p. 364-70.
90. Atai, N.A., et al., *Differential Activity of NADPH-Producing Dehydrogenases Renders Rodents Unsuitable Models to Study IDH1(R132) Mutation Effects in Human Glioblastoma.* Journal of Histochemistry & Cytochemistry, 2011. **59**(5): p. 489-503.
91. Bleeker, F.E., et al., *The prognostic IDH1 (R132) mutation is associated with reduced NADP(+)-dependent IDH activity in glioblastoma.* Acta Neuropathologica, 2010. **119**(4): p. 487-494.
92. Al-Khallaf, H., *Isocitrate dehydrogenases in physiology and cancer: biochemical and molecular insight.* Cell Biosci, 2017. **7**: p. 37.
93. Clark, O., K. Yen, and I.K. Mellinghoff, *Molecular Pathways: Isocitrate Dehydrogenase Mutations in Cancer.* Clin Cancer Res, 2016. **22**(8): p. 1837-42.
94. Watanabe, T., et al., *IDH1 mutations are early events in the development of astrocytomas and oligodendrogliomas.* Am J Pathol, 2009. **174**(4): p. 1149-53.

95. Dang, L., et al., *Cancer-associated IDH1 mutations produce 2-hydroxyglutarate.* Nature, 2009. **462**(7274): p. 739-44.
96. Xu, W., et al., *Oncometabolite 2-hydroxyglutarate is a competitive inhibitor of alpha-ketoglutarate-dependent dioxygenases.* Cancer Cell, 2011. **19**(1): p. 17-30.
97. Lu, C., et al., *IDH mutation impairs histone demethylation and results in a block to cell differentiation.* Nature, 2012. **483**(7390): p. 474-8.
98. Ceccarelli, M., et al., *Molecular Profiling Reveals Biologically Discrete Subsets and Pathways of Progression in Diffuse Glioma.* Cell, 2016. **164**(3): p. 550-63.
99. Noushmehr, H., et al., *Identification of a CpG island methylator phenotype that defines a distinct subgroup of glioma.* Cancer Cell, 2010. **17**(5): p. 510-22.
100. Wang, P., et al., *Oncometabolite D-2-Hydroxyglutarate Inhibits ALKBH DNA Repair Enzymes and Sensitizes IDH Mutant Cells to Alkylating Agents.* Cell Rep, 2015. **13**(11): p. 2353-2361.
101. Mayers, J.R. and M.G. Vander Heiden, *BCAT1 defines gliomas by IDH status.* Nat Med, 2013. **19**(7): p. 816-7.
102. Chesnelong, C., et al., *Lactate dehydrogenase A silencing in IDH mutant gliomas.* Neuro Oncol, 2014. **16**(5): p. 686-95.
103. Koivunen, P., et al., *Transformation by the (R)-enantiomer of 2-hydroxyglutarate linked to EGLN activation.* Nature, 2012. **483**(7390): p. 484-8.
104. Harris, A.L., *Hypoxia--a key regulatory factor in tumour growth.* Nat Rev Cancer, 2002. **2**(1): p. 38-47.
105. Kickingereder, P., et al., *IDH mutation status is associated with a distinct hypoxia/angiogenesis transcriptome signature which is non-invasively predictable with rCBV imaging in human glioma.* Sci Rep, 2015. **5**: p. 16238.
106. Shi, J., et al., *An IDH1 mutation inhibits growth of glioma cells via GSH depletion and ROS generation.* Neurol Sci, 2014. **35**(6): p. 839-45.
107. Baldewpersad Tewarie, N.M., et al., *NADP+ -dependent IDH1 R132 mutation and its relevance for glioma patient survival.* Med Hypotheses, 2013. **80**(6): p. 728-31.
108. Metallo, C.M., et al., *Reductive glutamine metabolism by IDH1 mediates lipogenesis under hypoxia.* Nature, 2011. **481**(7381): p. 380-4.
109. Koh, H.J., et al., *Cytosolic NADP+-dependent isocitrate dehydrogenase plays a key role in lipid metabolism.* J Biol Chem, 2004. **279**(38): p. 39968-74.
110. Johnson, B.E., et al., *Mutational analysis reveals the origin and therapy-driven evolution of recurrent glioma.* Science, 2014. **343**(6167): p. 189-193.
111. Kotredes, K. and A.M. Gamero, *Characterization of the effects of IDH2 mutations and (R)-2-HG in cancer progression.* Cancer Research, 2015. **75**.
112. Marcucci, G., et al., *IDH1 and IDH2 Gene Mutations Identify Novel Molecular Subsets Within De Novo Cytogenetically Normal Acute Myeloid Leukemia: A Cancer and Leukemia Group B Study.* Journal of Clinical Oncology, 2010. **28**(14): p. 2348-2355.
113. Green, C.L., et al., *The prognostic significance of IDH2 mutations in AML depends on the location of the mutation.* Blood, 2011. **118**(2): p. 409-412.
114. Navis, A.C., et al., *Increased mitochondrial activity in a novel IDH1-R132H mutant human oligodendroglioma xenograft model: in situ detection of 2-HG and alpha-KG.* Acta Neuropathologica Communications, 2013. **1**.
115. *An Slc1a5 Variant Transports Glutamine to Mitochondria in Cancer Cells.* Cancer Discovery, 2020. **10**(2): p. 173-173.
116. Robert, S.M. and H. Sontheimer, *Glutamate transporters in the biology of malignant gliomas.* Cellular and Molecular Life Sciences, 2014. **71**(10): p. 1839-1854.
117. Grassian, A.R., et al., *IDH1 mutations alter citric acid cycle metabolism and increase dependence on oxidative mitochondrial metabolism.* Cancer Research, 2014. **74**(19).
118. Seltzer, M.J., et al., *Inhibition of Glutaminase Preferentially Slows Growth of Glioma Cells with Mutant IDH1.* Cancer Research, 2010. **70**(22): p. 8981-8987.

119. de Groot, J.F., et al., *The excitatory amino acid transporter-2 induces apoptosis and decreases glioma growth in vitro and in vivo.* Cancer Research, 2005. **65**(5): p. 1934-1940.
120. van Lith, S.A.M., et al., *Glutamate as chemotactic fuel for diffuse glioma cells: Are they glutamate suckers?* Biochimica Et Biophysica Acta-Reviews on Cancer, 2014. **1846**(1): p. 66-74.
121. van Lith, S.A.M., et al., *Tumor cells in search for glutamate: an alternative explanation for increased invasiveness of IDH1 mutant gliomas.* Neuro-Oncology, 2014. **16**(12): p. 1669-1670.
122. Seltzer, M.J., et al., *Inhibition of glutaminase preferentially slows growth of glioma cells with mutant IDH1.* Cancer Res, 2010. **70**(22): p. 8981-7.
123. Ziskin, J.L., et al., *Vesicular release of glutamate from unmyelinated axons in white matter.* Nat Neurosci, 2007. **10**(3): p. 321-30.
124. de Groot, J.F., et al., *The excitatory amino acid transporter-2 induces apoptosis and decreases glioma growth in vitro and in vivo.* Cancer Res, 2005. **65**(5): p. 1934-40.
125. Robert, S.M. and H. Sontheimer, *Glutamate transporters in the biology of malignant gliomas.* Cell Mol Life Sci, 2014. **71**(10): p. 1839-54.
126. de Groot, J. and H. Sontheimer, *Glutamate and the biology of gliomas.* Glia, 2011. **59**(8): p. 1181-9.
127. Khurshed, M., et al., *In silico gene expression analysis reveals glycolysis and acetate anaplerosis in IDH1 wild-type glioma and lactate and glutamate anaplerosis in IDH1-mutated glioma.* Oncotarget, 2017. **8**(30): p. 49165-49177.
128. van Lith, S.A., et al., *Tumor cells in search for glutamate: an alternative explanation for increased invasiveness of IDH1 mutant gliomas.* Neuro Oncol, 2014. **16**(12): p. 1669-70.
129. van Lith, S.A., et al., *Glutamate as chemotactic fuel for diffuse glioma cells: are they glutamate suckers?* Biochim Biophys Acta, 2014. **1846**(1): p. 66-74.
130. Claes, A., A.J. Idema, and P. Wesseling, *Diffuse glioma growth: a guerilla war.* Acta Neuropathol, 2007. **114**(5): p. 443-58.
131. Ichimura, K., Y. Narita, and C.E. Hawkins, *Diffusely infiltrating astrocytomas: pathology, molecular mechanisms and markers.* Acta Neuropathol, 2015. **129**(6): p. 789-808.
132. Stupp, R., et al., *Effects of radiotherapy with concomitant and adjuvant temozolomide versus radiotherapy alone on survival in glioblastoma in a randomised phase III study: 5-year analysis of the EORTC-NCIC trial.* Lancet Oncol, 2009. **10**(5): p. 459-66.
133. Collins, V.P., D.T. Jones, and C. Giannini, *Pilocytic astrocytoma: pathology, molecular mechanisms and markers.* Acta Neuropathol, 2015. **129**(6): p. 775-88.
134. Vitanza, N.A. and S. Partap, *Pediatric Ependymoma.* J Child Neurol, 2016. **31**(12): p. 1354-66.
135. Gilbert, M.R., R. Ruda, and R. Soffietti, *Ependymomas in adults.* Curr Neurol Neurosci Rep, 2010. **10**(3): p. 240-7.
136. Louis, D.N., et al., *International Society Of Neuropathology--Haarlem consensus guidelines for nervous system tumor classification and grading.* Brain Pathol, 2014. **24**(5): p. 429-35.
137. Eckel-Passow, J.E., et al., *Glioma Groups Based on 1p/19q, IDH, and TERT Promoter Mutations in Tumors.* N Engl J Med, 2015. **372**(26): p. 2499-508.
138. Yang, P., et al., *Classification based on mutations of TERT promoter and IDH characterizes subtypes in grade II/III gliomas.* Neuro Oncol, 2016. **18**(8): p. 1099-108.
139. Ohgaki, H. and P. Kleihues, *The definition of primary and secondary glioblastoma.* Clin Cancer Res, 2013. **19**(4): p. 764-72.
140. Guan, X., et al., *Molecular subtypes of glioblastoma are relevant to lower grade glioma.* PLoS One, 2014. **9**(3): p. e91216.
141. Gupta, R., et al., *Expanding the spectrum of IDH1 mutations in gliomas.* Mod Pathol, 2013. **26**(5): p. 619-25.
142. Malzkorn, B. and G. Reifenberger, *Practical implications of integrated glioma classification according to the World Health Organization classification of tumors of the central nervous system 2016.* Curr Opin Oncol, 2016.

143. Verhaak, R.G., et al., *Integrated genomic analysis identifies clinically relevant subtypes of glioblastoma characterized by abnormalities in PDGFRA, IDH1, EGFR, and NF1.* Cancer Cell, 2010. **17**(1): p. 98-110.
144. Speidel, D., *The role of DNA damage responses in p53 biology.* Arch Toxicol, 2015. **89**(4): p. 501-17.
145. Pajtler, K.W., et al., *Molecular Classification of Ependymal Tumors across All CNS Compartments, Histopathological Grades, and Age Groups.* Cancer Cell, 2015. **27**(5): p. 728-43.
146. Chiang, J.C. and D.W. Ellison, *Molecular Pathology of Paediatric Central Nervous System Tumours.* J Pathol, 2016.
147. Sottoriva, A., et al., *Intratumor heterogeneity in human glioblastoma reflects cancer evolutionary dynamics.* Proc Natl Acad Sci U S A, 2013. **110**(10): p. 4009-14.
148. Patel, A.P., et al., *Single-cell RNA-seq highlights intratumoral heterogeneity in primary glioblastoma.* Science, 2014. **344**(6190): p. 1396-401.
149. Kim, H., et al., *Whole-genome and multisector exome sequencing of primary and post-treatment glioblastoma reveals patterns of tumor evolution.* Genome Res, 2015. **25**(3): p. 316-27.
150. Tirosh, I., et al., *Single-cell RNA-seq supports a developmental hierarchy in human oligodendroglioma.* Nature, 2016. **539**(7628): p. 309-313.
151. Snuderl, M., et al., *Mosaic amplification of multiple receptor tyrosine kinase genes in glioblastoma.* Cancer Cell, 2011. **20**(6): p. 810-7.
152. Johnson, B.E., et al., *Mutational analysis reveals the origin and therapy-driven evolution of recurrent glioma.* Science, 2014. **343**(6167): p. 189-93.
153. Penne, K., et al., *Gefitinib (Iressa, ZD1839) and tyrosine kinase inhibitors: the wave of the future in cancer therapy.* Cancer Nurs, 2005. **28**(6): p. 481-6.
154. Roskoski, R., Jr., *Cyclin-dependent protein kinase inhibitors including palbociclib as anticancer drugs.* Pharmacol Res, 2016. **107**: p. 249-75.
155. Rohle, D., et al., *An inhibitor of mutant IDH1 delays growth and promotes differentiation of glioma cells.* Science, 2013. **340**(6132): p. 626-30.
156. Osswald, M., et al., *Brain tumour cells interconnect to a functional and resistant network.* Nature, 2015. **528**(7580): p. 93-8.
157. Russell, W.L., et al., *Specific-locus test shows ethylnitrosourea to be the most potent mutagen in the mouse.* Proc Natl Acad Sci U S A, 1979. **76**(11): p. 5818-9.
158. Slikker, W., 3rd, N. Mei, and T. Chen, *N-ethyl-N-nitrosourea (ENU) increased brain mutations in prenatal and neonatal mice but not in the adults.* Toxicol Sci, 2004. **81**(1): p. 112-20.
159. Briancon-Marjollet, A., et al., *NG2-expressing glial precursor cells are a new potential oligodendroglioma cell initiating population in N-ethyl-N-nitrosourea-induced gliomagenesis.* Carcinogenesis, 2010. **31**(10): p. 1718-25.
160. Mukherjee, J., et al., *ENU administration causes genomic instability along with single nucleotide polymorphisms in p53 during gliomagenesis: T11TS administration demonstrated in vivo apoptosis of these genetically altered tumor cells.* Cancer Biol Ther, 2006. **5**(2): p. 156-64.
161. Zook, B.C., S.J. Simmens, and R.V. Jones, *Evaluation of ENU-induced gliomas in rats: nomenclature, immunochemistry, and malignancy.* Toxicol Pathol, 2000. **28**(1): p. 193-201.
162. Paugh, B.S., et al., *Novel oncogenic PDGFRA mutations in pediatric high-grade gliomas.* Cancer Res, 2013. **73**(20): p. 6219-29.
163. Koschmann, C., et al., *Characterizing and targeting PDGFRA alterations in pediatric high-grade glioma.* Oncotarget, 2016.
164. Puputti, M., et al., *Amplification of KIT, PDGFRA, VEGFR2, and EGFR in gliomas.* Mol Cancer Res, 2006. **4**(12): p. 927-34.
165. Wang, Q., et al., *Braf Mutations Initiate the Development of Rat Gliomas Induced by Postnatal Exposure to N-Ethyl-N-Nitrosourea.* Am J Pathol, 2016. **186**(10): p. 2569-76.

166. Reifenberger, G., et al., *Expression of vimentin and glial fibrillary acidic protein in ethylnitrosourea-induced rat gliomas and glioma cell lines.* Acta Neuropathol, 1989. **78**(3): p. 270-82.
167. Hambardzumyan, D., et al., *Genetic modeling of gliomas in mice: new tools to tackle old problems.* Glia, 2011. **59**(8): p. 1155-68.
168. Holland, E.C., *A mouse model for glioma: biology, pathology, and therapeutic opportunities.* Toxicol Pathol, 2000. **28**(1): p. 171-7.
169. de Vries, N.A., et al., *Rapid and robust transgenic high-grade glioma mouse models for therapy intervention studies.* Clin Cancer Res, 2010. **16**(13): p. 3431-41.
170. Bardella, C., et al., *Expression of Idh1R132H in the Murine Subventricular Zone Stem Cell Niche Recapitulates Features of Early Gliomagenesis.* Cancer Cell, 2016. **30**(4): p. 578-594.
171. Lin, F., et al., *PI3K-mTOR pathway inhibition exhibits efficacy against high-grade glioma in clinically relevant mouse models.* Clin Cancer Res, 2016.
172. Lin, F., et al., *ABCB1, ABCG2, and PTEN determine the response of glioblastoma to temozolomide and ABT-888 therapy.* Clin Cancer Res, 2014. **20**(10): p. 2703-13.
173. Barth, R.F. and B. Kaur, *Rat brain tumor models in experimental neuro-oncology: the C6, 9L, T9, RG2, F98, BT4C, RT-2 and CNS-1 gliomas.* J Neurooncol, 2009. **94**(3): p. 299-312.
174. Sonabend, A.M., et al., *Murine cell line model of proneural glioma for evaluation of anti-tumor therapies.* J Neurooncol, 2013. **112**(3): p. 375-82.
175. Ausman, J.I., W.R. Shapiro, and D.P. Rall, *Studies on the chemotherapy of experimental brain tumors: development of an experimental model.* Cancer Res, 1970. **30**(9): p. 2394-400.
176. Szatmari, T., et al., *Detailed characterization of the mouse glioma 261 tumor model for experimental glioblastoma therapy.* Cancer Sci, 2006. **97**(6): p. 546-53.
177. Beutler, A.S., et al., *Tumor gene therapy made easy: allogeneic major histocompatibility complex in the C6 rat glioma model.* Hum Gene Ther, 1999. **10**(1): p. 95-101.
178. Chung, C., et al., *Imaging biomarker dynamics in an intracranial murine glioma study of radiation and antiangiogenic therapy.* Int J Radiat Oncol Biol Phys, 2013. **85**(3): p. 805-12.
179. Tsiatas, M., G. Mountzios, and G. Curigliano, *Future perspectives in cancer immunotherapy.* Ann Transl Med, 2016. **4**(14): p. 273.
180. Li, M., S. Han, and X. Shi, *In situ dendritic cell vaccination for the treatment of glioma and literature review.* Tumour Biol, 2016. **37**(2): p. 1797-801.
181. Gielen, P.R., et al., *Increase in both CD14-positive and CD15-positive myeloid-derived suppressor cell subpopulations in the blood of patients with glioma but predominance of CD15-positive myeloid-derived suppressor cells in glioma tissue.* J Neuropathol Exp Neurol, 2015. **74**(5): p. 390-400.
182. Grauer, O.M., et al., *Elimination of regulatory T cells is essential for an effective vaccination with tumor lysate-pulsed dendritic cells in a murine glioma model.* Int J Cancer, 2008. **122**(8): p. 1794-802.
183. Zhou, X., et al., *Dendritic cell vaccination enhances antiangiogenesis induced by endostatin in rat glioma.* J Cancer Res Ther, 2016. **12**(1): p. 198-203.
184. Morton, J.J., et al., *Humanized Mouse Xenograft Models: Narrowing the Tumor-Microenvironment Gap.* Cancer Res, 2016. **76**(21): p. 6153-6158.
185. Bournazos, S., D.J. DiLillo, and J.V. Ravetch, *humanized mice to study FcgammaR function.* Curr Top Microbiol Immunol, 2014. **382**: p. 237-48.
186. Zitvogel, L., et al., *Mouse models in oncoimmunology.* Nat Rev Cancer, 2016. **16**(12): p. 759-773.
187. Yang, W., et al., *Development of a syngeneic rat brain tumor model expressing EGFRvIII and its use for molecular targeting studies with monoclonal antibody L8A4.* Clin Cancer Res, 2005. **11**(1): p. 341-50.
188. Westermark, B., J. Ponten, and R. Hugosson, *Determinants for the establishment of permanent tissue culture lines from human gliomas.* Acta Pathol Microbiol Scand A, 1973. **81**(6): p. 791-805.

189. Ponten, J. and E.H. Macintyre, *Long term culture of normal and neoplastic human glia.* Acta Pathol Microbiol Scand, 1968. **74**(4): p. 465-86.
190. Clark, M.J., et al., *U87MG decoded: the genomic sequence of a cytogenetically aberrant human cancer cell line.* PLoS Genet, 2010. **6**(1): p. e1000832.
191. Allen, M., et al., *Origin of the U87MG glioma cell line: Good news and bad news.* Sci Transl Med, 2016. **8**(354): p. 354re3.
192. Torsvik, A., et al., *U-251 revisited: genetic drift and phenotypic consequences of long-term cultures of glioblastoma cells.* Cancer Med, 2014. **3**(4): p. 812-24.
193. Huszthy, P.C., et al., *In vivo models of primary brain tumors: pitfalls and perspectives.* Neuro Oncol, 2012. **14**(8): p. 979-93.
194. Ernst, A., et al., *Genomic and expression profiling of glioblastoma stem cell-like spheroid cultures identifies novel tumor-relevant genes associated with survival.* Clin Cancer Res, 2009. **15**(21): p. 6541-50.
195. Freedman, L.P., et al., *Reproducibility: changing the policies and culture of cell line authentication.* Nat Methods, 2015. **12**(6): p. 493-7.
196. Reynolds, B.A. and S. Weiss, *Generation of neurons and astrocytes from isolated cells of the adult mammalian central nervous system.* Science, 1992. **255**(5052): p. 1707-10.
197. Balvers, R.K., et al., *Serum-free culture success of glial tumors is related to specific molecular profiles and expression of extracellular matrix-associated gene modules.* Neuro Oncol, 2013. **15**(12): p. 1684-95.
198. Conti, L., et al., *Niche-independent symmetrical self-renewal of a mammalian tissue stem cell.* PLoS Biol, 2005. **3**(9): p. e283.
199. Brewer, G.J., et al., *Optimized survival of hippocampal neurons in B27-supplemented Neurobasal, a new serum-free medium combination.* J Neurosci Res, 1993. **35**(5): p. 567-76.
200. Klink, B., et al., *A novel, diffusely infiltrative xenograft model of human anaplastic oligodendroglioma with mutations in FUBP1, CIC, and IDH1.* PLoS One, 2013. **8**(3): p. e59773.
201. Luchman, H.A., et al., *An in vivo patient-derived model of endogenous IDH1-mutant glioma.* Neuro Oncol, 2012. **14**(2): p. 184-91.
202. Stopschinski, B.E., C.P. Beier, and D. Beier, *Glioblastoma cancer stem cells--from concept to clinical application.* Cancer Lett, 2013. **338**(1): p. 32-40.
203. Son, M.J., et al., *SSEA-1 is an enrichment marker for tumor-initiating cells in human glioblastoma.* Cell Stem Cell, 2009. **4**(5): p. 440-52.
204. Holmberg Olausson, K., et al., *Prominin-1 (CD133) defines both stem and non-stem cell populations in CNS development and gliomas.* PLoS One, 2014. **9**(9): p. e106694.
205. Wee, B., N. Charles, and E.C. Holland, *Animal models to study cancer-initiating cells from glioblastoma.* Front Biosci (Landmark Ed), 2011. **16**: p. 2243-58.
206. Patru, C., et al., *CD133, CD15/SSEA-1, CD34 or side populations do not resume tumor-initiating properties of long-term cultured cancer stem cells from human malignant glio-neuronal tumors.* BMC Cancer, 2010. **10**: p. 66.
207. Lee, J., et al., *Tumor stem cells derived from glioblastomas cultured in bFGF and EGF more closely mirror the phenotype and genotype of primary tumors than do serum-cultured cell lines.* Cancer Cell, 2006. **9**(5): p. 391-403.
208. Claes, A., et al., *Phenotypic and genotypic characterization of orthotopic human glioma models and its relevance for the study of anti-glioma therapy.* Brain Pathol, 2008. **18**(3): p. 423-33.
209. Sundlisaeter, E., et al., *Primary glioma spheroids maintain tumourogenicity and essential phenotypic traits after cryopreservation.* Neuropathol Appl Neurobiol, 2006. **32**(4): p. 419-27.
210. Stieber, D., et al., *Glioblastomas are composed of genetically divergent clones with distinct tumourigenic potential and variable stem cell-associated phenotypes.* Acta Neuropathol, 2014. **127**(2): p. 203-19.

211. Bourgonje, A.M., et al., *Intracellular and extracellular domains of protein tyrosine phosphatase PTPRZ-B differentially regulate glioma cell growth and motility.* Oncotarget, 2014. **5**(18): p. 8690-702.
212. Caretti, V., et al., *Monitoring of tumor growth and post-irradiation recurrence in a diffuse intrinsic pontine glioma mouse model.* Brain Pathol, 2011. **21**(4): p. 441-51.
213. Roberts, W.G., et al., *Host microvasculature influence on tumor vascular morphology and endothelial gene expression.* Am J Pathol, 1998. **153**(4): p. 1239-48.
214. Wachsberger, P.R., et al., *VEGF trap in combination with radiotherapy improves tumor control in u87 glioblastoma.* Int J Radiat Oncol Biol Phys, 2007. **67**(5): p. 1526-37.
215. Navis, A.C., et al., *Increased mitochondrial activity in a novel IDH1-R132H mutant human oligodendroglioma xenograft model: in situ detection of 2-HG and alpha-KG.* Acta Neuropathol Commun, 2013. **1**: p. 18.
216. Molina, J.R., et al., *Invasive glioblastoma cells acquire stemness and increased Akt activation.* Neoplasia, 2010. **12**(6): p. 453-63.
217. Jacobs, V.L., et al., *Current review of in vivo GBM rodent models: emphasis on the CNS-1 tumour model.* ASN Neuro, 2011. **3**(3): p. e00063.
218. Gronych, J., et al., *An activated mutant BRAF kinase domain is sufficient to induce pilocytic astrocytoma in mice.* J Clin Invest, 2011. **121**(4): p. 1344-8.
219. Potter, N.E., et al., *Astrocytoma derived short-term cell cultures retain molecular signatures characteristic of the tumour in situ.* Exp Cell Res, 2009. **315**(16): p. 2835-46.
220. Meco, D., et al., *Ependymoma stem cells are highly sensitive to temozolomide in vitro and in orthotopic models.* Neuro Oncol, 2014. **16**(8): p. 1067-77.
221. Johnson, R.A., et al., *Cross-species genomics matches driver mutations and cell compartments to model ependymoma.* Nature, 2010. **466**(7306): p. 632-6.
222. Welker, A.M., et al., *Standardized orthotopic xenografts in zebrafish reveal glioma cell-line-specific characteristics and tumor cell heterogeneity.* Dis Model Mech, 2016. **9**(2): p. 199-210.
223. Vittori, M., H. Motaln, and T.L. Turnsek, *The study of glioma by xenotransplantation in zebrafish early life stages.* J Histochem Cytochem, 2015. **63**(10): p. 749-61.
224. Huang, X., et al., *Transcriptomic Analyses in Zebrafish Cancer Models for Global Gene Expression and Pathway Discovery.* Adv Exp Med Biol, 2016. **916**: p. 147-68.
225. Eden, C.J., et al., *Orthotopic models of pediatric brain tumors in zebrafish.* Oncogene, 2015. **34**(13): p. 1736-42.
226. Xie, J., et al., *A novel transgenic zebrafish model for blood-brain and blood-retinal barrier development.* BMC Dev Biol, 2010. **10**: p. 76.
227. Lam, S.H., et al., *Development and maturation of the immune system in zebrafish, Danio rerio: a gene expression profiling, in situ hybridization and immunological study.* Dev Comp Immunol, 2004. **28**(1): p. 9-28.
228. Witte, H.T., et al., *Modeling glioma growth and invasion in Drosophila melanogaster.* Neoplasia, 2009. **11**(9): p. 882-8.
229. Reiter, L.T. and E. Bier, *Using Drosophila melanogaster to uncover human disease gene function and potential drug target proteins.* Expert Opin Ther Targets, 2002. **6**(3): p. 387-99.
230. Read, R.D., et al., *A drosophila model for EGFR-Ras and PI3K-dependent human glioma.* PLoS Genet, 2009. **5**(2): p. e1000374.
231. LeBlanc, A.K., et al., *Creation of an NCI comparative brain tumor consortium: informing the translation of new knowledge from canine to human brain tumor patients.* Neuro Oncol, 2016. **18**(9): p. 1209-18.
232. Sancho-Martinez, I., et al., *Establishment of human iPSC-based models for the study and targeting of glioma initiating cells.* Nat Commun, 2016. **7**: p. 10743.
233. Kim, Y.W., et al., *Identification of novel synergistic targets for rational drug combinations with PI3 kinase inhibitors using siRNA synthetic lethality screening against GBM.* Neuro Oncol, 2011. **13**(4): p. 367-75.

234. Ettl, J., *Palbociclib: First CDK4/6 Inhibitor in Clinical Practice for the Treatment of Advanced HR-Positive Breast Cancer.* Breast Care (Basel), 2016. **11**(3): p. 174-6.
235. Cen, L., et al., *p16-Cdk4-Rb axis controls sensitivity to a cyclin-dependent kinase inhibitor PD0332991 in glioblastoma xenograft cells.* Neuro Oncol, 2012. **14**(7): p. 870-81.
236. de Gooijer, M.C., et al., *P-glycoprotein and breast cancer resistance protein restrict the brain penetration of the CDK4/6 inhibitor palbociclib.* Invest New Drugs, 2015. **33**(5): p. 1012-9.
237. Chu, E.C. and A.S. Tarnawski, *PTEN regulatory functions in tumor suppression and cell biology.* Med Sci Monit, 2004. **10**(10): p. RA235-41.
238. Cully, M., et al., *Beyond PTEN mutations: the PI3K pathway as an integrator of multiple inputs during tumorigenesis.* Nat Rev Cancer, 2006. **6**(3): p. 184-92.
239. Hatanpaa, K.J., et al., *Epidermal growth factor receptor in glioma: signal transduction, neuropathology, imaging, and radioresistance.* Neoplasia, 2010. **12**(9): p. 675-84.
240. Chu, C.T., et al., *Receptor dimerization is not a factor in the signalling activity of a transforming variant epidermal growth factor receptor (EGFRvIII).* Biochem J, 1997. **324 (Pt 3)**: p. 855-61.
241. Talasila, K.M., et al., *EGFR wild-type amplification and activation promote invasion and development of glioblastoma independent of angiogenesis.* Acta Neuropathol, 2013. **125**(5): p. 683-98.
242. Navis, A.C., et al., *Identification of a novel MET mutation in high-grade glioma resulting in an auto-active intracellular protein.* Acta Neuropathol, 2015. **130**(1): p. 131-44.
243. Navis, A.C., et al., *Effects of dual targeting of tumor cells and stroma in human glioblastoma xenografts with a tyrosine kinase inhibitor against c-MET and VEGFR2.* PLoS One, 2013. **8**(3): p. e58262.
244. Bauer, H. and A. Traweger, *Tight Junctions of the Blood-Brain Barrier - A Molecular Gatekeeper.* CNS Neurol Disord Drug Targets, 2016.
245. Krizbai, I.A., et al., *Pharmaceutical Targeting of the Brain.* Curr Pharm Des, 2016.
246. Breedveld, P., et al., *The effect of Bcrp1 (Abcg2) on the in vivo pharmacokinetics and brain penetration of imatinib mesylate (Gleevec): implications for the use of breast cancer resistance protein and P-glycoprotein inhibitors to enable the brain penetration of imatinib in patients.* Cancer Res, 2005. **65**(7): p. 2577-82.
247. de Vries, N.A., et al., *Restricted brain penetration of the tyrosine kinase inhibitor erlotinib due to the drug transporters P-gp and BCRP.* Invest New Drugs, 2012. **30**(2): p. 443-9.
248. Lin, F., et al., *Dual mTORC1 and mTORC2 inhibitor Palomid 529 penetrates the blood-brain barrier without restriction by ABCB1 and ABCG2.* Int J Cancer, 2013. **133**(5): p. 1222-33.
249. van Tellingen, O., et al., *Overcoming the blood-brain tumor barrier for effective glioblastoma treatment.* Drug Resist Updat, 2015. **19**: p. 1-12.
250. Georgieva, J.V., et al., *Peptide-mediated blood-brain barrier transport of polymersomes.* Angew Chem Int Ed Engl, 2012. **51**(33): p. 8339-42.
251. Tortorella, S. and T.C. Karagiannis, *The significance of transferrin receptors in oncology: the development of functional nano-based drug delivery systems.* Curr Drug Deliv, 2014. **11**(4): p. 427-43.
252. Karim, R., et al., *Nanocarriers for the treatment of glioblastoma multiforme: Current state-of-the-art.* J Control Release, 2016. **227**: p. 23-37.
253. Hersh, D.S., et al., *Emerging Applications of Therapeutic Ultrasound in Neuro-oncology: Moving Beyond Tumor Ablation.* Neurosurgery, 2016.
254. Cohen-Inbar, O., Z. Xu, and J.P. Sheehan, *Focused ultrasound-aided immunomodulation in glioblastoma multiforme: a therapeutic concept.* J Ther Ultrasound, 2016. **4**: p. 2.
255. Kobus, T., et al., *Safety Validation of Repeated Blood-Brain Barrier Disruption Using Focused Ultrasound.* Ultrasound Med Biol, 2016. **42**(2): p. 481-92.
256. Appelboom, G., et al., *Stereotactic modulation of blood-brain barrier permeability to enhance drug delivery.* Neuro Oncol, 2016.

257. Li, X.Q., et al., *Synergistic inhibition of angiogenesis and glioma cell-induced angiogenesis by the combination of temozolomide and enediyne antibiotic lidamycin.* Cancer Biol Ther, 2014. **15**(4): p. 398-408.
258. Bota, D.A., et al., *Proteasome inhibition with bortezomib induces cell death in GBM stem-like cells and temozolomide-resistant glioma cell lines, but stimulates GBM stem-like cells' VEGF production and angiogenesis.* J Neurosurg, 2013. **119**(6): p. 1415-23.
259. Narayana, A., et al., *Antiangiogenic therapy using bevacizumab in recurrent high-grade glioma: impact on local control and patient survival.* J Neurosurg, 2009. **110**(1): p. 173-80.
260. Chinot, O.L., W. Wick, and T. Cloughesy, *Bevacizumab for newly diagnosed glioblastoma.* N Engl J Med, 2014. **370**(21): p. 2049.
261. Gilbert, M.R., et al., *A randomized trial of bevacizumab for newly diagnosed glioblastoma.* N Engl J Med, 2014. **370**(8): p. 699-708.
262. Verhoeff, J.J., et al., *Tumour control by whole brain irradiation of anti-VEGF-treated mice bearing intracerebral glioma.* Eur J Cancer, 2009. **45**(17): p. 3074-80.
263. Brandsma, D. and M.J. van den Bent, *Pseudoprogression and pseudoresponse in the treatment of gliomas.* Curr Opin Neurol, 2009. **22**(6): p. 633-8.
264. Jain, R.K., *Normalization of tumor vasculature: an emerging concept in antiangiogenic therapy.* Science, 2005. **307**(5706): p. 58-62.
265. Verhoeff, J.J., et al., *Concerns about anti-angiogenic treatment in patients with glioblastoma multiforme.* BMC Cancer, 2009. **9**: p. 444.
266. Leenders, W.P., et al., *Antiangiogenic therapy of cerebral melanoma metastases results in sustained tumor progression via vessel co-option.* Clin Cancer Res, 2004. **10**(18 Pt 1): p. 6222-30.
267. Navis, A.C., et al., *Effects of targeting the VEGF and PDGF pathways in diffuse orthotopic glioma models.* J Pathol, 2011. **223**(5): p. 626-34.
268. Hamans, B., et al., *Multivoxel (1)H MR spectroscopy is superior to contrast-enhanced MRI for response assessment after anti-angiogenic treatment of orthotopic human glioma xenografts and provides handles for metabolic targeting.* Neuro Oncol, 2013. **15**(12): p. 1615-24.
269. de Groot, J.F., et al., *Tumor invasion after treatment of glioblastoma with bevacizumab: radiographic and pathologic correlation in humans and mice.* Neuro Oncol, 2010. **12**(3): p. 233-42.
270. Holash, J., et al., *Vessel cooption, regression, and growth in tumors mediated by angiopoietins and VEGF.* Science, 1999. **284**(5422): p. 1994-8.
271. Roodink, I., et al., *Development of the tumor vascular bed in response to hypoxia-induced VEGF-A differs from that in tumors with constitutive VEGF-A expression.* Int J Cancer, 2006. **119**(9): p. 2054-62.
272. Leenders, W.P., B. Kusters, and R.M. de Waal, *Vessel co-option: how tumors obtain blood supply in the absence of sprouting angiogenesis.* Endothelium, 2002. **9**(2): p. 83-7.
273. de Waal, R.M. and W.P. Leenders, *Sprouting angiogenesis versus co-option in tumor angiogenesis.* EXS, 2005(94): p. 65-76.
274. Gambarota, G., et al., *Characterisation of tumour vasculature in mouse brain by USPIO contrast-enhanced MRI.* Br J Cancer, 2008. **98**(11): p. 1784-9.
275. Altman, B.J., Z.E. Stine, and C.V. Dang, *From Krebs to clinic: glutamine metabolism to cancer therapy.* Nat Rev Cancer, 2016.
276. Cairns, R.A. and T.W. Mak, *Oncogenic isocitrate dehydrogenase mutations: mechanisms, models, and clinical opportunities.* Cancer Discov, 2013. **3**(7): p. 730-41.
277. Alexander, B.M. and M.P. Mehta, *Role of isocitrate dehydrogenase in glioma.* Expert Rev Neurother, 2011. **11**(10): p. 1399-409.
278. Duncan, C.G., et al., *A heterozygous IDH1R132H/WT mutation induces genome-wide alterations in DNA methylation.* Genome Res, 2012. **22**(12): p. 2339-55.
279. Piaskowski, S., et al., *Glioma cells showing IDH1 mutation cannot be propagated in standard cell culture conditions.* Br J Cancer, 2011. **104**(6): p. 968-70.

280. Tonjes, M., et al., *BCAT1 promotes cell proliferation through amino acid catabolism in gliomas carrying wild-type IDH1.* Nat Med, 2013. **19**(7): p. 901-8.
281. Hottinger, A.F., P. Pacheco, and R. Stupp, *Tumor treating fields: a novel treatment modality and its use in brain tumors.* Neuro Oncol, 2016. **18**(10): p. 1338-49.
282. Reardon, D.A. and P.Y. Wen, *Glioma in 2014: unravelling tumour heterogeneity-implications for therapy.* Nat Rev Clin Oncol, 2015. **12**(2): p. 69-70.
283. Baugh, E.H., et al., *Why are there hotspot mutations in the TP53 gene in human cancers?* Cell Death Differ, 2018. **25**(1): p. 154-160.
284. Basu, S. and M.E. Murphy, *Genetic Modifiers of the p53 Pathway.* Cold Spring Harb Perspect Med, 2016. **6**(4): p. a026302.
285. Bhattacharya, P. and T.N. Patel, *Microsatellite Instability and Promoter Hypermethylation of DNA repair genes in Hematologic Malignancies: a forthcoming direction toward diagnostics.* Hematology, 2018. **23**(2): p. 77-82.
286. Du, Z. and C.M. Lovly, *Mechanisms of receptor tyrosine kinase activation in cancer.* Mol Cancer, 2018. **17**(1): p. 58.
287. Hendriks, W., et al., *Proteinaceous Regulators and Inhibitors of Protein Tyrosine Phosphatases.* Molecules, 2018. **23**(2).
288. Choudhry, H. and A.L. Harris, *Advances in Hypoxia-Inducible Factor Biology.* Cell Metab, 2018. **27**(2): p. 281-298.
289. Petrova, V., et al., *The hypoxic tumour microenvironment.* Oncogenesis, 2018. **7**(1): p. 10.
290. Potente, M., H. Gerhardt, and P. Carmeliet, *Basic and therapeutic aspects of angiogenesis.* Cell, 2011. **146**(6): p. 873-87.
291. Ghosh, D., S. Nandi, and S. Bhattacharjee, *Combination therapy to checkmate Glioblastoma: clinical challenges and advances.* Clin Transl Med, 2018. **7**(1): p. 33.
292. Ariazi, E.A. and V.C. Jordan, *Estrogen-related receptors as emerging targets in cancer and metabolic disorders.* Curr Top Med Chem, 2006. **6**(3): p. 203-15.
293. Gaillard-Moguilewsky, M., *Pharmacology of antiandrogens and value of combining androgen suppression with antiandrogen therapy.* Urology, 1991. **37**(2 Suppl): p. 5-12.
294. Pant, S., et al., *Clinical update on K-Ras targeted therapy in gastrointestinal cancers.* Crit Rev Oncol Hematol, 2018. **130**: p. 78-91.
295. Agianian, B. and E. Gavathiotis, *Current Insights of BRAF Inhibitors in Cancer.* J Med Chem, 2018. **61**(14): p. 5775-5793.
296. Rubin, M.A. and F. Demichelis, *The Genomics of Prostate Cancer: emerging understanding with technologic advances.* Mod Pathol, 2018. **31**(S1): p. S1-11.
297. Mondesir, J., et al., *IDH1 and IDH2 mutations as novel therapeutic targets: current perspectives.* J Blood Med, 2016. **7**: p. 171-80.
298. Nicolaides, T.P., et al., *Targeted therapy for BRAFV600E malignant astrocytoma.* Clin Cancer Res, 2011. **17**(24): p. 7595-604.
299. Hyman, D.M., et al., *HER kinase inhibition in patients with HER2- and HER3-mutant cancers.* Nature, 2018. **554**(7691): p. 189-194.
300. Eijkelenboom, A., et al., *Reliable Next-Generation Sequencing of Formalin-Fixed, Paraffin-Embedded Tissue Using Single Molecule Tags.* J Mol Diagn, 2016. **18**(6): p. 851-863.
301. Neveling, K., et al., *BRCA Testing by Single-Molecule Molecular Inversion Probes.* Clin Chem, 2017. **63**(2): p. 503-512.
302. Gorgannezhad, L., et al., *Circulating tumor DNA and liquid biopsy: opportunities, challenges, and recent advances in detection technologies.* Lab Chip, 2018. **18**(8): p. 1174-1196.
303. Capper, D., et al., *DNA methylation-based classification of central nervous system tumours.* Nature, 2018. **555**(7697): p. 469-474.
304. Brien, G.L., D.G. Valerio, and S.A. Armstrong, *Exploiting the Epigenome to Control Cancer-Promoting Gene-Expression Programs.* Cancer Cell, 2016. **29**(4): p. 464-476.
305. Capper, D., et al., *Practical implementation of DNA methylation and copy-number-based CNS tumor diagnostics: the Heidelberg experience.* Acta Neuropathol, 2018. **136**(2): p. 181-210.

306. Kangsamaksin, T., I.W. Tattersall, and J. Kitajewski, *Notch functions in developmental and tumour angiogenesis by diverse mechanisms.* Biochem Soc Trans, 2014. **42**(6): p. 1563-8.
307. Saharinen, P., et al., *VEGF and angiopoietin signaling in tumor angiogenesis and metastasis.* Trends Mol Med, 2011. **17**(7): p. 347-62.
308. Kusters, B., et al., *Differential effects of vascular endothelial growth factor A isoforms in a mouse brain metastasis model of human melanoma.* Cancer Res, 2003. **63**(17): p. 5408-13.
309. Frampton, G.M., et al., *Activation of MET via diverse exon 14 splicing alterations occurs in multiple tumor types and confers clinical sensitivity to MET inhibitors.* Cancer Discov, 2015. **5**(8): p. 850-9.
310. Lowenstein, P.R. and M.G. Castro, *The value of EGFRvIII as the target for glioma vaccines.* Am Soc Clin Oncol Educ Book, 2014: p. 42-50.
311. Greenall, S.A. and T.G. Johns, *EGFRvIII: the promiscuous mutation.* Cell Death Discov, 2016. **2**: p. 16049.
312. de Bitter, T., et al., *Profiling of the metabolic transcriptome via single molecule molecular inversion probes.* Sci Rep, 2017. **7**(1): p. 11402.
313. Lenting, K., et al., *Isocitrate dehydrogenase 1-mutated human gliomas depend on lactate and glutamate to alleviate metabolic stress.* FASEB J, 2019. **33**(1): p. 557-571.
314. van den Heuvel, C., et al., *Quantification and localization of oncogenic receptor tyrosine kinase variant transcripts using molecular inversion probes.* Sci Rep, 2018. **8**(1): p. 7072.
315. van den Heuvel, C., et al., *Molecular Profiling of Druggable Targets in Clear Cell Renal Cell Carcinoma Through Targeted RNA Sequencing.* Front Oncol, 2019. **9**: p. 117.
316. Lenting, K., et al., *Isocitrate dehydrogenase 1-mutated human gliomas depend on lactate and glutamate to alleviate metabolic stress.* FASEB J, 2018: p. fj201800907RR.
317. O'Roak, B.J., et al., *Multiplex targeted sequencing identifies recurrently mutated genes in autism spectrum disorders.* Science, 2012. **338**(6114): p. 1619-22.
318. Galili, T., *dendextend: an R package for visualizing, adjusting and comparing trees of hierarchical clustering.* Bioinformatics, 2015. **31**(22): p. 3718-20.
319. Dobin, A., et al., *STAR: ultrafast universal RNA-seq aligner.* Bioinformatics, 2013. **29**(1): p. 15-21.
320. Tonjes, M., et al., *BCAT1 promotes cell proliferation through amino acid catabolism in gliomas carrying wild-type IDH1.* Nat Med, 2013. **19**(7): p. 901-908.
321. Gan, H.K., A.H. Kaye, and R.B. Luwor, *The EGFRvIII variant in glioblastoma multiforme.* J Clin Neurosci, 2009. **16**(6): p. 748-54.
322. *Catalogue of Somatic Mutations in Cancer, Sanger Institute*. 05-10-2018 [cited 2018 05-10]; Available from: https://cancer.sanger.ac.uk/cosmic/mutation/overview?id=14312.
323. Stone, T.J., et al., *Comprehensive molecular characterisation of epilepsy-associated glioneuronal tumours.* Acta Neuropathol, 2018. **135**(1): p. 115-129.
324. Dahiya, S., et al., *BRAF(V600E) mutation is a negative prognosticator in pediatric ganglioglioma.* Acta Neuropathol, 2013. **125**(6): p. 901-10.
325. Wang, J., et al., *Evaluation of EZH2 expression, BRAF V600E mutation, and CDKN2A/B deletions in epithelioid glioblastoma and anaplastic pleomorphic xanthoastrocytoma.* J Neurooncol, 2019.
326. Ekiz, H.A., et al., *Inhibition of RON kinase potentiates anti-CTLA-4 immunotherapy to shrink breast tumors and prevent metastatic outgrowth.* Oncoimmunology, 2018. **7**(9): p. e1480286.
327. Chen, Y., et al., *MGMT promoter methylation and glioblastoma prognosis: a systematic review and meta-analysis.* Arch Med Res, 2013. **44**(4): p. 281-90.
328. Hegi, M.E. and R. Stupp, *Withholding temozolomide in glioblastoma patients with unmethylated MGMT promoter--still a dilemma?* Neuro Oncol, 2015. **17**(11): p. 1425-7.
329. Molenaar, R.J., et al., *The combination of IDH1 mutations and MGMT methylation status predicts survival in glioblastoma better than either IDH1 or MGMT alone.* Neuro Oncol, 2014. **16**(9): p. 1263-73.

330. Phillips, A.C., et al., *ABT-414, an Antibody-Drug Conjugate Targeting a Tumor-Selective EGFR Epitope.* Mol Cancer Ther, 2016. **15**(4): p. 661-9.
331. Tredan, O., et al., *Molecular screening program to select molecular-based recommended therapies for metastatic cancer patients: analysis from the ProfiLER trial.* Ann Oncol, 2019. **30**(5): p. 757-765.
332. Eckhardt, S.G. and C. Lieu, *Is Precision Medicine an Oxymoron?* JAMA Oncol, 2018.
333. van den Heuvel, C., et al., *Selective MET Kinase Inhibition in MET-Dependent Glioma Models Alters Gene Expression and Induces Tumor Plasticity.* Mol Cancer Res, 2017.
334. Birkman, E.M., et al., *Protein phosphatase 2A (PP2A) inhibitor CIP2A indicates resistance to radiotherapy in rectal cancer.* Cancer Med, 2018. **7**(3): p. 698-706.
335. van den Heuvel, C., et al., *Selective MET Kinase Inhibition in MET-Dependent Glioma Models Alters Gene Expression and Induces Tumor Plasticity.* Mol Cancer Res, 2017. **15**(11): p. 1587-1597.
336. Nomura, N., et al., *Prostate specific membrane antigen (PSMA) expression in primary gliomas and breast cancer brain metastases.* Cancer Cell Int, 2014. **14**(1): p. 26.
337. Wernicke, A.G., et al., *Prostate-specific membrane antigen as a potential novel vascular target for treatment of glioblastoma multiforme.* Arch Pathol Lab Med, 2011. **135**(11): p. 1486-9.
338. Salas Fragomeni, R.A., et al., *Prostate-Specific Membrane Antigen-Targeted Imaging With [18F]DCFPyL in High-Grade Gliomas.* Clin Nucl Med, 2017. **42**(10): p. e433-e435.
339. Zalcman, N., et al., *Androgen receptor: a potential therapeutic target for glioblastoma.* Oncotarget, 2018. **9**(28): p. 19980-19993.
340. Haapasalo, J., et al., *Identification of an alternatively spliced isoform of carbonic anhydrase XII in diffusely infiltrating astrocytic gliomas.* Neuro Oncol, 2008. **10**(2): p. 131-8.
341. Mboge, M.Y., et al., *Carbonic Anhydrases: Role in pH Control and Cancer.* Metabolites, 2018. **8**(1).
342. Fiedler, L., et al., *Evaluation of (177)Lu-CHX-A''-DTPA-6A10 Fab as a radioimmunotherapy agent targeting carbonic anhydrase XII.* Nucl Med Biol, 2018. **60**: p. 55-62.
343. Balss, J., et al., *Analysis of the IDH1 codon 132 mutation in brain tumors.* Acta Neuropathol, 2008. **116**(6): p. 597-602.
344. Molenaar, R.J., et al., *The driver and passenger effects of isocitrate dehydrogenase 1 and 2 mutations in oncogenesis and survival prolongation.* Biochim Biophys Acta, 2014. **1846**(2): p. 326-41.
345. Dang, L., et al., *Cancer-associated IDH1 mutations produce 2-hydroxyglutarate.* Nature, 2009. **462**(7274): p. 739-44.
346. Kats, L.M., et al., *Proto-oncogenic role of mutant IDH2 in leukemia initiation and maintenance.* Cell Stem Cell, 2014. **14**(3): p. 329-41.
347. Chowdhury, R., et al., *The oncometabolite 2-hydroxyglutarate inhibits histone lysine demethylases.* EMBO Rep, 2011. **12**(5): p. 463-9.
348. Fan, J., et al., *Fatty acid labeling from glutamine in hypoxia can be explained by isotope exchange without net reductive isocitrate dehydrogenase (IDH) flux.* J Biol Chem, 2013. **288**(43): p. 31363-9.
349. Shi, J., et al., *Decreasing GSH and increasing ROS in chemosensitivity gliomas with IDH1 mutation.* Tumour Biol, 2015. **36**(2): p. 655-62.
350. Molenaar, R.J., et al., *Radioprotection of IDH1-Mutated Cancer Cells by the IDH1-Mutant Inhibitor AGI-5198.* Cancer Res, 2015. **75**(22): p. 4790-802.
351. Li, S., et al., *Overexpression of isocitrate dehydrogenase mutant proteins renders glioma cells more sensitive to radiation.* Neuro Oncol, 2013. **15**(1): p. 57-68.
352. Molenaar, R.J., et al., *Wild-type and mutated IDH1/2 enzymes and therapy responses.* Oncogene, 2018.
353. Jalbert, L.E., et al., *Metabolic Profiling of IDH Mutation and Malignant Progression in Infiltrating Glioma.* Sci Rep, 2017. **7**: p. 44792.

354. Khurshed, M., et al., *In silico gene expression analysis reveals glycolysis and acetate anaplerosis in IDH1 wild-type glioma and lactate and glutamate anaplerosis in IDH1-mutated glioma.* Oncotarget, 2017.
355. Esmaeili, M., et al., *IDH1 R132H mutation generates a distinct phospholipid metabolite profile in glioma.* Cancer Res, 2014. **74**(17): p. 4898-907.
356. Cuyas, E., et al., *Oncometabolic mutation IDH1 R132H confers a metformin-hypersensitive phenotype.* Oncotarget, 2015. **6**(14): p. 12279-96.
357. Mazor, T., et al., *Clonal expansion and epigenetic reprogramming following deletion or amplification of mutant IDH1.* Proc Natl Acad Sci U S A, 2017. **114**(40): p. 10743-10748.
358. Boyle, E.A., et al., *MIPgen: optimized modeling and design of molecular inversion probes for targeted resequencing.* Bioinformatics, 2014. **30**(18): p. 2670-2.
359. Trapnell, C., et al., *Differential gene and transcript expression analysis of RNA-seq experiments with TopHat and Cufflinks.* Nat Protoc, 2012. **7**(3): p. 562-78.
360. Conway, T., et al., *Xenome--a tool for classifying reads from xenograft samples.* Bioinformatics, 2012. **28**(12): p. i172-8.
361. Subramanian, A., et al., *Gene set enrichment analysis: a knowledge-based approach for interpreting genome-wide expression profiles.* Proc Natl Acad Sci U S A, 2005. **102**(43): p. 15545-50.
362. Botman, D., W. Tigchelaar, and C.J. Van Noorden, *Determination of glutamate dehydrogenase activity and its kinetics in mouse tissues using metabolic mapping (quantitative enzyme histochemistry).* J Histochem Cytochem, 2014. **62**(11): p. 802-12.
363. Botman, D., W. Tigchelaar, and C.J. Van Noorden, *Determination of phosphate-activated glutaminase activity and its kinetics in mouse tissues using metabolic mapping (quantitative enzyme histochemistry).* J Histochem Cytochem, 2014. **62**(11): p. 813-26.
364. Chieco, P., et al., *Image cytometry: protocols for 2D and 3D quantification in microscopic images.* Prog Histochem Cytochem, 2013. **47**(4): p. 211-333.
365. Guilfoyle, D.N., et al., *Quantitative measurements of proton spin-lattice (T1) and spin-spin (T2) relaxation times in the mouse brain at 7.0 T.* Magn Reson Med, 2003. **49**(3): p. 576-80.
366. de Graaf, R.A., et al., *High magnetic field water and metabolite proton T1 and T2 relaxation in rat brain in vivo.* Magn Reson Med, 2006. **56**(2): p. 386-94.
367. Xin, L., et al., *Proton T2 relaxation time of J-coupled cerebral metabolites in rat brain at 9.4 T.* NMR Biomed, 2008. **21**(4): p. 396-401.
368. Schwarcz, A., et al., *In vivo water quantification in mouse brain at 9.4 Tesla in a vasogenic edema model.* Magn Reson Med, 2001. **46**(6): p. 1246-9.
369. Provencher, S.W., *Automatic quantitation of localized in vivo 1H spectra with LCModel.* NMR Biomed, 2001. **14**(4): p. 260-4.
370. Min, J.L., et al., *Mutation analysis of candidate genes within the 2q33.3 linkage area for familial early-onset generalised osteoarthritis.* Eur J Hum Genet, 2007. **15**(7): p. 791-9.
371. Flaherty, A.L., J. Teer, and Y. Zhang, *IDH1 mutation in prostate cancer: R132H and beyond.* J Clin Oncol, 2014. **32** (4): p. 1.
372. Rossetto, M., et al., *Metabolism of glioma and IDH1/IDH2 mutations.* Rev Neurol (Paris), 2011. **167**(10): p. 699-703.
373. Massucci, F.A., et al., *Energy metabolism and glutamate-glutamine cycle in the brain: a stoichiometric modeling perspective.* BMC Syst Biol, 2013. **7**: p. 103.
374. Navis, A.C., et al., *Increased mitochondrial activity in a novel IDH1-R132H mutant human oligodendroglioma xenograft model: in situ detection of 2-HG and alpha-KG.* Acta Neuropathol Commun, 2013. **1**(1): p. 18.
375. Fack, F., et al., *Altered metabolic landscape in IDH-mutant gliomas affects phospholipid, energy, and oxidative stress pathways.* EMBO Mol Med, 2017.
376. Malzkorn, B., et al., *Unraveling the glioma epigenome: from molecular mechanisms to novel biomarkers and therapeutic targets.* Brain Pathol, 2011. **21**(6): p. 619-32.

377. Uhlen, M., et al., *A pathology atlas of the human cancer transcriptome.* Science, 2017. **357**(6352).
378. Faubert, B., et al., *Lactate Metabolism in Human Lung Tumors.* Cell, 2017. **171**(2): p. 358-371 e9.
379. Kasischke, K.A., et al., *Neural activity triggers neuronal oxidative metabolism followed by astrocytic glycolysis.* Science, 2004. **305**(5680): p. 99-103.
380. Mosienko, V., A.G. Teschemacher, and S. Kasparov, *Is L-lactate a novel signaling molecule in the brain?* J Cereb Blood Flow Metab, 2015. **35**(7): p. 1069-75.
381. Philips, T. and J.D. Rothstein, *Oligodendroglia: metabolic supporters of neurons.* J Clin Invest, 2017. **127**(9): p. 3271-3280.
382. Lerchundi, R., et al., *NH4(+) triggers the release of astrocytic lactate via mitochondrial pyruvate shunting.* Proc Natl Acad Sci U S A, 2015. **112**(35): p. 11090-5.
383. Chen, R., et al., *Hominoid-specific enzyme GLUD2 promotes growth of IDH1R132H glioma.* Proc Natl Acad Sci U S A, 2014. **111**(39): p. 14217-22.
384. Baldock, A.L., et al., *Invasion and proliferation kinetics in enhancing gliomas predict IDH1 mutation status.* Neuro Oncol, 2014. **16**(6): p. 779-86.
385. Ohgaki, H. and P. Kleihues, *Genetic pathways to primary and secondary glioblastoma.* Am J Pathol, 2007. **170**(5): p. 1445-53.
386. Mardis, E.R., et al., *Recurring mutations found by sequencing an acute myeloid leukemia genome.* N Engl J Med, 2009. **361**(11): p. 1058-66.
387. Amary, M.F., et al., *IDH1 and IDH2 mutations are frequent events in central chondrosarcoma and central and periosteal chondromas but not in other mesenchymal tumours.* J Pathol, 2011. **224**(3): p. 334-43.
388. Iannaci, G., et al., *Extraskeletal osteosarcoma: a very rare case report of primary tumor of the colon-rectum and review of the literature.* Pathol Res Pract, 2013. **209**(6): p. 393-6.
389. Borger, D.R., et al., *Frequent mutation of isocitrate dehydrogenase (IDH)1 and IDH2 in cholangiocarcinoma identified through broad-based tumor genotyping.* Oncologist, 2012. **17**(1): p. 72-9.
390. Fathi, A.T., et al., *Isocitrate dehydrogenase 1 (IDH1) mutation in breast adenocarcinoma is associated with elevated levels of serum and urine 2-hydroxyglutarate.* Oncologist, 2014. **19**(6): p. 602-7.
391. Hinsch, A., et al., *Immunohistochemically detected IDH1(R132H) mutation is rare and mostly heterogeneous in prostate cancer.* World J Urol, 2018. **36**(6): p. 877-882.
392. Leonardi, R., et al., *Cancer-associated isocitrate dehydrogenase mutations inactivate NADPH-dependent reductive carboxylation.* J Biol Chem, 2012. **287**(18): p. 14615-20.
393. Molenaar, R.J., et al., *Clinical and biological implications of ancestral and non-ancestral IDH1 and IDH2 mutations in myeloid neoplasms.* Leukemia, 2015. **29**(11): p. 2134-42.
394. Stein, E.M., et al., *Enasidenib in mutant IDH2 relapsed or refractory acute myeloid leukemia.* Blood, 2017. **130**(6): p. 722-731.
395. Khurshed, M., et al., *IDH1-mutant cancer cells are sensitive to cisplatin and an IDH1-mutant inhibitor counteracts this sensitivity.* FASEB J, 2018: p. fj201800547R.
396. Molenaar, R.J., et al., *IDH1/2 Mutations Sensitize Acute Myeloid Leukemia to PARP Inhibition and This Is Reversed by IDH1/2-Mutant Inhibitors.* Clin Cancer Res, 2018. **24**(7): p. 1705-1715.
397. Lu, Y., et al., *Chemosensitivity of IDH1-Mutated Gliomas Due to an Impairment in PARP1-Mediated DNA Repair.* Cancer Res, 2017. **77**(7): p. 1709-1718.
398. Fernandez, S.L., D.W. Russell, and P.J. Hurlin, *Development of human gene reporter cell lines using rAAV mediated homologous recombination.* Biol Proced Online, 2007. **9**: p. 84-90.
399. Vichai, V. and K. Kirtikara, *Sulforhodamine B colorimetric assay for cytotoxicity screening.* Nat Protoc, 2006. **1**(3): p. 1112-6.
400. Pusch, S., et al., *D-2-Hydroxyglutarate producing neo-enzymatic activity inversely correlates with frequency of the type of isocitrate dehydrogenase 1 mutations found in glioma.* Acta Neuropathol Commun, 2014. **2**: p. 19.

401. Lenting, K., et al., *Glioma: experimental models and reality.* Acta Neuropathol, 2017.
402. Shin, E.S., et al., *Catechin gallates are NADP+-competitive inhibitors of glucose-6-phosphate dehydrogenase and other enzymes that employ NADP+ as a coenzyme.* Bioorg Med Chem, 2008. **16**(7): p. 3580-6.
403. Zinellu, A., et al., *Human Serum Albumin Increases the Stability of Green Tea Catechins in Aqueous Physiological Conditions.* PLoS One, 2015. **10**(7): p. e0134690.
404. Redon, C., et al., *Histone H2A variants H2AX and H2AZ.* Curr Opin Genet Dev, 2002. **12**(2): p. 162-9.
405. Borodovsky, A., M.J. Seltzer, and G.J. Riggins, *Altered cancer cell metabolism in gliomas with mutant IDH1 or IDH2.* Curr Opin Oncol, 2012. **24**(1): p. 83-9.
406. Izquierdo-Garcia, J.L., et al., *IDH1 Mutation Induces Reprogramming of Pyruvate Metabolism.* Cancer Res, 2015. **75**(15): p. 2999-3009.
407. Salamanca-Cardona, L., et al., *In Vivo Imaging of Glutamine Metabolism to the Oncometabolite 2-Hydroxyglutarate in IDH1/2 Mutant Tumors.* Cell Metab, 2017. **26**(6): p. 830-841 e3.
408. McBrayer, S.K., et al., *Transaminase Inhibition by 2-Hydroxyglutarate Impairs Glutamate Biosynthesis and Redox Homeostasis in Glioma.* Cell, 2018. **175**(1): p. 101-116 e25.
409. Pedraz-Cuesta, E., et al., *The glutamate transport inhibitor DL-Threo-beta-Benzyloxyaspartic acid (DL-TBOA) differentially affects SN38- and oxaliplatin-induced death of drug-resistant colorectal cancer cells.* BMC Cancer, 2015. **15**: p. 411.
410. Izquierdo-Garcia, J.L., et al., *Glioma cells with the IDH1 mutation modulate metabolic fractional flux through pyruvate carboxylase.* PLoS One, 2014. **9**(9): p. e108289.
411. Garrett, M., et al., *Metabolic characterization of isocitrate dehydrogenase (IDH) mutant and IDH wildtype gliomaspheres uncovers cell type-specific vulnerabilities.* Cancer Metab, 2018. **6**: p. 4.
412. Li, J., et al., *Decreased expression of IDH1-R132H correlates with poor survival in gastrointestinal cancer.* Oncotarget, 2016. **7**(45): p. 73638-73650.
413. Weng, Z., et al., *Green tea epigallocatechin gallate binds to and inhibits respiratory complexes in swelling but not normal rat hepatic mitochondria.* Biochem Biophys Res Commun, 2014. **443**(3): p. 1097-104.
414. Khan, M.A., et al., *(-)-Epigallocatechin-3-gallate reverses the expression of various tumor-suppressor genes by inhibiting DNA methyltransferases and histone deacetylases in human cervical cancer cells.* Oncol Rep, 2015. **33**(4): p. 1976-84.
415. Gao, Y. and T.O. Tollefsbol, *Impact of Epigenetic Dietary Components on Cancer through Histone Modifications.* Curr Med Chem, 2015. **22**(17): p. 2051-64.
416. Nandakumar, V., M. Vaid, and S.K. Katiyar, *(-)-Epigallocatechin-3-gallate reactivates silenced tumor suppressor genes, Cip1/p21 and p16INK4a, by reducing DNA methylation and increasing histones acetylation in human skin cancer cells.* Carcinogenesis, 2011. **32**(4): p. 537-44.
417. Puig, T., et al., *Green tea catechin inhibits fatty acid synthase without stimulating carnitine palmitoyltransferase-1 or inducing weight loss in experimental animals.* Anticancer Res, 2008. **28**(6A): p. 3671-6.
418. Gelman, S.J., et al., *Consumption of NADPH for 2-HG Synthesis Increases Pentose Phosphate Pathway Flux and Sensitizes Cells to Oxidative Stress.* Cell Rep, 2018. **22**(2): p. 512-522.
419. Liang, Y.C., et al., *Suppression of extracellular signals and cell proliferation through EGF receptor binding by (-)-epigallocatechin gallate in human A431 epidermoid carcinoma cells.* J Cell Biochem, 1997. **67**(1): p. 55-65.
420. Kim, H.S., M.J. Quon, and J.A. Kim, *New insights into the mechanisms of polyphenols beyond antioxidant properties; lessons from the green tea polyphenol, epigallocatechin 3-gallate.* Redox Biol, 2014. **2**: p. 187-95.
421. Le, C.T., et al., *Effects of the Green Tea Polyphenol Epigallocatechin-3-Gallate on Glioma: A Critical Evaluation of the Literature.* Nutr Cancer, 2018. **70**(3): p. 317-333.

422. Kaur, H., et al., *A new therapeutic approach for brain delivery of Epigallocatechin gallate: Development and characterization studies.* Curr Drug Deliv, 2018.
423. Krupkova, O., S.J. Ferguson, and K. Wuertz-Kozak, *Stability of (-)-epigallocatechin gallate and its activity in liquid formulations and delivery systems.* J Nutr Biochem, 2016. **37**: p. 1-12.
424. Lin, L.C., et al., *Pharmacokinetics of (-)-epigallocatechin-3-gallate in conscious and freely moving rats and its brain regional distribution.* J Agric Food Chem, 2007. **55**(4): p. 1517-24.
425. Tyagi, N., et al., *Cancer therapeutics with epigallocatechin-3-gallate encapsulated in biopolymeric nanoparticles.* Int J Pharm, 2017. **518**(1-2): p. 220-227.
426. Velavan, B., et al., *Nano-chemotherapeutic efficacy of (-) -epigallocatechin 3-gallate mediating apoptosis in A549cells: Involvement of reactive oxygen species mediated Nrf2/Keap1signaling.* Biochem Biophys Res Commun, 2018.
427. Pardridge, W.M., *CSF, blood-brain barrier, and brain drug delivery.* Expert Opin Drug Deliv, 2016. **13**(7): p. 963-75.
428. Cecchelli, R., et al., *Modelling of the blood-brain barrier in drug discovery and development.* Nat Rev Drug Discov, 2007. **6**(8): p. 650-61.
429. Pardridge, W.M., *The blood-brain barrier: bottleneck in brain drug development.* NeuroRx, 2005. **2**(1): p. 3-14.
430. Perrin, S.L., et al., *Glioblastoma heterogeneity and the tumour microenvironment: implications for preclinical research and development of new treatments.* Biochem Soc Trans, 2019. **47**(2): p. 625-638.
431. Aum, D.J., et al., *Molecular and cellular heterogeneity: the hallmark of glioblastoma.* Neurosurg Focus, 2014. **37**(6): p. E11.
432. Inda, M.M., R. Bonavia, and J. Seoane, *Glioblastoma multiforme: a look inside its heterogeneous nature.* Cancers (Basel), 2014. **6**(1): p. 226-39.
433. Weller, M., et al., *EANO guidelines on the diagnosis and treatment of diffuse gliomas of adulthood.* Nature Reviews Clinical Oncology, 2021. **18**(3): p. 170-186.
434. Claes, A., et al., *Phenotypic and genotypic characterization of orthotopic human glioma models and its relevance for the study of anti-glioma therapy.* Brain Pathology, 2008. **18**(3): p. 423-433.
435. Piaskowski, S., et al., *Glioma cells showing IDH1 mutation cannot be propagated in standard cell culture conditions.* British Journal of Cancer, 2011. **104**(6): p. 968-970.
436. Pine, A.R., et al., *Tumor Microenvironment Is Critical for the Maintenance of Cellular States Found in Primary Glioblastomas.* Cancer Discovery, 2020. **10**(7): p. 964-979.
437. Lu, Y.X., et al., *Chemosensitivity of IDH1-Mutated Gliomas Due to an Impairment in PARP1-Mediated DNA Repair.* Cancer Research, 2017. **77**(7): p. 1709-1718.
438. Li, K.S., et al., *IDH1 R132H mutation regulates glioma chemosensitivity through Nrf2 pathway.* Oncotarget, 2017. **8**(17): p. 28865-28879.
439. Badur, M.G., et al., *Oncogenic R132 IDH1 Mutations Limit NADPH for De Novo Lipogenesis through (D)2-Hydroxyglutarate Production in Fibrosarcoma Cells (vol 25, pg 1018, 2018).* Cell Reports, 2018. **25**(6): p. 1680-1680.
440. Jin, G.L., et al., *Mutant IDH1 is required for IDH1 mutated tumor cell growth.* Oncotarget, 2012. **3**(8): p. 774-782.
441. van Lith, S.A., et al., *Identification of a novel inactivating mutation in Isocitrate Dehydrogenase 1 (IDH1-R314C) in a high grade astrocytoma.* Sci Rep, 2016. **6**: p. 30486.
442. Tonjes, M., et al., *BCAT1 promotes cell proliferation through amino acid catabolism in gliomas carrying wild-type IDH1.* Nature Medicine, 2013. **19**(7): p. 901-+.
443. Pusch, S., et al., *D-2-Hydroxyglutarate producing neo-enzymatic activity inversely correlates with frequency of the type of isocitrate dehydrogenase 1 mutations found in glioma.* Acta Neuropathologica Communications, 2014. **2**.
444. Fernandez, S.L., D.W. Russell, and P.J. Hurlin, *Development of human gene reporter cell lines using rAAV mediated homologous recombination.* Biological Procedures Online, 2007. **9**: p. 84-90.

445. Zhang, Y., et al., *IDH2 compensates for IDH1 mutation to maintain cell survival under hypoxic conditions in IDH1mutant tumor cells.* Mol Med Rep, 2019. **20**(2): p. 1893-1900.
446. Karpel-Massler, G., et al., *Induction of synthetic lethality in IDH1-mutated gliomas through inhibition of Bcl-xL.* Nature Communications, 2017. **8**.
447. Molenaar, R.J., et al., *Agi5198, an Inhibitor of Idh1r132h, Protects Idh1r132h Hct116 Cells against Irradiation.* Neuro-Oncology, 2014. **16**.
448. Steenbergen, R., et al., *Establishing normal metabolism and differentiation in hepatocellular carcinoma cells by culturing in adult human serum.* Sci Rep, 2018. **8**(1): p. 11685.
449. Gillet, J.P., S. Varma, and M.M. Gottesman, *The clinical relevance of cancer cell lines.* J Natl Cancer Inst, 2013. **105**(7): p. 452-8.
450. Kaur, G. and J.M. Dufour, *Cell lines: Valuable tools or useless artifacts.* Spermatogenesis, 2012. **2**(1): p. 1-5.
451. Marx, V., *Cell-line authentication demystified.* Nat Methods, 2014. **11**(5): p. 483-8.
452. You, S., et al., *Cellular characteristics of primary and immortal canine embryonic fibroblast cells.* Exp Mol Med, 2004. **36**(4): p. 325-35.
453. Cazzaniga, M. and B. Bonanni, *Relationship Between Metabolic Reprogramming and Mitochondrial Activity in Cancer Cells. Understanding The Anticancer Effect of Metformin and Its Clinical Implications.* Anticancer Research, 2015. **35**(11): p. 5789-5796.
454. DeBerardinis, R.J. and N.S. Chandel, *Fundamentals of cancer metabolism.* Science Advances, 2016. **2**(5).
455. Warburg, O., *On respiratory impairment in cancer cells.* Science, 1956. **124**(3215): p. 269-70.
456. Warburg, O., *On the origin of cancer cells.* Science, 1956. **123**(3191): p. 309-14.
457. Iurlaro, R., C.L. Leon-Annicchiarico, and C. Munoz-Pinedo, *Regulation of cancer metabolism by oncogenes and tumor suppressors.* Methods Enzymol, 2014. **542**: p. 59-80.
458. Laukka, T., et al., *Fumarate and Succinate Regulate Expression of Hypoxia-inducible Genes via TET Enzymes.* Journal of Biological Chemistry, 2016. **291**(8): p. 4256-4265.
459. Dalla Pozza, E., et al., *Regulation of succinate dehydrogenase and role of succinate in cancer.* Semin Cell Dev Biol, 2019.
460. Kim, W. and L.M. Liau, *IDH mutations in human glioma.* Neurosurg Clin N Am, 2012. **23**(3): p. 471-80.
461. Shah, S.H., W.E. Kraus, and C.B. Newgard, *Metabolomic profiling for the identification of novel biomarkers and mechanisms related to common cardiovascular diseases: form and function.* Circulation, 2012. **126**(9): p. 1110-20.
462. Kaushik, A.K. and R.J. DeBerardinis, *Applications of metabolomics to study cancer metabolism.* Biochim Biophys Acta Rev Cancer, 2018. **1870**(1): p. 2-14.
463. Wishart, D.S., et al., *HMDB 4.0: the human metabolome database for 2018.* Nucleic Acids Res, 2018. **46**(D1): p. D608-D617.
464. Wishart, D.S., et al., *Cancer Metabolomics and the Human Metabolome Database.* Metabolites, 2016. **6**(1).
465. Dekker, L.J.M., et al., *Metabolic changes related to the IDH1 mutation in gliomas preserve TCA-cycle activity: An investigation at the protein level.* FASEB J, 2020. **34**(3): p. 3646-3657.
466. Lenting, K., et al., *Mapping actionable pathways and mutations in brain tumours using targeted RNA next generation sequencing.* Acta Neuropathol Commun, 2019. **7**(1): p. 185.
467. Gottschalk, M., et al., *Refined modelling of the short-T2 signal component and ensuing detection of glutamate and glutamine in short-TE, localised, (1) H MR spectra of human glioma measured at 3 T.* NMR Biomed, 2016. **29**(7): p. 943-51.
468. Rijpkema, M., et al., *Characterization of oligodendrogliomas using short echo time 1H MR spectroscopic imaging.* NMR Biomed, 2003. **16**(1): p. 12-8.
469. Jung, E., et al., *Tumor cell plasticity, heterogeneity, and resistance in crucial microenvironmental niches in glioma.* Nat Commun, 2021. **12**(1): p. 1014.
470. Venkataramani, V., et al., *Synaptic input to brain tumors: clinical implications.* Neuro Oncol, 2021. **23**(1): p. 23-33.

471. Venkataramani, V., et al., *Glutamatergic synaptic input to glioma cells drives brain tumour progression.* Nature, 2019. **573**(7775): p. 532-+.
472. Venkatesh, H.S., et al., *Electrical and synaptic integration of glioma into neural circuits.* Nature, 2019. **573**(7775): p. 539-+.
473. Yu, K., et al., *PIK3CA variants selectively initiate brain hyperactivity during gliomagenesis.* Nature, 2020. **578**(7793): p. 166-171.
474. Monje, M., et al., *Roadmap for the Emerging Field of Cancer Neuroscience.* Cell, 2020. **181**(2): p. 219-222.
475. van den Heuvel, C., et al., *RNA-based high-risk HPV genotyping and identification of high-risk HPV transcriptional activity in cervical tissues.* Mod Pathol, 2019.
476. van den Heuvel, C.N.A.M., et al., *Molecular Profiling of Druggable Targets in Clear Cell Renal Cell Carcinoma Through Targeted RNA Sequencing.* Frontiers in Oncology, 2019. **9**.
477. van den Heuvel, C.N.A.M., et al., *Quantification and localization of oncogenic receptor tyrosine kinase variant transcripts using molecular inversion probes.* Scientific Reports, 2018. **8**.
478. Van der Velden, D.L., et al., *The Drug Rediscovery protocol facilitates the expanded use of existing anticancer drugs.* Nature, 2019. **574**(7776): p. 127-+.
479. Jain, K.K., *A Critical Overview of Targeted Therapies for Glioblastoma.* Front Oncol, 2018. **8**: p. 419.
480. Brennan, C.W., et al., *The somatic genomic landscape of glioblastoma.* Cell, 2013. **155**(2): p. 462-77.
481. Prasad, V., T. Fojo, and M. Brada, *Precision oncology: origins, optimism, and potential.* Lancet Oncol, 2016. **17**(2): p. e81-e86.
482. Tsimberidou, A.M., A.M. Eggermont, and R.L. Schilsky, *Precision cancer medicine: the future is now, only better.* Am Soc Clin Oncol Educ Book, 2014: p. 61-9.
483. Russo, A., et al., *Third generation EGFR TKIs in EGFR-mutated NSCLC: Where are we now and where are we going.* Crit Rev Oncol Hematol, 2017. **117**: p. 38-47.
484. Lynch, T.J., et al., *Activating mutations in the epidermal growth factor receptor underlying responsiveness of non-small-cell lung cancer to gefitinib.* N Engl J Med, 2004. **350**(21): p. 2129-39.
485. Bollag, G., et al., *Clinical efficacy of a RAF inhibitor needs broad target blockade in BRAF-mutant melanoma.* Nature, 2010. **467**(7315): p. 596-9.
486. Morris, V. and S. Kopetz, *BRAF inhibitors in clinical oncology.* F1000Prime Rep, 2013. **5**: p. 11.
487. Fong, P.C., et al., *Inhibition of poly(ADP-ribose) polymerase in tumors from BRCA mutation carriers.* N Engl J Med, 2009. **361**(2): p. 123-34.
488. Robson, M., et al., *Olaparib for Metastatic Breast Cancer in Patients with a Germline BRCA Mutation.* N Engl J Med, 2017. **377**(6): p. 523-533.
489. de Bono, J., J. Kang, and M. Hussain, *Olaparib for Metastatic Castration-Resistant Prostate Cancer. Reply.* N Engl J Med, 2020. **383**(9): p. 891.
490. Noch, E.K., R. Ramakrishna, and R. Magge, *Challenges in the Treatment of Glioblastoma: Multisystem Mechanisms of Therapeutic Resistance.* World Neurosurg, 2018. **116**: p. 505-517.
491. Zurth, C., et al., *Higher blood brain barrier penetration of [C-14]apalutamide and [C-14]enzalutamide compared to [C-14]darolutamide in rats using whole-body autoradiography.* Journal of Clinical Oncology, 2019. **37**(7).
492. Drilon, A., et al., *Efficacy of Larotrectinib in TRK Fusion-Positive Cancers in Adults and Children.* New England Journal of Medicine, 2018. **378**(8): p. 731-739.
493. Wu, G., et al., *The genomic landscape of diffuse intrinsic pontine glioma and pediatric non-brainstem high-grade glioma.* Nat Genet, 2014. **46**(5): p. 444-450.
494. Stransky, N., et al., *The landscape of kinase fusions in cancer.* Nat Commun, 2014. **5**: p. 4846.
495. Lange, A.M. and H.W. Lo, *Inhibiting TRK Proteins in Clinical Cancer Therapy.* Cancers (Basel), 2018. **10**(4).

496. Farber, S., et al., *Temporary Remissions in Acute Leukemia in Children Produced by Folic Acid Antagonist, 4-Aminopteroyl-Glutamic Acid (Aminopterin).* New England Journal of Medicine, 1948. **238**(23): p. 787-793.
497. Walling, J., *From methotrexate to pemetrexed and beyond. A review of the pharmacodynamic and clinical properties of antifolates.* Investigational New Drugs, 2006. **24**(1): p. 37-77.
498. Elion, G.B., *The Purine Path to Chemotherapy.* Science, 1989. **244**(4900): p. 41-47.
499. Heidelberger, C., et al., *Fluorinated Pyrimidines, a New Class of Tumour-Inhibitory Compounds.* Nature, 1957. **179**(4561): p. 663-666.
500. Parker, W.B., *Enzymology of Purine and Pyrimidine Antimetabolites Used in the Treatment of Cancer.* Chemical Reviews, 2009. **109**(7): p. 2880-2893.
501. Luengo, A., D.Y. Gui, and M.G. Vander Heiden, *Targeting Metabolism for Cancer Therapy.* Cell Chemical Biology, 2017. **24**(9): p. 1161-1180.
502. Vander Heiden, M.G., *Targeting cancer metabolism: a therapeutic window opens.* Nature Reviews Drug Discovery, 2011. **10**(9): p. 671-684.
503. Shaw, R.J. and L.C. Cantley, *Ras, PI(3)K and mTOR signalling controls tumour cell growth.* Nature, 2006. **441**(7092): p. 424-430.
504. Duvel, K., et al., *Activation of a Metabolic Gene Regulatory Network Downstream of mTOR Complex 1.* Molecular Cell, 2010. **39**(2): p. 171-183.
505. Pervin, M., et al., *Function of Green Tea Catechins in the Brain: Epigallocatechin Gallate and its Metabolites.* International Journal of Molecular Sciences, 2019. **20**(15).
506. Unno, T. and T. Takeo, *Absorption of (-)-Epigallocatechin Gallate into the Circulation System of Rats.* Bioscience Biotechnology and Biochemistry, 1995. **59**(8): p. 1558-1559.
507. Nakagawa, K. and T. Miyazawa, *Chemiluminescence high-performance liquid chromatographic determination of tea catechin, (-)-epigallocatechin 3-gallate, at picomole levels in rat and human plasma.* Analytical Biochemistry, 1997. **248**(1): p. 41-49.
508. Peeters, T.H., et al., *Isocitrate dehydrogenase 1-mutated cancers are sensitive to the green tea polyphenol epigallocatechin-3-gallate.* Cancer Metab, 2019. **7**: p. 4.
509. Le, C.T., et al., *Effects of the Green Tea Polyphenol Epigallocatechin-3-Gallate on Glioma: A Critical Evaluation of the Literature.* Nutrition and Cancer-an International Journal, 2018. **70**(3): p. 317-333.
510. Jarzyna, R., E. Lenarcik, and J. Bryla, *Chloroquine is a potent inhibitor of glutamate dehydrogenase in liver and kidney-cortex of rabbit.* Pharmacological Research, 1997. **35**(1): p. 79-84.
511. Molenaar, R.J., et al., *Study protocol of a phase IB/II clinical trial of metformin and chloroquine in patients with IDH1-mutated or IDH2-mutated solid tumours.* Bmj Open, 2017. **7**(6).
512. Harding, J.J., et al., *Isoform Switching as a Mechanism of Acquired Resistance to Mutant Isocitrate Dehydrogenase Inhibition.* Cancer Discovery, 2018. **8**(12): p. 1540-1547.
513. Intlekofer, A.M., et al., *Acquired resistance to IDH inhibition through trans or cis dimer-interface mutations.* Nature, 2018. **559**(7712): p. 125-+.

APPENDICES

Research Data Management
List of Publications
Curriculum Vitae
Dankwoord

Data management

Research data presented in this thesis was documented in paper labjournals as well as digitally in Labguru. Data was stored on a local server supported by de ICT department of the Radboudumc and replicated to a university server on a daily basis. The data was archived according to the FAIR principles (Findability, Accessibility, Interoperability, and Reuse of research data). All data generated or analysed in this thesis are included in the chapters of this thesis and in their corresponding publications. Additional data files are available on reasonable request through the corresponding author of the publication found in this thesis.

All experiments involving animals were conducted to according to international, national and institutional guidelines for the care and use of animals. All procedures that were performed were in accordance with the standards of the animal ethical committee of the Radboud University Nijmegen. All experiments and procedures were approved by the CCD (Centrale Commissie Dierproeven).

All studies involving human material were conducted in accordance with the principles of the Declaration of Helsinki. The Medical and Ethical Committee on Research Involving Human Subjects Region Arnhem Nijmegen, Nijmegen, the Netherlands has given approval to conduct these studies.

List of publications

Molenaar, R. J., Botman, D., Smits, M. A., Hira, V. V., van Lith, S. A., Stap, J., Henneman, P., Khurshed, M., **Lenting, K**., Mul, A. N., Dimitrakopoulou, D., van Drunen, C. M., Hoebe, R. A., Radivoyevitch, T., Wilmink, J. W., Maciejewski, J. P., Vandertop, W. P., Leenders, W. P., Bleeker, F. E., van Noorden, C. J. *Radioprotection of IDH1-Mutated Cancer Cells by the IDH1-Mutant Inhibitor AGI-5198.* Cancer Res, 2015. **75**(22): p. 4790-802

van Lith, S. A., Navis, A. C., **Lenting, K.,** Verrijp, K., Schepens, J. T., Hendriks, W. J., Schubert, N. A., Venselaar, H., Wevers, R. A., van Rooij, A., Wesseling, P., Molenaar, R. J., van Noorden, C. J., Pusch, S., Tops, B., Leenders, W. P. *Identification of a novel inactivating mutation in Isocitrate Dehydrogenase 1 (IDH1-R314C) in a high grade astrocytoma.* Sci Rep, 2016. 6: p. 30486

Khurshed, M., Molenaar, R. J., **Lenting, K**., Leenders, W. P., van Noorden, C. J. F. *In silico gene expression analysis reveals glycolysis and acetate anaplerosis in IDH1 wild-type glioma and lactate and glutamate anaplerosis in IDH1-mutated glioma*. Oncotarget, 2017. 8(30): p. 49165-49177.

Lenting, K., Verhaak, R., Ter Laan, M., Wesseling, P., Leenders, W. *Glioma: experimental models and reality*. Acta Neuropathol, 2017. 133(2): p. 263-282.

Lenting, K., Khurshed, M., Peeters, T. H., van den Heuvel, C.N.A.M., van Lith, S. A. M., de Bitter, T., Hendriks, W., Span, P. N., Molenaar, R. J., Botman, D., errijp, K., Heerschap, A., Ter Laan, M., Kusters, B., van Ewijk, A., Huynen, M., Van Noorden, C. J. F., Leenders, W. P. J. *Isocitrate dehydrogenase 1-mutated human gliomas depend on lactate and glutamate to alleviate metabolic stress*. FASEB J, 2019. 33(1): p. 557-571.

Lenting, K., van den Heuvel, C.N.A.M., van Ewijk, A., ElMelik, D., de Boer, R., Tindall, E., Wei, G., Kusters, B., Te , orsthorst, M., Ter Laan, M., Huynen, M. A., Leenders, W. P. *Mapping actionable pathways and mutations in brain tumours using targeted RNA next generation sequencing.* Acta Neuropathol Commun, 2019. 7(1): p. 185.

Peeters, T. H., Kobus, T., Breukels, V., **Lenting, K**., Veltien, A., Heerschap, A., Scheenen, T. W. J. *Imaging Hyperpolarized Pyruvate and Lactate after Blood-Brain Barrier Disruption with Focused Ultrasound*. ACS Chem Neurosci, 2019. 10(5): p. 2591-2601

Peeters, T. H., **Lenting, K**., Breukels, V., van Lith, S. A. M., van den Heuvel, Cnam, Molenaar, R., van Rooij, A., Wevers, Span, P. N., Heerschap, A., Leenders, W. P. J. *Isocitrate dehydrogenase 1-mutated cancers are sensitive to the green tea polyphenol epigallocatechin-3-gallate.* Cancer Metab, 2019. 7: p. 4

Curriculum Vitae

Krissie Lenting was born on the 11th of June, 1987 in Helmond, The Netherlands. She attended both primary and high school (atheneum) in Helmond. In 2007, she moved to Nijmegen to study Medical Biology at the Radboud University Nijmegen. After one year, she moved to study Biomedical Sciences at the Radboud University. Krissie performed research internships at the laboratory of dr. Egbert Oosterwijk (Department of Experimental Urology, RIMLS, Radboudumc), the laboratory of dr. William Leenders (Department of Pathology, Radboudumc), and the laboratory of dr. Wei Zhang (Department of Cancer Biology, MD Anderson Cancer Center, Houston, Texas). She also performed an science journalism internship at the Institute of Biology, 'Bionieuws' in Utrecht, The Netherlands. In 2015, she received her master's degree in Biomedical Sciences.

After her masters' degree, Krissie continued her research as a PhD student in the research group of dr. William Leenders, at the department of Pathology a the Radboudumc. In 2017, the Leenders' group moved to the department of Biochemistry at the Radboud Institute for Molecular Life Sciences (RIMLS), where Krissie's PhD research continued. The results of this research are described in this thesis. In March 2019, Krissie moved from academia to industry and now works in Medical Affais at a pharmaceutical company.

Dankwoord

Daar ligt hij dan, mijn proefschrit. **Het is eindelijk af!**

Ondanks vele goede voornemens om dit werk zo snel mogelijk af te maken en de door omstandigheden uitgestelde verdedigingsdatum, ben ik super blij dat ik de gedrukte versie nu toch in mijn handen mag houden. Ik denk dat menig persoon er wel eens aan getwijfeld heeft of ik ooit nog op dit punt zouden belanden en eerlijk is eerlijk, ikzelf heb er ook wel eens aan getwijfeld. Maar kijk eens aan, het is er toch van gekomen!

Natuurlijk is alles wat in voorgaande hoofdstukken beschreven staat niet mogelijk geweest zonder de hulp van een legio aan mensen, wie ik via deze weg graag wil bedanken. Ik hoop dat ik niemand vergeet, maar bij voorbaat al bedankt!

Allereerst het promotieteam **Pieter** en **Roland**, mijn promotoren. Ik wil jullie hartelijk danken voor jullie begeleiding in de proces. **Pieter**, bedankt voor de vele vruchtbare neuro-onco overleggen die we gehad hebben in de tijd dat je nog werkzaam was op het Radboudumc. Je input was altijd zinvol en gaf stof tot denken. Vanwege je verhuizing naar Utrecht (en Amsterdam) is de samenwerking wat minder geworden, maar je was altijd een luisterend oor wanneer nodig. **Roland**, hartelijk dank voor het welkom dat we gekregen hebben op de afdeling biochemie. Je input op de wekelijkse lab-overleggen was altijd scherp en natuurlijk zeer gewaardeerd.

William, we kennen onze goede en minder goede tijden, maar uiteindelijk overwinnen de goede tijden zeker. Bedankt dat je mij een kans hebt gegeven op dit project! Jij bent onderzoeker in hart en nieren, iets wat niet voor iedereen weggelegd is. Jouw 'out-of-the-box'-denken hebben er voor gezorgd dat het metabole monster van IDH-mutante gliomen in ieder geval voor een deel getemd lijkt te zijn. Voor elk onverwacht onderzoeksresultaat weet jij wel een passende hypothese te vinden. Bedankt voor de leuke en leerzame tijd. Ik wens je alle goeds in het opstarten van je bedrijf. Ik hoop dat het een daverend succes wordt en dat in de toekomst alle oncologische diagnostiek met een smMIP-assay gedaan zal worden.

Paul Span en **Wiljan Hendriks**, ook jullie bedankt voor alle vruchtbare overleggen op de woensdagochtend. De altijd zeer sprekende voorbeelden van Wiljan zullen me altijd bijblijven en maakten zelfs de meest complexe celbiologische processen begrijpelijk. Paul, hartelijk dank voor je input op het gebied van stralingsbiologie, zonder zou ik denk ik nog steeds kolonies aan het tellen zijn.

Onze partners in het Noorden; **Ron, Mohammed, Remco, Vashendria,** we hebben er een mooie en vruchtbare samenwerking van gemaakt. Dank voor de altijd nuttige overleggen en borreltjes die we aansluitend hielden. Zonder jullie input had dit proefschrift er heel anders uitgezien.

Dan mijn paranimfen, om te beginnen met **Marika:** we kennen elkaar van onze studie, waar het nooit een goed idee was om ons naast elkaar in de collegebanken te zetten vanwege de tranen die daar menig maal van plezier vloeiden. Wat was ik blij toen jij samen met Theo naar de afdeling pathologie kwam! Onze borrelkunsten zijn een mooie basis geweest voor een vriendengroep die op de pathologie is ontstaan en waar we allemaal menig mooie stapavond aan over hebben gehouden. Ik ben blij dat jij vandaag naast me staat, hopelijk kunnen we aan het einde van dit moordende uurtje ook weer tranen met tuiten lachen. Dan **Sanne**, toen ik

begon in de groep van William was jij een groot mysterie. Een stille kracht die niet het achterste van haar tong liet zien. Het duurde even voordat je los kwam, maar een bepaald personeelsfeest heeft daar gelukkig verandering in gebracht. Wat hebben wij een plezier gehad (en nog steeds), op het lab, de andere kant van de wereld én alles wat daartussen zit. Hopelijk beleven we nog veel avonturen samen, al zullen deze voortaan buiten het lab moeten plaatsvinden. Op het moment van schrijven ben jij nog steeds mijn paranimf, alleen weet ik niet of je op het moment van mijn daadwerkelijk verdediging naast mij kan staan. Mocht je er niet zijn dan is dit natuurlijk vanwege de mooiste reden die er is, namelijk de geboorte van een kindje. Ik wens jou en Thijs en jullie zoontje dan ook bij dezen alvast alle geluk van de wereld toe! **Kiek** zal de honeurs voor je waarnemen wanneer jij er niet bent.

Kiek, lieve Kiek, de steun en toeverlaat van zo'n beetje iedereen in de groep van William en ook zeker de mijne. Jouw wijsheid (zowel over labzaken als het leven) heeft me zo'n beetje door mijn PhD heen geloodst. Je nuchtere kijk was hard nodig wanneer ik weer eens chagrijnig was over de gang van zaken. Super bedankt voor alle steun en hulp bij eindeloze kleuringen, snijden van zebravissen of wat dan ook! Laten we snel maar weer eens een Aesculaafje of barbecue organiseren. Ik ben ook enorm verheugd dat je als paranimf op stand by wil staan voor wanneer Sanne niet beschikbaar is.

Corina, labmaatje tot het bittere eind. Gelukkig zijn we met z'n tweeën verhuisd van Pathologie naar Biochemie. Zonder jou was dit proces een stuk minder plezierig geweest. Bedankt voor de momenten van eindeloos geklaag vanachter onze computers en natuurlijk die vroeg startende en tot laat doorgaande SQL borrels.

Ook uit William's onderzoeksgroep: **Duaa**, **Karolina, Tessa, Anneke**. **Duaa** en **Karolina**, jullie komst betekende een nieuwe focus in de onderzoeksgroep: de SmMIPs. Bedankt voor jullie eindeloze inzet in pipetteren, analyseren en frustreren over deze nieuwe techniek die de basis is geworden van veel werk, ook in dit proefschrift. **Tessa**, jij bent de allereerste in onze groep geweest die deze techniek heeft opgepakt, bedankt daarvoor! **Anneke**, jouw metabole werk heeft ten grondslag gelegen aan het onderzoeksproject dat de basis heeft gevormd voor mijn PhD. Ik hoop dat je het in Zweden nog steeds naar je zin hebt.

Iedereen op het **Pathologie lab**, waar ik mijn PhD ben begonnen, bedankt voor jullie gezelligheid en expertise op alle vlakken van het onderzoek in de eerste twee jaar van mijn PhD. Iedereen op het **Biochemie lab**, bedankt voor jullie warme welkom en het wegwijs maken op een nieuw lab. Het **CMBI**, en dan met name **Martijn** en **Anne**: dank voor het helpen opzetten en analyseren van alle smMIP data. **Carlijn**, bedankt voor het design van de smMIPs.

Ook mijn collega's van de Nucleaire Geneeskunde: **Tom** en **Thiele**, het was altijd gezellig en enerverend in de kelder van het CDL, waar we menig muisje aan onze experimenten hebben onderworpen. Soms met succes, maar zeker ook zonder succes. **Tom**, jouw expertise op het gebied van NMR heeft voor mooie maar soms moeilijk interpreteerbare resultaten gezorgd waar menig koppen over gebroken zijn. Thiele, ook jij bedankt voor alle rust en expertise die je meenam in deze experimenten.
Over muizen gesproken, een warm bedankje aan **Jeroen**, jouw eindeloze inzet zorgde er altijd voor dat onze muisjes het goed hadden en met zo min mogelijk ongemak voorzien werden van een hersentumor. **Bianca**, ook jij bedankt voor alle input en hulp bij onze dierexperimenten.

Natuurlijk zijn er ook een heel scala aan personen te danken die niet in praktische zin hebben meegewerkt aan het tot stand komen van dit boekje. Elk promotietraject heeft ook een tegenhanger nodig van de serieuze kant van een promotieonderzoek en die heb ik zeker gehad in de vorm van de **Pathologie-Feest-groep**. De meeste avonden begonnen om vier uur stipt in de Aesculaaf en eindigden op vele verschillende plekken diep in de nacht. **Sanne, Marika, Corina, Carlijn, Thomas, Meyke, Peter, Daan, Laura** en alle anderen in deze app, bedankt! Wat hebben we een lol gehad met elkaar!
Ook de borrel-groep: **Manon, Anke, Marika, Ellen** en **Yvonne**. Vanuit de studie hebben we ons borreluurtje er goed in gehouden tijdens onze PhD's. We hebben nu allemaal onze eigen weg gekozen, maar ik kijk nog altijd met plezier terug op zowel de onze studie als alles daarbuiten.

Naast iedereen die op het 'professionele' vlak hebben bijgedragen aan dit boekje zijn degenen uit het privé-front minstens net zo belangrijk. Jullie hebben allen op jullie eigen manier bijgedragen aan het tot stand komen van dit boekje en daarom verdienen jullie je eigen bedankje

Strakboord: **Anna, Hanna, Marjolijn en Mirjam,** jullie steun begon eigenlijk al vroeg in onze studies, waar jullie mij wisten aan te sporen tot het afronden van mijn studie met een pannenkoekentaart toen in mijn bachelor haalde. Bedankt hiervoor! We zien elkaar inmiddels wat minder dan vroeger, maar dat maakt onze vriendschap niet minder waardevol.

Mijn schoonfamilie: **Rob, Inge, Elly, Marco en de rest**. Jullie honger naar een feestje hebben er toch ook zeker voor gezorgd dat dit boekje er nu ligt. Ik hoop dat de situatie het toelaat dat er ook daadwerkelijk een klein feestje gevierd kan worden. **Marco** voor jou ook nog een bijzonder bedankje voor je creatieve geest en je design voor dit boekje.

Pap, helaas kun je dit werk niet meer zien. Ik ben blij dat we uiteindelijk de stap hebben gezet om elkaar weer te zien, ook al was dat maar van korte duur. Ik had je mijn boekje graag nog willen laten zien.

Mam & Eric, hier is 'ie dan eindelijk, het 'ding-waarover-niet-gesproken-mocht-worden'. Mam, Ik weet dat jij van mening bent dat je hier niet aan bij hebt gedragen, maar niets in minder waar. Door jou sta ik waar ik nu sta en heb je dus wel degelijk een belangrijke rol gehad in het uiteindelijk in je hand kunnen houden van dit werk. Ik weet hoe trots je op me bent. Bedankt!

Lieve **Thomas,** we hebben elkaar ontmoet tijdens mijn stage in de groep van William en jij bent uiteindelijk degene die er voor heeft gezorgd dat dit boekje er nu écht ligt. Je aansporingen tot afronding werden je vrijwel nooit in dank afgenomen, maar ik stel ze (achteraf) zeker op prijs. Bedankt voor je geduld. Ik ben enorm blij met jou en met wat we samen aan het opbouwen zijn, ik hou van je!

De laatste woorden van dit dankwoord gaan uit naar **Fenne.** Wat ben ik enorm trots op hoe jij je afgelopen jaar hebt ontwikkeld. Je bent een enorme leuke, pittige dame aan het worden. Ik kijk er naar uit hoe jij je verder gaat ontwikkelen in de toekomst. Je vader en ik houden zo ontzettend veel van je!

Radboudumc
university medical center
IN·DEI·NOMINE·FELICITER
Radboud University